

Charles University
Faculty of Science

DOCTORAL THESIS

Prague 2021

Sabina Jolanta Horodecka

Charles University

Faculty of Science

Department of Physical and Macromolecular Chemistry

Ph.D. study program: Macromolecular chemistry

Doctoral Thesis



Oriented copolymers with liquid crystalline building blocks

Eng. Sabina Jolanta Horodecka M.Sc.

Supervisor:

Eng. Adam Strachota Ph.D.



Institute of Macromolecular Chemistry
Academy of Sciences of the Czech Republic

Prague 2021

Univerzita Karlova v Praze

Přírodovědecká fakulta

Katedra fyzikální a makromolekulární chemie

Doktorský studijní program: Makromolekulární chemie

Disertační práce



**Orientované kopolymery obsahující kapalně krystalické
stavební bloky**

Ing. Sabina Jolanta Horodecka M.Sc.

Školitel:

Ing. Adam Strachota Ph.D.



Ústav makromolekulární chemie
Akademie věd České republiky, v.v.i.

Praha 2021

Declaration:

I hereby declare that this Thesis is my own work and that all the sources are accurately mentioned in the References section. To the best of my knowledge and belief, it contains neither material previously published or written by another person nor material, which to a substantial extent has been accepted for the award of any other degree or diploma of the University or other Institute of higher education, except for the already published results, which are included in the list of attachments. I have written this doctoral thesis independently, under the guidance of my supervisor Eng. Adam Strachota, Ph.D.

Prague, 04.01.2021

.....

Sabina Horodecka

Nawet mądryemu potrzebny jest przyjaciel, a silnemu – oparcie.

prysłowie chińskie

Acknowledgement

Firstly, I would like to express my sincere gratitude to my supervisor Eng. Adam Strachota Ph.D., for the continuous support of my Ph.D. study and related research, for his patience, motivation, and immense knowledge. His guidance helped me in all the time of research and writing of this Thesis. I could not have imagined having a better advisor and mentor for my Ph.D. study.

My thanks belong also to the Charles University in Prague for the opportunity of carrying out doctoral studies, and to the Institute of Macromolecular Chemistry, which was my place of work during these studies.

Then, I would like to thank colleagues from the Department of Nanostructured Polymers and Composites, to all coauthors and people who were involved in all projects in which I took a part. I would like to express my profound gratitude to all „the members of the team“, who shared the knowledge, supported and helped me in different cases, also in my private life.

Na końcu chciałabym serdecznie podziękować najważniejszym osobom w moim życiu: rodzicom, siostrze i mężowi, za wszystko co dla mnie zrobili, za duchowe wsparcie w życiu i podczas pisania tej pracy. Dziękuję za Waszą miłość, cierpliwość, opiekuńczość i modlitwę o ostateczny sukces. Wielkie dzięki za Wasz czas i świadomość, że zawsze mogę wrócić do domu rodzinnego. Bez Was nie znaczy nic.

Contents

Abstract	17
Shrnutí	19
List of abbreviations	21
List of symbols	23
1 Introduction	25
1.1 Liquid crystals	25
1.1.1 Classifications of liquid crystals	27
1.1.1.1 In view of formation conditions	27
1.1.1.2 In view of ordering type	28
1.1.1.3 Liquid crystals based on other than rod-like mesogen molecules	30
1.1.2 Applications of liquid crystals	31
1.2 Liquid crystalline polymers (LCPs)	33
1.2.1 Classification of LCPs	33
1.2.2 Main-chain liquid crystalline polymers (MC-LCPs)	34
1.2.3 Side-chain liquid crystalline polymers (SC-LCPs)	35
1.2.4 Rheology of liquid crystals and of liquid-crystalline polymers (LCPs)	35
1.2.4.1 Models of flow behaviour of LCPs	36
1.2.4.2 Effect of LCP architecture	37
1.3 Liquid crystalline polymer networks (LCPNs)	38
1.3.1 Rigid epoxy-LC resins	38
1.3.2 Liquid crystalline elastomers (LCEs)	39
1.3.3 Polydimethylsiloxane-LC copolymers	41
1.3.4 The basic polydimethylsiloxane (PDMS) polymer and its derivatives	42
1.3.5 Hydrosilylation coupling	44

1.4	Reversibly crosslinked polymers.....	45
1.4.1	Reversibly crosslinked PDMS	47
2	Aims of the Thesis.....	49
3	Experimental part	51
3.1	Chemicals	51
3.1.1	Commercial hydrido-functional PDMS precursors.....	51
3.1.1.1	Determination of precise equivalent molar mass per SiH function (¹ H-NMR).....	52
3.1.2	Vinyl-functional mesogens (LC-units).....	62
3.2	Syntheses	64
3.2.1	Synthesis of PDMS copolymers with pendant “BAFKU” LC groups.....	64
3.2.2	Synthesis of polydimethylsiloxane α,ω -terminated (end-capped) with “BAFKU” LC units.....	67
3.2.3	Synthesis of ‘infinite’ alternating copolymers of PDMS and linearly bonded LC units of azo-type (“A1”, “A12”)	70
3.2.4	Synthesis of ‘infinite’ alternating copolymers of PDMS and linearly bonded LC units of aromatic polyeter type (“M12”, “M22” and “M32”).....	75
3.3	Methods of characterization of the prepared LC-PDMS copolymers	84
3.3.1	Verification of chemical microstructure	85
3.3.1.1	Nuclear Magnetic Resonance (NMR) spectroscopy.....	85
3.3.1.2	Fourier transform infrared (FTIR) spectroscopy	85
3.3.1.3	Gel permeation chromatography (GPC)	86
3.3.1.4	Matrix-assisted laser desorption ionization / time of flight (MALDI-TOF).....	87
3.3.2	Phase properties and transitions	88
3.3.2.1	Differential scanning calorimetry (DSC).....	88
3.3.2.2	X-ray diffraction	89
3.3.2.3	Polarized light microscopy (PLM).....	90
3.3.3	Material properties	91

3.3.3.1	Dynamic-mechanical thermal analysis (DMTA).....	91
3.3.3.2	Microtensile tests and self-healing evaluation.....	92
3.3.3.3	Advanced mechanical analyses.....	93
3.3.3.4	Rheological properties	95
4	Statement about work contribution	99
5	Results and discussion.....	101
5.1	Synthesis of the copolymers via hydrosilylation coupling.....	102
5.1.1	Grafted PDMS-LC copolymers.....	102
5.1.2	LC-end-capped copolymers	104
5.1.3	Linear ‘infinite’ LC-PDMS copolymers	105
5.1.4	Chemical aspects of the syntheses: optimization and side reactions	106
5.1.5	General properties of the prepared copolymers	110
5.1.5.1	Grafted PDMS-LC copolymers	110
5.1.5.2	LC-end-capped copolymers.....	111
5.1.5.3	Linear infinite PDMS-LC copolymers of azo type.....	113
5.1.5.4	Azo-free linear infinite PDMS-LC copolymers.....	115
5.1.6	Efficiency of the hydrosilylation coupling.....	118
5.1.7	Molecular masses of the copolymers	120
5.2	Thermo-mechanical properties of the copolymers (DMTA).....	125
5.3	Self-healing behaviour of the LC-PDMS copolymers	134
5.4	Phase behaviour of the LC-PDMS copolymers.....	136
5.4.1	DSC: thermal transitions	136
5.4.2	X-ray scattering analysis of the phase behaviour.....	145
5.4.3	PLM observation of anisotropy and of mesophase textures	155
5.4.4	Aggregation behaviour of the copolymers	169

5.5	Advanced tests of mechanical properties: disconnection of crosslinks in the reversible elastomers.....	172
5.5.1	Strain sweep tests	173
5.5.2	Creep test.....	175
5.5.3	Stress relaxation	176
5.5.4	Frequency stiffening tests and ability to self-healing.....	177
5.6	Rheological properties	180
5.6.1	Reversible gelation near the melting point.....	180
5.6.2	Rate of thermally induced physical gelation	185
5.6.3	Thixotropic properties	187
6	Conclusions	191
7	List of publications.....	195
7.1	List of the articles constituting the Thesis:.....	195
7.2	List of articles not included in the Thesis:.....	195
8	APPENDICES.....	197
9	References	199

Abstract

Several series of reversible physical networks based on polydimethylsiloxane (PDMS) chains and liquid crystalline (LC) structural units were synthesized and studied, which belong to three different architecture types:

- (1) LC-grafted PDMS (with LC quartets at the grafting sites),
- (2) LC-end-capped linear PDMS,
- (3) and linear 'infinite' LC-PDMS copolymers (with alternating LC and PDMS segments).

PDMS spacers of different lengths were tested, as well as 6 different polyaromatic mesogens of azo type and azo-free type.

Hydrosilylation coupling of vinyl-functional mesogens, obtained as part of an international cooperation, with commercial Si-H-functional PDMS was employed to synthesize all the studied materials.

The copolymers were physically crosslinked by the nano-aggregation of the LC units contained in their macromolecules. The thermotropic properties of the LC-nano-aggregates lent interesting physical properties to the whole material, making some of the copolymers attractive as potential smart materials.

The PDMS spacer segments were selected for the sake of their extreme flexibility, which should provide elastic properties to the physically crosslinked copolymers, and also because of their (desired) incompatibility with the mesogens. This latter effect was highly helpful for achieving the desired physical crosslinking.

The LC-grafted architecture achieved the strongest physical crosslinking, if copolymers with identical (or nearly) identical mesogens, and with PDMS spacers of the same length were compared. The linear infinite copolymers were less strongly crosslinked, and the crosslinking was the weakest in the LC-end-capped ones. The latter materials were rubbery only at low temperatures, but behaved like temperature-sensitive smart oils (containing physical crosslinks)

at ambient T . The efficiency of the crosslinking in the grafted copolymers is apparently greatly enhanced by the occurrence of LC units as quartets at the graft sites.

In the series of the linear ‘infinite’ LC-PDMS copolymers, it was possible to vary the strength of the physical crosslinking by changing the size of the incorporated mesogen. The melting point of the elastomers could be increased up to temperatures exceeding 160°C in the extreme case.

The presented work includes a comprehensive characterization of the copolymers by mechanical, thermo-mechanical and rheological methods. The complex phase behaviour of the nano-segregated LC-copolymers was elucidated by correlating DSC, X-ray and PLM analyses with thermo-mechanical and rheological ones.

Very attractive, application-related material properties of the copolymers include their re-processibility (useful e.g. for 3D printing, recycling, or simple processing), multiple temperature-induced viscoelastic transitions in the rubbery or molten state (interesting for smart applications), melt thixotropy with very rapid recovery of the initial properties, as well as self-healing in the rubbery state (connected with the physical nature of the crosslinking).

Shrnutí

Bylo syntetizováno a studováno několik sérií reverzibilních fyzikálních sítí založených na polydimetylsiloxanových (PDMS) řetězcích a kapalně krystalických (LC) strukturních jednotkách. Materiály patřily do tří různých typů architektury:

- (1) PDMS s ‘naroubovanými’ bočními skupinami LC (čtveřice LC v každé pozici naroubování),
- (2) PDMS ukončený na obou koncích makromolekul jednotkami LC,
- (3) a lineární ‘nekonečné’ kopolymery LC-PDMS s pravidelně se střídajícími jednotkami LC a řetězci PDMS.

V rámci syntéz byly testovány řetězce PDMS o různých délkách a 6 různých polyaromatických mezogenů se skupinami azo i bez nich.

K syntéze všech studovaných materiálů byla použita hydrosilylační reakce mezi mezogeny s vinylovými funkčními skupinami (získaných v rámci mezinárodní spolupráce) a komerčními Si-H-funkčními polydimetylsiloxany.

Kopolymery byly fyzikálně sesíťovány nano-agregací jednotek LC obsažených v jejich makromolekulách. Termotropní vlastnosti nano-agregátů LC propůjčily celému materiálu zajímavé fyzikální vlastnosti, díky nimž jsou některé z kopolymerů atraktivní coby potenciální ‘inteligentní’ materiály.

Řetězce PDMS byly vybrány coby stavební jednotky z důvodu jejich extrémní flexibility, která měla propůjčit elastické vlastnosti fyzikálně sesíťovaným kopolymerům. Dalším důvodem byla také (žádoucí) nekompatibilita PDMS s mezogeny, která byla velmi užitečná pro dosažení potřebného fyzikálního síťování.

Architektura s bočními (‘naroubovanými’) jednotkami LC vedla k nejsilnějšímu fyzikálnímu síťování, což vyplynulo ze srovnání kopolymerů se stejnými (nebo téměř stejnými) mezogeny a s řetězci PDMS o stejné délce. Lineární nekonečné kopolymery LC-PDMS byly méně silně

sesít'ovány, a sesít'ování bylo pak vůbec nejslabší v kopolymerech jednotkami LC na koncích řetězců. Posledně jmenované materiály byly kaučukovité pouze při nízkých teplotách, ale okolo pokojové teploty se chovaly jako teplotně citlivé 'inteligentní oleje' (obsahující fyzikální síť'ování). Účinnost síť'ování v kopolymerech s 'naroubovanými' bočními jednotkami LC je zřejmě značně posílena tím, že jsou tyto jednotky navázány vždy ve čtveřicích.

V rámci série lineárních 'nekonečných' kopolymerů LC-PDMS bylo možné měnit sílu fyzikálního síť'ování cestou změny velikosti zabudovaného mezogenu. Bod tání elastomerů tak mohl být v krajním případě zvýšen až na teploty přesahující 160°C.

Tato disertační práce zahrnuje také komplexní charakterizaci kopolymerů mechanickými, termomechanickými a reologickými metodami. Složitě fázové chování nano-segregovaných kopolymerů LC-PDMS bylo objasněno korelací analýz DSC, rentgenových i PLM s termomechanickými a reologickými.

Mezi velmi atraktivní materiálové vlastnosti kopolymerů související s jejich možnými aplikacemi patří jejich opětovná zpracovatelnost (užitečná například pro 3D tisk, recyklaci nebo i pro jednoduché zpracování), vícenásobné teplotně indukované viskoelastické přechody v kaučukovitém nebo roztaveném stavu (zajímavé pro aplikace coby inteligentní materiály), tixotropie tavenin s velmi rychlou obnovou počátečních vlastností, stejně jako samo-regenerace v kaučukovitém stavu (která souvisí s fyzikální podstatou síť'ování).

List of abbreviations

LC	liquid crystal, liquid-crystalline phase, liquid crystalline
PAA	p-azoxyanizole
N	nematic phase
N*	cholesteric phase
Sm	smectic phase
2D	two-dimensional
MC-LCP	main-chain liquid-crystalline polymer
SC-LCP	side-chain liquid-crystalline polymer
1D	one-dimensional
LCDs	liquid crystal displays
LCTFs	liquid crystal tunable filters
LCPs	liquid crystalline-polymers
MC/SC-LCP	main-chain/side-chain liquid-crystalline polymer
PLM	polarized light microscopy
LCPNs	liquid crystalline polymer networks
LCEs	liquid crystalline elastomers
MC-LCEs	main-chain liquid-crystalline elastomers
SC-LCEs	side-chain liquid-crystalline elastomers
MC/SC-LCEs	main-chain/side-chain liquid-crystalline elastomers
PDMS	polydimethylsiloxane
ATRP	atom transfer radical polymerization
UV	ultraviolet
PDMS-PEO	polydimethylsiloxane-poly(ethylene oxide)
RAFT	reversible addition-fragmentation chain-transfer polymerization
POSS	polyhedral oligomeric silsesquioxane
3D	three-dimensional
bio-MEMS	biomedical microelectromechanical systems
D4	the cyclic dimethylsiloxane tetramer
BAFKU	4-[(4-butylphenyl)diazenyl]phenyl undec-10-enoate
A1	azobenzene-4,4'-diyl bis(pent-4-enoate)
A12	azobenzene-4,4'-diyl bis(undec-10-enoate)
M12	4-(undec-10-enoyloxy)phenyl 4-(undec-10-enoyloxy)benzoate
M22	p-phenylene bis[4-(undec-10-enoyloxy)benzoate]
M32	biphenyl-4,4'-diyl bis[4-(undec-10-enoyloxy)benzoate]
Pt(IV)	platinum complex in the fourth oxidation state
Pt ⁰ or Pt (0)	platinum in the free state (at zero oxidation state)
Pt-H	the Pt-H bond (hydrometallation)
Ni (0)	nickel in the free state (at zero oxidation state)
Pd (0)	palladium in the free state (at zero oxidation state)
Rh(I)	rhodium in the first oxidation state
Co (III)	cobalt in the third oxidation state

EqMW	equivalent molecular masses per SiH function
¹ H-NMR	proton nuclear magnetic resonance spectroscopy
HMS 301	dimethylsiloxane-methylhydrosiloxane (25–35%) copolymer M _n = 1 900–2 100 g/mol
HMS 064	dimethylsiloxane-methylhydrosiloxane (4–8%) copolymer M _n = ca. 60 000–65 000 g/mol
DMS H03	hydrido-terminated polydimethylsiloxane M _n = 400–500 g/mol
DMS H11	hydrido-terminated polydimethylsiloxane M _n = 1 000–1 100 g/mol
DMS H21	hydrido-terminated polydimethylsiloxane M _n = 4 000–5 000 g/mol
DMS Hxx	hydrido-terminated polydimethylsiloxane precursor
ppm	parts per million
HMS xxx	HMS precursor
RUT	Rzeszow University of Technology
Pt	platinum
Vol%	volume percent [%]
CDCl ₃	deuterated chloroform
FTIR	Fourier-transform infrared spectroscopy
MALDI-TOF	matrix-assisted laser desorption ionization / time of flight
DSC	differential scanning calorimetry
DMTA	dynamic-mechanical thermal analysis
TMS	tetramethylsilane
ATR	attenuated total reflection
GPC	gel permeation chromatography
SEC	size exclusion chromatography
ELSD	evaporative light scattering detector
UV-vis	refraction index detector
THF	tetrahydrofuran
CHCl ₃	chloroform
DCTB	(trans-2-[3-(4-t-butyl-phenyl)-2-methyl-2-propenylidene]malonitrile matrix
DPSS	diode-pumped solid-state
SAXS	small-angle X-ray scattering
WAXS	wide-angle X-ray scattering
XRD	X-ray diffraction
m.p.	melting point

List of symbols

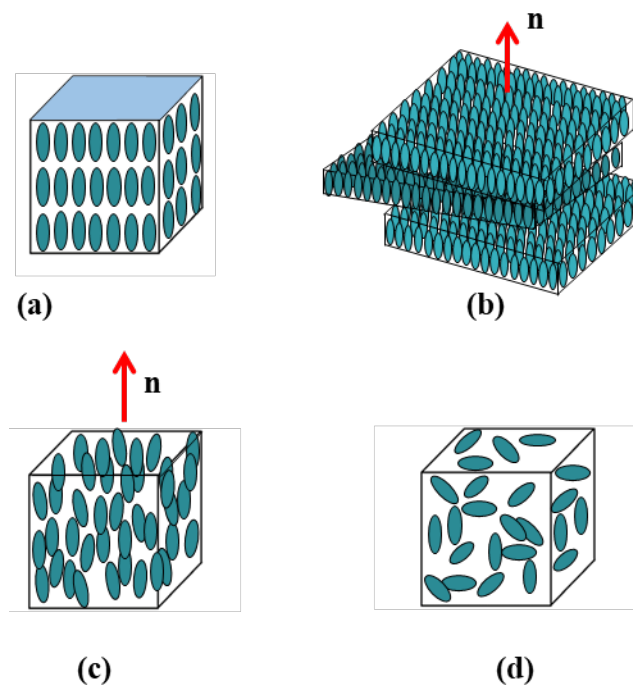
n	an axis describing the preferred molecular orientation in the liquid crystals
S	the degree of molecular orientational order
φ	the angle between molecular axis and the director n
$\langle \cos^2 \varphi \rangle$	an average value of $\cos^2 \varphi$ over many LC molecules
T_g	glass temperature
γ	shear rate
T	temperature
M_n	the number average molecular weight
x	coefficient describing number of quatets with Si-H grups from the Scheme 2 structure formula
y	coefficients from the Scheme 2 structure formula
z	coefficients from the Scheme 2 structure formula
n	the number of internal repeat units from the structure formula in Scheme 14
H	molecular mass of the block $[(CH_3)(H)SiO]_4 = 240.5094$ g/mol
D	molecular mass of the block $[(CH_3)_2SiO]_4 = 296.6158$ g/mol
E	molecular mass of both end groups $\equiv (CH_3)_3Si-O-Si(CH_3)_3 = 162.3775$ g/mol
M	molecular mas of the whole HMS molecule (as shown in above structure formula): the value stated by the manufacturer was used
R	apparent ratio of the number of ‘normal’ PDMS repeat units to the number of methyl-hydrido-functional repeat units, which does not take into account the trimethylsilyl end groups (it is similar but not equal to y, it comes close to y at high z values)
m	number of all siloxane repeat units
RU	molecular mass of an internal repeat unit (of the block $[(CH_3)_2SiO]$) = 74.154 g/mol
ρ	density [g/cm ³]
m	mass [g]
δ	chemical shift [ppm]
M_w	the weight average molecular weight
M_z	the Z-average molecular weight
M_v	the viscosity molecular weight
\bar{M}_M	the dispersity index (traditional name: polydispersity)
λ	wavelength
q	scattering vector
2θ	scattering angle
G'	storage modulus [Pa]
G''	loss modulus [Pa]
$\tan(\delta)$	loss factor [-]
d	diameter

1 Introduction

1.1 Liquid crystals

This Thesis is dedicated to self-assembling copolymers which are physically crosslinked by the aggregation of liquid crystalline moieties in their structure.

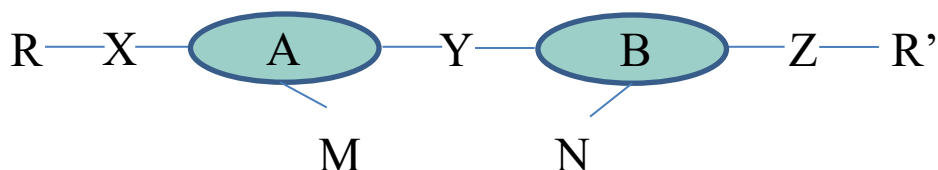
Liquid crystals (LCs) or liquid crystalline phases, possess properties of both liquid (fluidity, molecular mobility) and crystal (long range of order), respectively. They can be considered to be a new state of matter alongside the well-known ones, gas, solid and liquid [1,2]. The liquid crystals hence represent an ordered liquid state, which is intermediate between the rigid and fully ordered crystals, and the fluid and fully disordered ‘normal liquid phase’. A solid state analogue of the liquid crystals are the so-called plastic crystals [3], which are rigid like ‘normal crystals’, but partly disordered (like liquids) due to rotational movements of molecules.



Scheme 1. Schematic representation of molecular packing in the a) crystal, b) and c) liquid crystal, d) liquid.

Liquid crystalline behaviour was first noticed by the Austrian botanist Friedrich Reinitzer (while working at the German branch of the Charles University). In 1888, during his studies on cholesteryl benzoate, he discovered that this substance apparently had two melting points [4]: when he heated it, a first (sharp) melting point occurred where the substance turned into cloudy liquid, while it became fully transparent after a second (equally sharp) melting point. The mentioned compound was further studied by Vorländer, who coined the name „*mesophase*“ for the cloudy liquid, to stress the intermediate nature of this phase between the fully ordered crystalline solid and the completely disordered liquid. This is the reason why Vorländer is called the “father” of liquid crystalline polymeric systems [5]. In *Scheme 1*, an example is shown of a crystalline compound, which via two mesophases gradually melts to an isotropic liquid (it has three apparent melting points). The cloudy appearance of the liquid-crystalline phase is connected with its (normally occurring) polydomain morphology, in analogy to opaque polycrystalline solids (while amorphous or single crystalline solid phases are transparent).

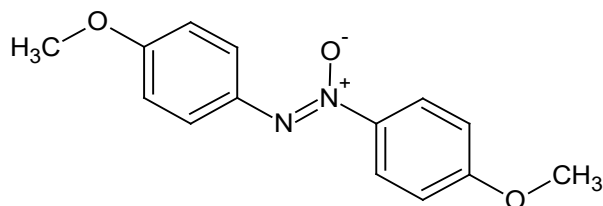
Until present, a large number of liquid crystals have been synthesized, and structure requirements for liquid crystalline behaviour are already well understood [1]. In order to possess mesophases, a compound must consist of molecules with anisotropic properties (e.g. with distinctly elongated-, or disc-like shape), which are then called mesogens.



Scheme 2. Schematic representation of the general structure of a calamitic liquid crystal [6].

Scheme 2 shows the **most common structure of liquid crystalline molecules** [1, 6, 7]: This **rigid-rod-like** molecule is also called ‘calamitic mesogen’. In the center of the structure, A and B cores composed of aromatic groups are located, whereas Y is a linking group between them. It can be azo, imine, ester, ethylene group, or a direct link. M and N are lateral substituents (-F, -Cl, -CH₃, -CN, etc.), which modify the physical properties and thus the mesogenic behaviour of the molecule. At the ends of the elongated structure, flexible terminal groups are attached (R and R’). They are linked to the rigid cores directly, or through linking groups X and Z. They stabilize the molecular alignment and have influence on the melting point. As such terminal groups, most commonly alkyl and alkoxy units are used.

For example p-azoxyanizole (PAA) is a typical calamitic mesogen as shown in *Scheme 3*. In this compound, an azoxy-group connects two aromatic rings. The linearity of the molecule is preserved thanks to para-substitution at of the benzene rings. Methoxy are the terminal groups on the benzene rings.



Scheme 3. Chemical structure of p-azoxyanizole (PAA) [8].

In the 1950s, the liquid crystals attracted numerous researchers, both to experimental and to theoretical studies. In 1956, after analyzing the behaviour of rigid molecules in solution, Flory [9, 10] postulated the conditions for the formation of different anisotropic phases. These criteria concerned the formation of lyotropic mesophases in solutions, but they also can be applied to thermotropic polymers, by approaching solvent concentration of zero.

1.1.1 Classifications of liquid crystals

1.1.1.1 In view of formation conditions

A very important classification criterion of liquid crystals are the conditions, which induce the formation of the mesophases.

Thermotropic mesophases are such ones, which are created by temperature changes. They are formed, when due to thermal motion, a part of the long-range positional and orientational order is lost in an initially perfectly ordered molecular crystal. Sufficiently high shape anisotropy of the molecules is necessary for such a behavior. Materials able of liquid crystallinity often undergo several thermotropic transitions between crystalline solid and isotropic liquid. The mechanical as well as the symmetry properties of the obtained mesophases are intermediate between the ones of a solid and the ones of a liquid. The temperature point at which a perfectly ordered crystal is transformed into a mesophase is called the melting point, whereas the transition from the last mesophase to isotropic liquid is called the clearing point (because the mesophases usually are cloudy, due to polydomain character). If a mesophase appears only

during cooling, it is called *monotropic*. If it appears both during heating and cooling, it is called *enantiotropic*.

Lytropic LC phases are such ones, which are obtained in solution [2]. A typical example is amphiphilic compounds, e.g. polysorbate surfactants or phospholipids found in cell membranes [2], which in an appropriate solvent, at a suitable concentration and temperature undergo self-assembly to anisotropic superstructures, e.g. columnar or lamellar ones. Also simple ionic surfactants like soap dissolved in water form lyotropic phases [11]. The mentioned amphiphilic compounds typically consist of a lipophilic chain ('tail') and of a polar 'head' group (ionic or non-ionic), which facilitates their self-assembly. Another group of common lyotropes are rod-like macromolecules like poly(γ -benzyl glutamate) [12], hydroxypropylcellulose [12], or helical polypeptides [13].

Amphotropic phases [14] are interesting systems, which combine the features of the above two groups: they are mesophases which form under simultaneous influence of both the temperature and the solvent in some mesogen/solvent systems.

1.1.1.2 In view of ordering type

The type of order of the rigid mesogen molecules is the next criterion of classification of liquid crystals. In case of **rod-like molecules**, the most prominent types of ordering are *nematic*, *smectic* and *cholesteric (twisted nematic)* phases [1, 2]. In case of the lyotropic systems based on self-assembly of amphiphilic molecules, different phases like *columnar* or *lamellar* are typically formed, as mentioned further above (which are analogous to morphologies in immiscible polymer blends).

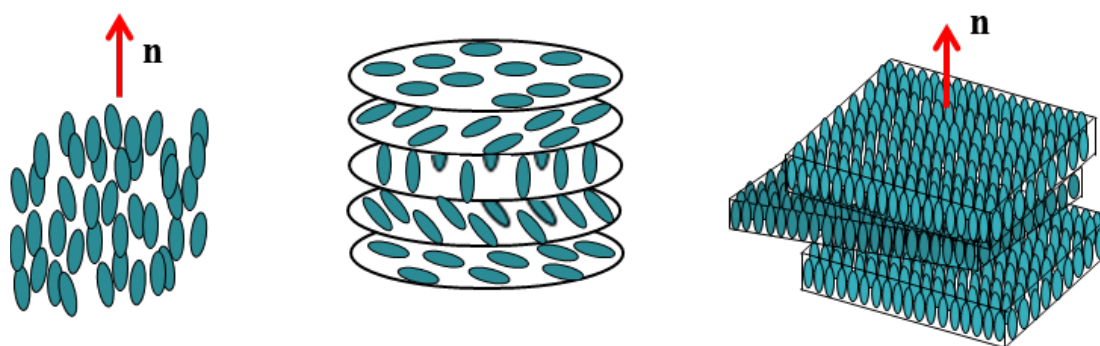
For evaluating the degree of orientation in liquid crystals, which significantly differs among the above groups, it is important to introduce the director n , an axis describing the preferred molecular orientation. The degree of molecular orientational order S can be calculated using Hermann's equation as follows [15]:

$$S = \frac{3 \langle \cos^2 \varphi \rangle - 1}{2}$$

where φ is the angle between molecular axis and the director. $\langle \cos^2 \varphi \rangle$ means an average value of $\cos^2 \varphi$ over many LC molecules. $S = 0$ describes a completely random orientation of molecules, whereas $S = 1$ indicates molecules perfectly oriented along the director.

A **nematic (N) phase** is the simplest one among the liquid crystalline phases. It occurs at temperatures just below the isotropic phase, and possesses a viscosity comparable to the one of an isotropic liquid. In this phase, the mesogens are oriented in a particular direction called the director (n) but they have no positional order and their centers of gravity are randomly located [16]. The degree of molecular orientational order S for nematic phase is when $0.45 < S < 0.65$. The alignment of molecules in a nematic phase is illustrated in **Scheme 4**.

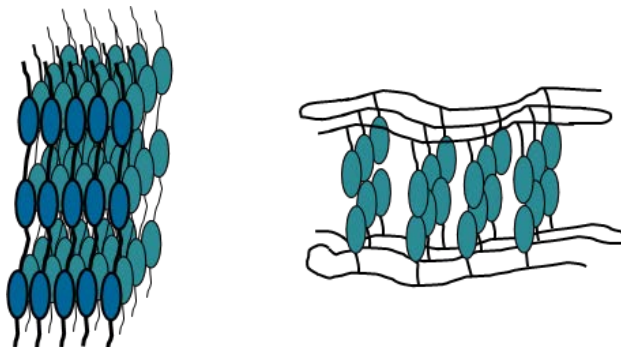
A **cholesteric (N*) phase** (see **Scheme 4** center), also called a twisted nematic or chiral nematic, is a special mesophase which occurs only in chiral LC compounds [17]. The name comes from history, as this particular type of organization was first observed in esters of cholesterols [16]. In this type of mesophase, the chiral nematic mesogens align at small angle relative to each other, so that over longer distances, the nematic alignment is twisted. The director does not have a constant direction, but it 'moves' as a tangent on a helix. The phases (like the helices) can be right-handed or left-handed, depending on the shape of the chiral molecule. Because of the helical type of arrangement, a selective light reflection property is obtained, which is interesting for advanced optical applications.



Scheme 4. Comparison of nematic, cholesteric (N*) and smectic phase.

A **smectic (Sm) phase** (see **Scheme 4** right, or **Scheme 5** with polymeric liquid crystals) occurs if the mesogen molecules arrange to a layered structure. While the nematic phase is aligned in one dimension, the smectic one is 2D-aligned. This phase (in case that it is formed)

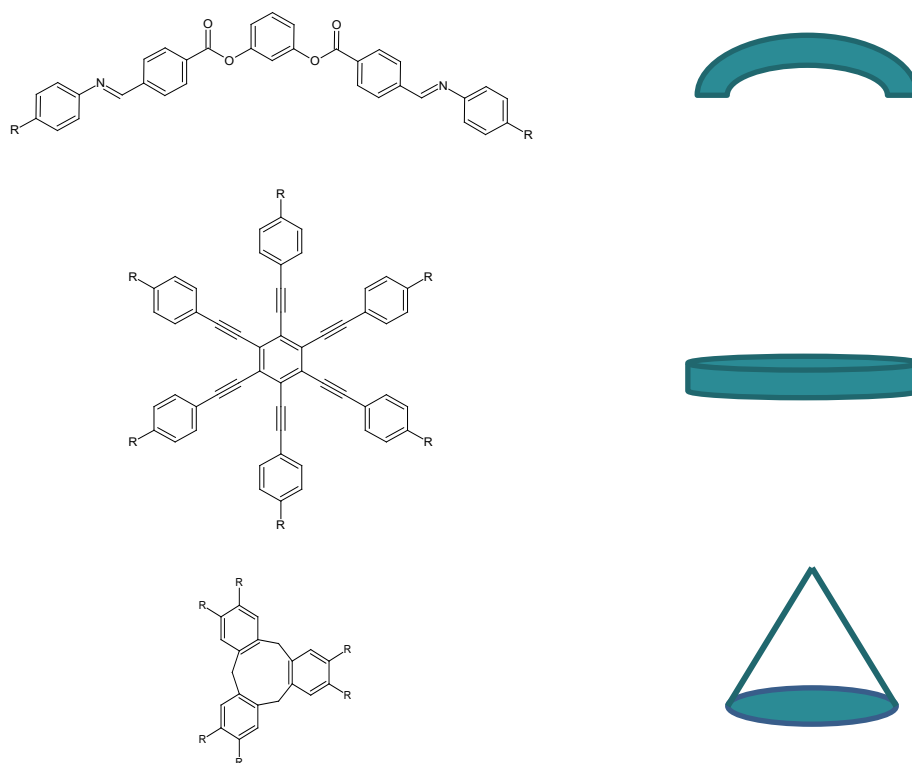
appears at lower temperatures than the nematic one, and possesses a higher viscosity (the primary flow mechanism is the sliding of 2D-lamellae of mesogens). There are several types of smectic phases, named smectic A to smectic K. The degree of molecular orientational order S for smectic phases typically is high: $0.85 < S < 0.95$ [18, 19].



Scheme 5. Scheme of smectic phase in linear polymer (MC-LCP and SC-LCP).

1.1.1.3 Liquid crystals based on other than rod-like mesogen molecules

In addition to the most common rod-like mesogens, liquid crystalline molecules can possess banana [2, 20, 21], discotic [2, 22], or hat-like (also called bowl-like) shape [2, 23] (see *Scheme 6*). Banana-shaped mesogens form classical smectic and nematic phases, including their more exotic varieties, but also novel ones, like the phases called “B1” to “B8” [24] and hence attract a considerable research interest. They are also attractive materials for ferroelectric applications [25].



Scheme 6. Examples of different shape of LC molecules (banana, discotic and hat shape).

The discotic and the hat-like (bowl-like) mesogens are anisotropic molecules extended in two dimensions (in contrast to 1D-extended rods). The bowl-like mesogens represent bent 2D molecules, in analogy to banana-type mesogens as bent rods. Most typical for the discotic and hat-like mesogens are the so-called columnar mesophases [22, 23]. Molecules which are extended in all three dimensions automatically are of spheroidal symmetry, and hence not anisotropic. However, in some analogy to liquid crystals, some spheroidal molecules form the above-mentioned plastic-crystalline mesophases, in which the molecules keep their precise positions in the lattice, but lose their spatial orientation, due to molecular rotation enabled by the transition to the plastic crystals [3]. The viscous liquid-like liquid crystals, as well as the waxy solid-like plastic crystals are often referred-to as ‘soft matter’ [3].

1.1.2 Applications of liquid crystals

By far the most important application of liquid crystals in view of sales volume, as well as tonnage is their use in various types of **liquid crystal displays (LCDs)** [26]. The basic principle

is that the above-mentioned twisted (and thus chiral) nematic phase is able to rotate polarized light, while non-twisted phases like ‘normal nematic’ are not. The liquid crystalline film (consisting of polar mesogens) is placed between two crossed polarizers and is switched by electric field between the nematic (enforced by field) and the twisted nematic (relaxed, no field) states. In this way light is either transmitted (field OFF, twisted nematic) or stopped (nematic field ON, nematic) by the device.

Another relatively widespread mass application are so-called ‘**smart films**’ used to make ‘**smart windows**’ which can switch between an opaque translucent and a transparent state. The LC-variety of the smart films is based on liquid crystal droplets dispersed in a polymer film [27]. The anisotropic micro-droplets are randomly oriented and hence scatter light (like polycrystalline materials), thus causing a white opaque color. Application of electrical field forcibly aligns the orientation of the droplets and causes the film to be transparent.

One more household application are **thermochromic liquid crystalline thermometers** [28], which indicate temperature by color change. Similarly, application of a liquid crystalline fluid is used for detection of (defective) hot spots in semiconductor industry.

Liquid crystal tunable filters (LCTFs) use electronically controlled liquid crystal elements to transmit a selectable wavelength (from 400 up to 2 450 nm) of light and exclude others [29]. The filters are based on electronically controlled birefringence of the liquid crystals employed.

Liquid crystal lenses continuously tunable by external electric field or temperature [30, 31] via adjusting the refractive index of the liquid crystal layer with applied voltage, are another high-tech optical application.

Liquid crystal lasers [32] use a liquid crystal as the resonator cavity, and allow the controlled selection of polarization, as well as of emission wavelength, typically in a range of several tens of nanometers. The lasing medium is usually a dye doped into the liquid crystal.

Other advanced applications attract considerable research interest such as **ferroelectric devices** [25], **liquid-crystalline elastomeric actuators** [33–35] or **optical memory devices** [36].

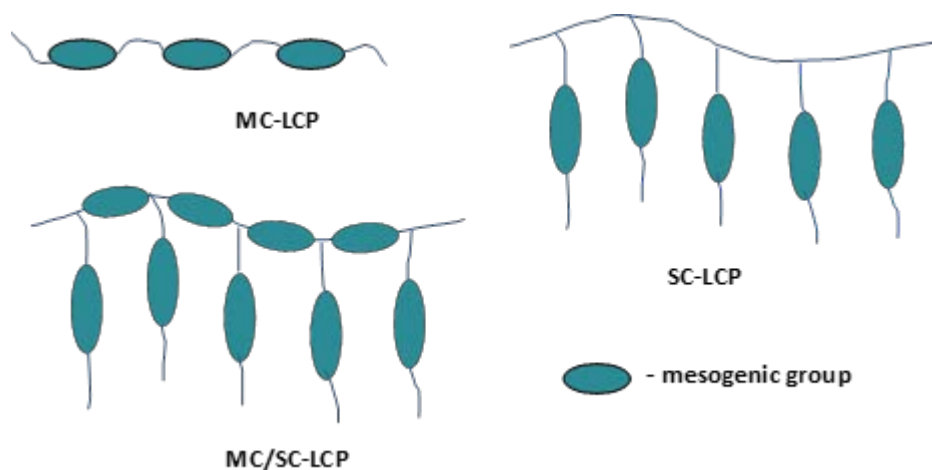
1.2 Liquid crystalline polymers (LCPs)

Because of their ability of self-organization and alignment, the liquid crystals attracted interest in the field of synthesis of special materials, namely the liquid crystalline polymers, which combine the properties of liquid crystals with those of ‘simple’ macromolecules. Also the materials synthesized and studied in this Thesis belong in a broader sense to the liquid crystalline polymers.

1.2.1 Classification of LCPs

Generally, most polymers can be divided into two groups: *thermoplastics* (linear or moderately branched ones) and *polymer networks*, traditionally referred-to as *thermosets*. The same classification can be used also for liquid crystalline polymers (LCPs).

Liquid-crystalline polymers (LCPs) can be divided in analogy to the ‘simple ones’ into *thermoplastic* (linear or moderately branched ones) polymers and *polymer networks* (traditionally referred-to as *thermosets*). Typical rigid or elastomeric polymer networks are covalently cross-linked and are hence no longer fusible or soluble after their synthesis is finalized. Therefore, they cannot be processed by injection-moulding or recycled. Thermoplastic LCPs based on linear and comb-like macromolecules already are well described in the literature [1–10, 14, 15]. Among attractive properties of LCPs [37–46], high elastic moduli in the direction of mesogens’ orientation and high impact resistance are of considerable importance.



Scheme 7. Possible location of mesogens in the macromolecule.

From an additional structural point of view, considering the location of LC units, the LCPs can be further divided into **main-chain-** (MC-LCPs), **side-chain-** (SC-LCPs), and **‘mixed’ MC/SC-LCPs** [43] (see *Scheme 7*). These can occur as simple linear structures, shown in *Scheme 7*, or as networks (eventually as branched molecules).

1.2.2 Main-chain liquid crystalline polymers (MC-LCPs)

Main-chain LCPs are typically synthesized via polycondensation or polyaddition. Most studied are liquid-crystalline polyamides [47, 48], polyesters [37–54], polyurethanes [55–57], while polyacetylenes [58, 59], polycarbonates [60, 61], polyethers [62, 63] or polyimides [64] received less attention. Mesogenic (LC) structural units in MC-LCPs are linearly incorporated into the backbone of MC-LCPs and are usually based on previously characterized low-molecular liquid crystals. They have a strong effect on the segmental mobility and alignment tendency of the whole MC-LCPs macromolecules. The MC-LCPs usually can be easily processed by injection-moulding. By injection-moulding or extrusion, an orientation of polymer chain is induced in the direction of polymer flow. Hence, after cooling down, the obtained product is considerably aligned (which causes a sort of ‘self-reinforcement’). Aligned MC-LCPs are characterized by high mechanical durability, stretching resistance (due to chain orientation), low permeability by gases, and enhanced chemical resistance (both latter properties due to the compact molecular packing).

The MC-LCPs often possess high temperatures of mesophase transitions, in some cases even close to the limit of thermal degradation of the macromolecules, due to the reduced mobility of the mesogenic groups. This reduced mobility results from the direct linking of LC units by usually relatively short building blocks (in typical MC-LCPs). In order to reduce the phase transition temperatures to ‘safe values’, approaches were employed: one method is the introduction of ‘connector moieties’ of irregular length between the LC units, which leads to an irregular structure of the macromolecules, which in turn hinders the crystallization and ordering of the LC segments and whole macromolecules, reduces the size of nanocrystallites and crystallites and thus enhances the segmental mobility and lowers phase transition temperatures. Another, similar approach is based on introducing monodisperse but somewhat longer ‘spacer segments’ between the LC units, so that the flexibility of the linear macromolecules is improved, but their high regularity is preserved. Such MC-LCPs are called semi-rigid. Typical flexible

spacers are aliphatic hydrocarbon chains of various lengths $-(\text{CH}_2)_n-$ [65], or short polydimethylsiloxane spacers [66, 67].

Crosslinked (main-chain-) LCPs with attractive properties, which are structurally related to the above-described linear MC-LCPs, were studied by Giamberini and co-workers and were obtained by reactions between liquid-crystalline diepoxides and dicarboxylic acids [68–71] or aromatic amines [70]. The mentioned products are characterized by a low crosslinking density (the occasional crosslinks originate from epoxy group homopolymerization – a side reaction). Such loosely cross-linked MC-LCPs were shown to display similar reversible phase transitions during heating or cooling like the ideally linear MC-LCPs. After heating above the glass transition temperature (T_g), the now elastomeric cross-linked MC-LCPs can be subjected to orientation, or conversely, to order destruction via mechanical deformation.

1.2.3 Side-chain liquid crystalline polymers (SC-LCPs)

Side-chain LCPs, which are often referred-to as comb-like liquid-crystalline polymers, are usually obtained by attaching low-molecular-weight mesogenic groups to pendant positions of a (typically flexible) macromolecular chain [40]. Most studied were such grafted co-polymers obtained by coupling small liquid-crystalline building blocks to suitably functionalized (in pendant positions) polysiloxane-, polymethacrylate- and polyacrylate- chains, in more exotic cases to polycarbosilane, polyester, polyether, polyphosphazene, polystyrene, polyurethane etc. [39–43, 72–80]. The properties of SC-LCPs are controlled by the structure of the mesogenic groups, as well as by the segmental mobility and the length of the flexible ‘spacer segments’ of the polymer backbone (length of polymer backbone between two LC-grafted positions) [40]. In comparison with MC-LCPs, the SC-LCPs are more readily oriented in the magnetic field [49] (via the diamagnetic exclusion effect), which attracts a considerable research interest in these materials.

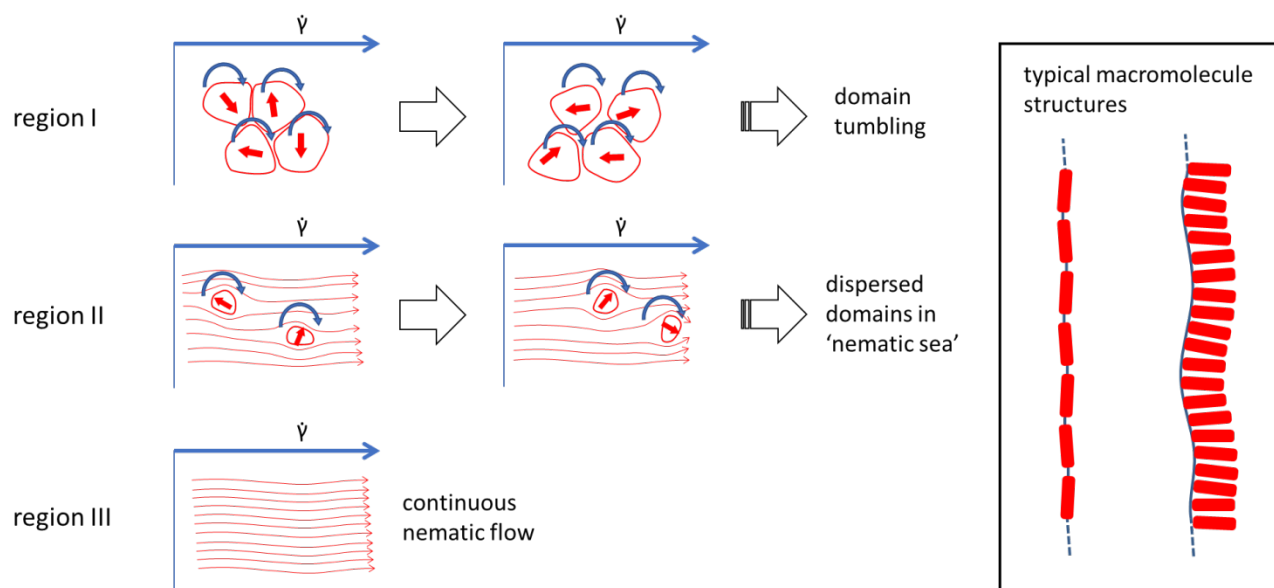
1.2.4 Rheology of liquid crystals and of liquid-crystalline polymers (LCPs)

The presently studied copolymers display highly interesting viscoelastic properties due to the presence of significant amounts of liquid-crystalline building blocks in their structure. The rheology and viscoelasticity of rod-like molecular liquid crystals, as well as of liquid-crystalline polymers (LCPs) attracted a considerable research interest since early on, see reviews [81–85], in

view of unusual and promising material properties of LCPs, especially of oriented ones, and in view of their extraordinary flow behaviour during processing. Lyotropic and thermotropic LCPs generally display similar rheology, but the lyotropic ones were studied earlier and more frequently (see e.g. [13, 86, 87]) than thermotropic ones [83], due to the easier in-situ observation of the former by polarized light microscopy (PLM).

1.2.4.1 Models of flow behaviour of LCPs

Based on their studies of LCPs rheology with polarized light, Onogi, Asada and co-workers [88, 89] proposed three regions (see *Scheme 8*) of the dependence of viscosity on shear rate: a polydomain region with piled and randomly oriented and tumbling LC domains, which occurs at low shear rates (“region I”) – associated with thixotropic behaviour; at higher shear rates, the “region II” occurs, characterized by dispersed domains in a nematic continuum and by a plateau of the viscosity dependence on shear rate; finally, at the highest shear rates (“region III”), the morphology transforms to nematic monodomain-type (flow alignment), and thixotropic behaviour again is observed. Generally, in the aligned nematic state, the LCPs are observed to possess a distinctly lower viscosity than in the isotropic state [81].



Scheme 8. Typical three-region flow behaviour of liquid crystalline polymers [88–91].

The flow behaviour of single LCPs macromolecules (and also of LC molecules) was described by two models, which apply depending on material properties: the ‘molecular (Doi-) model’ [90, 91], which assumes an uniform phase of the flowing fluid with some director wagging or tumbling in this phase. The viscoelasticity arises from the interplay of LC-distortional- (Frank-) elasticity and of hydrodynamic forces. On the other hand, the ‘polydomain (Larson-Doi-) model’ [92, 93] is based on a polydomain morphology (similar to the polycrystalline one in solid materials), where not the director in the uniform fluid, but the small domains undergo wagging and tumbling [12]. If the rheological behaviour of lyotropic and thermotropic LCPs was compared [94, 95], it was found that the molecular (Doi) theory well fits diluted lyotropic LCPs, while concentrated lyotropic LCPs and thermotropic LCPs are better described by the polydomain model (Larson-Doi). The latter is favoured by topological exclusion and insufficient flexibility of the macromolecules.

1.2.4.2 *Effect of LCP architecture*

Several studies compared the rheology of the two main structural families of LCPs:

In case that thermotropic main-chain-LCPs (**MC-LCPs**) possess semi-flexible properties due to suitable spacers, flow aligning behaviour was found to be greatly favoured [85, 96], even in a moderately crosslinked MC-LCPs [97]. Because of this, MC-LCPs are also subjected to rather durable consequences of previous shear flow (‘thermal and shear history’), which are difficult to reset, even by isotropic melting [85, 98, 99].

The side-chain-LCPs (**SC-LCPs**) were reported to possess a much more extended linear viscoelastic region than MC-LCPs [100], and even to lack the rheological ‘region I’ [98], as well as having a tendency to persistent domain tumbling during flow [85], instead of flow alignment. In contrast to MC-LCPs, shear history effects quickly disappear in SC-LCPs (rapid ‘reset’ of initial viscoelastic properties) [85]. SC-LCPs with the rod-like mesogens attached side-on (laterally) [101] are generally similar to ‘normal’ SC-LCPs with end-on-attached LC units, but they can be oriented by creep, while subsequent isotropization easily occurs via oscillatory deformation. Their rheology is controlled mainly by their backbone.

Spacer moieties in MC-LCPs influence their tendency to flow alignment by their flexibility [85, 96], as well as their viscosity (odd/even effect in shorter polymethylene spacers)

[102]. In SC-LCPs, a longer spacer favours stronger LC-LC interaction and eventually the formation of a smectic phase [103, 104], while shorter spacers favour nematic ordering. Smectic SC-LCPs display a specific shear behaviour [105].

1.3 Liquid crystalline polymer networks (LCPNs)

The materials synthesized and studied in this Thesis are physical networks based on copolymers with LC building blocks. Hence they also are related to the interesting material group of liquid crystalline networks.

Cross-linking of reactive liquid crystalline molecules leads to anisotropic solids with an ordered structure. In their case, the term ‘liquid crystalline’ does not refer to the state of matter, but to the similar physical properties like in case of ordered low-molecular-weight liquid crystals (LCs). The organized structure of the LC melt, which is preserved during the curing reaction, leads to a high rigidity. The liquid crystalline monomers (calamitic molecules) used for LCPNs synthesis consist of a rigid aromatic core and of flexible tail groups, which are terminated with reactive moieties able of crosslinking reactions. The length of the flexible tail groups controls the rigidity of the final LCPNs [106, 107].

Liebert and Strzelecki for the first time synthesized a “true” liquid crystalline network via a polymerization reaction of a mesogenic diacryl mesogen with a Schiff base [108]. Later, Blumstein’s group used a system similar to the one of Liebert and Strzelecki, but prepared their network in a strong magnetic field: a long-range aligned structure was then confirmed by X-ray diffraction [109]. Due to their excellent thermal and mechanical stability, the LCPNs easily found use in high-tech applications, for example as foils in electronics, or as matrices in advanced composites, etc. [45, 110, 111, 112].

1.3.1 Rigid epoxy-LC resins

Epoxy resins (which belong to liquid-crystalline networks) are one of the most produced ‘families’ of thermosets and are widely used as a matrix in advanced composites, but not only. They found application in the aviation industry, as coating- or encapsulation materials and also as glues. They are characterized by good mechanical, thermal and dielectric properties, resistance to corrosion and a relatively low shrinkage upon cure. The properties of the epoxy resins can be further improved by incorporation of rigid mesogenic (LC) groups into their network, which can

enhance thermal stability, toughness, flexibility, corrosion resistance, as well as adhesion to various surfaces [113].

The epoxy-LC resins are 'diluted LCPN systems, which besides the LC monomer (which is usually the epoxy component) contain also the hardener component. Hence, these resins are copolymers. The epoxy-LC component is obtained via a modified synthesis route of the basic LC molecule, so that the epoxy functions are introduced for example via LC-diol reaction with epichlorohydrin [70, 114–116] or via condensation of LC-bis(acyl chloride) with glycydyl alcohol [117]. Another method is the oxidation of mesogenic diolefins with terminal double bonds [118, 119]. Curing of LC-epoxy monomers follows the same reaction paths as in case of commercial epoxy networks. As hardeners, primary or secondary aliphatic and aromatic amines, as well as di- or more- functional carboxylic acids are mainly used. More seldom, diphenols, polyphenols and polymercaptans can be employed too [120]. However, the aromatic hardeners are most widely used in epoxy-LC resins. By carefully selecting curing conditions, the size of aligned domains and the network structure can be controlled [68, 70, 71, 121]. In general, the curing of the system should be done within the temperature range of the desired mesophase and should be relatively slow in order not to disturb the LC order. Epoxy-LC-resins cured without special precautions are obtained with a polydomain liquid crystalline structure [122]. Several methods were successfully tested to achieve the monodomain alignment. A simple, safe, and efficient one was found to be the alignment with strong magnetic fields (diamagnetic exclusion effect), achieving values of the order parameter between 0.8 and 0.9, with magnetic field strength varied from 1.45 to 13.5 T [70, 123–130].

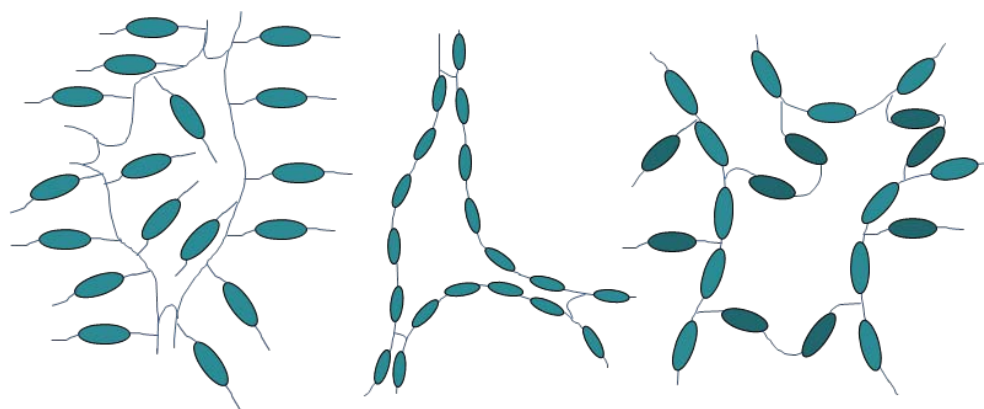
1.3.2 Liquid crystalline elastomers (LCEs)

The liquid crystalline elastomers (LCEs), which were for the first time introduced by De Gennes [131], combine the elastic properties of classical rubbery elastomers with special effects caused by self-organization behaviour of the LC units in the polymer structure. The volume fraction of LC units is dominant in these interesting materials, while the crosslinking density is low, which allows strong effects of ordering phenomena in linear LCP chains between the network junctions. In order to achieve significant LCE-effects, the LC units in the network have to be aligned during the synthesis [132]. The most typical effect in LCEs is the anomalous and abrupt one-direction-expansion of an (internally aligned) LCE sample upon cooling below the isotropic→nematic transition temperature (clearing point): at the lower temperature, the nematic

order favours the straight and hence longer conformation of the linear LCP segments between junctions. If the temperature raises again and reaches the isotropic region, the sample contracts. The LCEs hence are of interest as actuators or even as sensors-actuators [132]. In addition to temperature, the mechanical response also can be triggered by light in some cases, e.g. in LCEs rich in azo-type LC units [133].

Synthesis and properties of different LCE systems are widely discussed in the literature [1, 46, 132–139]. They are conveniently synthesized from selected functionalized mesogens and can be divided into three groups (*Scheme 9*), MC-LCEs, SC-LCEs, MC/SC-LCEs [108, 132, 136, 137, 139], similarly like liquid crystalline polymers in general. Attractive LCE products were described by Giamberini and coworkers, and are based on reactions between liquid crystalline diepoxides and dicarboxylic acids [68–71] or aromatic diamines [70].

The application potential of a given LCE product very strongly depends on the degree of long-range alignment of its mesogenic groups, which controls the extent of their mechanical response to stimuli. The orientation of mesogens in LCEs can be achieved in different ways: a sample which gradually cures and already achieved gelation, but which is still far before quantitative conversion, can be strongly stretched and subsequently cured until full conversion [140]. Another employed method was the photo-alignment of suitable LC units, which even made possible aligning them in different directions at different places in the sample during its cure [141].



Scheme 9. Possible structures of liquid crystalline elastomers.

1.3.3 Polydimethylsiloxane-LC copolymers

Polysiloxane copolymers with liquid crystalline (mesogenic) building blocks are compounds which can offer fascinating material properties due to the combination of the highly flexible and hydrophobic polysiloxane with the phase behaviour of the mesogenic (LC) units [142, 143]. The copolymers which were synthesized and studied in this Thesis also belong to this broader family. These materials attract deserved research interest since Finkelmann's pioneering works in the 1980s [144–148]. Since then, most of the studies were dedicated to liquid-crystalline siloxane polymers (LCPs) **with mesogens as side chains**, whereas **main-chain copolymers** were studied much less frequently (see e.g. [66, 67, 149, 150]). In 1991, Finkelmann prepared mono-domain-oriented nematic LCPs (with side-chain mesogens) via a two-step-crosslinking process [151]. A structural variation of the 'side-chain polysiloxane LCPs' are copolymers with side-on bonded pendant mesogens, i.e. via a linker in the central part of the rod-like LC, which leads to a different ordering behaviour [152]. Long pendant LC chains consisting of multiple mesogen units have also been attached to functionalized polydimethylsiloxane (PDMS), namely via ATRP grafting polymerization [153]. All **the above-discussed polysiloxane LCPs are very rich in the LC component** (typically one LC per siloxane repeat unit), which makes up a dominant volume fraction and the behaviour of the usually more or less fixed (via chemical crosslinking) mesogens is responsible for practically all the material properties. In contrast to that, **in the presented work, the mesogen makes up a relatively small volume fraction** of the copolymer. The elastic product properties originate from the PDMS component, while melting, solidification, sensitivity to strain damage, as well as self-healing are controlled by the phase behaviour of the mesogen.

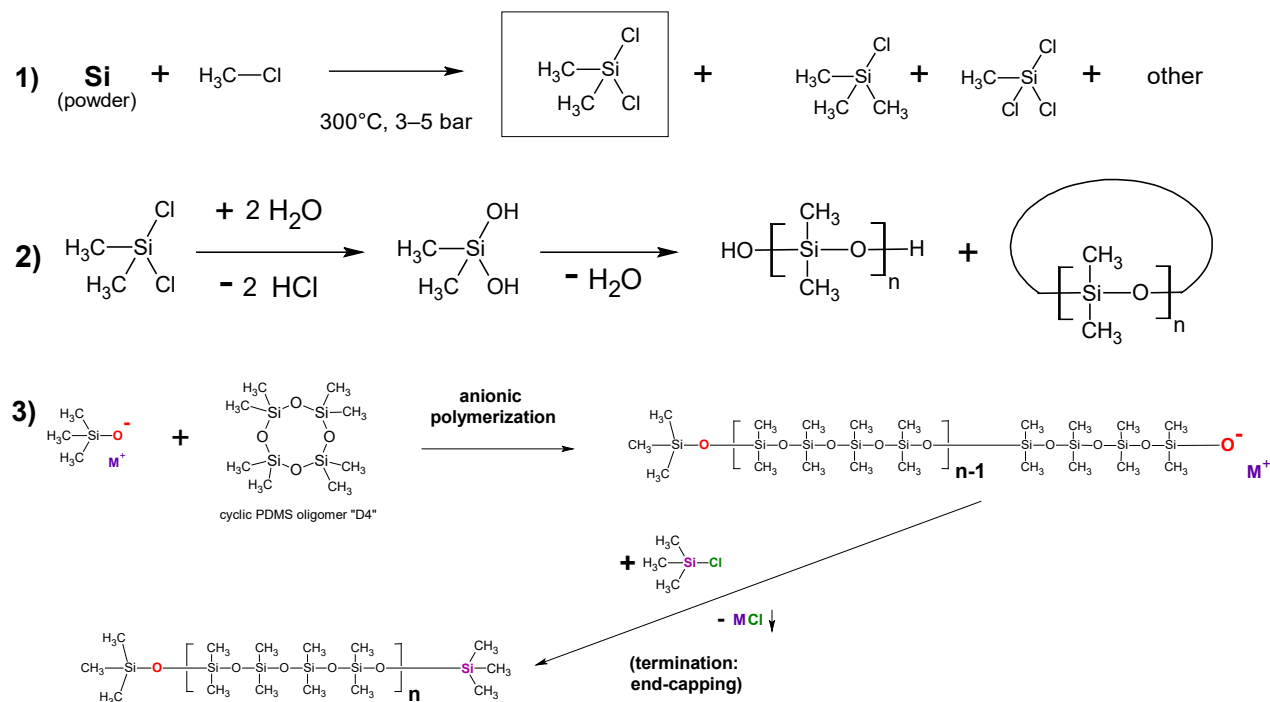
Polysiloxane LCPs are most frequently **synthesized** via hydrosilylation (as is the case in this work), namely by grafting vinyl-functional mesogens onto hydrido-functional (Si-H) PDMS. Alternative routes include the use of alkynyl-functional mesogens in the hydrosilylation reaction [154] leading to a more rigid link between PDMS and the mesogen, the thiol-ene addition using vinyl-functionalized PDMS and mesogenic thiol [34, 152, 168], or the azide-yne cycloaddition (Huisgen 'click reaction') [155, 166].

From the **application** point of view, the **polysiloxane LCPs** have been investigated as electro-optic- [156], as light-emitting- [157], gas-separation- (membrane-) [158, 159] and chromatography materials [160] as well as actuators (see e.g. [67, 161–163]). The latter, often referred-to as ‘liquid-crystalline elastomers’ (LCEs), gained by far the most research attention, especially in recent years. The mechanisms of stimulus response include UV-triggered *cis/trans* isomerization of azobenzene mesogens (e.g. [33, 152, 164–166]) or the nematic → isotropic transition of polyaromatic mesogens (*T*-triggering), e.g. [34, 67, 167, 168]). Other remarkable polysiloxane LCEs include electrostrictive [35], multiple-stimuli-responsive [168] or stimulus-converting systems [167] as well as actuators with programmable shape-memory [33]. In contrast to that, **in this work, the polysiloxane LCPs were studied as potential structural smart materials.**

1.3.4 The basic polydimethylsiloxane (PDMS) polymer and its derivatives

Polydimethylsiloxane (PDMS, see *Scheme 10 bottom*) played an important role as a component of the copolymers synthesized and studied in this Thesis. PDMS is an important commercial polymer, which is supplied either in the linear form as various silicone oils (including functional derivatives) or in the crosslinked form as silicone rubbers [169]. The popular silicone sealants are partly cured linear silicones with pendant reactive (crosslinking) groups. PDMS is characterized by a low glass transition temperature (T_g) of about -125°C , a unique flexibility and a high gas permeability. It is essentially non-toxic (orally, dermally or via inhalation) and biocompatible. PDMS also is optically clear, colourless and odourless. The polymer further displays a high thermal, UV and chemical resistance as well as non-flammable behavior. Due to its unique properties, PDMS has a wide range of industrial and domestic applications [170, 171]. Its world production is estimated to be ca. 150 000 tons per year [169]. Linear PDMS (oil) [171] is used in lubricants, shampoos, antifoaming agents and hydraulic fluids. Rubbery (crosslinked) PDMS [171] is used for producing tubes, cords, sealings and other elastic parts for the automotive industry, but also in electronics, textile manufacturing, as baking mould material, in medical devices, or contact lenses, etc. More recently, PDMS resins have been used in soft lithography [171], a key process in biomedical microelectromechanical systems (bio-MEMS). One of the greatest advantages of PDMS is its low cost, but on the other hand they have some limitations like hydrophobicity, easy contamination by bacteria, cells or some pollutants [170].

PDMS (*Scheme 10 bottom*) can be considered to be an organic-inorganic polymer, because its backbone $-\text{[Si-O]}_n-$ is purely inorganic, while the pendant methyl groups make up the organic part. In contrast to the rigid 3D network of silica, the 1D $-\text{[Si-O]}_n-$ chains are unusually flexible, which manifests itself as the above-mentioned very low T_g value.



Scheme 10. *Synthesis of PDMS: 1) Muller–Rochow reaction, 2) Hydrolysis of dimethyldichlorosilane, 3) Anionic polymerization of octamethyl-cyclotetrasiloxane (D4).*

The commercial synthesis path to PDMS is shown in **Scheme 10**: at first, dimethyldichlorosilane is obtained from elemental silicon and methyl chloride in the Muller–Rochow reaction. The purified dimethyldichlorosilane is subsequently hydrolysed to a mixture of linear and cyclic polydimethylsiloxanes. From this mixture, the cyclic dimethylsiloxane tetramer (“D4”) is obtained by distillation combined with cracking. Pure D4 is then finally polymerized via an anionic ring-opening polymerization to yield PDMS. Different functional derivatives can be obtained by employing special anionic initiator groups and end-capping groups (see **Scheme 10**, last stage) or / and by adding modified D4 monomer (e.g. with H-atoms or vinyl groups in place of four methyl groups) to the ‘normal D4’. Further derivatization is possible in follow-on reactions.

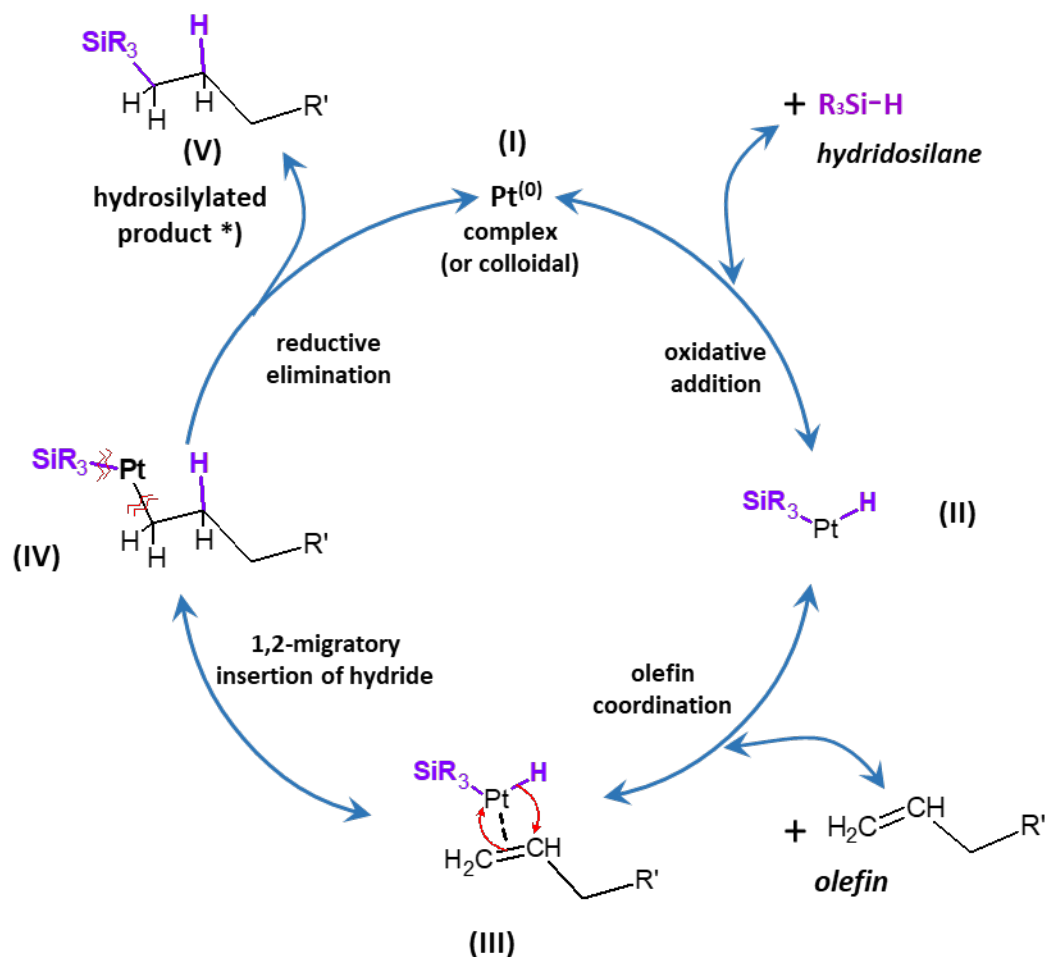
1.3.5 Hydrosilylation coupling

The hydrosilylation coupling [172] was typically employed in the literature in order to obtain the further-above-discussed PDMS-LC copolymers. It also played an important role in this work, as it was used to attach vinyl-functional LC building blocks to PDMS precursors of self-assembling copolymers.

This hydrosilylation reaction is well known as the addition of a Si-H group onto a C=C bond of olefins (and eventually onto acetylenes), catalysed by platinum compounds [172]. With a suitable choice of catalyst, however, Si-H also can be added onto carbonyl or imino groups [173]. The reaction also can be started by transition metal complexes or by Lewis acids as catalysts, but also by radical initiators and even by heat (radical dissociation of SiH) [172, 173].

The earliest transition metal catalyst was hexachloroplatinic acid, $\text{H}_2\text{PtCl}_6 \cdot 6\text{H}_2\text{O}/i\text{PrOH}$ [174, 172], commonly known as Speier catalyst in this specific function. This Pt(IV) compound undergoes reduction to Pt^0 upon contact with SiH. Karstedt's catalyst, Pt^0 complexed by divinyl-tetramethyl-disiloxane, is also very popular [172]. In any case, the zero-valent platinum species enters the catalytic cycle shown in *Scheme 11*, which proceeds according to the Chalk-Harrod mechanism [175]. The first step is an oxidative addition of hydridosilane onto platinum (0), which yields the hydrido-silyl complex (II). Thereafter, the hydrido-silyl complex is coordinated with the alkene, yielding the complex (III). The latter undergoes a 1,2-migratory insertion of the alkene into the Pt-H bond (hydrometallation), in order to give the alkyl-silyl species (IV). Finally, reductive elimination takes place and the hydrosilylated product is set free.

Besides Pt (0), electron-rich complexes of Ni (0) and Pd (0) [176], as well as of Rh (I) [177, 176], were found to be relatively prospective catalytic systems, but also Co (III) complexes [178, 176]. The platinum catalyst is well-suited for the hydridosilanes: $\text{HSiCl}_n\text{Me}_{3-n}$ ($n=1\sim 3$), $\text{HSi}(\text{OR})_3$ or $\text{H}_n\text{SiR}_{4-n}$ ($n=1\sim 3$, R=alkyl or phenyl), while palladium complexes can be used for $\text{HSiCl}_n\text{R}_{3-n}$ (where $n=2, 3$), and the rhodium catalyst prefers HSiR_3 [176].



Scheme 11. Chalk-Harrod mechanism for the hydrosilylation reaction of olefins; (*) it should be noted that as product (V), usually both the thinkable isomers are formed: in the depicted case with Si bonded to the primary or to the secondary C-atom of the vinyl group; sterical effects might favour one of the isomers.

1.4 Reversibly crosslinked polymers

Reversibly crosslinked polymers are an attractive material class, to which also the copolymers synthesized and studied in this Thesis belong: Achieving strong but reversible (by heat or by solvent) physical crosslinking in elastomeric PDMS-LC copolymers was one of the main aims of this Thesis.

As it was already mentioned further above, two principal classes of commercial polymers exist: thermosets and thermoplastics. A drawback of the thermosets is the lack of reprocessibility. From economical and environmental point of view, it is therefore interesting to develop

reversibly crosslinked polymers, which would combine the material properties of the polymer networks (thermosets: shape constancy, high elasticity) with the processibility and recyclability of the thermoplastics, i.e. which would be melt- or solution processible.

Reversible crosslinking in polymers can be achieved in several ways. Most studied is the reversible crosslinking by hydrogen bridges, which is considered to be a form of **physical crosslinking**. An example from the nature are the skleroproteins (polypeptides = polyamides) like keratin, which is comparable to classical thermosets, displays a very high density of crosslinking and is found in horn and nails. Besides hydrogen bridges, keratin also is reinforced by covalent disulfide bridges. The structurally related **synthetic polyamides** can be considered to be an industrial analogue of the skleroproteins. Inspired by the polyamides was the development of polyurethanes, including polyurethane elastomers (H-bridges between carbamate groups are the main or the only type of crosslink), in which very good elastic properties can be achieved, if suitable monomers and macro-monomers are chosen [179]. Also the comparatively weaker H-bridging between aliphatic hydroxyl groups can be very efficient in some cases, as found in the natural polysaccharide cellulose. A spectacular example of synthetic materials physically crosslinked by hydrogen bridges are the elastomers synthesized by Leibler et al. [180], in which the H-bridges are responsible for both lateral (crosslinking-), as well as for a part of the main-chain bonds and which display very efficient self-healing in addition to attractive elastic properties. This kind of structure is referred-to as **dynamer**, which highlights the reversible nature of the bonding in the polymer backbone.

Other well-studied **mechanisms of physical crosslinking** in polymers include π -stacking of pendant (crosslinker-) groups [181] or crosslinking by aggregation of ionic pendant groups [182, 183]. Crystallization or at least nano-phase-separation of polymer chain segments, for example of terminal polyethyleneoxide blocks in a triblock copolymer with polydimethylsiloxane [184] also can be regarded as physical crosslinking (if the central block is much larger than the terminal ones).

Reversible covalent crosslinking is another possibility, how to obtain processable, recyclable and self-healing networks. The name ‘covalent adaptable networks’ was coined for this kind of materials. The numerous chemical systems which display ‘dynamic bonding’ are discussed in several reviews, e.g. [185, 186]. The oldest known example are **disulphide bridges**

in rubbers: already in the 1940s, Tobolsky et al. noticed that these bridges break and re-connect, if vulcanized rubber is extruded [187] and named the effect ‘chemorheology’. Since then, disulphidic structural units were employed to prepare self-healing [188], photo-responsive (reversible fragmentation by light) [189] or redox-sensitive [190] dynamic networks.

A popular mechanism for obtaining reversible covalent crosslinking is the **Diels-Alder/retro-Diels-Alder reaction** (sterically weakened reversible carbon-carbon bonds) [191–194]. Another promising approach is the employment of **transesterification chemistry**, for example if epoxides are cured by carboxylic acids or by acid anhydrides [195]: this type of cure leads to the presence of ester moieties in the network structure, as well as of dangling alcohol hydroxyl groups. The latter can attack the ester moieties in exchange reactions, which in turn make possible the spatial rearrangement of the network. The ‘dynamics’ of the crosslinking starts at elevated temperatures and needs the presence of the original transesterification catalyst. At room temperature, such networks behave like classical thermosets. A very interesting example from this group is a structurally highly rigid epoxy network, which melts (via transesterification) in an analogous way like silica or window glass (where exchange reactions involve anionic silanolate units and SiO₄ tetraeders) and also shows a similar viscoelastic behaviour of the melt (Leibler et al. [196]). Such polymers are sometimes referred-to as vitrimers. Other in principle similar reaction types include **transimination** [197], or the long-known **polysiloxane/silanolate living system** [198], which can generate ‘adaptable crosslinking’ in rubbery polydimethylsiloxane. Finally, **addition–fragmentation chain transfer exchange reactions** (which also are part of the modern RAFT polymerization mechanism) can be employed as mechanism in reversible covalent networks [199].

Another variety of reversible crosslinking can be achieved by sufficiently weak **coordination bonds to transition metal cations** [200]. This mechanism can be considered as intermediate between the physical and the covalent reversible crosslinking.

1.4.1 Reversibly crosslinked PDMS

Related to the focus of this **Thesis** is the broader topic of **reversible crosslinking of PDMS**. Several interesting approaches were studied in the literature, mainly concerned with **physical (non-covalent) crosslinking**, which was achieved for example by the attachment of

hydrogen-bridging groups [201–204] or of π -stacking units [181, 205, 206]. Other physically crosslinked PDMS derivatives include such with grafted side chains consisting of long hydrocarbons with polar end-fragments [207] or A-B-A triblock copolymers with PDMS as central block [184, 208]. Combinations of Lewis-acidic and -basic functional substituents on PDMS [209] or of attached mildly bonding ligands and free metal cations [200] also were tested, as well as coordinative crosslinking by **borate** units [210, 211]. The latter systems already rather represent **PDMS networks with reversible covalent crosslinking**. More typical ‘covalent adaptive networks’ based on PDMS were obtained using the further-above mentioned trans-amination mechanism of adaptation of the network structure [212, 213].

In contrast to the different types of above mentioned so-called ‘thermoplastic elastomers’, the **PDMS copolymers studied in this Thesis** are **crosslinked by** a rather **mild** variety of **non-covalent interactions**: the aggregation of the ‘active’ structural units is driven by their crystallization tendency, with no hydrogen bridging, no strong π -stacking and no strong electrostatic attraction or reversible covalent bonds

2 Aims of the Thesis

This Thesis is dedicated to the synthesis and study of non-covalently and reversibly crosslinked elastomeric copolymers of polydimethylsiloxane (PDMS) with liquid crystalline (LC) nano-building blocks as physical crosslinking agent. The study had to fulfil several partial aims:

- The fundamental scientific aim was to evaluate the ability of single, ‘normal-sized’ mesogenic moieties to act as efficient physical crosslinkers in polymeric physical networks, where they would crosslink relatively long polymeric chains.

- Secondly, it had to be elucidated, how the thermotropic properties of the crosslinking agent will project themselves onto the material properties of the physically crosslinked copolymer.

To this end:

- Copolymers belonging to three different architecture types had to be synthesized:

(1) LC-grafted PDMS,

(2) LC-end-capped linear PDMS,

(3) and linear ‘infinite’ LC-PDMS copolymers (with alternating LC and PDMS segments).

- PDMS spacers of different lengths had to be tested, as well as calamitic polyaromatic mesogens of different size.

- The optimal product had to be a network with an extended temperature region of the rubbery state (‘rubbery plateau’), which could be reprocessed by melting or by dissolution.

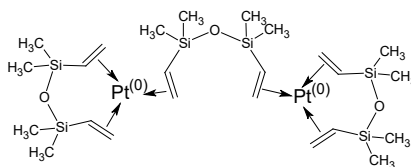
- Structure-property relationships had to be investigated, especially concerning the size and type of mesogen, the length of the PDMS polymer chain between the LC units and the copolymer architecture.

- Material properties like thermal, thermo-mechanical, tensile, and rheological had to be investigated, as well as the phase- and aggregation behaviour of the LC units.

3 Experimental part

3.1 Chemicals

‘Simple’ commercial chemicals: Chlorofom (solvent) was purchased from Sigma-Aldrich, St. Louis, MO, USA, while a 2% solution of the Karstedt’s catalyst in xylene (see *Scheme 12*) was purchased from Merck, Darmstadt, Germany. These chemicals were used as received.

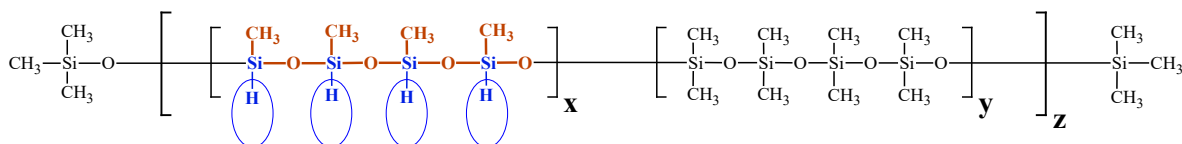


Scheme 12: Karstedt’s catalyst containing zero-valent platinum.

3.1.1 Commercial hydrido-functional PDMS precursors

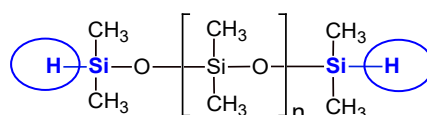
Two types of hydrido-functional PDMS (see *Scheme 13* and *14*) were used in this work: pendant-hydrido-functional (for obtaining grafted derivatives) and α,ω -SiH-terminated PDMS. All these PDMS precursors were purchased from Gelest, Morrisville, PA, USA. These chemicals were used as received, but their equivalent molecular masses per SiH function (*EqMW*) were analytically determined ($^1\text{H-NMR}$) prior to use.

As **SiH grafted PDMS** precursors, the “dimethylsiloxane-methylhydrosiloxane(25–35%) copolymer HMS 301” (supplier: $M_n = 1\,900\text{--}2\,100\text{ g/mol}$; analysis ($^1\text{H-NMR}$): *EqMW(per SiH): 248.700 g/mol*), and the “dimethylsiloxane-methylhydrosiloxane(4–8%) copolymer HMS 064” (supplier: $M_n = \text{ca. } 60\,000\text{--}65\,000\text{ g/mol}$; analysis ($^1\text{H-NMR}$): *EqMW(per SiH): 1\,320.558 g/mol*) were employed, see structures in *Scheme 13*.



Scheme 13: The structure of the used SiH-grafted PDMS precursors HMS301 and HMS064; in both cases the coefficient x was equal to 1.

As **α,ω -SiH-terminated PDMS** precursors, the “hydrido-terminated polydimethylsiloxanes”: “DMS H03” (supplier: $M_n = 400\text{--}500$ g/mol; analysis ($^1\text{H-NMR}$): $EqMW(per\ SiH): 311.9325$ g/mol), “DMS H11” (supplier: $M_n = 1\ 000\text{--}1\ 100$ g/mol; analysis ($^1\text{H-NMR}$): $EqMW(per\ SiH): 598.241$ g/mol), and “DMS H21” (supplier: $M_n = 4\ 000\text{--}5\ 000$ g/mol; analysis ($^1\text{H-NMR}$): $EqMW(per\ SiH): 2\ 382.2$ g/mol) were used for the synthesis of α,ω -LC end-capped PDMS, as well as for the synthesis of ‘infinite’ alternating copolymers of PDMS and linearly bonded LC units, see structures in **Scheme 14**.



Scheme 14: The structure of the used hydrido-terminated “DMS Hxx” PDMS precursors.

As mentioned above, the molecular masses given by the supplier were only approximate, so that the determination of precise equivalent molecular masses (= number average molecular mass / average number of SiH functions per molecule) was necessary, which was done by means of $^1\text{H-NMR}$ analysis, as described below.

3.1.1.1 Determination of precise equivalent molar mass per SiH function ($^1\text{H-NMR}$)

3.1.1.1.1 Molecular mass of PDMS with pendant SiH functions

The y , z : coefficients from the structure formula in **Scheme 13**, as well as the equivalent molecular weight per SiH function ($EqMW$), which is needed to calculate accurate reactant amounts for synthesis, were calculated as follows, using the $^1\text{H-NMR}$ spectra of the hydrido-PDMS:

Magnitudes for calculation:

y , z : coefficients from above structure formula

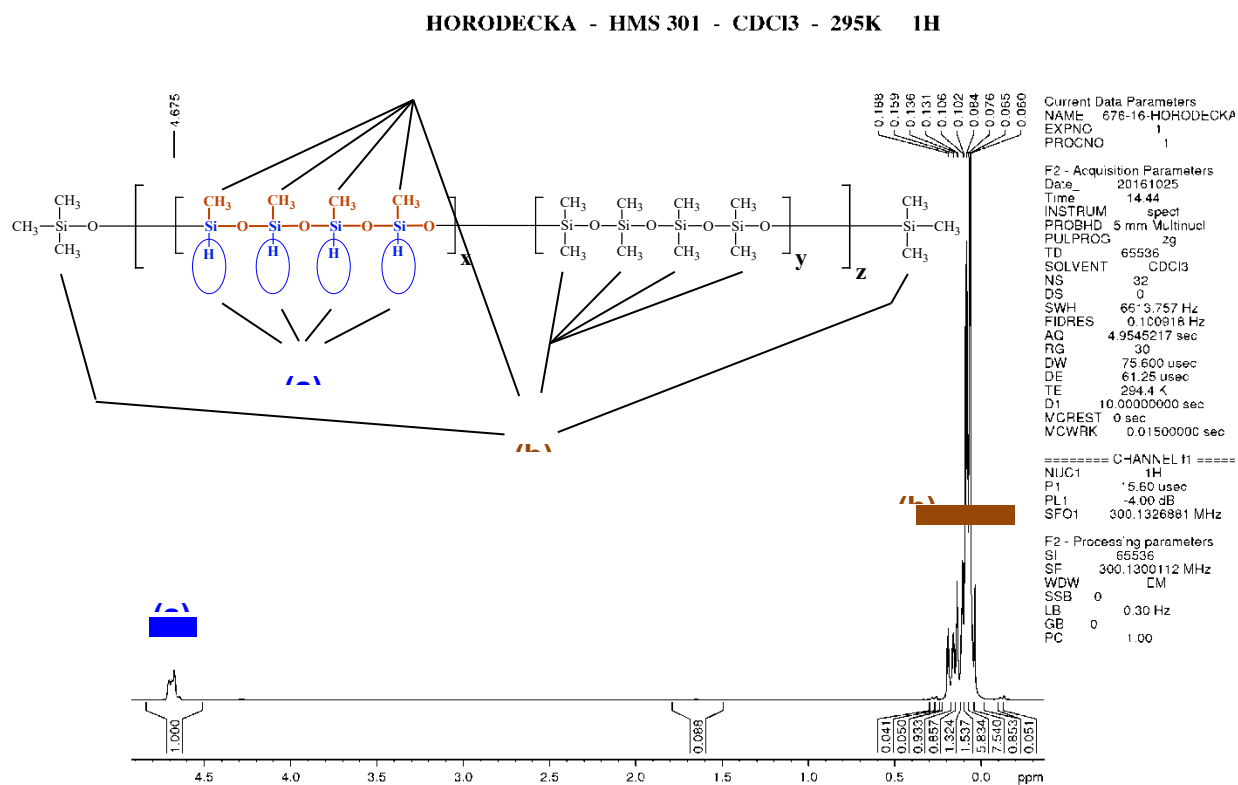
H \equiv molecular mass of the block $[\{(CH_3)(H)SiO\}_4] = 240.5094$ g/mol

D \equiv molecular mass of the block $[\{(CH_3)_2SiO\}_4] = 296.6158$ g/mol

$E \equiv$ molecular mass of both end groups $\equiv (\text{CH}_3)_3\text{Si-O-Si}(\text{CH}_3)_3 = 162.3775 \text{ g/mol}$

$M =$ molecular mass of the whole HMS molecule (as shown in above structure formula):
the value stated by the manufacturer was used

$R =$ apparent ratio of the number of 'normal' PDMS repeat units to the number of methyl-hydrido-functional repeat units, which does not take into account the trimethylsilyl end groups (it is similar but not equal to y , it comes close to y at high z values); its calculation from the $^1\text{H-NMR}$ spectra in **Figure 1** is described below:



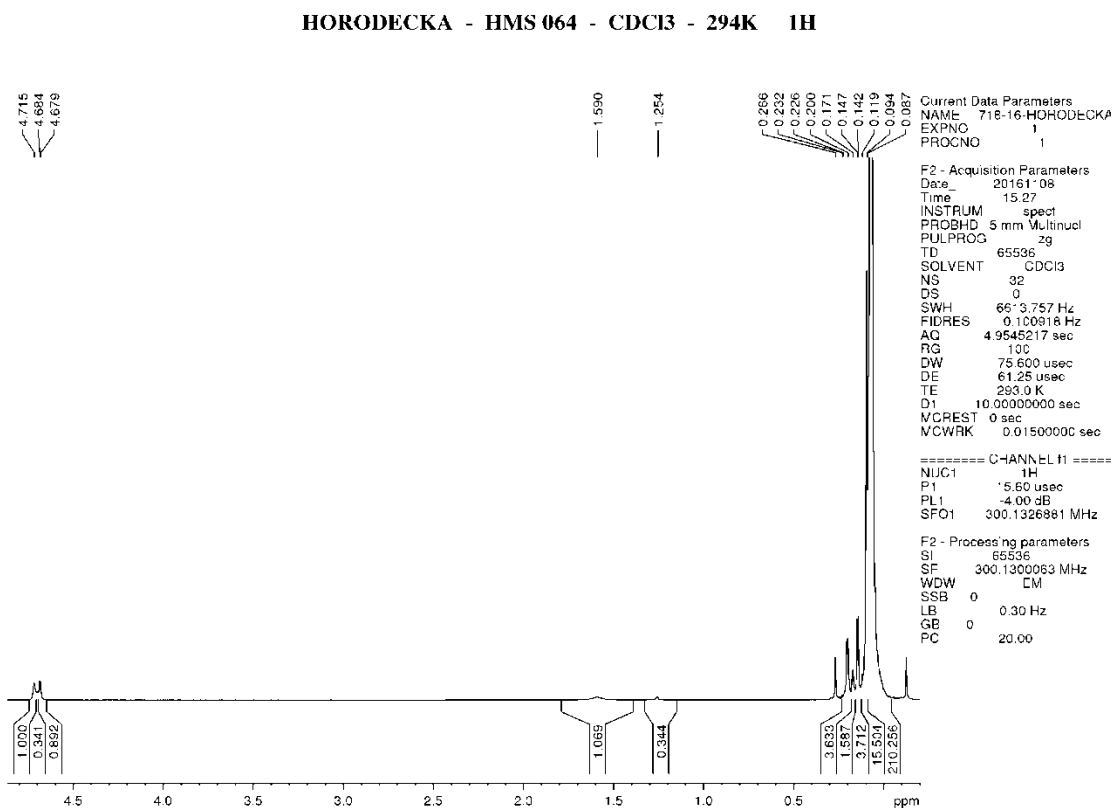


Figure 1: ^1H -NMR spectra of the SiH-grafted PDMS precursors: (top): HMS 301; (bottom): HMS 064; the peak of the methyl groups is near 0.06 ppm, the Si-H peak near 4.68 ppm.

Obtaining ratio R from the ^1H -NMR spectra in **Figure 1**:

at first, the integrals are normalized so, that the value of the integral of the SiH peak is equal to 1.00 (as done in **Figure 1 top**)

next, the sum of all integrals of the $\text{CH}_3(-\text{Si})$ peak group, ' CH_3_norm ' is calculated

as every SiH repeat unit also contains one methyl group (see structure), the corresponding intensity (threefold of SiH integral, normalized to 1.00) has to be subtracted from CH_3_norm in order to obtain the integral of normal PDMS units (including the trimethylsilyl end groups, which cannot be resolved):

$$\text{CH}_3_PDMS_norm = \text{CH}_3_norm - 3.00$$

in order to use the integrals $CH3_PDMS_norm$ and $CH3_from_SiH_norm$ for the calculation of the ratio of the repeat units, it has to be taken into account that the ‘normal’ units have the double number of methyl groups than the hydrido-functional ones

hence:

$$R = CH3_PDMS_norm / CH3_from_SiH_norm$$

$$R = \{(CH3_norm - 3) / 2\} / (3 * SiH_norm)$$

$$R = \{(CH3_norm - 3) / 2\} / 3$$

$$R = (CH3_norm - 3) / 6$$

in this way, the apparent (inaccurate) ratio **R** of PDMS to SiH repeat units is obtained from the ¹H-NMR-spectra in **Figure 1** (this R does not take into account the end groups)

the experimentally determined **R** values for HMS-301 and HMS-064 are listed in **Table 1**.

¹H-NMR signal integrals and the precise structure of the precursor polymers:

If the further-above-depicted structure of the precursor (HMS) polymers is taken into account, the following relations concerning the numbers of protons (H) and hence also integral values can be stated:

SiH (in hydrido-quartets)	CH ₃ (in hydrido-quartets)	(CH ₃) ₂ (in ‘normal’ quartets of PDMS units)	((CH ₃) ₃) ₂ (in end groups)
$z * 1 * 4 * H1$	$z * 1 * 4 * H3$	$z * y * 4 * H6$	$2 * 3 * H3$
$4z$	$4z * 3$	$4z * y * 6$	18
SiH integral normalized to 1.0 => division of all values by $4z$			
1	3	$y * 6$	$18 / 4z = 4.5 / z$

The ¹H-NMR peaks of the above listed structural units occur in two groups which were used for determining the above-discussed apparent ratio R of the both types of repeat units; their integral ratios then are:

Peak group	SiH peak	all CH ₃ -Si peaks
Integral value	1	3 + y*6 + 4.5/z

if the experimentally determined ratio **R** is expressed using the structural coefficients **y** and **z** , we obtain:

$$R = \{(6*y + 4.5/z)/2\}/3 = (6*y + 4.5/z)/6$$

$$R = y + 0.75/z$$

a second equation is needed for determining **y** and **z**

the relation describing the known molecular mass of the polymer can serve this purpose:

$$M = E + (H*1 + D*y)*z$$

Determining y and z:

The set of equations

$$1) M = E + (H*1 + D*y)*z$$

$$2) R = y + 0.75/z$$

yields the solution for **y** and **z** :

$$y = (R*M - R*E - 0.75*H) / (0.75*D + M - E)$$

$$z = 0.75/(R - y)$$

using the structural coefficients **y** and **z** , other molecular parameters, like the average number of functional groups per molecule, the equivalent molecular weight per SiH functional group and other, can be calculated and are listed in **Table 1**.

Final results:**Table 1:** Molecular parameters of the HMS precursor polymers determined by $^1\text{H-NMR}$.

precursor polymer name	M_n ‡ (supplier) [g/mol]	R from NMR	y^*	z^*	number of all repeat units (= number of Si atoms)*	functionality (number of SiH groups)	EqMW [g/mol]
HMS-301	1 950	2.646	2.264	1.960	27.59	7.841	248.70 0
HMS-064	55 000	17.01 7	16.94 5	10.41 2	749.389	41.65	1320.5 58

‡) It should be noted, that the molecular mass of the “HMS xxx” hydridosilanes could not be determined by $^1\text{H-NMR}$, because the difference in chemical shifts of the trimethylsilyl end caps and of the ‘central’ dimethylsilyl units was negligible. The *EqMW* (per SiH) which depends on the ratio of hydrido-functional to ‘normal’ (dimethyl-type) siloxane repeat units, is not sensitive to the molecular mass of the whole macromolecule, except in case of very short macromolecules (where the fraction of end caps is significant). As molecular masses of the “HMS xxx” precursors, the average values stated by the supplier were used for calculating the stoichiometric coefficients from *Scheme 13*, as well as the numbers of SiH functions per molecule.

*) the average length of elastic spacers between the functional (‘grafting’) SiH quartets is equal to $4y$ according to the structure in *Scheme 13*, and is equal to **9.05** repeat units for **HMS-301** and to **67.8** repeat units for **HMS-064** (real spacer lengths in real molecule segments always must be divisible by 4, due to above structure).

3.1.1.1.2 Molecular mass of α,ω -SiH-terminated PDMS

The number of internal repeat units (n) from the structure formula in *Scheme 14*, as well as the equivalent molecular weight per SiH function (*EqMW*), which is needed to calculate accurate reactant amounts for synthesis, was calculated as follows, using the $^1\text{H-NMR}$ spectra of the hydrido-PDMS:

Ratios of signal integrals from the ^1H -NMR spectra (*Figure 2* and *3*) in relation to the above structure formula:

H in SiH end groups	H in CH₃ groups in all siloxane repeat units
2	$(2*3)*n$
if the SiH integral is normalized to 1.0, the following integral ratios are obtained:	
1	$3*n$

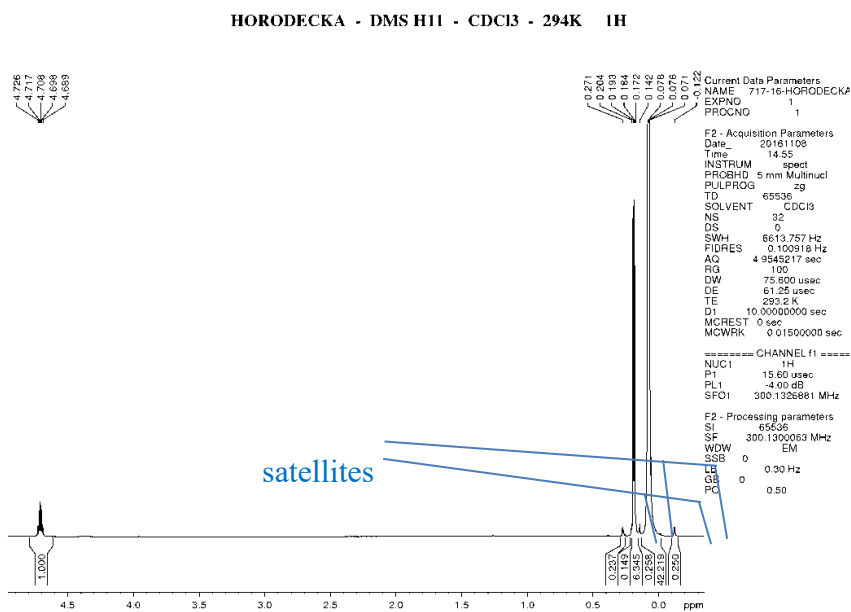
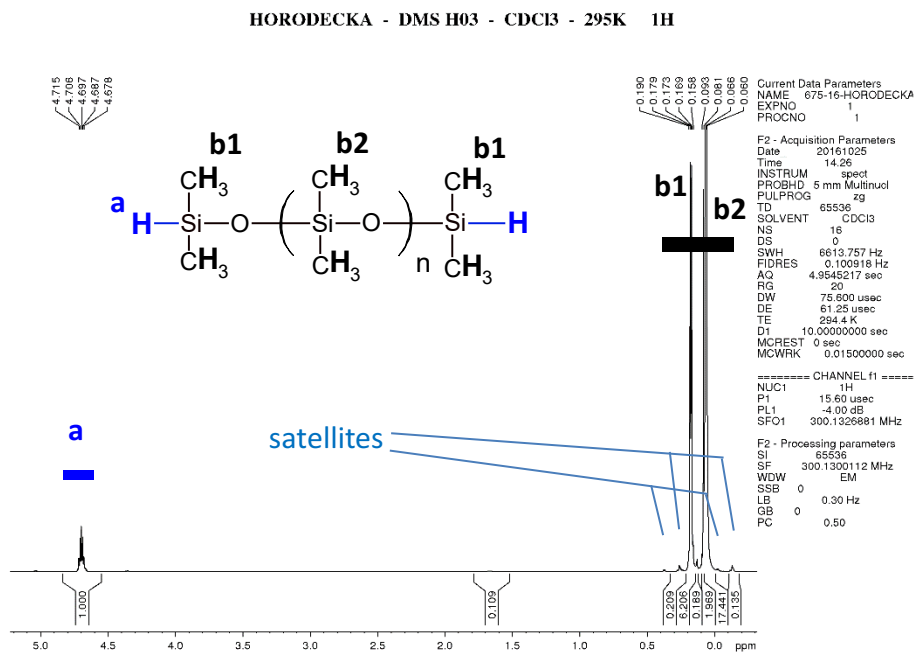


Figure 2: ¹H-NMR spectra of the hydrido-terminated “DMS Hxx” PDMS precursors: (top): H03; (bottom): H11; the peak of the methyl groups is near 0.1 ppm, the Si-H peak near 4.70 ppm.

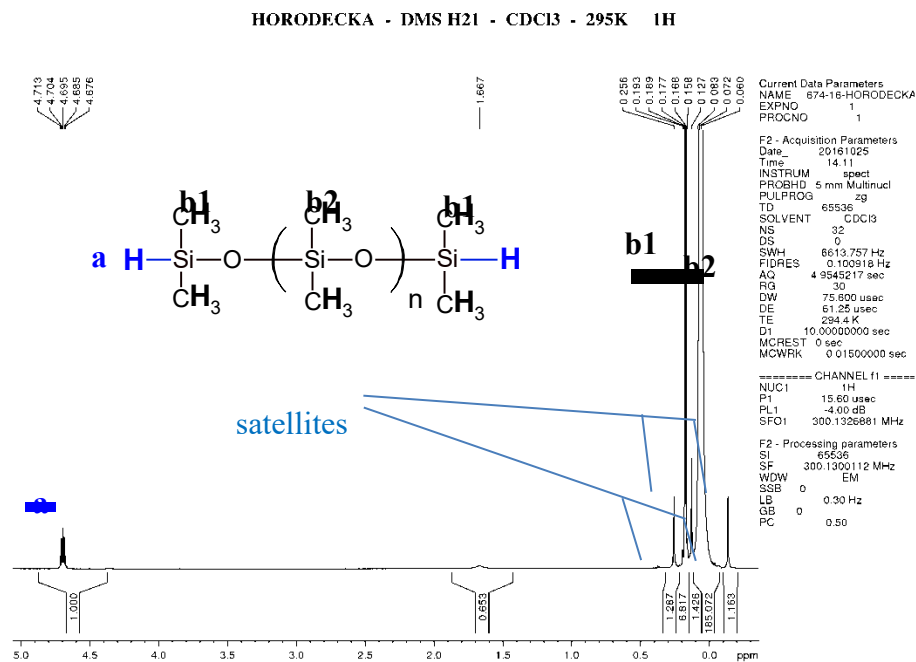


Figure 3: ^1H -NMR spectrum of the hydrido-terminated “DMS Hxx” PDMS precursor H21; the peak of the methyl groups is near 0.1 ppm, the Si-H peak near 4.70 ppm.

Magnitudes for calculation:

n: coefficient from above structure formula (number of internal repeat units)

m = n + 2 : number of all siloxane repeat units

RU = molecular mass of an internal repeat unit (of the block $[(\text{CH}_3)_2\text{SiO}]$)

$$= 74.154 \text{ g/mol}$$

E = molecular mass of both end groups taken together, hence of $(\text{CH}_3)_2(\text{H})\text{Si}-\text{O}-\text{Si}(\text{H})(\text{CH}_3)_2$

$$= 134.325 \text{ g/mol}$$

M = molecular mass of the whole “DMS” molecule (as shown in the above structure formula)

Obtaining n from the ^1H -NMR spectra in **Figure 2** and **3**:

-at first, the integrals in the spectra are normalized so, that the value of the integral of the SiH peak is equal to 1.00 (as done in **Figure 2** and **3**); it is then assigned 1 = ‘SiH_norm’; each molecule contains two hydrogens from SiH groups;

-next, the sum of all integrals of the peaks of $(\text{CH}_3)_2\text{Si}<$ groups, ‘CH3’ is calculated; each siloxane repeat unit in the DMS molecule contains 6 hydrogens from two methyl groups; as result of the above normalization of the SiH signal, an integral value of 3 corresponds to one siloxane repeat unit; the normalized value ‘CH3_norm’ is calculated by dividing ‘CH3’ by three;

-finally, the coefficients **m** (number of all Si-containing units) and **n** (number of internal siloxane units) are calculated, using ‘CH3_norm’ and ‘SiH_norm’:

$$m = \text{CH3_norm} / \text{SiH_norm} = \text{CH3_norm} / 1 = \text{CH3_norm} = \text{‘CH3’} / 3$$

hence $m = \text{‘CH3’} / 3$

and $n = m - 2$

$M = E + n \cdot \text{RU}$ (with molecular masses of the constants E, RU taken from above)

$\text{EqMW} = M/2$

Final Results:

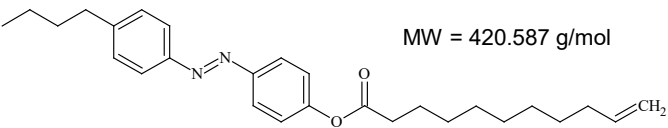
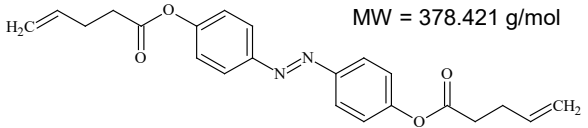
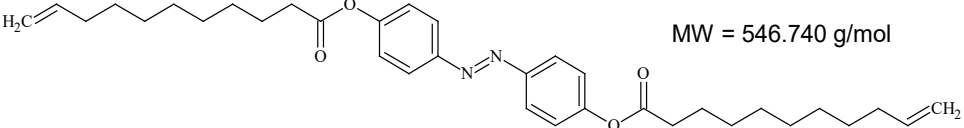
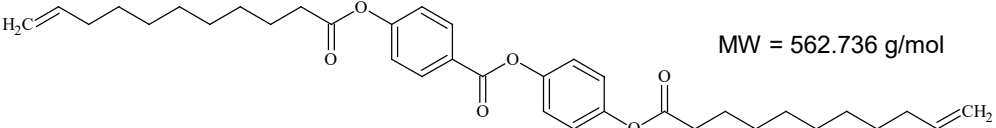
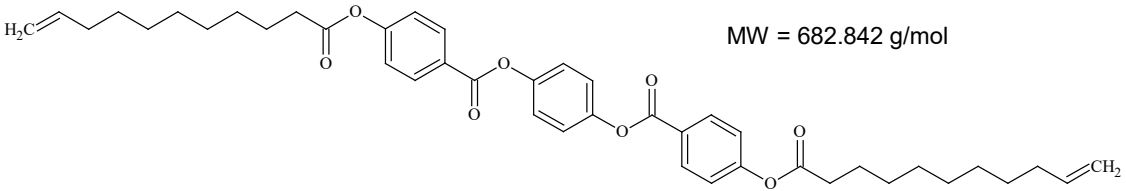
Table 2: Molecular parameters of the PDMS precursor polymers as determined by ¹H-NMR, compared with the data given by the manufacturer (last two columns, italics).

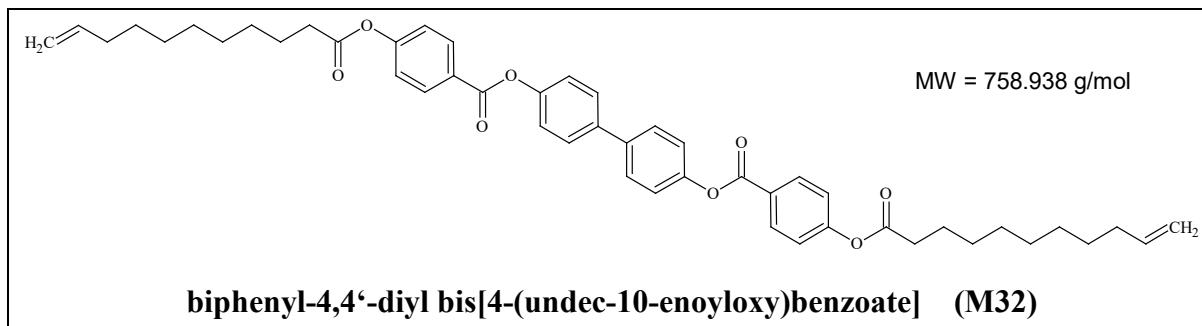
name of siloxane precursor	‘CH ₃ ’ from NMR	<i>m</i> (number of all repeat units) from NMR	<i>n</i> (number of internal repeat units) from NMR	<i>M_n</i> (= ‘M’) from NMR [g/mol]	EqMW = <i>M_n</i> /2 [g/mol]	<i>M_n</i> (supplier) [g/mol]	<i>m</i> (supplier, calculated)
H03	25.805	8.602	6.602	623.865	311.9325	<i>450±50</i>	<i>6.257</i>
H11	48.971	16.324	14.324	1196.482	598.241	<i>1 050±50</i>	<i>14.348</i>
H21	193.315	64.438	62.438	4764.377	2382.189	<i>4 500±500</i>	<i>60.873</i>

3.1.2 Vinyl-functional mesogens (LC-units)

Vinyl-functional mesogens, which are shown in **Table 3** were employed as the liquid-crystalline component in the copolymers studied in this work.

Table 3. Collection of the LC mesogens, which were used to the synthesis with their structure, name and temperature of phase transitions.

Structure, name and temperature of LC transitions of mesogens	
 <p>MW = 420.587 g/mol</p>	4-[(4-butylphenyl)diazenyl]phenyl undec-10-enoate (BAFKU)
 <p>MW = 378.421 g/mol</p>	azobenzene-4,4'-diyl bis(pent-4-enoate) (A1)
 <p>MW = 546.740 g/mol</p>	azobenzene-4,4'-diyl bis(undec-10-enoate) (A12)
 <p>MW = 562.736 g/mol</p>	4-(undec-10-enoxy)phenyl 4-(undec-10-enoxy)benzoate (M12)
 <p>MW = 682.842 g/mol</p>	p-phenylene bis[4-(undec-10-enoxy)benzoate] (M22)



The mesogens were attached via hydrosilylation coupling to the above-described commercial hydrido-functional PDMS precursors. The mesogens were obtained from the Rzeszow University of Technology (RUT), as part of international scientific cooperation. The mesogen “BAFKU” from *Table 3* was synthesized at RUT according to [214], “A1” and “A12” according to [215], and “M12”, “M22”, as well as “M32” according to [216].

3.2 Syntheses

3.2.1 Synthesis of PDMS copolymers with pendant “BAFKU” LC groups

Appropriate quantities of PDMS of HMS-type and of the BAFKU mesogen (see *Table 4*) were placed into a small vessel equipped with a magnetic stirring bar. 2 mL of chloroform were added and after flushing the reactants with argon, they were dissolved by brief stirring at 60°C. Subsequently, Karstedt's catalyst (8.7 mg of a 2 wt% solution \equiv 0.0228 mmol Pt) was added and the solution was stirred at 60°C for 5 min. Thereafter, the reaction mixture was cooled down to room temperature and the solvent was removed under reduced pressure. The BAFKU₈–HMS 301 product was free of side-products, but the BAFKU₄₁–HMS 064 copolymer contained a crosslinked fraction, which prevented the melting or full dissolution of the raw product. Hence, the raw BAFKU₄₁–HMS064 obtained after solvent removal was further purified by dissolving it in tetrahydrofuran, filtering through a syringe filled with 1 cm of cotton wool, after which the solvent was evaporated again. Finally, both solvent-free copolymers were further dried under vacuum (10 mbar) for 30 min at 90°C (molten state). Thereafter, they were cooled to room temperature and stored.

Yield: BAFKU₈–HMS 301: 0.783 g (1.17 mmol) \equiv 100% of theory.

BAFKU₄₁–HMS 064: 1.082g (0.622 mmol) \equiv 53.1% of theory.

Table 4: Amounts of the components used in the synthesis of the copolymers based on PDMS grafted with BAFKU.

Component		Sample name	
		BAFKU ₈ - HMS301	BAFKU ₄₁ - HMS064
BAFKU	[g]	0.492	0.492
	[mmol] *	1.17	1.17
	wt%	61.9	24.14
	Vol% ‡	60.26	22.72
HMS301	[g]	0.291	-
	[mmol] *	1.17	-
	wt%	38.1	-
	Vol% ‡	39.74	-
HMS064	[g]	-	1.545
	[mmol] *	-	1.17
	wt%	-	75.86
	Vol% ‡	-	77.28
CHCl₃	[g]	2.978	2.978
Karstedt's catalyst as 2 wt.% solution	[g]	0.0087	0.0087
	[mmol]	0.0228	0.0228

* as mmol of respective functional groups (not whole molecules).

‡ The volume fractions of the aggregation-able mesogen BAFKU were calculated using the below **Equation** under consideration of the densities ($\rho_{(\text{BAFKU})} = 1.05 \text{ g/cm}^3$, $\rho_{(\text{HMS301})} = 0.98 \text{ g/cm}^3$, and $\rho_{(\text{HMS064})} = 0.97 \text{ g/cm}^3$) and of the stoichiometric synthesis amounts (see above **Table 5**) of the individual components.

$$\text{volume percent (Vol\%)} = \frac{m(\text{component})/\rho(\text{component})}{\sum \left(\frac{m(i)}{\rho(i)}\right)} * 100\%$$

Characterization by ¹H-NMR (CDCl₃), δ (ppm):

(BAFKU)₈-HMS 301: 7.95 (16H, d, arom.), 7.84 (16H, d, arom.), 7.30 (16H, d, arom.), 7.21 (16H, d, arom.), 2.55 (16H, m, CH₂), 1.7 (48H, m, CH₂), 1.28 (144H, m, CH₂), 0.96 (24H, m, CH₃), 0.07 (144H, m, CH₃).

(BAFKU)₄₅-HMS 064: 8.15 (90H, d, arom.), 7.85 (90H, d, arom.), 7.4 (90H, d, arom.), 7.32 (90H, d, arom.), 2.73 (90H, m, CH₂), 2.65 (135H, m, CH₂), 2.08 (270H, m, CH₃), 1.25 (810H, m, CH₃), 0.1 (3963H, m, CH₃).

for comparison:

neat BAFKU: 7.90 (2H, d, arom.), 7.82 (2H, d, arom.), 7.31 (2H, d, arom.), 7.22 (2H, d, arom.), 5.79 (1H, m, CH), 4.94 (2H, m, CH₂), 2.59 (2H, m, CH₂), 2.56 (2H, m, CH₂), 2.03 (2H, m, CH₂), 1.65 (2H, m, CH₂), 1.60 (2H, m, CH₂), 1.31 (12H, m, CH₂), 0.92 (3H, m, CH₃).

neat HMS 301: 4.68 (8H, Si-H), 0.1 (42H, m, CH₃), 0.07 (120H, m, CH₃).

neat HMS 064: 4.72 (45H, Si-H), 0.01 (153H, m, CH₃), 0.07 (4590H, m, CH₃).

Check of quantitative coupling reaction:

FTIR (Fourier-transform infrared spectroscopy): Complete disappearance of the peak of the Si-H bond stretching at about 2120 cm⁻¹ (see *SI-Fig. 1 – 3 / Appendix 1*).

NMR (Nuclear magnetic resonance spectroscopy): Complete disappearance of the peaks near 4.68 ppm (Si-H) and of the multiplets near 5.79 and 4.94 ppm (vinyl groups of BAFKU) see *SI-Fig. 1 and 6 / Appendix 1*.

3.2.2 Synthesis of polydimethylsiloxane α,ω -terminated (end-capped) with “BAFKU” LC units

Appropriate quantities of the BAFKU mesogen and of PDMS (see *Table 5*) were placed into a small vessel equipped with a magnetic stirring bar. 2 mL of chloroform were added and after flushing the reactants with argon, they were dissolved by brief stirring at 60°C. Subsequently, Karstedt's catalyst (8.7 mg of a 2 wt.% solution \equiv 0.0228 mmol Pt) was added and the solution was stirred at 60°C for 5 min. Thereafter, the reaction mixture was cooled down to room temperature and the solvent was removed under reduced pressure. The so-obtained copolymer was further dried under vacuum (10 mbar) for 30 min at 90°C (molten state). The product was then cooled-down to room temperature and stored. The trace amounts of the Karstedt's catalyst (between 0.008 and 0.02 wt.%) were tolerated as non-problematic impurity in case of standard syntheses (it was possible to remove them by adsorption on silica or on activated carbon at the cost of reduced yield).

Yield:

H03–BAFKU₂: 0.8715 g (1.19 mmol) \equiv 100% of theory (one-pot synthesis).

H11–BAFKU₂: 1.2069 g (1.19 mmol) \equiv 100% of theory (one-pot synthesis).

H21–BAFKU₂: 3.311 g (1.19 mmol) \equiv 100% of theory (one-pot synthesis).

Table 5. Amounts of the components used in the synthesis of polydimethylsiloxane α,ω -terminated (end-capped) with “BAFKU” LC units.

Component		Sample name		
		H03– BAFKU ₂	H11– BAFKU ₂	H21– BAFKU ₂
BAFKU	[g]	0.5	0.5	0.5
	[mmol] *	1.19	1.19	1.19
	wt%	57.4	41.43	15.1
	Vol% ‡	52.4	37.3	13.5
H03	[g]	0.371	-	-
	[mmol] *	1.19	-	-
	wt%	42.6	-	-
	Vol% ‡	47.6	-	-
H11	[g]	-	0.711	-
	[mmol] *	-	1.19	-
	wt%	-	58.57	-
	Vol% ‡	-	62.7	-
H21	[g]	-	-	2.832
	[mmol] *	-	-	1.19
	wt%	-	-	84.9
	Vol% ‡	-	-	86.5
CHCl₃	[g]	2.956	2.956	2.956
Karstedt's catalyst	[g]	0.0087	0.0087	0.0087
	[mmol]	0.0228	0.0228	0.0228

* as mmol of respective functional groups (not whole molecules).

‡ The volume fractions of the aggregation-able mesogen BAFKU were calculated using the below *Equation* under consideration of the densities ($\rho_{(\text{BAFKU})} = 1.05 \text{ g/cm}^3$, $\rho_{(\text{H03})} = 0.90 \text{ g/cm}^3$, $\rho_{(\text{H11})} = 0.93 \text{ g/cm}^3$ and $\rho_{(\text{H21})} = 0.97 \text{ g/cm}^3$) and of the stoichiometric synthesis amounts (see above *Table 5*) of the individual components.

$$\text{volume percent (Vol\%)} = \frac{m(\text{component})/\rho(\text{component})}{\sum \left(\frac{m(i)}{\rho(i)} \right)} * 100\%$$

Characterization by ¹H-NMR, in CDCl₃, δ (ppm) (see also spectra in *SI-Fig. 7–8 / Appendix 2*):

H03–BAFKU₂: 7.94 (4H, d, arom.), 7.84 (4H, d, arom.), 7.33 (4H, d, arom.), 7.26 (4H, d, arom.), 2.69 (4H, m, CH₂), 2.58 (4H, m, CH₂), 1.75 (4H, m, CH₂), 1.65 (4H, m, CH₂), 1.55 (s, H₂O: moisture in CDCl₃), 1.29 (32H, m, CH₂), 0.94 (6H, m, CH₃), 0.53 (4H, m, CH₂), 0.06 (52H, m, CH₃).

H11–BAFKU₂: 7.92 (4H, d, arom.), 7.82 (4H, d, arom.), 7.30 (4H, d, arom.), 7.22 (4H, d, arom.), 2.69 (4H, m, CH₂), 2.58 (4H, m, CH₂), 1.77 (4H, m, CH₂), 1.63 (4H, m, CH₂), 1.29 (32H, m, CH₂), 0.91 (6H, m, CH₃), 0.53 (4H, m, CH₂), 0.07 (96H, m, CH₃).

H21–BAFKU₂: 7.92 (4H, d, arom.), 7.84 (4H, d, arom.), 7.33 (4H, d, arom.), 7.24 (4H, d, arom.), 2.69 (4H, m, CH₂), 2.58 (4H, m, CH₂), 1.65 (4H, m, CH₂), 1.55 (4H, m, CH₂), 1.29 (32H, m, CH₂), 0.94 (6H, m, CH₃), 0.52 (4H, m, CH₂), 0.06 (392H, m, CH₃).

for comparison (see also spectra in *SI-Fig. 4–6 / Appendix 2*):

neat BAFKU: 7.90 (2H, d, arom.), 7.82 (2H, d, arom.), 7.31 (2H, d, arom.), 7.22 (2H, d, arom.), 5.79 (1H, m, CH), 4.94 (2H, m, CH₂), 2.59 (2H, m, CH₂), 2.56 (2H, m, CH₂), 2.03 (2H, m, CH₂), 1.65 (2H, m, CH₂), 1.60 (2H, m, CH₂), 1.31 (12H, m, CH₂), 0.92 (3H, m, CH₃).

neat DMS H03: 4.70 (2H, m, SiH), 0.18 (12H, m, CH₃), 0.06 (40H, m, CH₃).

neat DMS H11: 4.71 (2H, m, SiH), 0.17 (12H, m, CH₃), 0.08 (84H, m, CH₃).

neat DMS H21: 4.69 (2H, m, SiH), 0.13 (12H, m, CH₃), 0.06 (380H, m, CH₃).

Check of quantitative conversion:

FTIR Complete disappearance of the peak of the Si–H bond stretching at about 2120 cm⁻¹ (see *SI-Fig. 1–3 / Appendix 2*).

¹H-NMR: Complete disappearance of the peaks near 4.7 ppm (Si-H) and of the multiplets near 5.79 and 4.94 ppm (vinyl groups of LC mesogen), see spectra in *SI-Fig. 7–8 / Appendix 2*.

3.2.3 Synthesis of ‘infinite’ alternating copolymers of PDMS and linearly bonded LC units of azo-type (“A1”, “A12”)

Appropriate quantities of LC mesogens and of PDMS (see *Table 6* and *7*) were placed into a small vessel equipped with a magnetic stirring bar. 2 mL of toluene were added and after flushing the reactants with argon, they were dissolved by brief stirring at 60°C. Subsequently, Karstedt’s catalyst (8.7 mg of a 2 wt% solution \equiv 0.02 mmol Pt) was added and the solution was stirred at 60°C for 5 min. Thereafter, the reaction mixture was cooled down to room temperature and the solvent was removed under reduced pressure. In some mixtures, side reactions occurred to a varying degree, which led to the formation of a crosslinked fraction. For this reason, all the raw products were further purified by dissolution in toluene and filtration through a syringe filled with 1 cm of cotton wool, after which the solvent was evaporated again, and the products dried under vacuum at 80°C. The products were then cooled-down to room temperature and stored. The trace amounts of the Karstedt’s catalyst were tolerated as non-problematic impurity in case of standard syntheses (it was possible to remove them by adsorption on silica or on activated carbon at the cost of reduced yield).

Table 6. Amounts of the components used in the synthesis of ‘infinite’ alternating copolymers of PDMS and linearly bonded LC units of azo type “A1”.

Component		Sample name		
		A1-H03	A1-H11	A1-H21
A1	[g]	0.5	0.5	0.5
	[mmol] *	2.64	2.64	2.64
	wt%	37.72	24.14	7.41
	Vol% ‡	34.17	21.99	6.88
H03	[g]	0.8257	-	-
	[mmol] *	2.64	-	-
	wt%	62.28	-	-
	Vol% ‡	65.83	-	-
H11	[g]	-	1.5712	-
	[mmol] *	-	2.64	-
	wt%	-	75.9	-
	Vol% ‡	-	78.01	-
H21	[g]	-	-	6.249
	[mmol] *	-	-	2.64
	wt%	-	-	92.59
	Vol% ‡	-	-	93.12
Toluene	[g]	1.734	1.734	1.734
Karstedt's catalyst	[g]	0.0087	0.0087	0.0087
	[mmol]	0.02	0.02	0.02

* as mmol of respective functional groups (not whole molecules).

‡ The volume fractions of the aggregation-able mesogen A1 were calculated using the below *Equation* under consideration of the densities ($\rho_{(A1)} = 1.05 \text{ g/cm}^3$, $\rho_{(H03)} = 0.90 \text{ g/cm}^3$, $\rho_{(H11)} = 0.93 \text{ g/cm}^3$ and $\rho_{(H21)} = 0.97 \text{ g/cm}^3$) and of the stoichiometric synthesis amounts (see above *Table 5*) of the individual components.

$$\text{volume percent (Vol\%)} = \frac{m(\text{component})/\rho(\text{component})}{\sum \left(\frac{m(i)}{\rho(i)}\right)} * 100\%$$

Table 7. Amounts of the components used in the synthesis of ‘infinite’ alternating copolymers of PDMS and linearly bonded LC units of azo type “A1”.

Component		Sample name		
		A12- H03	A12-H11	A12- H21
A12	[g]	0.5	0.5	0.5
	[mmol] *	1.83	1.83	1.83
	wt%	46.66	31.5	10.18
	Vol% ‡	42.85	28.94	9.47
H03	[g]	0.5715	-	-
	[mmol] *	1.83	-	-
	wt%	53.54	-	-
	Vol% ‡	57.15	-	-
H11	[g]	-	1.0875	-
	[mmol] *	-	1.83	-
	wt%	-	68.5	-
	Vol% ‡	-	71.06	-
H21	[g]	-	-	4.413
	[mmol] *	-	-	1.83
	wt%	-	-	89.82
	Vol% ‡	-	-	90.53
Toluene	[g]	1.734	1.734	1.734
Karstedt's catalyst	[g]	0.0087	0.0087	0.0087
	[mmol]	0.02	0.02	0.02

* as mmol of respective functional groups (not whole molecules).

‡ The volume fractions of the aggregation-able mesogen A12 were calculated using the below *Equation* under consideration of the densities ($\rho_{(A12)} = 1.05 \text{ g/cm}^3$, $\rho_{(H03)} = 0.90 \text{ g/cm}^3$, $\rho_{(H11)} = 0.93 \text{ g/cm}^3$ and $\rho_{(H21)} = 0.97 \text{ g/cm}^3$) and of the stoichiometric synthesis amounts (see above *Table 5*) of the individual components.

$$\text{volume percent (Vol\%)} = \frac{m(\text{component})/\rho(\text{component})}{\sum \left(\frac{m(i)}{\rho(i)} \right)} * 100\%$$

Yield:

A1-co-H03: 1.2556 g (2.50 mmol) \equiv 95% of theory.

A1-co-H11: 1.8241 g (2.33 mmol) \equiv 88% of theory.

A1-co-H21: 6.1526 g (2.41 mmol) \equiv 91% of theory

A12-co-H03: 1.0422 g (1.78 mmol) \equiv 97% of theory.

A12-co-H11: 1.3186 g (1.52 mmol) \equiv 83% of theory.

A12-co-H21: 4.5644 g (1.70 mmol) \equiv 93% of theory.

Characterization by $^1\text{H-NMR}$ (proton nuclear magnetic resonance), in CDCl_3 , δ (ppm) (see also spectra in **Appendix 4**):

A1-co-H03: 7.93 (4H, d, arom.), 7.24 (4H, d, arom.), 2.59 (4H, m, CH₂), 1.79 (4H, m, CH₂), 1.56 –H₂O, 1.48 (4H, m, CH₂), 0.62 (4H, m, CH₂), 0.09 (52H, m, CH₃).

A1-co-H11: 7.93 (4H, d, arom.), 7.24 (4H, d, arom.), 2.59 (4H, m, CH₂), 1.79 (4H, m, CH₂), 1.56 –H₂O, 1.48 (4H, m, CH₂) 0.61 (4H, m, CH₂), 0.09 (111H, m, CH₃).

A1-co-H21: 7.93 (4H, d, arom.), 7.24 (4H, d, arom.), 3.73 – 1,2-dichloroethane, 2.58 (4H, m, CH₂), 1.79 (4H, m, CH₂), 1.56 –H₂O, 1.49 (4H, m, CH₂) 0.62 (4H, m, CH₂), 0.09 (452H, m, CH₃).

A12-co-H03: 7.93 (4H, d, arom.), 7.24 (4H, d, arom.), 2.58 (4H, m, CH₂), 1.77 (4H, m, CH₂), 1.56 –H₂O, 1.30 (30H, m, CH₂), 0.52 (4H, m, CH₂), 0.09 (51H, m, CH₃).

A12-co-H11: 7.93 (4H, d, arom.), 7.23 (4H, d, arom.), 2.58 (4H, m, CH₂), 1.77 (4H, m, CH₂), 1.56 –H₂O, 1.27 (32H, m, CH₂), 0.52 (4H, m, CH₂), 0.14 (109H, m, CH₃).

A12-co-H21: 7.96 (4H, d, arom.), 7.24 (4H, d, arom.), 2.59 (4H, m, CH₂), 1.77 (4H, m, CH₂), 1.56 –H₂O, 1.28 (32H, m, CH₂), 0.54 (4H, m, CH₂), 0.15 (454H, m, CH₃).

for comparison:

neat A1: 7.92 (4H, d, arom.), 7.23 (4H, d, arom.), 5.88 (2H, m, CH), 5.12 (4H, m, CH₂), 2.69 (4H, m, CH₂), 2.52 (4H, m, CH₂), 1.53 ppm (H₂O - moisture).

neat A12: 7.92 (4H, d, arom.), 7.22 (4H, d, arom.), 5.78 (2H, m, CH), 4.95 (4H, m, CH₂), 2.56 (4H, m, CH₂), 2.02 (4H, m, CH₂), 1.74 (4H, m, CH₂), 1.53 ppm (H₂O - moisture), 1.38 (20H, m, CH₂).

neat DMS H03: 4.70 (2H, m, SiH), 0.18 (12H, m, CH₃), 0.06 (40H, m, CH₃).

neat DMS H11: 4.71 (2H, m, SiH), 0.17 (12H, m, CH₃), 0.08 (84H, m, CH₃).

neat DMS H21: 4.69 (2H, m, SiH), 0.13 (12H, m, CH₃), 0.06 (380H, m, CH₃).

Check of quantitative conversion:

FTIR Complete disappearance of the peak of the Si–H bond stretching at about 2120 cm⁻¹ (see spectra in **Appendix 4**).

¹H-NMR: Complete disappearance of the peaks near 4.7 ppm (Si-H) and of the multiplets near 5.79 and 4.94 ppm (vinyl groups of LC mesogen), see spectra in **Appendix 4**.

3.2.4 Synthesis of ‘infinite’ alternating copolymers of PDMS and linearly bonded LC units of aromatic polyeter type (“M12”, “M22” and “M32”)

Appropriate quantities of LC mesogens and of PDMS (see *Table 8–10*) were placed into a small vessel equipped with a magnetic stirring bar. 2 mL of chloroform or of toluene (in case of copolymers with the M12 mesogen, see *Table 8*) were added and after flushing the reactants with argon, they were dissolved by brief stirring at 60°C or 100°C (in case of M12-containing mixtures in toluene). Subsequently, Karstedt’s catalyst (8.7 mg of a 2 wt% solution \equiv 0.02 mmol Pt) was added and the solution was stirred at 60°C or 100°C (in case of M12-containing mixtures in toluene) for 5 min. Thereafter, the chloroform-containing reaction mixture was cooled down to room temperature and the solvent was removed under reduced pressure. In case of toluene-containing reaction mixture (with M12), triethylsilane was added to avoid crosslinking of terminal LC-vinyl groups and Karstedt’s catalyst also was added again (8.7 mg of a 2 wt% solution \equiv 0.02 mmol Pt). The M12-based reaction mixture was then stirred for additional 5 min, and was subsequently cooled down to room temperature and the solvent was removed under reduced pressure, similarly like chloroform from the other mixtures. In some mixtures, side reactions occurred to a varying degree, which led to the formation of a crosslinked fraction. For this reason, all the raw products were further purified by dissolution in tetrahydrofuran and filtration through a syringe filled with 1 cm of cotton wool, after which the solvent was evaporated again, and the products dried under vacuum at 80°C. The products were then cooled-down to room temperature and stored. The trace amounts of the Karstedt’s catalyst in the copolymers were tolerated as non-problematic impurity in case of standard syntheses (although it was possible to remove them by adsorption on silica or on activated carbon at the cost of reduced yield).

Yield:

M12-co-H03: 0.9564 g (1.61mmol) \equiv 90% of theory.

M12-co-H11: 0.7346 g (0.84 mmol) \equiv 47% of theory.

M12-co-H21: 4.5698 g (1.73 mmol) \equiv 97% of theory

M22-co-H03: 0.9576 g (1.46 mmol) \equiv 100% of theory.

M22-co-H11: 0.6031 g (0.64 mmol) \equiv 44% of theory.

M22-co-H21: 3.3385 g (1.23 mmol) \equiv 84% of theory.

M32-co-H03: 0.9117 g (1.32 mmol) \equiv 100% of theory.

M32-co-H11: 0.5125 g (0.53 mmol) \equiv 40% of theory.

M32-co-H21: 3.6156 g (1.32 mmol) \equiv 100% of theory.

Table 8. Amounts of the components used in the synthesis of ‘infinite’ alternating copolymers of PDMS and linearly bonded LC units of aromatic polyester type “M12”.

Component		Sample name		
		M12-H03	M12-H11	M12-H21
M12	[g]	0.5	0.5	0.5
	[mmol] *	1.78	1.78	1.78
	wt%	47.38	32.12	10.63
	Vol% ‡	43.56	29.53	9.9
H03	[g]	0.5553	-	-
	[mmol] *	1.78	-	-
	wt%	52.62	-	-
	Vol% ‡	56.44	-	-
H11	[g]	-	1.057	-
	[mmol] *	-	1.78	-
	wt%	-	67.88	-
	Vol% ‡	-	70.47	-
H21	[g]	-	-	4.202
	[mmol] *	-	-	1.78
	wt%	-	-	89.37
	Vol% ‡	-	-	90.1
Toluene	[g]	2.956	2.956	2.956
Karstedt's catalyst	[g]	0.0087	0.0087	0.0087
	[mmol]	0.02	0.02	0.02

* as mmol of respective functional groups (not whole molecules).

‡ The volume fractions of the aggregation-able mesogen M12 were calculated using the below *Equation* under consideration of the densities ($\rho_{(M12)} = 1.05 \text{ g/cm}^3$, $\rho_{(H03)} = 0.90 \text{ g/cm}^3$, $\rho_{(H11)} =$

0.93 g/cm^3 and $\rho_{(H_2I)} = 0.97 \text{ g/cm}^3$) and of the stoichiometric synthesis amounts (see above **Table 5**) of the individual components.

$$\text{volume percent (Vol\%)} = \frac{m(\text{component})/\rho(\text{component})}{\Sigma\left(\frac{m(i)}{\rho(i)}\right)} * 100\%$$

Table 9. Amounts of the components used in the synthesis of ‘infinite’ alternating copolymers of PDMS and linearly bonded LC units of aromatic polyester type “M22”.

Component		Sample name		
		M22-H03	M22-H11	M22-H21
M22	[g]	0.5	0.5	0.5
	[mmol] *	1.46	1.46	1.46
	wt%	52.25	36.47	12.62
	Vol% ‡	48.36	33.71	11.76
H03	[g]	0.4576	-	-
	[mmol] *	1.46	-	-
	wt%	47.75	-	-
	Vol% ‡	51.64	-	-
H11	[g]	-	0.8708	-
	[mmol] *	-	1.46	-
	wt%	-	63.53	-
	Vol% ‡	-	66.29	-
H21	[g]	-	-	3.463
	[mmol] *	-	-	1.46
	wt%	-	-	87.38
	Vol% ‡	-	-	88.24
CHCl₃	[g]	2.956	2.956	2.956
Karstedt's catalyst	[g]	0.0087	0.0087	0.0087
	[mmol]	0.02	0.02	0.02

* as mmol of respective functional groups (not whole molecules).

‡ The volume fractions of the aggregation-able mesogen M22 were calculated using the below *Equation* under consideration of the densities ($\rho_{(M22)} = 1.05 \text{ g/cm}^3$, $\rho_{(H03)} = 0.90 \text{ g/cm}^3$, $\rho_{(H11)} = 0.93 \text{ g/cm}^3$ and $\rho_{(H21)} = 0.97 \text{ g/cm}^3$) and of the stoichiometric synthesis amounts (see above *Table 5*) of the individual components.

$$\text{volume percent (Vol\%)} = \frac{m(\text{component})/\rho(\text{component})}{\Sigma\left(\frac{m(i)}{\rho(i)}\right)} * 100\%$$

Table 10. Amounts of the components used in the synthesis of ‘infinite’ alternating copolymers of PDMS and linearly bonded LC units of aromatic polyester type “M32”.

Component		Sample name		
		M32-H03	M32-H11	M32-H21
M32	[g]	0.5	0.5	0.5
	[mmol] *	1.32	1.32	1.32
	wt%	54.88	38.96	13.83
	Vol%	51	36.12	12.91
H03	[g]	0.4117	-	-
	[mmol] *	1.32	-	-
	wt%	45.12	-	-
	Vol%	49	-	-
H11	[g]	-	0.7834	-
	[mmol] *	-	1.32	-
	wt%	-	61.04	-
	Vol%	-	63.88	-
H21	[g]	-	-	3.116
	[mmol] *	-	-	1.32
	wt%	-	-	86.17
	Vol%	-	-	87.09
CHCl₃	[g]	2.956	2.956	2.956
Karstedt's catalyst	[g]	0.0087	0.0087	0.0087
	[mmol]	0.02	0.02	0.02

* as mmol of respective functional groups (not whole molecules).

‡ The volume fractions of the aggregation-able mesogen M32 were calculated using the below *Equation* under consideration of the densities ($\rho_{(M32)} = 1.05 \text{ g/cm}^3$, $\rho_{(H03)} = 0.90 \text{ g/cm}^3$, $\rho_{(H11)} =$

0.93 g/cm^3 and $\rho_{(H21)} = 0.97 \text{ g/cm}^3$) and of the stoichiometric synthesis amounts (see above **Table 5**) of the individual components.

$$\text{volume percent (Vol\%)} = \frac{m(\text{component})/\rho(\text{component})}{\sum \left(\frac{m(i)}{\rho(i)}\right)} * 100\%$$

Characterization by $^1\text{H-NMR}$ in CDCl_3 , δ (ppm) (see also spectra in **Appendix 6**):

M12-co-H03: 8.22 (2H, d, arom.), 7.24 (4H, m, arom.), 7.14 (2H, m, arom.), 5.43 (stabilizer impurity: substituted phenol), 2.58 (4H, m, CH₂), 1.98 (2H, m, CH₂), 1.76 (4H, m, CH₂), 1.30 (25H, m, CH₂), 0.07 (39H, m, CH₃).

M12-co-H11: 8.22 (2H, d, arom.), 7.23 (4H, m, arom.), 7.14 (2H, m, arom.), 5.43 (stabilizer impurity: substituted phenol), 2.56 (4H, m, CH₂), 1.76 (4H, m, CH₂), 1.26 (25H, m, CH₂), 0.95 (2H, m, CH₂), 0.536 (3H, m, CH₃), 0.08 (80H, m, CH₃).

M12-co-H21: 8.22 (2H, d, arom.), 7.26 (4H, m, arom.), 7.13 (2H, m, arom.), 5.43 (stabilizer impurity: substituted phenol), 2.57 (4H, m, CH₂), 1.76 (4H, m, CH₂), 1.27 (32H, m, CH₂), 0.533 (2H, m, CH₂), 0.07 (252H, m, CH₃).

M22-co-H03: 8.21 (4H, d, arom.), 7.25 (4H, m, arom.), 7.21 (4H, m, arom.), 5.40 (stabilizer impurity: substituted phenol), 2.57 (4H, m, CH₂), 1.75 (4H, m, CH₂), 1.27 (26H, m, CH₂), 0.04 (52H, m, CH₃)

M22-co-H11: 8.23 (4H, d, arom.), 7.27 (4H, m, arom.), 7.23 (4H, m, arom.), 5.42 (stabilizer impurity: substituted phenol), 2.58 (4H, m, CH₂), 1.99 (2H, m, CH₂), 1.77 (4H, m, CH₂), 1.25 (24H, m, CH₃), 0.11 (105H, m, CH₃).

M22-co-H21: 8.26 (4H, d, arom.), 7.27 (8H, d, arom.), 5.43 (stabilizer impurity: substituted phenol), 2.67 (4H, m, CH₂), 2.02 (4H, m, CH₂), 1.79 (4H, m, CH₂), 1.29 (56H, m, CH₃), 0.87 (12H, m, CH₂), 0.4 (50H, m, CH₃), 0.15 (380H, m, CH₃).

M32-co-H03: 8.26 (4H, d, arom.), 7.62 (4H, d, arom.), 7.27 (4H, m, arom.), 7.25 (4H, m, arom.), 5.43 (stabilizer impurity: substituted phenol), 2.60 (4H, m, CH₂), 1.76 (4H, m, CH₂), 1.55 (12H, m, CH₂), 1.27 (30H, m, CH₂), 0.07 (46H, m, CH₃).

M32-co-H11: 8.28 (4H, d, arom.), 7.65 (4H, d, arom.), 7.28 (8H, m, arom.), 5.43 (stabilizer impurity: substituted phenol), 2.68 (4H, m, CH₂), 2.01 (4H, m, CH₂), 1.80 (4H, m, CH₂), 1.28 (52H, m, CH₂), 0.78 (14H, m, CH₂), 0.39 (24H, m, CH₃), 0.1 (92H, m, CH₃).

M32-co-H21: 8.26 (4H, d, arom.), 7.63 (4H, d, arom.), 7.31 (4H, m, arom.), 7.24 (4H, m, arom.), 3.73 (2H, m, CH₂), 2.60 (4H, m, CH₂), 1.78 (4H, m, CH₂), 1.55 (10H, m, CH₂), 1.25 (30H, m, CH₂), 0.07 (502H, m, CH₃).

starting compounds for comparison:

neat M12: 8.20 (2H, m, arom.), 7.23 (4H, d, arom.), 7.13 (2H, m, arom.), 5.79 (2H, m, CH), 4.94 (4H, m, CH₂), 2.55 (4H, m, CH₂), 2.03 (4H, m, CH₂), 1.74 (4H, m, CH₂), 1.33 (20H, m, CH₂).

neat M22: 8.21 (4H, d, arom.), 7.25 (4H, d, arom.), 7.21 (4H, d, arom.), 5.80 (2H, m, CH), 4.94 (4H, m, CH₂), 2.58 (4H, m, CH₂), 2.02 (4H, m, CH₂), 1.77 (4H, m, CH₂), 1.33 (20H, m, CH₂).

neat M32: 8.25 (4H, d, arom.), 7.63 (4H, d, arom.), 7.30 (4H, d, arom.), 7.24 (4H, d, arom.), 5.82 (2H, m, CH), 4.96 (4H, m, CH₂), 2.60 (4H, m, CH₂), 2.07 (4H, m, CH₂), 1.78 (4H, m, CH₂), 1.37 (20H, m, CH₂).

neat DMS H03: 4.70 (2H, m, SiH), 0.18 (12H, m, CH₃), 0.06 (40H, m, CH₃).

neat DMS H11: 4.71 (2H, m, SiH), 0.17 (12H, m, CH₃), 0.08 (84H, m, CH₃).

neat DMS H21: 4.69 (2H, m, SiH), 0.13 (12H, m, CH₃), 0.06 (380H, m, CH₃).

Check of quantitative conversion:

FTIR: Complete disappearance of the peak of the Si-H bond stretching at about 2120 cm⁻¹ (see spectra in **Appendix 6**).

¹H-NMR: Complete disappearance of the peaks near 4.7 ppm (Si-H) and of the multiplets near 5.79 and 4.94 ppm (vinyl groups of LC mesogen), see spectra in **Appendix 6**.

3.3 Methods of characterization of the prepared LC-PDMS copolymers

The success of the syntheses via hydrosilylation coupling, as well as the final properties of the studied LC-PDMS copolymers were investigated by a large variety of physico-chemical methods.

The copolymers' chemical microstructure was verified by $^1\text{H-NMR}$ spectroscopy, while the completeness of the coupling reaction was rapidly and easily checked by FT-IR. $^1\text{H-NMR}$ spectroscopy also was used to determine precise equivalent molecular weights per SiH function of the hydrido-functional PDMS precursors, as described further above. The molecular masses of the copolymers were analysed using size exclusion chromatography (GPC) and in some cases also by MALDI-TOF or $^1\text{H-NMR}$ (end group analysis).

The phase behaviour of the copolymers was studied by differential scanning calorimetry (DSC), which identified the thermal transitions and their specific heat values, by polarized light microscopy (PLM: mesophase textures), as well as by X-ray scattering (characteristic distances connected with different types of ordering).

Among the material properties, the thermo-mechanical ones were investigated by DMTA. Also tested were tensile properties of some samples, in 'intact' state, as well as after self-healing of disrupted specimens. Advanced mechanical tests included creep-, stress-relaxation-, strain-sweep-, and frequency sweep experiments, which helped to evaluate the strength and reversibility of the physical crosslinking in the copolymers at different temperatures.

Purely rheological properties also were investigated, namely the gelation of melt to rubber vs. rubber melting as result of continuously changing temperature (T -sweep), or the kinetics of gelation after abrupt cooling of copolymer melt (time sweep at constant T). Thixotropy (shear-thinning) effects also were evaluated for selected copolymers. The results of these investigations will be discussed together with the advanced mechanical tests, because they are all related to the topic of reversibility and dynamics of the physical crosslinking.

From the application point of view, the DMTA (determining glassy, elastic, plastic and melt regions) and the rheological gelation tests (illustrating steps in viscoelasticity) were the most important.

3.3.1 Verification of chemical microstructure

3.3.1.1 Nuclear Magnetic Resonance (NMR) spectroscopy

The ^1H -NMR spectroscopy was employed to verify the chemical microstructure of the prepared copolymers, as well as the purity of the starting compounds (including determination of the equivalent molar masses per SiH of the PDMS precursors). The success of the employed coupling reaction (hydrosilylation) also could be evaluated with a high accuracy, as the disappearance in the spectra of the copolymers of the characteristic vinyl peaks (of the functional mesogens) near 4.94 and 5.77 ppm and of the SiH-peak (from hydrido-PDMS) at 4.7 ppm.

Equipment: The ^1H -NMR spectra were recorded on an Avance DPX 300 spectrometer (from Bruker, Karlsruhe, Germany) at 300 MHz. $\text{CDCl}_3\text{-d}_1$ was used as solvent for all analyses. Tetramethylsilane (TMS; $\delta = 0$ ppm) was employed as internal standard.

3.3.1.2 Fourier transform infrared (FTIR) spectroscopy

In case of the infrared spectroscopy (FTIR), there is a much more complex relationship between molecular structure and spectrum than in case of ^1H -NMR. This cheap and easily accessible method is especially efficient for confirming the purity of highly pure and well-known compounds, for studying physical effects which shift the positions of characteristic peaks, or also, if the appearance or disappearance of compounds is studied, which are characterized by isolated highly specific peaks (in regions which are normally 'empty' in the FTIR spectra). This latter case applied to the present work, because the SiH bonds in the hydrido-functional PDMS generate a very specific and isolated vibration peak near 2120 cm^{-1} . Its disappearance meant the full consumption of the SiH groups in the hydrosilylation coupling. Hence FTIR was used to determine the minimum reaction times needed for the completion of the employed coupling reactions, during their optimization.

Equipment: FTIR spectra were recorded in the attenuated total reflection (ATR) mode using a Nicolet 8700 spectrometer (from Thermo Scientific, Waltham, MA, USA). The ATR setup used a Golden Gate™ heatable Diamond ATR Top-Plate (MKII single reflection ATR system, from Specac, Orprington, UK).

3.3.1.3 Gel permeation chromatography (GPC)

The gel permeation chromatography (GPC – traditional name) or more properly size exclusion chromatography (SEC) is a method that separates analytes on the basis of size, typically in organic solvents. This technique is used for the analysis of molecular masses, as well as of their distribution in polymers. Mathematical analysis of the GPC chromatogram yields the number average molecular weight (M_n), the weight average molecular weight (M_w), the Z-average molecular weight (M_z) or the viscosity molecular weight (M_v), as well as the dispersity index (traditional name: polydispersity): $D_M = M_w/M_n$, which characterizes the width of the molecular mass distribution. The method is widely used as a universal one for analysing molecular masses and polydispersities of polymers. The accuracy of the results depends on calibration: usually, the obtained masses are calibrated to polystyrene standard. In praxis, this calibration is used for all polymers, which however generally have different relationships between the size of the molecular coil in solution and its molecular mass, depending on size and mass of the rigid structural segments, which are flexibly connected to the molecular coil. Also, intra- (ev. denser coiling) and inter-molecular (association of two or more molecules) interactions can play a role. Calibration in principle is possible for any polymer (e.g. GPC coupled to MALDI-TOF analysis of the fractions exiting the GPC column), but is done very rarely in praxis. In this work, GPC was used as an universal method to evaluate the molecular masses of all the prepared copolymers (alternative methods were not working well with all samples).

Equipment: The GPC analysis system consisted of a Deltachrom pump with computer-controlled piston movement (from Watrex Praha, s.r.o., Praha, Czech Republic), the autosampler MIDAS (from Spark, Emmen, Holland), as well as of two columns “PLgel 5 μ m MIXED-B” (10 μ m particles; from Polymer Laboratories, now Agilent Technologies, Santa Clara, CA, USA), which according to the manufacturer, separate in the molecular mass range of approximately $1 \times 10^2 \leq M \leq 1 \times 10^6$. Evaporative light scattering detector (ELSD) PL ELS 1000 (from Polymer

Laboratories, Church Stretton, Shropshire, UK, laser wavelength: 658 nm) and a UV–vis (refraction index) DeltaChrom UVD 200 detector (from Watrex Praha, s.r.o., Praha, Czech Republic) with a flow-cell volume of 8 μ L, operating at wavelength $\lambda = 264$ nm, were the detectors in the order of flow. The data were collected into the Clarity software (from DataApex Ltd., Praha, Czech Republic), which communicated with the detectors using a U-PAD2 USB acquisition device (also from DataApex). The mobile phase was tetrahydrofuran (Thermo Fisher Scientific, Waltham, MA, USA) at 25°C (controlled ambient temperature), used as received. The concentration of measured solutions was 5 mg/mL. Polystyrene standards obtained from Polymer Standards Services (Mainz, Germany) were used for calibration.

3.3.1.4 *Matrix-assisted laser desorption ionization / time of flight (MALDI-TOF)*

MALDI TOF is a kind of mass spectrometry, which is based on direct measurement of the molecular mass. Polymer samples are dissolved to obtain thin solutions with spatially isolated macromolecular coils. These solutions are blended (solvent is subsequently evaporated) with a suitable low-molecular matrix material, which can be vaporized by laser pulses. A well-selected ionization agent (which adsorbs onto the polymer) also is added to the blend. The laser pulse which hits the blend consisting mainly of the matrix thus ejects isolated and ionized polymer molecules into the gas phase in the analysis chamber. The charged molecules are subsequently accelerated by electric field and recorded upon impact onto a detector plate. The molecular masses are calibrated in view of the time of flight (“TOF”). A great advantage of MALDI-TOF is the direct measurement of molecular masses. There are also some limitations, however. Large macromolecules are more difficult to vaporize, so that molecular distributions determined by MALDI-TOF can be biased in favour of low molecular masses. Large macromolecules also can fragment and hence be absent in the MALDI TOF mass spectrum, while ‘fake’ low molecular products appear in their place.

The method was applied with varying success in this work: generally, low-molecular-mass copolymers could be characterized with great accuracy, while PDMS copolymers (or precursors) with masses of 5 000 g/mol fragmented quantitatively. Additionally, SiH-rich PDMS precursors were found to undergo radical coupling reactions during the MALDI-TOF analysis.

Sample preparation: The samples were prepared by the ‘dried droplet method’: THF (tetrahydrofuran, $\geq 99.9\%$, from Sigma-Aldrich, St. Louis, MO, USA) solutions of the analyzed

polymer (10 mg mL⁻¹), of the matrix DCTB (trans-2-[3-(4-t-butyl-phenyl)-2-methyl-2-propenyli-dene]malonitrile, Sigma–Aldrich, 10 mg mL⁻¹), and of the cationization agent sodium trifluoroacetate (CF₃COONa; Sigma–Aldrich, 10 mg mL⁻¹) were mixed in the volume ratio 4:20:1. 1 μL of the mixture (the ‘droplet’) was then deposited on the ground-steel target plate and dried at ambient atmosphere.

Equipment: The MALDI-TOF mass spectra were acquired with an **UltrafleXtreme** apparatus (from Bruker Daltonics, Bremen, Germany) in the positive ion reflectron and linear mode. Each spectrum was the sum of 25 000 shots with a DPSS (diode-pumped solid-state) Nd : YAG laser (neodymium-doped yttrium-aluminum garnet laser; 355 nm, 2000 Hz). Delayed extraction and external calibration was used.

3.3.2 Phase properties and transitions

3.3.2.1 *Differential scanning calorimetry (DSC)*

DSC is a technique widely used for examining phase transitions in solid or liquid (non-volatile) materials in general. Important in the context of this work are for example thermotropic transitions in liquid crystals, crystallization- or glass transition phenomena in polymers. Degradation endotherms or reaction exotherms also can be observed by DSC, which however did not occur in the studied products (in the given temperature range).

Equipment: Standard DSC experiments were performed on a DSC Q2000 instrument from TA Instruments (New Castle, DE, USA) under a nitrogen atmosphere. The temperature range was from -90 to 100°C. The heating and cooling rate was always 10°C/min. The samples were first cooled down to -90°C, after which they were subjected to the first heating scan from -90 to 80°C (with final temperature corresponding to the isotropic state of the polymer melt), followed by the first cooling scan (80 to -90°C) and the second heating scan.

Low-temperature experiments in the range from -140 up to -80°C were performed in addition to the above standard experiments, in order to observe the freezing/unfreezing of the mobility of pendant methyl groups in PDMS (in selected samples only). The low-temperature DSC analyses were carried out under nitrogen atmosphere using a “8500” calorimeter from PerkinElmer (Waltham, MA, USA). The cooling medium was liquid nitrogen. The heating and cooling rate

was always 10°C/min. The samples were first cooled down to -140°C, after which the first heating scan (finishing at -80°C) was performed, followed by the first cooling scan (-80 → -140°C) and the second heating scan.

3.3.2.2 X-ray diffraction

Small- and wide-angle X-ray scattering (SAXS and WAXS) was employed in order to elucidate the phase behaviour of the studied copolymers (also by comparison with neat mesogens). Reflection peaks in the WAXS and the SAXS/WAXS border region yielded information about characteristic distances in crystalline or liquid-crystalline states of the pure mesogens, as well as in LC nano-aggregates in the copolymers, but also about inter-aggregate distances in the copolymers. SAXS scattering patterns were of interest for estimating the size of eventual larger nano-domains. Temperature-induced changes in the WAXS and SAXS patterns hence were helpful in explaining the involved phase transitions.

Equipment: X-ray scattering experiments were performed using a pinhole camera (MolMet, Rigaku, Japan, modified by SAXSLAB/Xenocs) attached to a microfocused X-ray beam generator (Rigaku MicroMax 003) operating at 50 kV and 0.6 mA (30 W). The camera was equipped with a vacuum version of Pilatus 300K detector. Variable detector positioning cover q range of 0.004 – 3.6 Å⁻¹ was chosen. Scattering vector, q , is defined as: $q = (4\pi/\lambda)\sin\theta$, where $\lambda = 1.54$ Å is the wavelength of the installed source and 2θ is the scattering angle. Calibration of primary beam position and sample-to-detector distances was performed using AgBehenate and Si powder sample. Exposure time for recording one XRD pattern was 1 hour. In order to obtain accurate positions of reflection (interference) peaks, these were fitted by Gaussian peak function.

Sample preparation: The tested materials were placed into thin glass capillaries of 2 mm internal width and of 0.01 mm wall thickness, which were sealed after sample filling. The capillaries with the specimens were subsequently placed into a heated holder and were measured at several temperatures. Except the initial measurement at room temperature, all the following patterns were recorded after the specimens dwelt 10 min at the selected temperature.

3.3.2.3 Polarized light microscopy (PLM)

The assignment of the phase transitions connected with the observed DSC peaks, as well as of the ordering in the mesophases, which occurred between the transitions was further supported by observing characteristic textures with polarized light microscopy (PLM).

Equipment: PLM micrographs were recorded with a microscope Nikon Eclipse 80i (from Nikon, Shinagawa, Tokyo, Japan) equipped with a digital camera ProgRes CT3 (from Jenoptik, Jena Germany) and THMS 600 heating stage (from Linkam Scientific Instruments Ltd., Tadworth, Surrey, UK).

Specimen preparation: Thin specimens for PLM (thickness $<10\ \mu\text{m}$) were prepared by compression molding on a heating bar (temperature of the bar 120°C , compression between two glasses, load 5 kg for 10 min). In some of the copolymers, especially in the ones with alternating PDMS and LC or in the LC-grafted ones; the best PLM micrographs were obtained for the thinnest polymer films after slight shear deformation, which was induced by manual shift of the two glasses used for compression molding. On the other hand, in the LC-end-capped copolymers, distinct textures appeared without any shear treatment.

Experimental procedure: All PLM experiments started at room temperature. In case of expected transitions above room temperature, the sample was gradually heated with the rate of $1^\circ\text{C}/\text{min}$ up to the desired final temperature, where the melt was fully isotropic. After a short pause at the maximum temperature (5 min), the sample was cooled down to room temperature using the same rate. In case of transitions starting below room temperature, the sample was cooled down to the ‘start temperature’ with the rate of $1^\circ\text{C}/\text{min}$, dwelt at this temperature for 5 min, after which the heating scan (at $1^\circ\text{C}/\text{min}$) was started. The cooling scan was performed with the same rate after dwelling 5 min at the maximum temperature. In case of the maximum temperature, it had to be taken into account, that above 180°C , rapid depolymerisation of PDMS occurs, so that a ‘safe’ maximum temperature for the copolymers was ca. 160°C , if degradation damage had to be prevented.

Analysis of mean polarized light intensity: Eventual anisotropic features smaller than $1\ \mu\text{m}$ were not directly visible by PLM, but their presence was analysed by measuring the mean intensity of the polarized light from the whole observed area. Distinct ‘hidden effects’ were proven in this way in some of the copolymers. The mean transmitted intensity of the polarized

light (while sample illumination intensity was constant) was evaluated using the software NIS Elements 4.0 from Laboratory Imaging, Prague, Czech Republic; morphological descriptor *MeanIntensity*). As the final output, the normalized *MeanIntensity* as a function of temperature was plotted. The polarized light intensity recorded in this way is proportional to the amount of crystalline/anisotropic structures in the investigated specimen.

3.3.3 Material properties

3.3.3.1 Dynamic-mechanical thermal analysis (DMTA)

The basic temperature-dependent mechanical properties of the studied copolymers, namely the temperature regions of glassy, rubbery and liquid state, as well as the storage and loss moduli in these regions, were determined by the dynamic-mechanical thermal analysis (DMTA).

Equipment: An advanced multi-functional rheometer ARES-G2 (from TA Instruments, New Castle, DE, USA – part of Waters, Milford, MA, USA) was used for the DMTA analyses.

Sample preparation / geometry: The DMTA analyses of the fusible physically crosslinked polymers stretched over a wide range of sample consistence, from glassy state down to melt. In order to carry out the DMTA analysis in one step for the whole consistence range, the specimens were measured between small parallel plates (exchangeable stainless-steel plates, diameter: 6.1 mm, plate distance between 1 and 1.5 mm): sample installation consisted in melting the specimen and subsequently establishing capillary contact with the upper plate. Subsequently, the specimen was frozen to the rubbery state. An advantage was that practically all the studied copolymers displayed good adhesion to the steel plates even in the glassy state. The flat cylindrical geometry made possible a very high accuracy of moduli measurement in the rubbery state, as well as in adjacent regions of vitrification or of gradual melting. The accuracy in the glassy state still was relatively good, while for characterizing the well-molten state, accurate experiments with large parallel plates were necessary (see further below).

Procedure: An oscillatory shear deformation at the constant frequency of 1 Hz and at a small strain amplitude (0.001 to 4%, adjusted by auto-strain function) was applied. In a first scan, the samples were cooled down to -135°C (in standard experiments) from the molten state, at the rate of 3°C/min. Subsequently, in the heating scan, the samples were heated with the same rate up

to the temperature of the thin melt. For both scans, the temperature dependences of the storage- and of the loss shear modulus were recorded, as well as of the loss factor (G' , G'' , and $\tan(\delta)$, respectively).

3.3.3.2 *Microtensile tests and self-healing evaluation*

An interesting property of the studied copolymers, which were solid at room temperature was their tensile behaviour, namely the shape of the stress-strain curve, the elongation at break and the stress at break. The efficiency of self-healing of disrupted samples was evaluated by subsequent tensile tests and the comparison of the tensile curves of self-healed and intact samples.

Equipment: The tensile tests were performed using the same ARES-G2 from TA Instruments, which was used for DMTA and rheology tests.

Sample preparation / geometry: Rectangular specimens ('standard tensile specimens') of total specimen length of 20 mm, width of 5 mm and thickness of 2 mm were used for the tests. They were obtained via melting of the necessary material amount in a teflon mould and subsequent cooling. The samples were installed in the clamps of the ARES-G2 in such a way that the length between the jaws was 3 mm (size of the deformed part of the sample: height: 3 mm, width 5 mm, thickness: 2 mm; 8.5 mm of the sample were inserted into the jaws on the top and on the bottom of the sample). For the chosen geometry, the material properties and the limitations of the ARES-G2 apparatus (which was not conceived as tensile tester) were to be taken into account: maximum allowed tensile force is 20 N, and maximum elongation is 135 mm. The sample dimensions had to be selected in such a way that these limits do not need to be exceeded before the specimen fails.

Disruption and subsequent self-healing of specimens: Among the studied copolymers, BAFKU₄₁-HMS064 was selected for simple self-healing tests, because it is rubbery at room temperature, but also easily meltable and displays thermotropic transitions starting not far above room temperature (starting above 40°C). Two self-healing tests were carried out:

1) At room temperature: a standard rectangular specimen, which failed (ca. in the middle of its length) during a tensile test, was 're-assembled' and pressed together for 48 h by a force of

ca. 100 g at room temperature (22°C), which was below the region of thermotropic transitions in BAFKU₄₁–HMS064, but still in its rubbery range.

2) At 45°C, in the thermotropic region: a standard rectangular specimen was cut into two pieces, which were subsequently pressed together by a force of ca. 100 g at 45°C for 48 h. The healing temperature already was in the range of the thermotropic transitions (DSC) of the copolymer, but still well below the range of gradual melting, so that the sample did not ‘flow’.

Procedure (tensile test itself): The tensile tests were carried out using the method “Axial” of ARES-G2. The experiments were performed at room temperature, with a cross-head speed set to 0.25 mm/s and the final elongation set to 130 mm.

3.3.3.3 *Advanced mechanical analyses*

The ‘advanced mechanical analyses’ were carried out in order to more deeply investigate the reversible nature of the physical crosslinks in the studied elastomeric copolymers.

Equipment: The advanced mechanical analyses were performed using the same ARES-G2 from TA Instruments, which was used for DMTA and rheology tests.

Sample geometry: The samples were measured between parallel plates, the diameter of which was: 35 mm for H21-BAFKU₂, 25 mm for H11-BAFKU₂ and most experiments with H03-BAFKU₂ and 12.6 mm for the most viscous samples of H03-BAFKU₂. Pure polysiloxane components H03, H11, H21 were measured as references using the 12.6 mm plates. BAFKU₄₁–HMS064 samples were measured between 6.1 mm plates. The thickness of the tested samples was always between 0.2 and 0.25 mm (1 mm for BAFKU₄₁–HMS064). The samples of copolymers with the A1, A12, M12, M22 and M32 mesogens were measured between the 25 mm plates at distances between 0.2 and 0.25 mm.

3.3.3.3.1 Strain sweep tests

The possibility to disconnect the reversible physical networks by mechanical deformation at different temperatures was investigated via strain sweep tests.

Procedure: The method “Oscillation Amplitude” in ARES-G2 software was selected for this test: the samples were measured between parallel plates, the geometry of which is specified further above. At a constant deformation frequency of 1 Hz, the strain was gradually increased from 0.1% to 1000% and strain-dependent G' , G'' as well as $\tan(\delta)$ were recorded. Such

experiments were carried out at several constant temperatures positioned in characteristic regions of the studied samples.

3.3.3.3.2 Frequency-stiffening tests (frequency sweep)

Eventual stiffening (or even transition from liquid-like to solid-like behaviour) of the copolymers at moderately high oscillatory deformation frequencies was studied by means of the frequency sweep tests.

Procedure: The method “Oscillation Frequency” in ARES-G2 software was selected for this test: the oscillatory deformation frequency was gradually increased from 0.001 Hz to 100 Hz. The data were recorded in five logarithmic series of points – ‘decades’ with a constant deformation amplitude in each decade, namely 50% (at 0.001 to 0.01 Hz), 20%, 10%, 5% and 1% (at 10 to 100 Hz). The samples were measured between parallel plates, the geometry of which is specified further above. Such frequency sweep tests were carried out at several constant temperatures positioned in characteristic regions of the studied samples.

3.3.3.3.3 Creep and Creep Recovery Tests

The creep and creep recovery tests were performed in order to further evaluate the strength of the physical crosslinks in the studied materials at different temperatures. In weaker-crosslinked samples, yield stress values could be obtained in these experiments.

Procedure: The method “Step (Transient) Creep” (method name in ARES-G2 software) was used for this test. The experiment consisted of several subsequent stages, each of which contained a loading step followed by an un-loading one (two subsequent “Step (Transient) Creep” modules). During the loading step, a constant stress was applied for a pre-defined time period and the deformation (strain) adjusted automatically in order to maintain the constant stress. In the subsequent un-loading step, the value of the applied constant stress was set to be zero. The measured time-dependent values of the automatically adjusted strain were the final results. The subsequent two-step stages differed in the strain values applied in their respective first step. The creep and creep recovery tests were performed at several characteristic temperatures for each studied copolymer. The standard sequence of applied stress loadings (in the

first steps of each stage) was: 0.1, 1, 200, 500, 1 000, 2 000 and finally 10 000 Pa. In view of the properties of the studied samples, the duration of the loading and un-loading steps was set to 3 min, with 200 data points recorded during this time.

3.3.3.3.4 Stress relaxation tests

Stress relaxation tests (method name in ARES-G2 software: “Step (Transient) Stress Relaxation”) were used as an additional method to further evaluate the strength of the physical crosslinks and the dynamics of their splitting and reconnection.

Procedure: The samples were measured in the torsion regime between parallel plates, the geometry of which is specified further above. During each test, a pre-defined constant deformation (strain) was applied and the time-dependence of the resulting stress was recorded by the force detector and later evaluated as the final experiment result. The experiment was stopped after the stress value apparently reached equilibration. For each copolymer sample, a series of tests was done at several characteristic temperatures. Each of the series consisted of tests with the applied deformation (strain) values of: 0.4, 1, 2, 3, 4, 5, 10 and 20% (in some cases also 40, 60 and 100%). A sufficient length of the experiment was given in order to reach equilibrium of stress versus time. The data sampling rate was 1 point/s. The time-dependent stress was recorded.

3.3.3.4 *Rheological properties*

Purely rheological investigations were carried out in order to evaluate the effects of physical crosslinking in the studied copolymers in the melt phase (and in the bordering soft rubbery state). The investigations focused on gelation / melting processes induced by temperature changes, on the kinetics of the build-up of physical crosslinking after melt cooling, as well as on thixotropy effects in viscoelastic regions of molten copolymers.

3.3.3.4.1 Determination of temperatures of gelation

The temperature-controlled gelation behaviour of the studied copolymers was evaluated using the multi-frequency temperature sweep test (method name in ARES-G2 software: “Oscillation Multiwave”).

Procedure: The samples were loaded as melt between parallel plates, the geometry of which is specified above and were isotropized by a 5 min dwell at 80°C. Subsequently, two tests were run, the first one in cooling regime and a second one in heating regime. The first test started at the ‘loading temperature’ of +80°C, where all samples were isotropic and all history effects in them erased. The final temperature of the cooling run depended on the sample: 0°C for H03–BAFKU₂, -15°C for H11–BAFKU₂ and -40°C for H21–BAFKU₂. The heating scan started at the final cooling temperature of each sample and ended at +70°C. The rate of temperature change was 1°C/min in both scans. The deformation regime in both scans consisted in simultaneously applied (‘multi-frequency’) deformations of following frequencies and amplitudes: 1 Hz / strain amplitude of 1%, 2 Hz / 1%, 4 Hz / 0.8%, 8 Hz / 0.6%, 16 Hz / 0.4%, 32 Hz / 0.3%, and 64 Hz / 0.1%. The results were depicted as curves sets of temperature dependent storage shear modulus $G' = f(T)$, of the loss shear modulus $G'' = f(T)$, and of the loss factor $\tan(\delta) = f(T)$. The latter sets of curves were used to determine the gel points (as $\tan \delta$ crossover points) according to the theory of Chambon and Winter [217].

3.3.3.4.2 Kinetics of thermally induced physical gelation

In order to evaluate the rate with which the physical network is formed after abrupt cooling of molten copolymer to different temperatures, oscillatory time sweep tests (method name in ARES-G2 software: “Oscillation/Time”) have been performed.

Procedure: A constant oscillatory strain amplitude of 1% was applied at a constant frequency of 1 Hz. The samples were measured between parallel plates, the geometry of which is specified further above. The copolymer samples were rapidly cooled from the isotropic melt state (most often from +70°C) to different final temperatures, which were positioned in the rubbery region, in the liquid-crystalline melt region and in the isotropic melt region. The “oscillatory time sweep test” recorded G' , G'' and $\tan(\delta)$ as function of time, as well as the actual temperature, beginning with the start of the rapid melt cooling. In this way, eventual rapid crosslinking prior to temperature equilibration also could be observed, in addition to slower crosslinking which occurred after the temperature of the cooled melt stabilized.

3.3.3.4.3 Thixotropy: simple oscillatory tests

The destruction of physical crosslinking by high deformations, as well as its recovery upon substantial reduction of such deformations was tested in simple oscillatory time sweep tests (method name in ARES-G2 software: “Oscillation/Time”).

Procedure: The experiments were carried out as multi step procedures. In each step, a constant oscillatory frequency (1 Hz) and at constant oscillatory deformation was applied, and the time-dependent values of storage shear modulus and of loss shear modulus were recorded. The individual steps in the procedure differed by highly contrasting values of the deformation amplitudes, which ranged between 0.1 and 5030%. The duration of each step was between 50 and 150s.

3.3.3.4.4 Thixotropic Loop tests

Thixotropy loop tests were performed in order to evaluate changes in viscosity caused by continuous shear flow (destruction of physical branching points), as well as the degree of eventual recovery vs. ‘persistent shear damage’ in short-time term. The samples were measured between parallel plates, the geometry of which is specified further above.

Procedure: Two experimental setups were used: “Flow Ramp” and “Flow Sweep” (method names in ARES-G2 software):

In the “**Flow Ramp**” tests, in the first step, the materials were subjected to a continuously increasing shear rate (during continuous rotatory mode), while the stress generated by the shearing was recorded. The shear-rate-dependent viscosity values were calculated from the stress values. In the second step, the shear rate was continuously reduced down to 0 s^{-1} . In a standard test, the range of applied shear rates was 0 to 100 s^{-1} , followed by 100 to 0 s^{-1} . The duration of each step was set to 10 min. In case of highly viscous or semi-solid samples, shorter “Thixotropy ramp” tests were performed, with shear rate ranges of 0 to 0.1 s^{-1} , 0 to 1 s^{-1} or 0 to 10 s^{-1} . The values of stress and of viscosity in dependence of shear rate were obtained in the result plot.

The “**Flow Sweep**” tests were used to perform a rapid scan of the shear rate region from 100 to 400 s^{-1} . The experiments were performed in two steps: in the first step, the shear rate was step-wise increased, with measured points at: 100 , 200 , 300 and 400 s^{-1} and with equilibration

time of 2 min per each point (while the point's data were measured and averaged for an additional 30 s). In the second analogous step, the shear rate was step-wise decreased, to 300, 200 and 100 s⁻¹. The values of stress and of viscosity in dependence of shear rate were obtained in the result plot.

The thixotropy loop tests were carried out at several characteristic temperatures of each copolymer, in order to characterize their semi-liquid and liquid regions.

4 Statement about work contribution

My own work on this dissertation included:

- Synthesis of the studied copolymers, based on three structural families and on 6 different LC building blocks. This also included the optimization of reaction conditions and reaction times, conversion kinetics evaluation, as well as copolymer stabilization in some cases.
- Investigation of basic thermo-mechanical properties of all the copolymers (DMTA analysis).
- Advanced tests of mechanical properties: creep- and creep recovery tests, stress-relaxation-, strain-sweep- and frequency sweep tests; these experiments were carried out at characteristic temperatures of each studied copolymer.
- Self-healing experiments.
- Microtensile tests.
- Rheology experiments including temperature-controlled gelation studies, studies of gelation kinetics upon melt cooling and thixotropic loop tests.
- Optimization of experimental parameters for the above physical methods.
- Measurement of a part of the FTIR analyses.

The following characterization results have been obtained from colleagues from the Institute of Macromolecular Chemistry:

¹H-NMR: D. Kankova, GPC: Dr. M. Netopilík, MALDI-TOF: Z. Walterová,

DSC: Dr. M. Vyroubalova, SAXS/WAXS: Dr. A. Zhigunov and Ms. E. Miškovská, PLM: Dr. M. Šlouf and Dr. S. Krejčíková, development of self-healing techniques and micro-tensile characterization procedure: Dr. Beata Strachota.

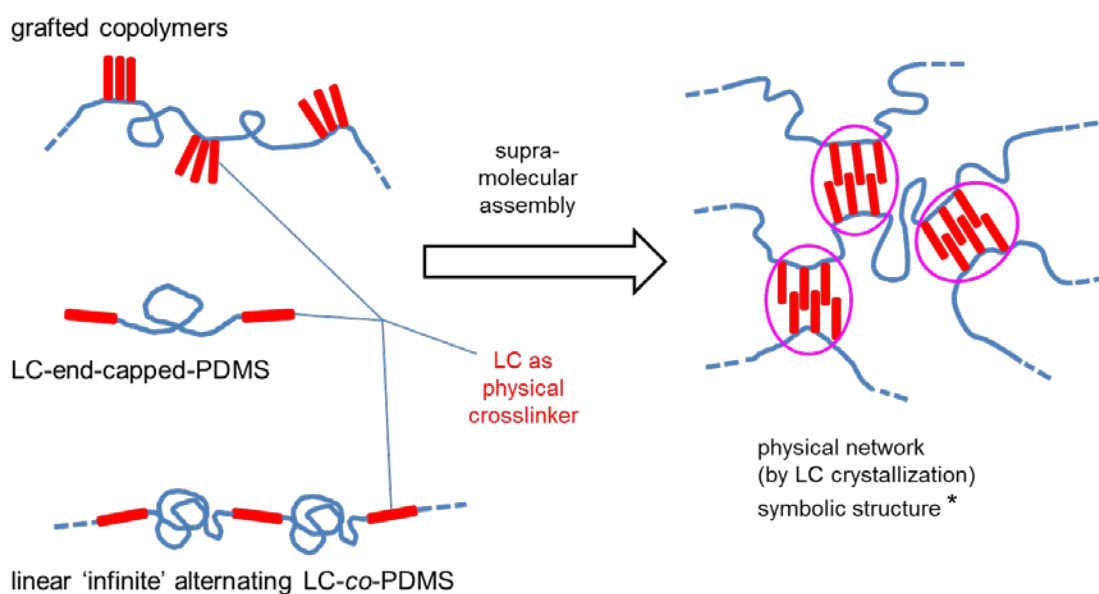
The following work contribution was received via cooperation with the Rzeszow University of Technology, Faculty of Chemistry:

Synthesis of the vinyl-functional mesogens (LCs) tested as building blocks in this work: Assoc. Prof. Dr. Beata Mossety-Leszczak.

Their support and enthusiasm are gratefully acknowledged.

5 Results and discussion

In this work, several families of copolymers based on highly flexible PDMS chains and on rod-like liquid crystalline (LC) units of different size and length were synthesized (see *Scheme 15*), as reversible elastomers with widely varied melting points. These copolymers self-assemble to physical networks due to the phase-separation tendency of the LC units (see *Scheme 15*). The elastomers are attractive due their re-processibility (either by melting, or by dissolution), and also due to the thermotropic behaviour of the physical crosslinks (LC nano-aggregates) in them (as potential smart materials).



Scheme 15: The architectures of the synthesized copolymers and the self-assembly of their macromolecules to physical networks; () the self-assembled structure in the Scheme is the one for the 'grafted copolymers'; the other networks are basically similar and their structures are shown further below.*

Three copolymer architectures were studied (see *Scheme 15*), as reversible elastomers with widely varied melting points. These copolymers self-assemble to physical networks due to the phase-separation tendency of the LC units (see *Scheme 15*): 'grafted copolymers', which consist of alternating polydimethylsiloxane (PDMS) 'spacer' segments and pendant quartets of mesogenic (LC) units; ' α,ω -LC terminated copolymers' in which PDMS chains are end-capped

by LC units; and linear ‘infinite’ LC-PDMS copolymers whose structure is based on alternating polyaromatic mesogens and elastic polydimethylsiloxane chains.

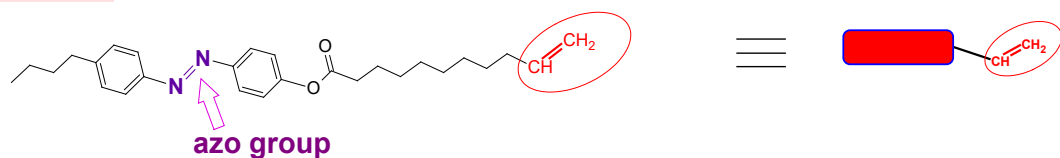
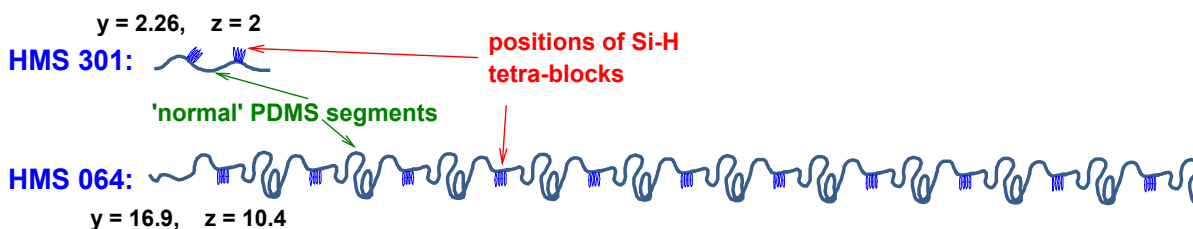
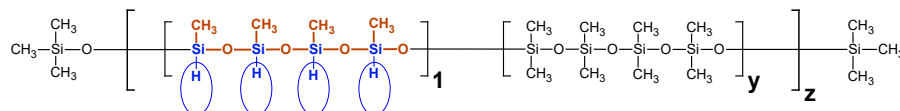
In the Results and Discussion section, the following aspects will be debated in this sequence: (1) the synthesis of the copolymers (including their basic characterization), (2) the copolymers’ thermomechanical properties; (3) self-healing behaviour and tensile tests of a selected copolymer; (4) the phase behaviour of these complex thermotropic materials; (5) the results of advanced mechanical tests which were carried out to evaluate the strength of the physical crosslinking at different temperatures; and (6) the rheological behaviour (temperature-controlled gel formation from melt, gelation kinetics, thixotropy). The mentioned results are part of three published articles and of three unpublished works, which will be referred-to as *Appendix 1 – 6*.

5.1 Synthesis of the copolymers via hydrosilylation coupling

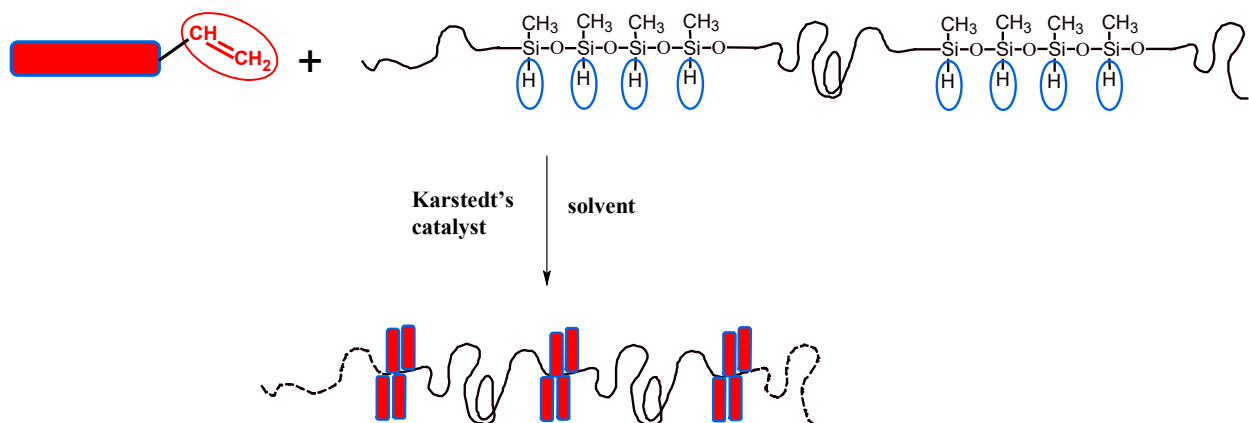
The components of the copolymers were chosen in order to combine highly flexible polymer chains having a low glass transition temperature (PDMS) with readily crystallizing rigid building blocks (LC mesogens). Important was the immiscibility (in absence of solvent) of both components, which favoured the aggregation (nano-phase-separation) of the mesogen units, and thus physical crosslinking. The synthesis of the different studied copolymer types is described below.

5.1.1 Grafted PDMS-LC copolymers

The grafted PDMS-LC copolymers used the mono-vinyl-functional mesogen “BAFKU” (see *Scheme 16*) as the LC building block, and the pendant-hydrido-functional polysiloxanes HMS301 (short and SiH-rich), and HMS064 (long macromolecule, long spacers between SiH quartets) as the polymeric precursors (see *Scheme 16*).

mesogen: BAFKU**PDMS precursors with pendant SiH functions:***Scheme 16: Components of the grafted PDMS-LC copolymers.*

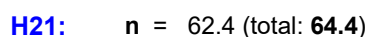
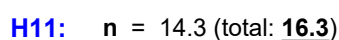
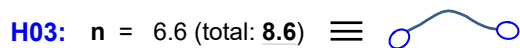
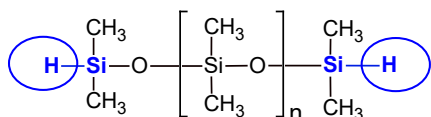
The synthesis reaction, in which the components of the copolymers were coupled via hydrosilylation, is shown in *Scheme 17*. The preparation, the phase- and the material properties of this copolymer were published, and a detailed discussion can be found in *Appendix 1*. A specific structural feature was the occurrence in quartets of the SiH functions, and later of the grafted mesogens. This feature is given by the technical synthesis of PDMS, where cyclic tetrasiloxanes are used as (co-)monomers (see also Introduction – synthesis of PDMS).

*Scheme 17: Synthesis of the grafted BAFKU-PDMS copolymers.*

5.1.2 LC-end-capped copolymers

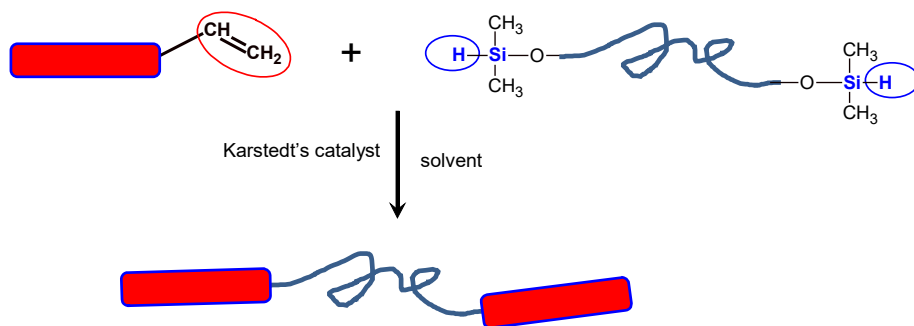
The LC-end-capped copolymers also contained the mono-vinyl-functional BAFKU (shown in *Scheme 16*) as the LC building block, while as the PDMS component, three α,ω -hydrido-functional PDMS precursors of different length were used (see *Scheme 18*).

α,ω -hydrido-functional PDMS precursors:



Scheme 18: The linear α,ω -hydrido-functional PDMS precursors.

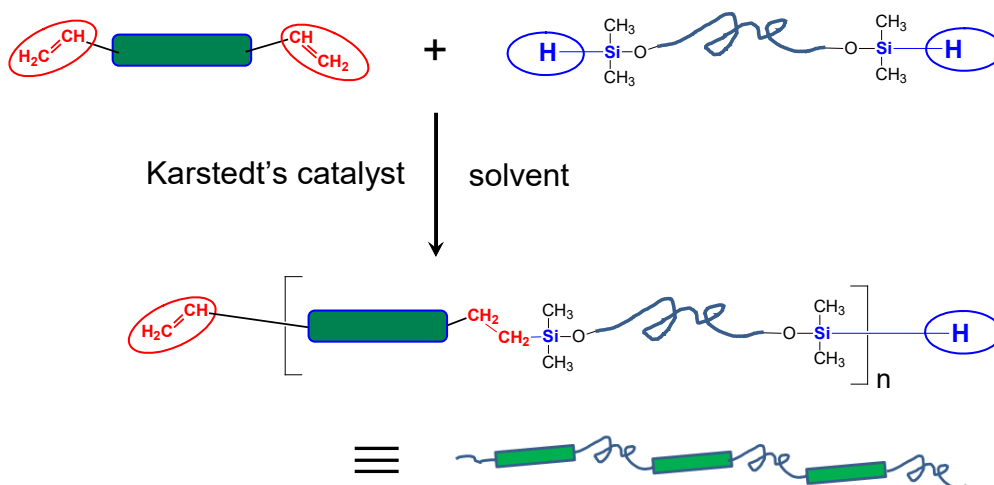
The synthesis was carried out via hydrosilylation coupling of the copolymer components, as shown in *Scheme 19*. The synthesis, the phase- and the material properties of these copolymers were published, and a detailed discussion can be found in *Appendix 2*).



Scheme 19: Synthesis of the LC-end-capped copolymers.

5.1.3 Linear ‘infinite’ LC-PDMS copolymers

The linear ‘infinite’ LC-PDMS copolymers contained the further-above-mentioned α,ω -hydrido-functional PDMS precursors (see *Scheme 18*) as ‘spring component’. These were coupled (*Scheme 20*) with several different divinyl-functional mesogens (see *Scheme 21*) via hydrosilylation, which for the given architecture had a character of a polyaddition. The synthesis procedures for all the prepared copolymers are described in the Experimental Part. Unpublished results concerning the characterization, the phase- and the material properties of two different groups of these copolymers are summarized in *Appendix 4* and *6*.

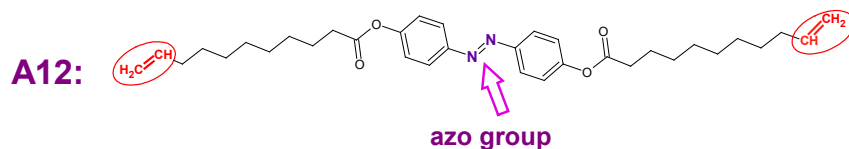
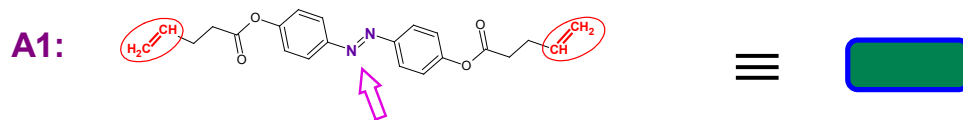


Scheme 20: Synthesis of the linear ‘infinite’ LC-PDMS copolymers.

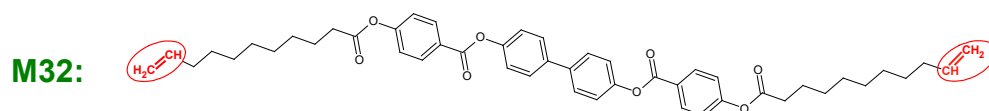
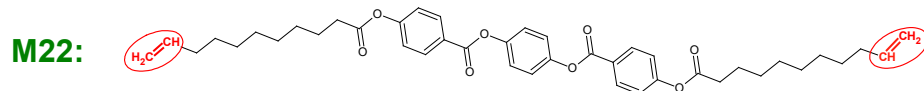
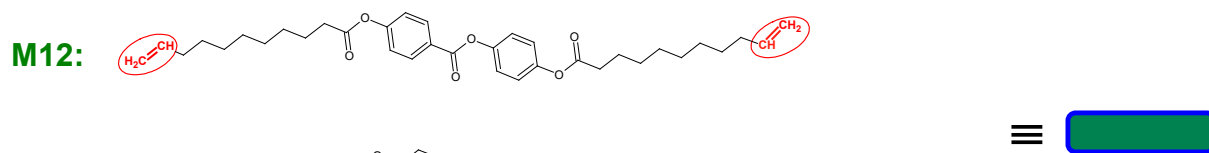
The divinyl-functional mesogens which were incorporated into the linear ‘infinite’ LC-PDMS copolymers belonged to two groups (see *Scheme 21*):

One group were **azo-type mesogens** similar to the mono-functional BAFKU, namely “A1” and “A12”. A1 has distinctly shorter aliphatic tail units than BAFKU, while A12 has one identical and one longer (the second vinyl-functional tail) tail unit, if compared to BAFKU. These mesogens were tested as the difunctional variety of the basic BAFKU structure, in order to compare the effect of the (practically) same mesogenic structure in all the three studied copolymer architectures. The effect of ‘LC-tail-length’ on the aggregation behaviour also was compared.

Divinyl-functional azo mesogens:



Divinyl-functional azo-free polyaromatic mesogens:



Scheme 21: The two groups of divinyl-functional mesogens employed for copolymer synthesis in this work: top: azo-type mesogens closely structurally related to the mono-functional BAFKU; bottom: azo-free polyaromatic divinyl-mesogens of different size.

The other group of divinyl mesogens incorporated into the linear infinite LC-PDMS copolymers were the **azo-free polyaromatic mesogens** “M12”, “M22” and “M32”. The first of these mesogens, M12 has the identical size, and a nearly identical shape (except for the central carboxyl unit replacing azo) like A12. The other azo-free mesogens have a similar basic structure like M12, but their rigid aromatic part is increased in size by incorporating a phenyl, or a biphenyl unit, respectively, in the molecule centre. This series of mesogens was selected to demonstrate the effect of mesogen size on the aggregation behaviour of the LC units in the supramolecularly assembling physical networks.

5.1.4 Chemical aspects of the syntheses: optimization and side reactions

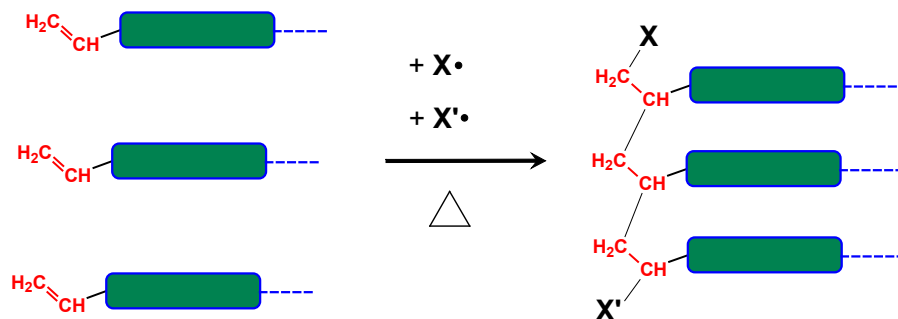
The above hydrosilylation reactions all have been optimized for maximum yield and product purity. The precursor polymer and the vinyl-functional mesogens were deliberately

selected as non-miscible materials (for the sake of physical crosslinking), so that a suitable solvent for the synthesis had to be selected. Especially in case of the larger M22 and M32 mesogens, also a moderately high temperature (60°C) was needed in order to achieve their dissolution and compatibilization with PDMS. As solvents, chloroform, tetrahydrofuran and toluene were especially efficient. Chloroform was preferred due to its easy removal. Because chloroform and tetrahydrofuran (THF) can start radical reactions (C-Cl bond splitting, THF reactions with oxygen), the vinyl-functional mesogens, which displayed the highest tendency to radical crosslinking side-reactions, were coupled with hydrido-PDMS in toluene (albeit its removal was more difficult than that of CHCl₃). In this way, toluene was used as solvent for preparing all the copolymers with the mesogens A1 and A12, and also with M12.

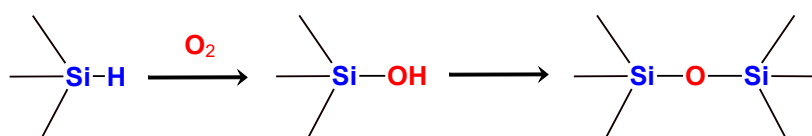
The coupling reactions, the kinetics of which was assessed in a simple way in this work, proved to be very fast. Eventually, the temperature of 60°C was selected as the standard one. At this temperature, full conversion already was achieved in less than 5 min, as verified by FTIR spectroscopy for each reactant pair.

While the hydrosilylation reaction generally is considered to be one of the click-type, it is known to produce problematic side-reactions in some cases, for example the formation of crosslinked polymers instead of linear grafted ones [152, 153]. In this work, the crosslinking side-reactions were found to be most prominent in case of the synthesis of the linear infinite LC-PDMS copolymers, but also in case of the grafted copolymers, if the PDMS precursor HMS 064 was used, which possesses long macromolecules and numerous grafting positions. The side-reactions and some of the crosslinked structures are illustrated in *Scheme 22–24*.

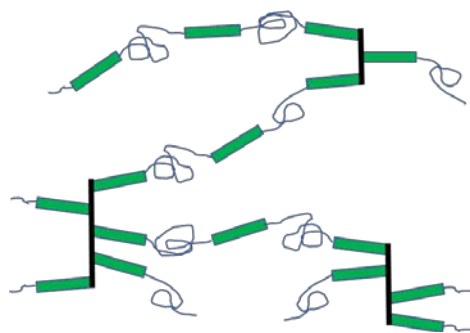
The most problematic side-reaction which was observed during the synthesis of linear infinite LC-PDMS copolymers is the polymerization of the vinyl groups shown in *Scheme 22*: This oligomerization of the LC units theoretically can occur prior to the coupling, during its course, but also in the final LC-PDMS copolymer, the macromolecules of which contain one unreacted terminal vinyl group (see *Scheme 20* further above).



Scheme 22: Polymerization of the vinyl groups before, during, and after the hydrosilylation coupling.



Scheme 23: Oxidative coupling of unreacted SiH groups.

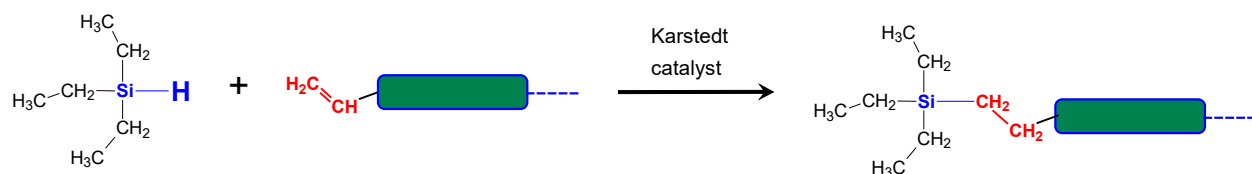


Scheme 24: Crosslinked structure based on the one of the infinite linear LC-PDMS copolymer, in which some of the divinyl-functional-LC units are oligomerized, and hence polyfunctional instead of linearly bonding.

Incorporation of the defect oligomerized LC-units (which are poly-vinyl-functional) during the coupling reaction in **Scheme 20** (further above) automatically leads to the formation of branched or even of crosslinked products. Macromolecules of the linear infinite LC-PDMS copolymer that are only branched, can be eventually crosslinked by inter-molecular side-reactions of the SiH groups, like the oxidative coupling shown in **Scheme 23**, or by similar radical-induced reactions of SiH. Unreacted SiH groups also occur as terminal groups of the ideal linear infinite LC-PDMS copolymers (see **Scheme 20** further above). The crosslinked structure of a defect-rich linear infinite LC-PDMS copolymer is shown in **Scheme 24**.

In case of the LC-grafted copolymers, only the side-reactions of the SiH groups (like in *Scheme 23*) can lead to crosslinking, because an oligomerization of the mono-vinyl-functional LC component yields non-functional oligomers.

Measures to minimize the side-reactions: Eventual oligomers of the vinyl-functional mesogens were removed via recrystallization of the employed LCs (with subsequent purity check by $^1\text{H-NMR}$), but the crosslinking tendency of the linear infinite LC-PDMS copolymers during their synthesis was not markedly reduced by this measure. As result of optimization of synthesis conditions (mentioned further above), the fast coupling at the moderately elevated temperature of 60°C helped to minimize the fraction of crosslinked products, from which the soluble linear infinite LC-PDMS copolymers were subsequently extracted. The so-isolated products further tended to gelation (via crosslinking) upon heat treatment, or during longer storage. Hence, in the final version of the optimized synthesis of the linear infinite LC-PDMS copolymers, the terminal vinyl groups in these products were deactivated by a follow-on hydrosilylation reaction shown in *Scheme 25* (using an excess of a volatile hydridosilane), which was carried out after the completed polymerization, before product isolation. The copolymers subsequently extracted from the crosslinked byproducts proved to be stable, so that no deactivation of the terminal SiH groups was undertaken (which theoretically could be done as another additional hydrosilylation step, this time with a volatile α -olefin).



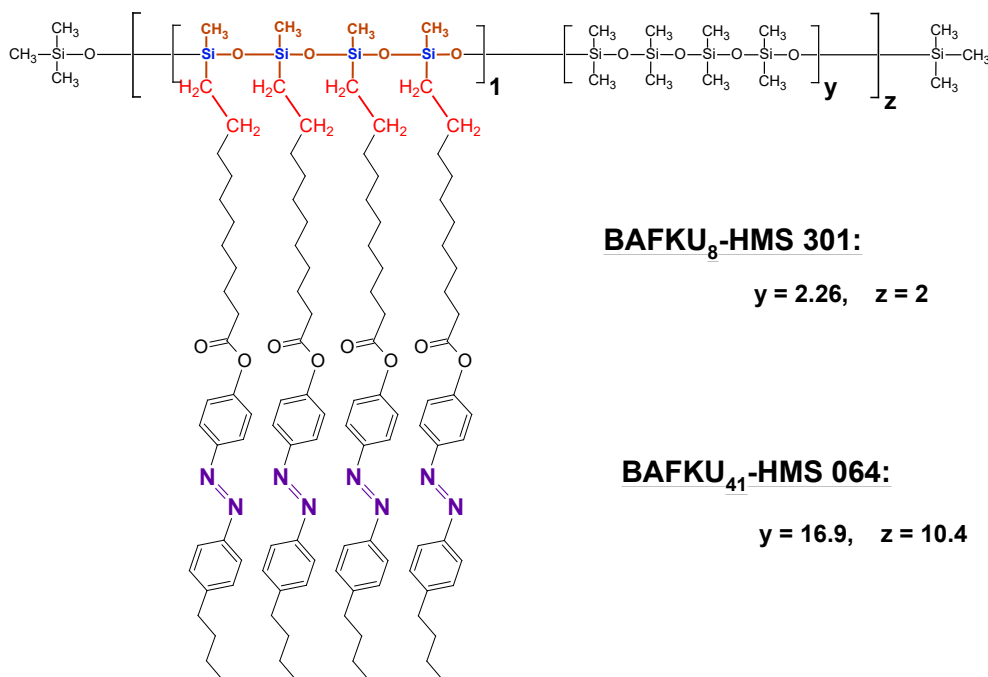
Scheme 25: Protection of the terminal vinyl groups in the linear infinite LC-PDMS copolymers.

In case of the grafted copolymer with the H 064 PDMS precursor, the crosslinking side-reactions of the SiH groups always occurred during the reaction with the mesogen, while after the isolation of the soluble copolymer fraction, the latter was thermally fairly stable. For this reason, no deactivation of the residual SiH groups was done in case of the grafted copolymers.

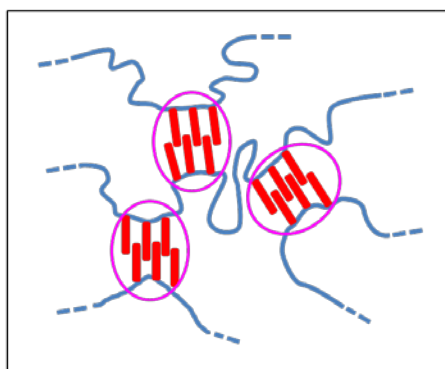
5.1.5 General properties of the prepared copolymers

5.1.5.1 Grafted PDMS-LC copolymers

Two LC-grafted PDMS copolymers were synthesized and studied in this work: BAFKU₈-HMS301 and BAFKU₄₁-HMS064. Their general formulas, the symbolic representations of their macromolecules (based on the known molecular masses of the PDMS precursors, and on their spectroscopically determined functionality), as well as the principle of physical crosslinking in them, is shown in *Scheme 26*.



BAFKU₈-HMS 301



BAFKU₄₁-HMS 064



Scheme 26: Grafted PDMS-LC copolymers: (top): general chemical structure; (bottom): symbolic representation of the macromolecules of the studied copolymers BAFKU₈-HMS301 and BAFKU₄₁-HMS064, as well as of the physical crosslinking in them.

Both grafted copolymers (see photograph in **Figure 4**) are dark orange solids, of similar colour like molten BAFKU. The mesogen-rich BAFKU₈-HMS301 (60.3 Vol.%, see volume fractions of mesogens in **Table 11** further below) is brittle and waxy, due to the high content of BAFKU and to short PDMS spacers between the LC grafts (typically 8 PDMS repeat units, in average 9.04 – see **Scheme 26**). The PDMS-rich copolymer BAFKU₄₁-HMS064 (22.7 Vol.% BAFKU) is a rubbery translucent material, which can be re-melted to different shapes – see platelet in **Figure 4**. Interestingly, both the fairly different copolymers reversibly melt at the same temperature of ca. 60°C, where also the pure BAFKU mesogen melts. Both copolymers are well soluble in chloroform, tetrahydrofuran and in toluene.

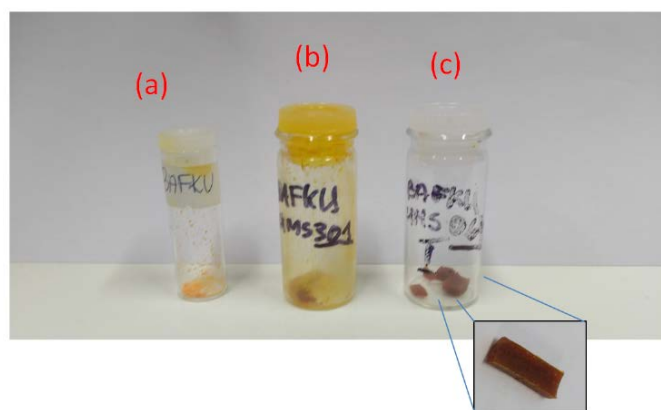
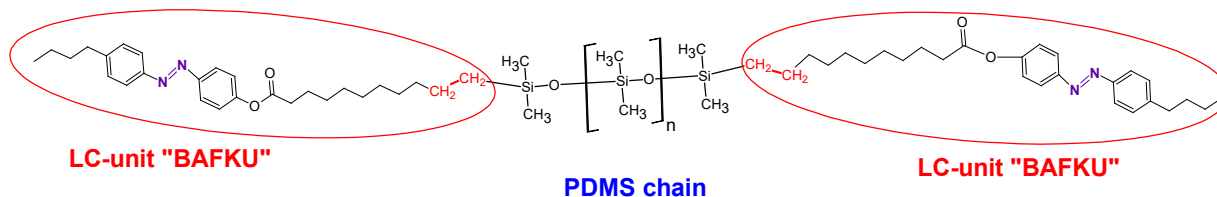


Figure 4: Appearance of the grafted PDMS-LC copolymers (a) neat BAFKU mesogen; (b) the waxy BAFKU₈-HMS301 copolymer; (c) BAFKU₄₁-HMS064.

5.1.5.2 LC-end-capped copolymers

In this work, three LC-end-capped PDMS copolymers were prepared and investigated: H03-BAFKU₂, H11-BAFKU₂, and H21-BAFKU₂. Their chemical formula, the symbolic representation of their macromolecules, and also the principle of crosslinking in the bulk materials is shown in **Scheme 27**, while their outward appearance can be seen in **Figure 5**. These copolymers used the same mesogen BAFKU like the grafted ones, and the LC volume fraction was in a similar range (52.4 to 13.5 Vol.%). However, the different bonding situation of the LC units had profound effects on material properties.

In contrast to the above-discussed grafted copolymers, the LC-end-capped ones were all nominally liquid at standard room temperature (25°C). The approximate melting points were 22°C (H03-BAFKU₂), 8°C (H11-BAFKU₂), and -15°C (H21-BAFKU₂). The two copolymers with the longer PDMS chains (H11-BAFKU₂ and H21-BAFKU₂) are oily liquids at laboratory temperature, which possess a dark red colour (transparent in thin layer; see **Figure 5**), the same like molten BAFKU.



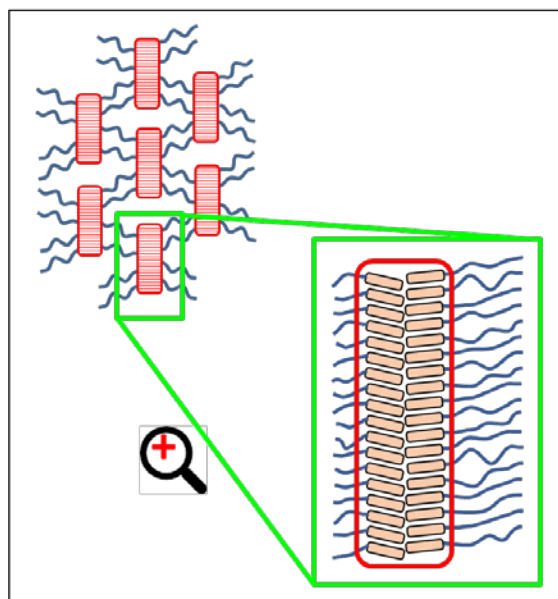
H03-BAFKU₂



H11-BAFKU₂



H21-BAFKU₂



Scheme 27: LC-end-capped copolymers: (top): general chemical structure; (bottom): symbolic representation of the macromolecules of the studied copolymers H03-BAFKU₂, H11-BAFKU₂, and H21-BAFKU₂, as well as of the physical crosslinking in them.

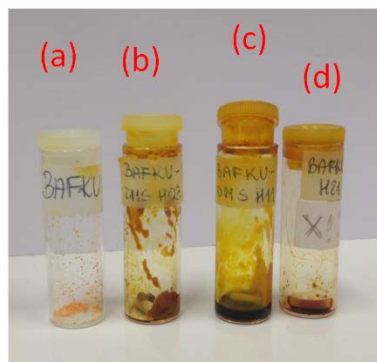
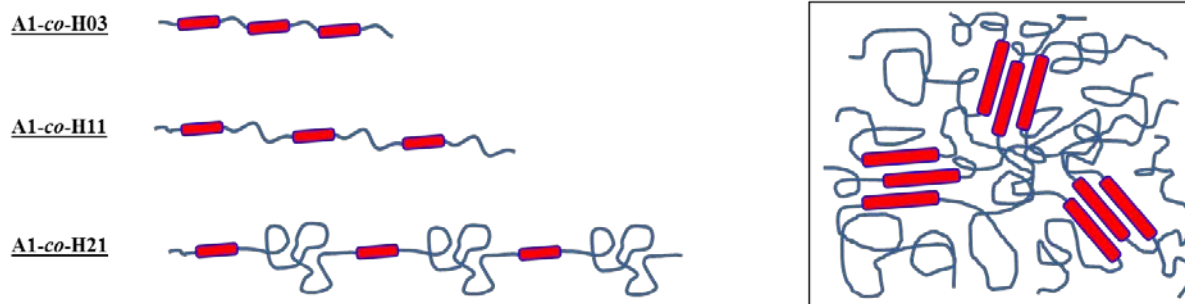
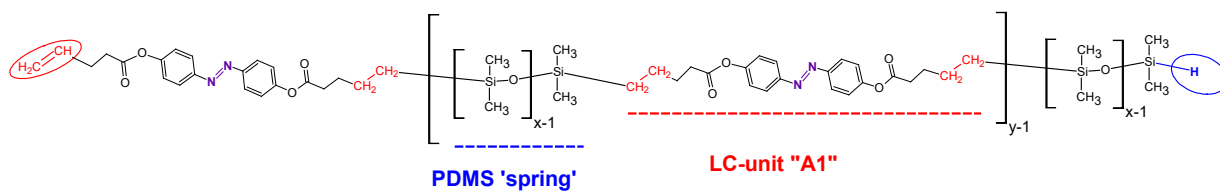


Figure 5: Appearance of the grafted LC-end-capped copolymers (a) neat BAFKU mesogen; (b) the soft waxy H03–BAFKU₂; (c) the oily H11–BAFKU₂; (d) the oily H21–BAFKU₂.

The shortest copolymer, which is the richest in BAFKU: 52.4 Vol.%, see **Table 11** further below), has a pasteous consistence at the typical laboratory temperature, albeit it can freeze to a waxy brittle material on colder days. Its colour is orange, somewhat darker than that of polycrystalline BAFKU. At higher temperatures, as a thin melt, H03–BAFKU₂ also is dark red, like the other (liquid) copolymers from this family. All the BAFKU-end-capped copolymers can be dissolved in chloroform, tetrahydrofuran or toluene.

5.1.5.3 Linear infinite PDMS-LC copolymers of azo type

Copolymers based on the divinyl-functional azo-type mesogens A1 and A12 are related to the above-discussed PDMS-BAFKU copolymer families, because the A-type mesogens are highly similar to BAFKU: A12 practically is a vinyl-bifunctional modification of BAFKU. A1 also is highly similar, but it has distinctly shorter alkyl tails attached to the aromatic core. Hence, it was of interest to evaluate the effect of the alkyl tails on the calamitic LC units A1 and A12 in case of copolymers with highly flexible PDMS chains.



Scheme 28: Linear infinite PDMS-LC copolymers of azo type: (top): general chemical structure on the example of a copolymer containing the A1 mesogen ; (bottom): symbolic representation of the macromolecules of the studied copolymers with incorporated PDMS 'spring segments' H03, H11, and H21, as well as of the physical crosslinking in this type of copolymers; copolymers with the A12 mesogen (shown in **Scheme 21**) have an analogous structure.

The general chemical formula (on the example of A1-co-PDMS), the symbolic representation of the macromolecules (which have the same architecture with A1 and A12), and also the principle of crosslinking in the bulk materials is shown in **Scheme 28**. The outward appearance of the synthesized and studied copolymers A1-co-H03, A1-co-H11, A1-co-H21, A12-co-H03, A12-co-H11, and A12-co-H21 can be seen in **Figure 6**.

All the copolymers based on A1 or A12 (see **Figure 6**) have a dark red colour in the liquid or in the rubbery state, similarly like molten A1, A12 or BAFKU. The A1-based copolymers are all liquid or nearly liquid at standard laboratory temperature: A1-co-H03 starts to melt between 25 and 30°C, A1-co-H11 gradually melts between -40 and 0°C, while A1-co-H21 relatively abruptly melts between -40 and -30°C. The analogous copolymers with the A12 mesogen display distinctly higher melting points: A12-co-H03: between 40 and 60°C, A12-co-H11 between 0 and 50°C (gradual) and A12-co-H21 between -10 and +30°C (gradual). The latter copolymer appears liquid-like at laboratory temperature, while the other A12 copolymers are rubbery or very soft rubbery at the same conditions (see **Figure 6 f, g**). All of the above-discussed copolymers can be dissolved in chloroform, tetrahydrofuran or toluene.

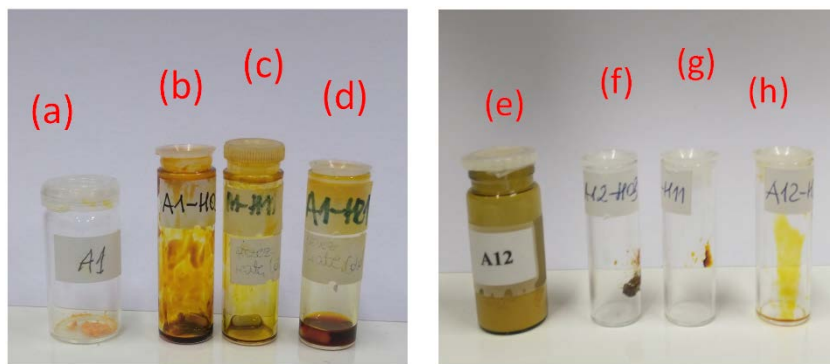
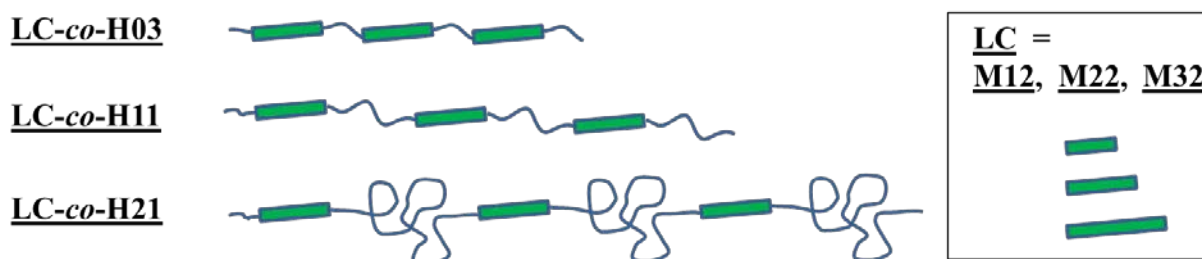


Figure 6: Appearance of the linear infinite LC-PDMS copolymers of azo-type: (a) neat A1 mesogen; (b) the oily A1-co-H03; (c) the oily A1-co-H11; (d) the oily A1-co-H21; (e) neat A12 mesogen; (f) the rubbery A12-co-H03; (g) the soft rubbery A12-co-H11; (h) the oily A12-co-H21; the powdered mesogens A1 and A12 have an orange colour similarly like BAFKU.

5.1.5.4 Azo-free linear infinite PDMS-LC copolymers

The last group of synthesized and studied copolymers also belonged to the linear infinite LC-PDMS type. These copolymers were fully analogous to the ones with azo mesogens, but contained instead the azo-free divinyl-functional M12, M22 or M32 LC units which had the same (M12) or a distinctly larger size M22 and M32 than A12 or BAFKU. Each mesogen was combined with the hydrido-PDMS precursors H03, H11 and H21 (see *Scheme 29*). The appearance of the copolymers' series based on M12 and on M32 is shown in *Figure 7*.

The pure copolymers were colourless (see example in *Figure 7 h*), but usually, if the residue of the Karstedt catalyst was not removed by adsorption on carbon black, these products had a dark coloration due to the presence of a precipitate of colloidal platinum (see *Figure 7*).



Scheme 29: Symbolic representation of azo-free linear infinite PDMS-LC copolymers, based on three different PDMS 'spring segments' H03, H11, and H21, and on three different linearly bonding LC units: M12, M22 and M32.

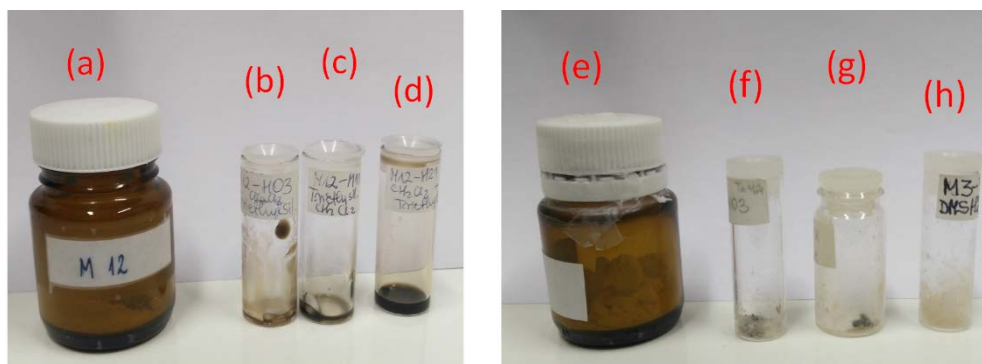


Figure 7: Appearance of the azo-free linear infinite LC-PDMS copolymers: (a) neat M12 mesogen; (b) the oily M12-co-H03; (c) the oily M12-co-H11; (d) the oily M12-co-H21; (e) neat M32 mesogen; (f) the brittle M32-co-H03; (g) the rubbery M32-co-H11; (h) the rubbery M32-co-H21.

The samples based on M12 (similarly like with A1) were either oily or close to melting at laboratory temperature. The nominal melting points of the M12-based copolymers, however, were even higher than in case of the copolymers with A12: ca. 40°C for M12-co-H03, 10 to 60°C (gradual, M12-co-H11), and 0 to 60°C (gradual, M12-co-H21).

The linear infinite copolymers based on M22 displayed dramatically higher melting points than those containing M12 (or its analogues A1 and A12), but they all can be molten without decomposition (PDMS rapidly depolymerizes at 180°C, so that experiment temperatures close to, or above 160°C were problematic). The melting points were: ca. 137°C for M22-co-H03, 112°C for M22-co-H11, and 110°C for M22-co-H21.

The copolymers with the even larger M32 mesogen displayed already very strong physical crosslinking, and most of them could not be ‘safely’ molten without at least partial damage to the PDMS segments. All could be dissolved in suitable solvents, however. The melting points were: 173°C for M32-co-H03, 152°C for M32-co-H11 and 95°C (+ viscoelastic step at 160°C) for M32-co-H21. The latter copolymer was processible by melting without any problems.

All of the above-mentioned copolymers were soluble in chloroform, tetrahydrofuran or toluene.

Table 11: Volume fraction of liquid crystalline component in the prepared copolymers.

Name of the sample	Volume % of LC component *
Grafted copolymers	
BAFKU ₈ -HMS 301	60.26
BAFKU ₄₁ -HMS 064	22.72
α,ω -LC terminated PDMS copolymers	
H03-BAFKU ₂	52.44
H11-BAFKU ₂	37.29
H21-BAFKU ₂	13.47
linear infinite LC-PDMS copolymers with azo-type mesogens	
A1- <i>co</i> -H03	34.17
A1- <i>co</i> -H11	21.99
A1- <i>co</i> -H21	6.88
A12- <i>co</i> -H03	42.85
A12- <i>co</i> -H11	28.94
A12- <i>co</i> -H21	9.47
azo-free linear infinite LC-PDMS copolymers	
M12- <i>co</i> -H03	43.56
M12- <i>co</i> -H11	29.53
M12- <i>co</i> -H21	9.90
M22- <i>co</i> -H03	48.36
M22- <i>co</i> -H11	33.71
M22- <i>co</i> -H21	11.76
M32- <i>co</i> -H03	51.00
M32- <i>co</i> -H11	36.12
M32- <i>co</i> -H21	12.91

*) The volume fractions of the mesogens were calculated as described in the Experimental Part.

5.1.6 Efficiency of the hydrosilylation coupling

As the reactants used in the synthesis of the studied copolymers were non-volatile, and also otherwise difficult to separate from the final products, a precise stoichiometric ratio, as well as a quantitative conversion was desired in all the syntheses. Achieving good precision in stoichiometric ratios was possible thanks to the precise determination of equivalent molar masses per SiH function via $^1\text{H-NMR}$, as described in the Experimental Part. The completion of the hydrosilylation coupling reaction between SiH-functional polydimethylsiloxanes and the vinyl-functional mesogens was quickly verified by means of FT-IR spectroscopy, as shown on two examples in **Figure 8**: Disappearance of the SiH stretching peak at 2120 cm^{-1} indicated the consumption of SiH, but the method was not very accurate, if the volume concentration of SiH was small. The $^1\text{H-NMR}$ spectroscopy was a highly sensitive and comprehensive analysis (see **Figure 9**: NMR spectra of the same samples which were analysed by FT-IR in **Figure 8**): The disappearance of both the SiH peak (near 4.7 ppm) and of vinyl peaks (near 4.9 and 5.7 ppm) could be followed. The rapid FT-IR analyses were very helpful in developing optimized (temperature, reaction time) synthesis procedures, while the NMR analyses were used for quantitative conversion analysis (and product purity check).

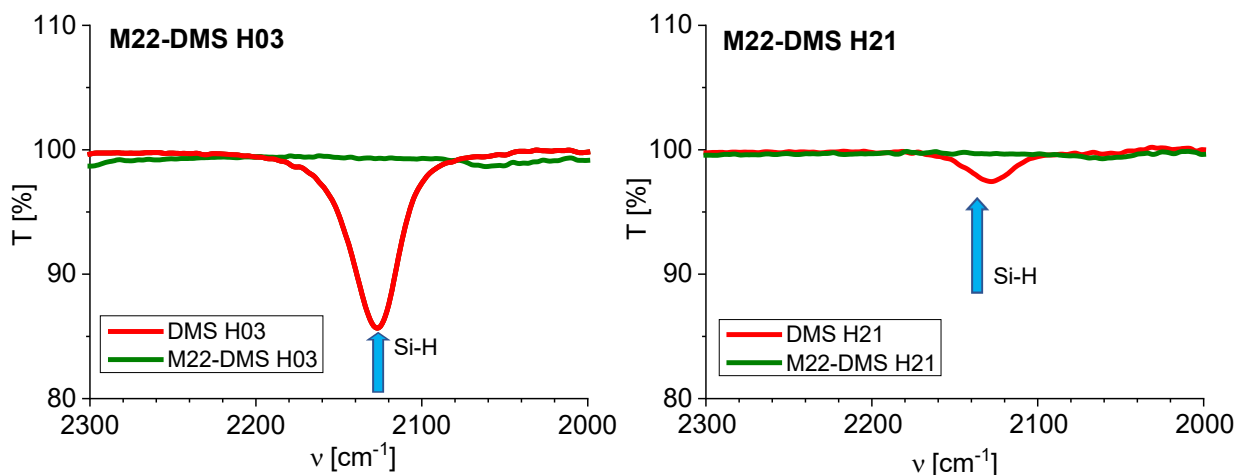


Figure 8: FT-IR analysis of the consumption of SiH groups on the example of the copolymers M22-co-H03 and M22-co-H21 (from the azo-free linear infinite LC-PDMS copolymers group).

Among the **grafted LC-PDMS copolymers**, the reaction went smoothly for the reactant pair HMS301/BAFKU, while it was more difficult with HMS064/BAFKU, which was documented by its $^1\text{H-NMR}$ spectrum (see **Appendix 1 - Supplementary Information**). There, for BAFKU₄₁-HMS064 synthesized using the optimized procedure, a small residue peak from

unreacted SiH groups still persists, as well as less visible residue signals of un-reacted vinyl groups. The signals correspond to ca. 3.3% of un-reacted functions. Longer reaction times or higher synthesis temperatures led to an increasing prominence of side reactions. The dilution of the functional groups on one hand, as well as the sterical crowding at the quartets of SiH groups on the precursor on the other, might have contributed to the less than quantitative conversion.

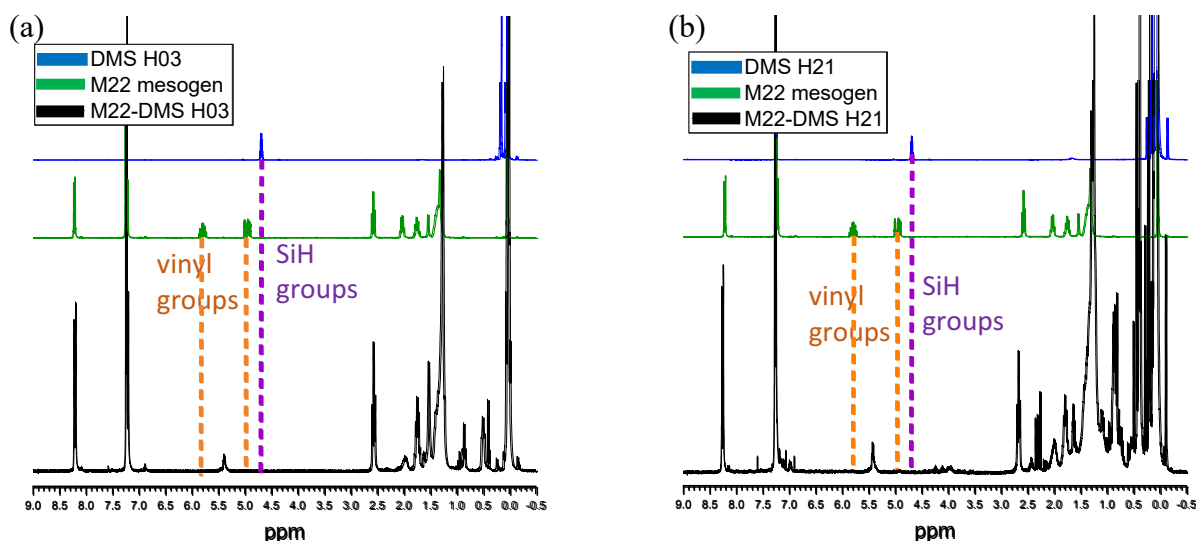


Figure 9: ¹H-NMR analysis – overlay of spectra demonstrating the consumption of SiH groups and of vinyl groups on the example of the copolymers M22-co-H03 (a) and M22-co-H21 (b) from the azo-free linear infinite LC-PDMS copolymers group; the overlays include the spectra of the respective neat hydrido-silanes (top, blue line), of the neat M22 mesogen (middle, green line) and of the respective copolymer (bottom, black line); the copolymer spectra are strongly zoomed, so that 3 mol % of residual functional groups would generate peaks of similar size like the reference signals of the functional groups.

For **LC-end-capped PDMS polymers**, a quantitative (100%) conversion was easily achieved in all cases, as confirmed by the sensitive ¹H-NMR analysis (see *Appendix 2 - Supplementary Information*).

In case of the **linear infinite LC-PDMS copolymers** with the vinyl-bifunctional **azo mesogens A1 and A12**, the conversion of the SiH and vinyl groups was rapid, but the crosslinking side-reactions discussed further above presented the most serious problem, especially with smaller mesogen molecules and short PDMS spacers (which led to high concentrations of vinyl groups in the reaction mixtures). This led to reduced yields of soluble

linear polymers. $^1\text{H-NMR}$ spectra, in which, typically, there were no functional group residues at all, are shown in *Appendix 4*.

The **azo-free linear infinite LC-PDMS copolymers** with the vinyl-bifunctional **mesogens M12, M22 and M32** displayed similar behaviour during synthesis like their azo analogues (rapid and easy reaction, but also crosslinking side reactions). Their $^1\text{H-NMR}$ spectra are shown in *Appendix 6*.

5.1.7 Molecular masses of the copolymers

The molecular masses of the prepared copolymers were characterized by several methods, which showed different accuracy. Most universal, albeit not always highly accurate, was the size exclusion chromatography (SEC, “GPC”) with polystyrene standard calibration for the range of 100–500 000 g/mol, and with simultaneous UV/Vis-refraction-index- (at $\lambda = 254$ nm) and evaporative-light-scattering- (ELSD; laser: $\lambda = 658$ nm) detection. Alternative methods, which yielded highly accurate results in selected cases, but which could not be applied on the whole collection of prepared copolymers, were the MALDI-TOF- (matrix-assisted laser desorption ionization / time of flight mass spectroscopy: applicable only for smaller macromolecules) and the $^1\text{H-NMR}$ -end-group analysis (often not applicable because of absence of such groups with isolated easily integrable signals).

In case of the **grafted LC-PDMS copolymers**, (see *Appendix 1* and its *Supplementary Information*), all the above-mentioned methods of molecular mass determination proved to be of problematic accuracy. The GPC analysis provided some valuable information about these copolymers, but it was not well-suited to analyse their molecular masses with high precision. Probably due to inter- and intra-molecular interactions of LC units, the copolymers displayed marked deviations from expected mass spectra: the molecular mass increase expected to arise from the grafting could not be verified by GPC, albeit the order of magnitude of the measured molecular masses was correct. Due to detector specifics (and in contrast to NMR), the content of non-bonded BAFKU mesogen was grossly over-estimated by GPC, because of the high sensitivity of both detectors wavelengths to BAFKU (see details in *Appendix 1 - Supplementary Information*). MALDI-TOF was not suitable for analysing the most interesting product, BAFKU₄₁–HMS064, because of its high molecular mass (72 000 g/mol), while for molecular

mass evaluation by $^1\text{H-NMR}$ -end-group analysis, suitable end groups with isolated signals were missing. Hence, the nominal molecular masses of the grafted copolymers only could be obtained using the (viscosimetrically determined) molecular masses of the PDMS precursors provided by the supplier, the known molecular mass of BAFKU, and the analytic information ($^1\text{H-NMR}$) about the number of SiH grafting positions per nominal average precursor molecule, as well as the confirmation of (nearly) quantitative conversion by $^1\text{H-NMR}$.

In case of the **LC-end-capped PDMS polymers**, the molecular masses were evaluated using $^1\text{H-NMR}$ spectroscopy (end group analysis: ratio of terminal groups to PDMS repeat units), as well as by GPC, and by MALDI-TOF (the results are shown in *Appendix 2* and its *Supplementary Information*). The latter two methods were useful for characterizing molecular mass distributions. The $^1\text{H-NMR}$ spectroscopy provided highly accurate values of the number average molecular masses of the PDMS precursors. In combination with the confirmed quantitative conversion ($^1\text{H-NMR}$), these results made it possible to obtain highly precise number-average molecular masses of the copolymers. A direct molecular mass determination using the signals of the LC moieties as end groups also theoretically is possible, but because of great differences in relaxation behaviour of protons on PDMS and on the benzene rings of the LC units, special precautions are to be taken for the analysis (long relaxation times between pulses, see also *Appendix 2 - Supplementary Information*). As for the GPC analysis, it generally provided relatively accurate molecular mass values for all the PDMS–BAFKU₂ copolymers (albeit the content of non-bonded BAFKU is over-estimated, similarly like in the grafted copolymers). MALDI-TOF yielded very accurate values for the copolymers H03–BAFKU₂ and H11–BAFKU₂, but the vaporization of H21–BAFKU₂ was no more successful, similarly like in case of neat H21, due to the too high molecular mass.

In case of the **linear infinite LC-PDMS copolymers with azo-type mesogens A1 and A12** (similarly like in case of their azo-free analogues), the determination of molecular masses was very interesting, also for evaluating the subsequently studied material properties. In case of the further-above-discussed LC-grafted and LC-end-capped copolymers, the molecular masses of defect-free products were determined by the molecular masses of their PDMS precursors. In the

linear infinite copolymers, however, the synthesis reaction is a polyaddition of two bifunctional components, which could yield very different molecular masses of the resulting products.

The linear infinite LC-PDMS copolymers theoretically possess one vinyl and one SiH end group per macromolecule (see *Scheme 20* or *28*), if these groups are not destroyed by a defect. However, these groups were usually not visible after completed synthesis, so that end group analysis by $^1\text{H-NMR}$ could not be employed. As for MALDI-TOF, the unknown molecular masses could be potentially too high, so that accurate results could not be guaranteed. Hence, the only method to evaluate the molecular masses of the linear infinite LC-PDMS copolymers was GPC.

The GPC results obtained for the **A1-co-PDMS** and **A12-co-PDMS** copolymers are shown in *Appendix 4*, while the results are summarized in *Table 12*.

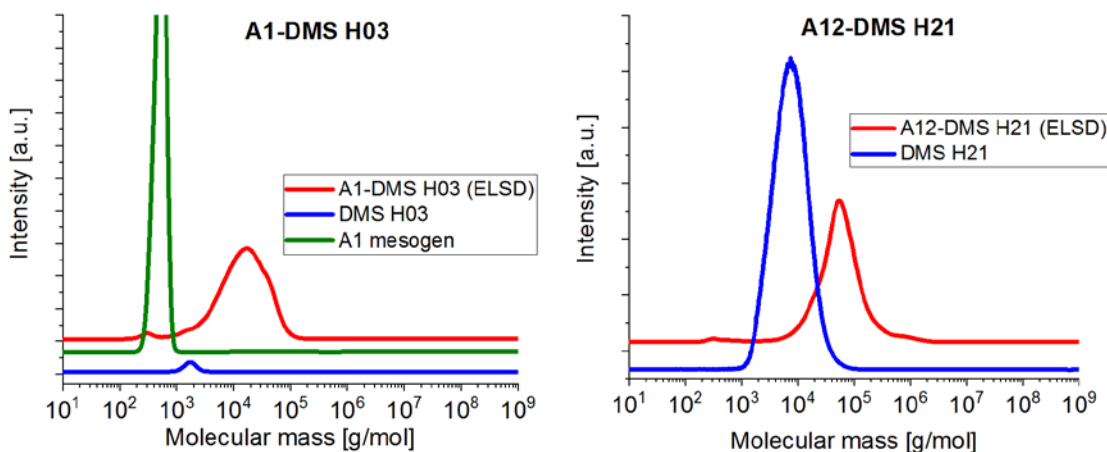


Figure 10: Exemplary GPC traces of linear infinite LC-PDMS copolymers based on azo-type mesogens, with overlaid traces of the neat PDMS and LC components.

As can be noted from *Table 12*, the molecular masses achieved in the A1-co-PDMS and A12-co-PDMS copolymers ranged approximately between 10 000 and 40 000 g/mol (compare: H03 precursor: 624 g/mol; H21 precursor: 4 764 g/mol), according to polystyrene standard, while the polydispersities were in the range between 1.6 and 3.7; the highest molecular weight was achieved in the copolymer A12-co-H21. The number of ‘macro-repeat-units’ LC-PDMS (e.g. A12-H11) per average copolymer macromolecule was also calculated in *Table 12*: It can be seen, that this number (which ranged between 5 and 13) initially moderately increases if going from the shorter PDMS spacer H03 to the longer H11. But in case of the longest PDMS spacer H21, the

number of macro-repeat-units always is the lowest (see **Table 12**), in spite of the highest molecular weight, which was always achieved with the longest spacer. This effect seems to be connected with reaction statistics: The functional groups are relatively diluted in the LC / H21 mixture, and as the reaction progresses, it is increasingly difficult for the rare and spatially separated chain ends to achieve reactive contact with each other (the H21 spacer alone has 64 repeat units). Similarly like in case of the BAFKU-based copolymers, the peaks of “unreacted” mesogens appear over-estimated in some of the GPC spectra in **Appendix 4**, as they do not correspond with eventual residual vinyl signals in the NMR spectra.

Table 12: Results of GPC analysis of the linear ‘infinite’ LC-PDMS copolymers based on azo-type mesogens A1 and A12: number-average molecular masses, polydispersity, as well as number of alternating LC-PDMS ‘pairs’ (= coefficient *n* in **Scheme 20** or *y* in **Scheme 28**).

Names of samples	M_n according to GPC [g/mol]	Polydispersity index []	Number of alternating LC-PDMS ‘pairs’
A1-co-H03	8 472	2.43	8.45
A1-co-H11	19 558	1.59	12.42
A1-co-H21	25 046	1.77	4.87
A12-co-H03	13 266	2.32	11.33
A12-co-H11	22 459	3.73	12.88
A12-co-H21	36 408	2.56	6.86

In case of the **azo-free linear infinite LC-PDMS copolymers with the mesogens M12, M22 and M32** (see GPC traces in **Appendix 6**), the achieved nominal molecular masses (according to polystyrene standard) were approximately two times lower, between 6 000 and 22 000 g/mol, than in case of the analogous copolymers with A1 and A12, as can be seen in **Table 13**. Correspondingly, also the number of macro-repeat-units in the azo-free linear infinite

copolymers is approximately two times smaller than in the azo-analogues: it ranges between 2.5 and 7 (see **Table 13**). The copolymers based on the mesogens of “M-type” also have a narrower distribution of molecular masses: their polydispersity index ranges between 1.5 and 2.6. The highest molecular mass (22 000 g/mol) was achieved in the copolymer M22-*co*-H21. Similarly like in case of the infinite linear copolymers with azo LCs, also in the azo-free systems the copolymers with the longest PDMS spacer H21 achieved the highest molecular masses but contained the fewest macro-repeat units (LC-PDMS pairs).

Table 13: Results of GPC analysis of the azo-free linear ‘infinite’ LC-PDMS copolymers based on the mesogens M12, M22, and M32: number-average molecular masses, polydispersity, as well as number of alternating LC-PDMS ‘pairs’ (= coefficient “*n*” in **Scheme 20** or “*y*” in **Scheme 28**).

Names of samples	M_n according to GPC [g/mol]	Polydispersity index []	Number of alternating LC-PDMS ‘pairs’
M12- <i>co</i> -H03	6 299	2.58	5.31
M12- <i>co</i> -H11	8 391	2.40	4.77
M12- <i>co</i> -H21	13 541	2.39	2.54
M22- <i>co</i> -H03	9 028	1.82	6.91
M22- <i>co</i> -H11	10 826	2.51	5.76
M22- <i>co</i> -H21	21 676	1.76	3.98
M32- <i>co</i> -H03	8 100	1.50	5.86
M32- <i>co</i> -H11	11 925	1.84	6.10
M32- <i>co</i> -H21	14 431	1.72	2.61

In view of the results, it should be noted, that the true molecular masses of the linear infinite LC-PDMS copolymers could be different from the ones determined by GPC, because of the calibration with polystyrene standard, and secondly, because of possible inter- or intramolecular interactions of LC units of the macromolecules. In case of the grafted high-molecular copolymer BAFKU₄₁-HMS064, which contained numerous LC quartets separated by

long spacers (68 repeat units long, similar like H21 which has 64), the intramolecular effects obviously prevailed (internal physical crosslinks, tighter-packed polymer coils) and led to an apparently lowered ‘GPC mass’. As the LC-LC interactions become very strong if going from linear copolymers with M12 to the ones with M32, such interactions might play a greater role in the latter.

Finally, it should be noted, that even a moderate (ca. 6 in M22-*co*-H11, or in M32-*co*-H11), or a relatively low (4 or 2.6 in M22-*co*-H21, or M32-*co*-H21, respectively) number of macro-repeat units was able to support very strong reversible crosslinking, as will be discussed below in view of the thermo-mechanical properties. The copolymer M32-*co*-H11 even could not be safely molten (m.p.: ca 150°C), due to the danger of an onset of thermal degradation of its PDMS segments. The mentioned copolymer was re-processible only by dissolution. Higher molecular masses (more macro-repeat units) in the linear infinite copolymers hence could be even disadvantageous in some cases, where an excessive number of physically crosslinking LC units could raise the melting point too much.

5.2 Thermo-mechanical properties of the copolymers (DMTA)

The thermo-mechanical properties of the copolymers are important characteristics in view of their possible application field, such as reversible elastomers, as smart viscoelastic liquids or coupling materials, or as energy-absorbing damping materials. In **Figure 11**, an overview is shown of the prepared copolymers, grouped into structural families: Each copolymer is labelled with an icon describing its thermo-mechanical characteristics, as well as its consistence at room temperature. The main groups are: “waxes”, which are brittle (vitrimeric) in the solid state, and which melt without forming a rubbery phase (see characteristics of exemplary copolymers in **Figure 12**); “rubbers”, which are glassy at very low temperatures, rubbery in a significant temperature region (including laboratory temperature), and which can be re-melted at sufficiently high T (see examples in **Figure 14**); and finally “smart oils” which are liquid at room temperature, but which typically still contain physical crosslinks in the liquid phase (see examples in **Figure 15** and **16**).

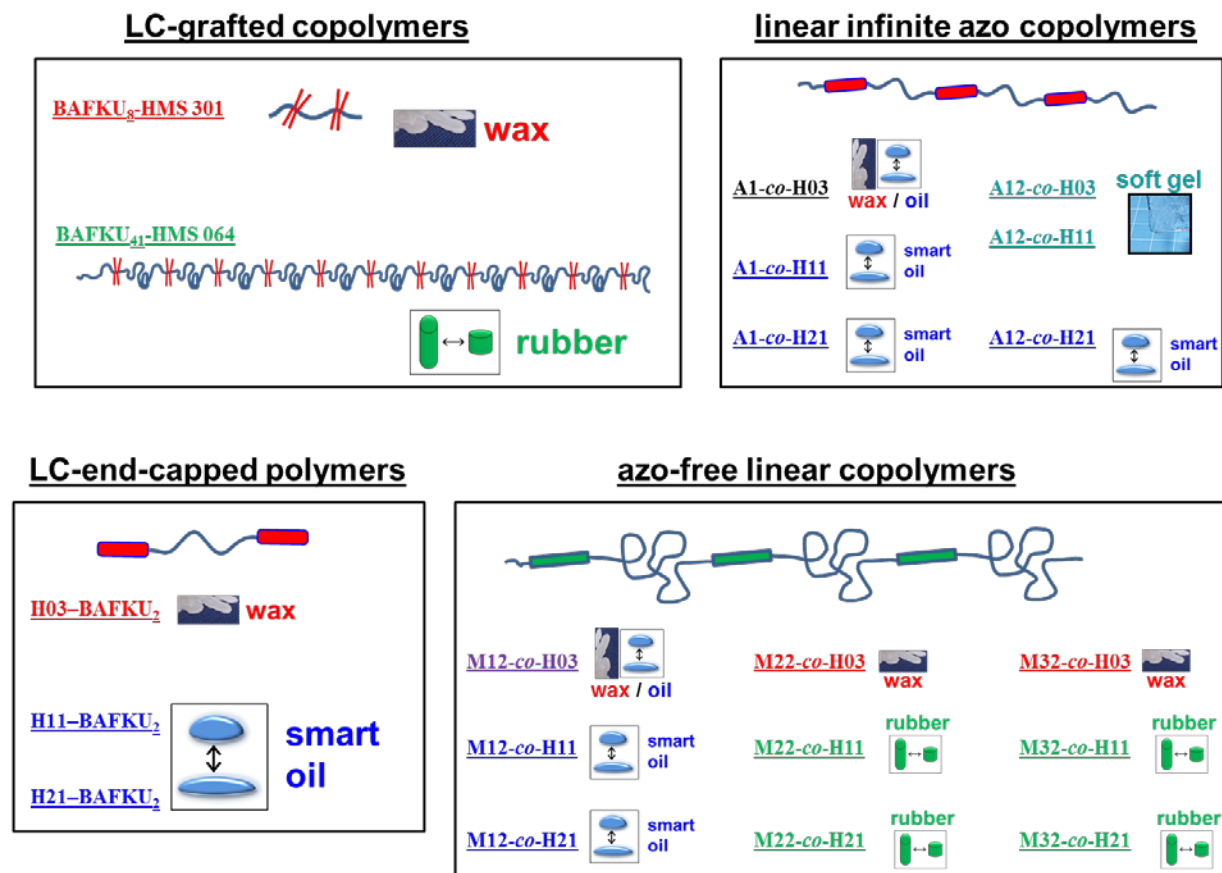


Figure 11: Overview of the prepared copolymers with respect to their thermo-mechanical properties and their consistence at laboratory temperature.

Special cases were “wax / oil” or “soft gel” materials, which represent waxy or rubbery products close to melting at laboratory temperature.

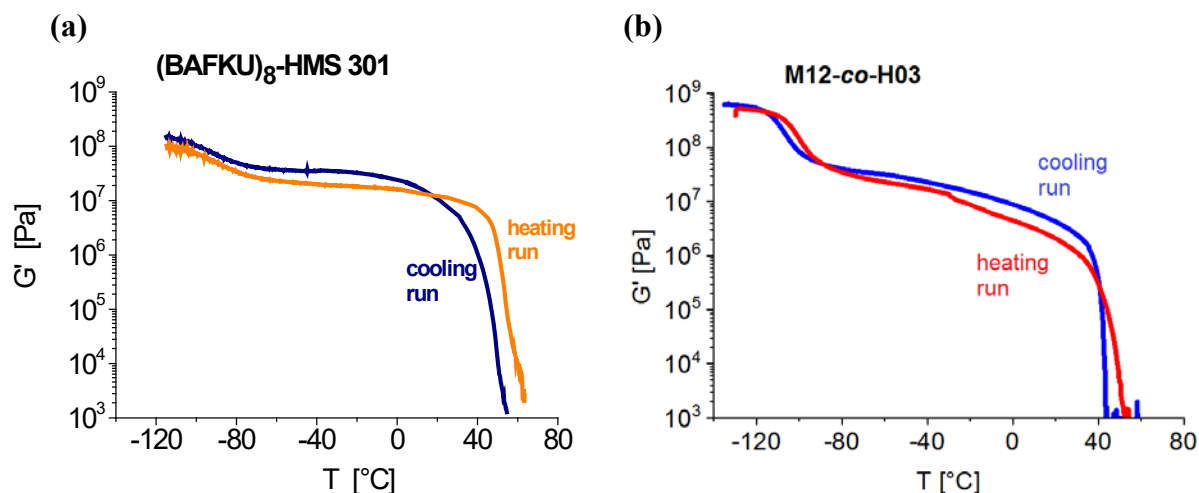


Figure 12: DMTA profiles (temperature-dependent storage modulus G' only) of two exemplary waxy, LC-rich copolymers: (a) $(\text{BAFKU})_8\text{-HMS301}$ and (b) M12-co-H03 , recorded as heating and cooling scans.

As can be read from **Figure 11**, the materials which are the richest in mesogens, namely such with the shortest PDMS spacers, typically belong to the group of “waxes”. Strong rubbers were obtained in copolymers based on medium or longer PDMS spacers, in case of the grafted- and of the linear infinite copolymer families (in the latter case only with larger mesogens). The LC end-capped-, and also the linear infinite copolymers with small mesogen units mainly belonged to the group of “smart liquids”.

In **Figure 12–16**, selected results of dynamic-mechanical thermal analysis (DMTA) of the prepared copolymers are shown, in order to illustrate the discussed structure-property relationships in the studied copolymers. The complete sets of result data are in **Appendix 1 - Supplementary Information**, **Appendix 2 - Supplementary Information**, **Appendix 4**, and in **Appendix 6**). The performed DMTA tests extended over a wide range of sample consistence, ranging between glassy material and polymer melt. The tests were nevertheless performed using a single experimental setup, namely small parallel-plates (diameter: 6.1 mm). This geometry made possible reasonably accurate characterization in the glassy state, as well as in the early stage of melting, and ideally accurate characterization in the rubbery state.

The **effect of copolymer architecture** can be evaluated, if products are compared which are based on the same (or nearly identical) LC units and on PDMS spacers of the same length

between them. Such an exemplary set is given in **Figure 13**, where the DMTA profiles of BAFKU₄₁-HMS064 (grafted type, contains 10–11 grafting sites with LC quartets, separated by long PDMS spacers; $M_n = \text{ca. } 72\,000 \text{ g/mol}$), A12-co-H21 (linear ‘infinite’ one, contains ca. 7 LC-PDMS macro-repeat-units, $M_n = \text{ca. } 36\,000 \text{ g/mol}$), and of H21-BAFKU₂ (LC-end-capped: one macromolecule contains 2 LC units; $M_n = \text{ca. } 5\,600 \text{ g/mol}$) are shown. It can be observed in **Figure 13**, that the grafted copolymer distinctly has the highest melting point of the rubbery phase and the widest rubbery plateau, while the LC-end-capped copolymer displays the ‘worst’ results in this respect.

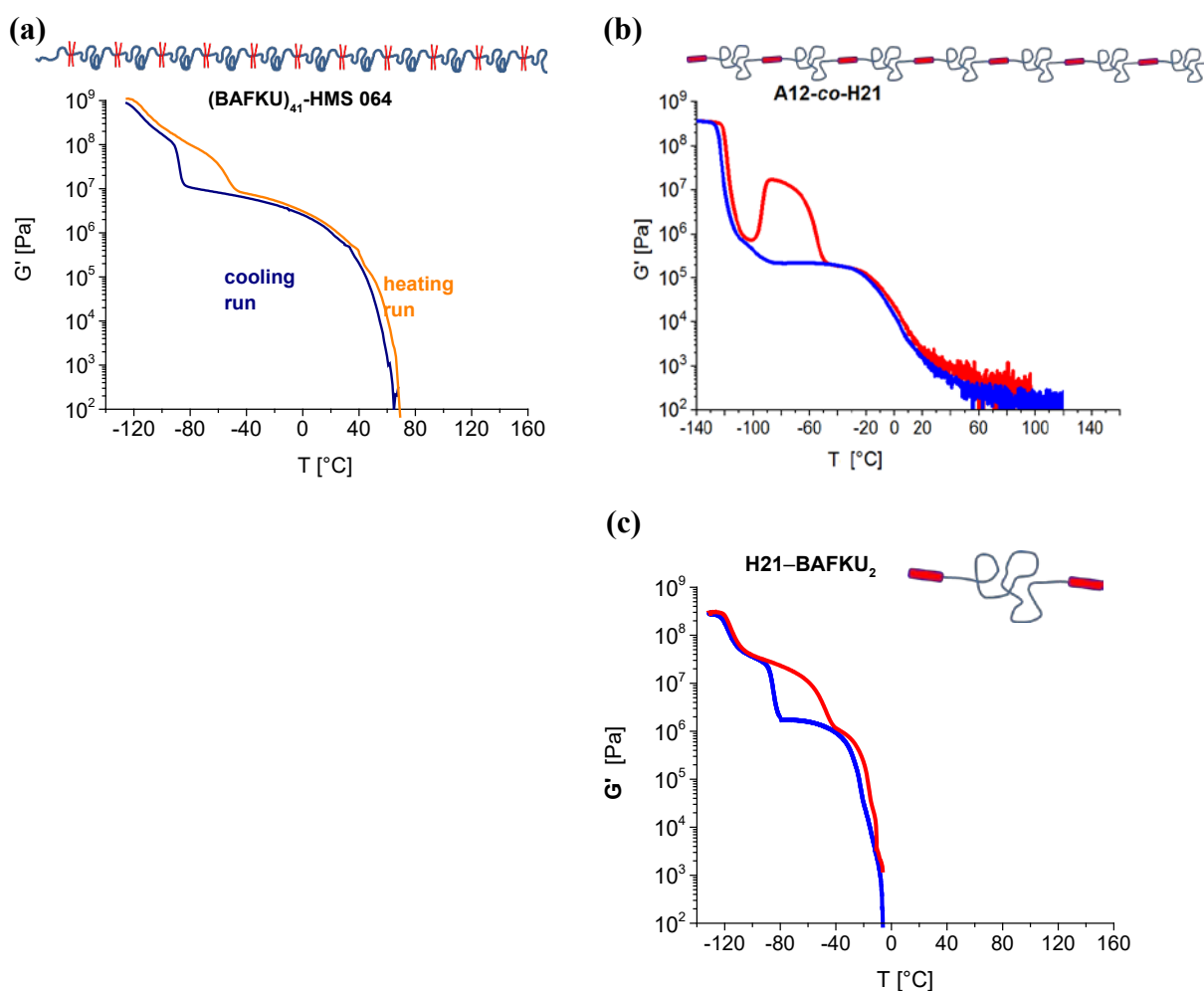


Figure 13: DMTA profiles (temperature-dependent storage modulus G' only) of three copolymers physically crosslinked by BAFKU, or by its divinyl-analogue A12, and containing PDMS spacer segments of the same length (68 repeat units in HMS064 and 64 r.u. in H21): (a) BAFKU₄₁-HMS064, (b) A12-co-H21, and (c) H21-BAFKU₂, recorded as heating and cooling scans; the “x” and “y” axes are at the same scale in all three graphs.

The efficiency of crosslinking in BAFKU₄₁–HMS064 most likely is enhanced by the high number of BAFKU graft positions, namely 10.4 in average (see structure in *Scheme 26* further above), as well as by the fact that four mesogen units are attached at each graft position. In this way, even a small crystallizing pendant group like BAFKU achieves a considerable crosslinking effect. In case of A12-*co*-H21, the number of crosslinking positions per molecule (= number of isolated LC units in this case) is comparable but smaller (7), while the molecular mass, and also the mesogen volume fraction is two times smaller (9.5% vs. 22.7%, see *Table 11*). However, if the linear copolymer A12-*co*-H11 is considered (DMTA: see *Figure 17b*), which contains even more mesogen than BAFKU₄₁–HMS064 (28.9 Vol.% vs. 22.7 Vol.%), and also more crosslinking sites (ca. 13 per macromolecule, see *Table 12*), it still melts at lower temperatures than BAFKU₄₁–HMS064, namely at ca. +15°C (melting region: 0 to 40°C), while the grafted copolymer melts near +60°C. Also in case of the LC-end-capped copolymer H21–BAFKU₂, the LC volume fraction is lower than in BAFKU₄₁–HMS064 (13.5% vs. 22.7%), but again, if the LC-end-capped copolymer H11–BAFKU₂, which contains 37.3 Vol.% of mesogen is compared with BAFKU₄₁–HMS064, it is still the grafted product, which has a distinctly higher melting point (+60°C vs. ca +10°C) and a (moderately) wider temperature region of the rubbery phase. The physical crosslinking in the LC-end-capped copolymers appears to be limited by the fact, that only 2 LC units are bonded per macromolecule. On the other hand, the LC-end-capped architecture displayed very interesting phase behaviour, as will be discussed further below. Concerning the comparison of the linear infinite and grafted architectures it should be noted, that **the melting points of the grafted copolymers were close to the clearing point of the grafted mesogens** (albeit also not far above the first solid→liquid crystal transition), while **in case of all the linear infinite copolymers, the melting points were observed at temperatures distinctly lower than the ones of the first respective solid→liquid crystal transition. In the LC end-capped copolymers, the melting point was even further depressed.**

The length of the PDMS spacer segment in the studied copolymers expectedly had a marked effect on the thermo-mechanical properties: the shortest spacer segments H03 (8.6 repeat units) or the ones in HMS301-based systems (9 repeat units) yield waxy LC-PDMS copolymers. Longer PDMS chains, such as H11 (16 repeat units) or H21 (64 repeat units) were needed to achieve rubbery elasticity (in the region between T_g and melting point) in the copolymers physically crosslinked by LC units (see *Figure 14* and *15*). The mid-sized elastic chains H11 yielded rubbery materials which had higher moduli (due to shorter chains), higher melting points,

and a wider rubbery plateau (due to easier aggregation of LC units), while in case of the H21 chains, dilution effects lead to less efficient physical crosslinking and to lower melting points (see **Figure 14** and **15**). Entanglements of the longer H21 chains are not efficient enough for compensating the dilution effect, but they cause more gradual melting in comparison to copolymers with H11 chains (see **Figure 14** vs. **15**). In case of the grafted copolymers, only one elastomer was obtained so that the effect of dilution by longer PDMS chains could not be studied, but it can be expected to occur in analogy to the other copolymers.

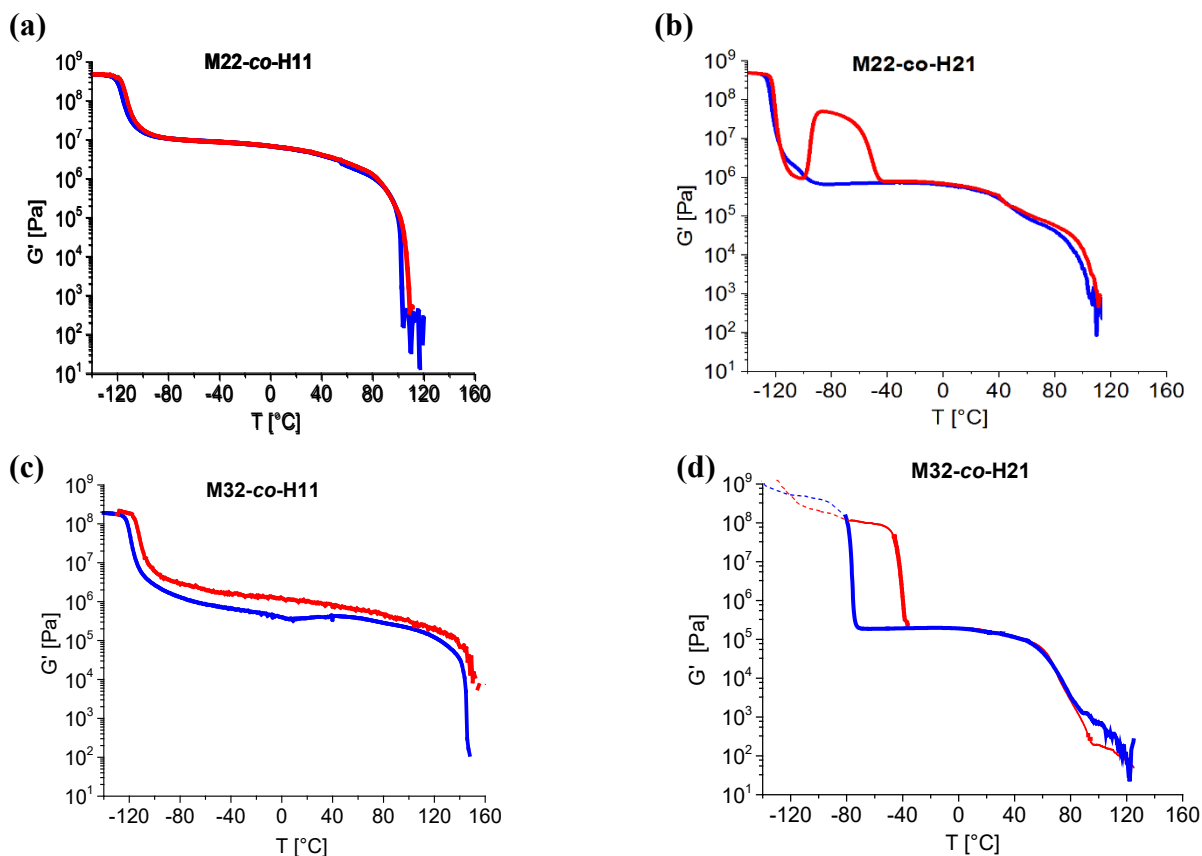


Figure 14: DMTA profiles the rubbery azo-free linear infinite copolymers: (a) M22-co-H11, (b) M22-co-H21, (c) M32-co-H11, and (d) M32-co-H21, recorded as heating and cooling scans.

The size of the incorporated LC units expectedly had a tremendous effect on the thermo-mechanical properties of the copolymers: In **Figure 14** and **16**, the DMTA profiles of the rubbery azo-free linear infinite copolymers based on the “M” mesogens are shown. The diaromatic mesogen M12 displays only a moderate crosslinking effect, as can be seen in **Figure 16**, which leads to low melting points and small rubbery plateaus. Replacing M12 with its triaromatic homologue M22 led to a tremendous increase in the melting point (by ca. 100°C, and to the occurrence of an extended well-established rubbery region (see **Figure 14** a, b). In case of

the tetraaromatic mesogen M32, the melting point is further increased (by 40°C) and the rubbery plateau widened, if the spacer is H11. Between the diluted systems with H21 chains, there is little difference if M22 is replaced by M32, however.

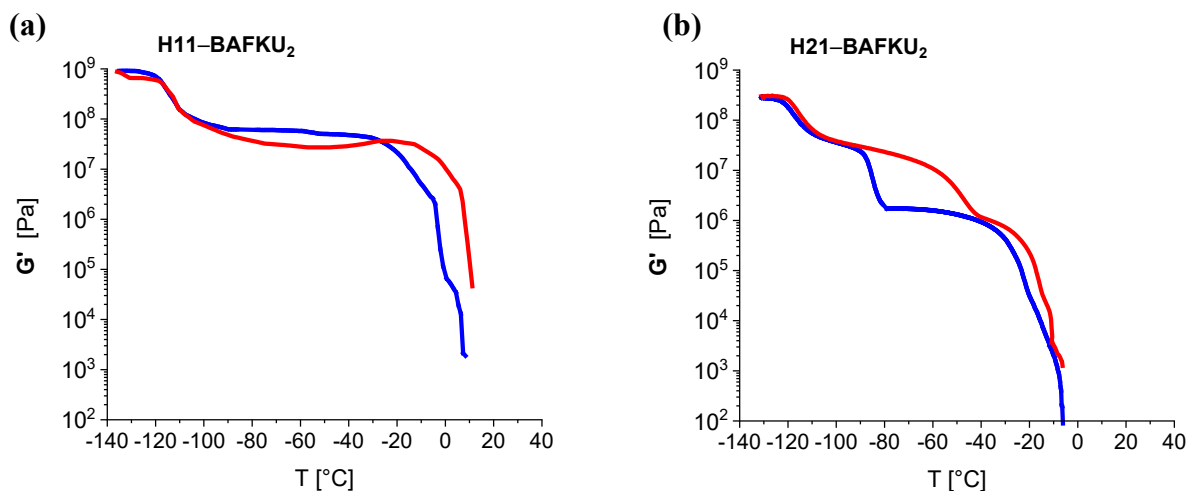


Figure 15: DMTA profiles (temperature-dependent storage modulus G' only) of the LC-end-capped copolymers (a) H11-BAFKU₂ and (b) H21-BAFKU₂, which are oily at ambient conditions and rubbery at low temperatures, recorded as heating and cooling scans.

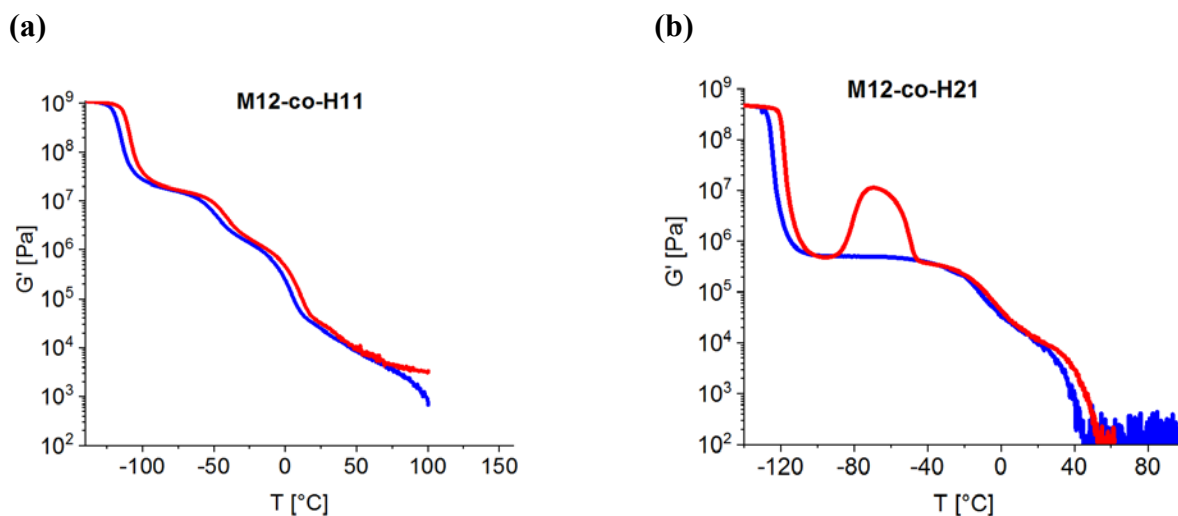


Figure 16: DMTA profiles (temperature-dependent storage modulus G' only) of the weakly crosslinked linear infinite copolymers containing the M12 mesogen: (a) M12-co-H11 and (b) M12-co-H21, which are oily at ambient conditions and rubbery at low temperatures, recorded as heating and cooling scans.

Hence, the most efficiently crosslinked system is M32-co-H11, which melts near 160°C, so that its re-melting becomes problematic due to the possible onset of PDMS degradation. Also, the solubility of M32 in the mentioned good solvents chloroform, THF and toluene was only moderate at room temperature, so that a moderately elevated temperature (60°C) was needed to dissolve this mesogen during copolymer synthesis. Larger mesogens of similar structure hence could be expected to be difficultly compatibilized with the PDMS component during copolymer synthesis.

Effect of the **different length of alkyl tails in the mesogens A1 and A12**: The linear infinite copolymers based on the azo-mesogens A1 and A12 generally display similar DMTA profiles like the copolymers based on M12. The A1-based products have distinctly lower melting points than their M12 analogues, however. The A12-derivatives have distinctly higher melting points than the A1-analogues, and they even exceed the melting points of the M12-based copolymers. The different consistence of the A1- and A12-based copolymers also is noted in the **Figure 11** further above. The **Figure 17** shows DMTA profiles of two analogous linear infinite copolymers of azo-type, namely A1-co-H11 (an oil) and (b) A12-co-H21(a soft gel). The

comparison demonstrates the much more efficient physical crosslinking with the mesogen A12, which possesses distinctly larger alkyl tail units than A1 (see structures in *Scheme 21* further above). Obviously, the flexible alkyl chains in the azo-LCs behave highly differently from the extremely flexible PDMS spacer chains: The alkyl tail units support the phase separation of A1 or A12 from PDMS, as well as the crystallization of the azo LCs, so that longer alkyl tail units cause stronger physical crosslinking.

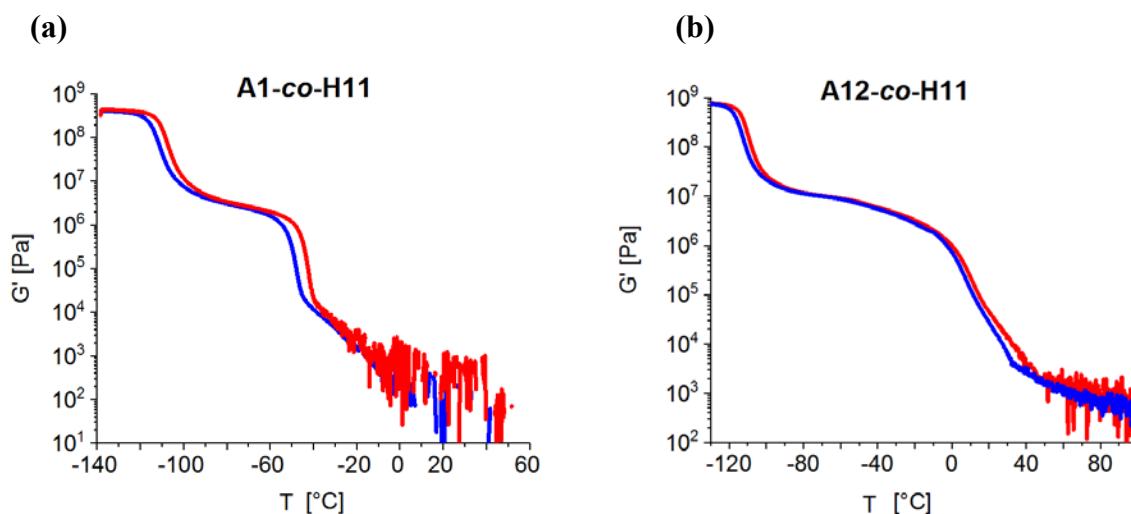


Figure 17: DMTA profiles, recorded as heating and cooling scans, of exemplary weakly crosslinked linear infinite copolymers containing the mesogens A1 and A12: (a) A1-co-H11 (an oil) and (b) A12-co-H21 (a soft gel), which are rubbery at low temperatures.

5.3 Self-healing behaviour of the LC-PDMS copolymers

The studied LC-PDMS copolymers are all reversibly physically crosslinked by aggregation of the LC units. Because of the physical nature and of the reversibility of this crosslinking, it could be expected, that all these copolymers would display self-healing behavior at favourable conditions.

In this work, the self-healing ability was preliminary studied on the example of the well-characterized rubbery copolymer **BAFKU₄₁-HMS 064** (see also *Appendix 1*). Tests were carried out at two temperatures, namely 22 and 45°C, and both were partly successful. The obtained results indicate that the self-healing of fully disrupted samples of BAFKU₄₁-HMS 064 (and most likely also of the other PDMS-LC copolymers) is relatively slow, if they are not brought close to melting.

The efficiency of self-healing was evaluated by means of tensile tests (see *Figure 18*). For these tests, the original ‘intact’ samples were prepared by re-melting of BAFKU₄₁-HMS 064 in open Teflon moulds, and had the dimensions of 20 mm x 5 mm x 2 mm. In the subsequent micro-tensile tests, which could be conveniently carried out on the multi-functional ARES-G2 rheometer, the deformed length of the sample was 3 mm (from 20 mm; 8.5 + 8.5 mm were in the clamps).

One sample selected for **self-healing** was a specimen which failed in its central region during a tensile test. In course of the self-healing procedure, it was re-assembled and pressed together for 48 h by a force of ca. 100 g **at room temperature** (22°C) (see *Figure 18 top / Appendix 1*). The BAFKU₄₁-HMS 064 sample is not sticky at room temperature, and its pieces fell immediately apart, if they were pressed together only for seconds or minutes. At 22°C, the temperature was **below the region of thermotropic transitions** in the copolymer (see DSC further below, in *Figure 21*), but still in the rubbery range (DMTA: *Figure 13a* further above).

The second sample for self-healing was obtained by cutting an intact re-melted platelet into two pieces. The latter were subsequently pressed together by a force of ca. 100 g **at 45°C** for 48 h (see *Figure 18 bottom / Appendix 1*). In this second test, the **healing temperature** already was **in the range of the thermotropic transitions** (DSC) of the copolymer, **but** still well **below** the range of gradual **melting**.

Both experiments yielded grown-together specimens (photographs can be seen in *Figure 18 / Appendix 1*). The tensile tests depicted in *Figure 18* confirm that **self-healing was partly successful at both the tested temperatures**, albeit it was not complete after 48 h in both cases: Both the healed samples failed at the self-healing joint, and both reached only partly the initial extensibility: 1/6 of original value in case of self-healing at room temperature, and 1/3 of it after healing at 45°C. The moduli (slopes of the tensile curves in *Figure 18*), however, can be considered as fully restored. In case of the sample healed at 45°C, some moderate creep occurred during the healing.

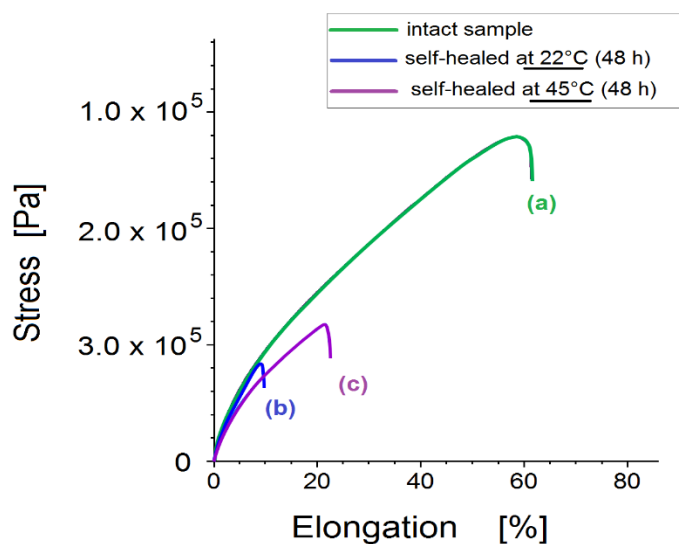


Figure 18: Stress-strain curves of intact and self-healed samples of the grafted LC-PDMS copolymer BAFKU₄₁-HMS 064: (a) intact, previously re-melted sample; (b) sample self-healed at 22°C for 48h (which was previously disrupted); (c) sample self-healed at 45°C for 48h (which was previously disrupted).

To sum up, the above results prove the presence of the self-healing effect in the rubbery copolymer BAFKU₄₁-HMS 064 in the solid rubbery state, but they also indicate, that a careful optimization of the healing temperature (key parameter), healing time, as well as of contact pressure (to prevent permanent deformation at higher temperatures) is needed to achieve 100% restoration of tensile properties by solid-state self-healing (all properties can be easily restored by re-melting). The self-healing of the disrupted samples was much slower, than the further below-discussed self-healing of structural damage caused by strain, which occurs nearly immediately. This difference is likely due to the spatial separation of the disconnected LC nano-domains (whose volume fraction is rather small), during the disruption, so that slow diffusion-like

processes are necessary to establishing new contacts between the LC domains in both (rubbery) solid fragments of the healed sample.

5.4 Phase behaviour of the LC-PDMS copolymers

5.4.1 DSC: thermal transitions

Differential scanning calorimetry (DSC) was employed in order to investigate the thermal transitions in the studied LC-PDMS copolymers, especially the involved values of specific heat of each transition. Interesting was the correlation of the temperatures of the thermal transitions with the above-discussed changes in the thermo-mechanical behaviour of the copolymers. In order to better understand the thermotropic changes occurring in the LC nano-aggregates in the physically crosslinked copolymers, the DSC traces of all of the copolymers were compared with the DSC traces of the neat mesogens. The complete DSC results are shown in *Appendix 1, 2, 4* and *6*.

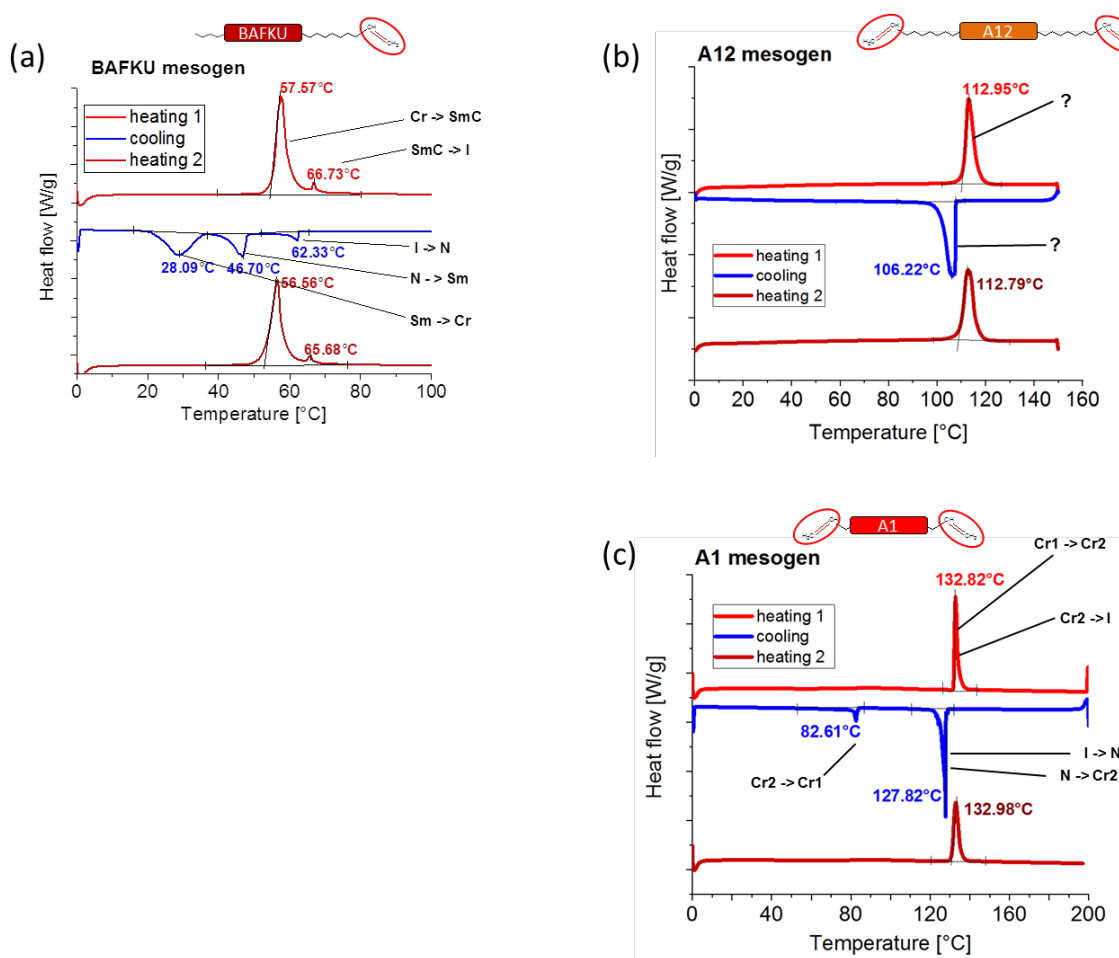


Figure 19: DSC traces of neat mesogens of the azo-type: (a) BAFKU; (b) A12; (c) A1.

The DSC traces of the employed **mesogens of azo-type** (both monovinyl- and divinyl-functional) are compared in **Figure 19**. All these structurally similar (see **Scheme 21**) mesogens have one common DSC feature: They have a single very dominant thermal transition in the heating scan. In case of BAFKU (whose transitions were assigned in [214]), there is still one more weak transition in the heating scan (SmC \rightarrow I), while there are three transitions in the cooling scan (assignment: see **Figure 19**). The mesogens A1 and A12 show a simpler behaviour, with practically only one apparent transition in heating and cooling scans (an exception is a weak Cr2 \rightarrow Cr1 transition in the solid state during the cooling of A1). In reality, the behaviour of A1 and probably also of A12 is more complex: The investigation of A1 with polarized light indicated (**Appendix 4**), that its single dominant peaks in the heating and in the cooling scan both consist of cumulated adjacent phase transitions in both scans (assignment: see **Figure 19**). Hence, to sum-up, all the azo mesogens have the potential to display interesting thermotropic behaviour in the physical crosslinks of copolymers with PDMS, more complex than just melting/freezing of nanocrystallites.

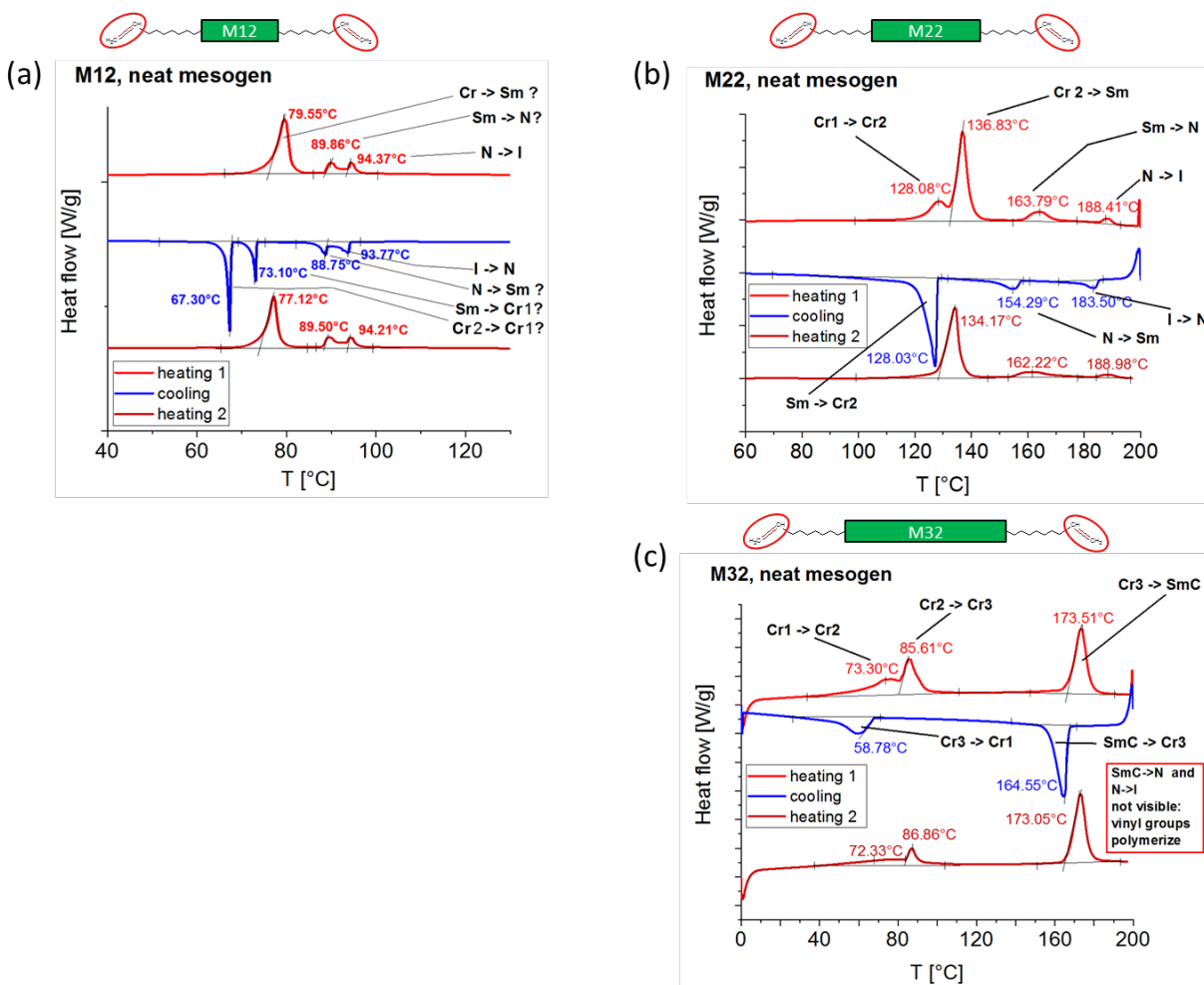


Figure 20: DSC traces of the azo-free vinyl-difunctional mesogens of “M”-type (azo-free): (a) M12; (b) M22; (c) M32.

The DSC traces of the employed **azo-free divinyl-functional mesogens** (M12, M22 and M32) are compared in **Figure 20**. It can be noted that the “M”-mesogens display a very rich transition behaviour in comparison to the ones of azo-type. Even in case of M12, which is structurally nearly identical with A12 (compare in **Scheme 21**), the high number of phase transitions is striking (vs. an apparent single one in A12). The transitions are tentatively assigned in **Figure 20**, albeit the investigation of these mesogens was not fully finished in this work. The “M-type” mesogens hence have a great potential for interesting thermotropic behaviour in physically crosslinked polymers. However, as will be discussed further below, the copolymer architecture in which they were used, does not favour highly ordered nano-aggregates with multiple discrete internal phase transitions.

The **LC-grafted copolymer** architecture proved highly efficient in physical crosslinking, as demonstrated by DMTA analysis (see *Figure 13a*), where an extended rubbery plateau was observed for the copolymer BAFKU₄₁-HMS 064.

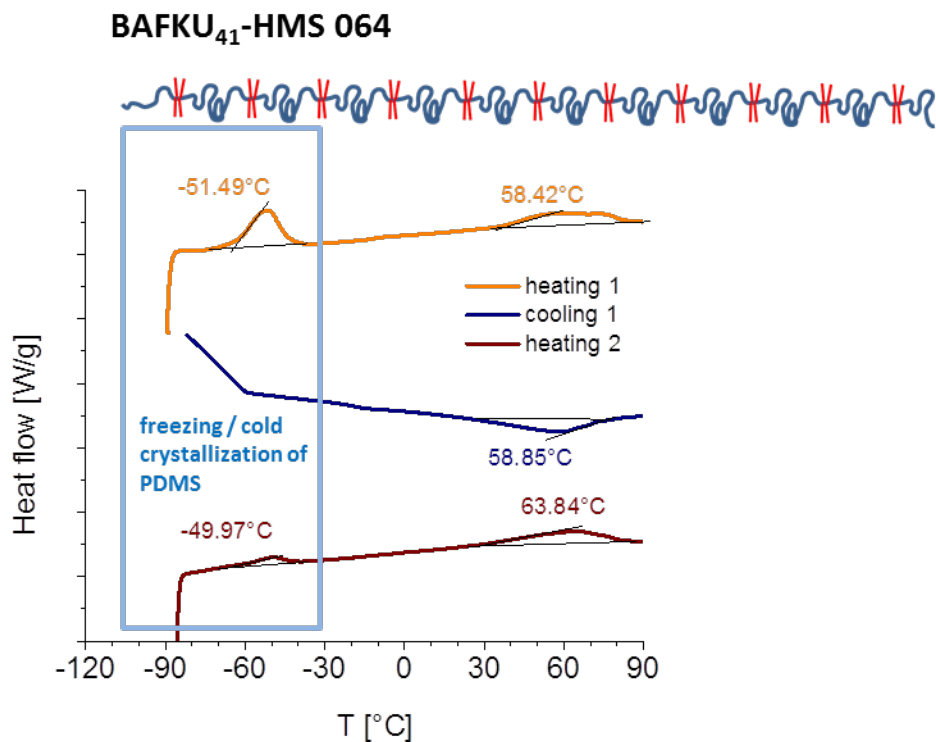


Figure 21: DSC traces of the grafted copolymer BAFKU₄₁-HMS 064.

Both the studied LC-grafted copolymers, the LC-rich waxy BAFKU₈-HMS 301, and the PDMS-rich elastomer BAFKU₄₁-HMS 064, display very similar DSC traces (including the transition temperatures; see also results in *Appendix I*). As example, the trace of BAFKU₄₁-HMS 064 is shown in *Figure 21*. It can be seen, that this copolymer displays a **single broad transition region**, the temperature range of which approximately corresponds to the range of the multiple transitions observed during heating and cooling of neat BAFKU. This region also corresponds to the temperature region where the rubbery phase softens and starts to melt (compare DMTA: *Figure 13a*); the copolymer becomes fully liquid at the end of the DSC transition region. The DSC transitions are joined into a single broad and continuous transition region in the copolymer, and this broad DSC feature also displays approximately the same shape and position in heating

and cooling scans (in contrast to the complex behaviour of neat BAFKU). The broad transition region suggests that the **mesophases in the grafted copolymers are less ordered than in neat BAFKU**. On the other hand, the nearly identical range of transitions in pure BAFKU and in both the fairly different grafted copolymers also indicates, that **phase transitions characteristic of neat BAFKU control the thermal behaviour in the LC nanoaggregates in the grafted copolymers**, with little interference from the PDMS component. The thermal effects connected with freezing and cold crystallization of PDMS are also visible in the DSC trace of the grafted copolymer with long PDMS spacer segments (see *Figure 21*), but not in BAFKU₈-HMS 301 (see *Appendix 1*).

The **LC-end-capped copolymers** displayed moderately strong crosslinking (with BAFKU end-caps), but their phase behaviour which included also transitions in the liquid state, was very interesting (their DSC results are extensively discussed in *Appendix 2*). In contrast to the grafted copolymers, the LC-end-capped copolymers often displayed multiple well-separated thermotropic transitions, at least if a mid-sized or short PDMS spacer was incorporated (see *Figure 22*). The first transition always was associated with the mechanically observable melting (see example DMTA: *Figure 15a* vs. DSC *Figure 22b*: both melting and DSC transition near +10°C), while the next transition(s) was (were) associated with changes in viscoelasticity of the copolymer melt. The thermotropic phases in the LC-nano-aggregates of H03-BAFKU₂ (*Figure 22a*) were assigned as crystalline / smectic / nematic / isotropic, while in the two remaining copolymers the phases were assigned as crystalline / nematic / isotropic. In case of the copolymer H21-BAFKU₂, which has the longest PDMS spacer, the transitions are practically thermally neutral in the heating scan (see *Figure 22c*), but they were observed indirectly as change in melt viscoelasticity, and (at lower temperature) as melt freezing to rubber (in analogy to the behaviour of H11-BAFKU₂). The freezing of H21-BAFKU₂ to a rubbery phase (but not the reverse process) nevertheless still is visible by DSC. The distinct and discrete transitions in the LC nano-domains in the LC-end-capped copolymers were found to be the result of a specific morphology in the nano-phase-separated copolymers, namely a lamellar structure (the proof of which will be discussed further below). The arrangement of the LC units in lamellae made possible a high degree of their ordering, and hence the distinct thermotropic transitions in the lamellae. In a great contrast to the grafted copolymers, the **temperature region of the phase transitions** (as far as it

is visible by DSC) **distinctly moves to lower temperatures with increasing length of the PDMS spacer**, albeit the width of the whole region of thermal transitions remains similar like in neat BAFKU. Hence, the **interference of the highly mobile PDMS chains with the thermal transitions in the lamellar nano-aggregates of LC units plays a key role in the LC-end-capped PDMS copolymers**.

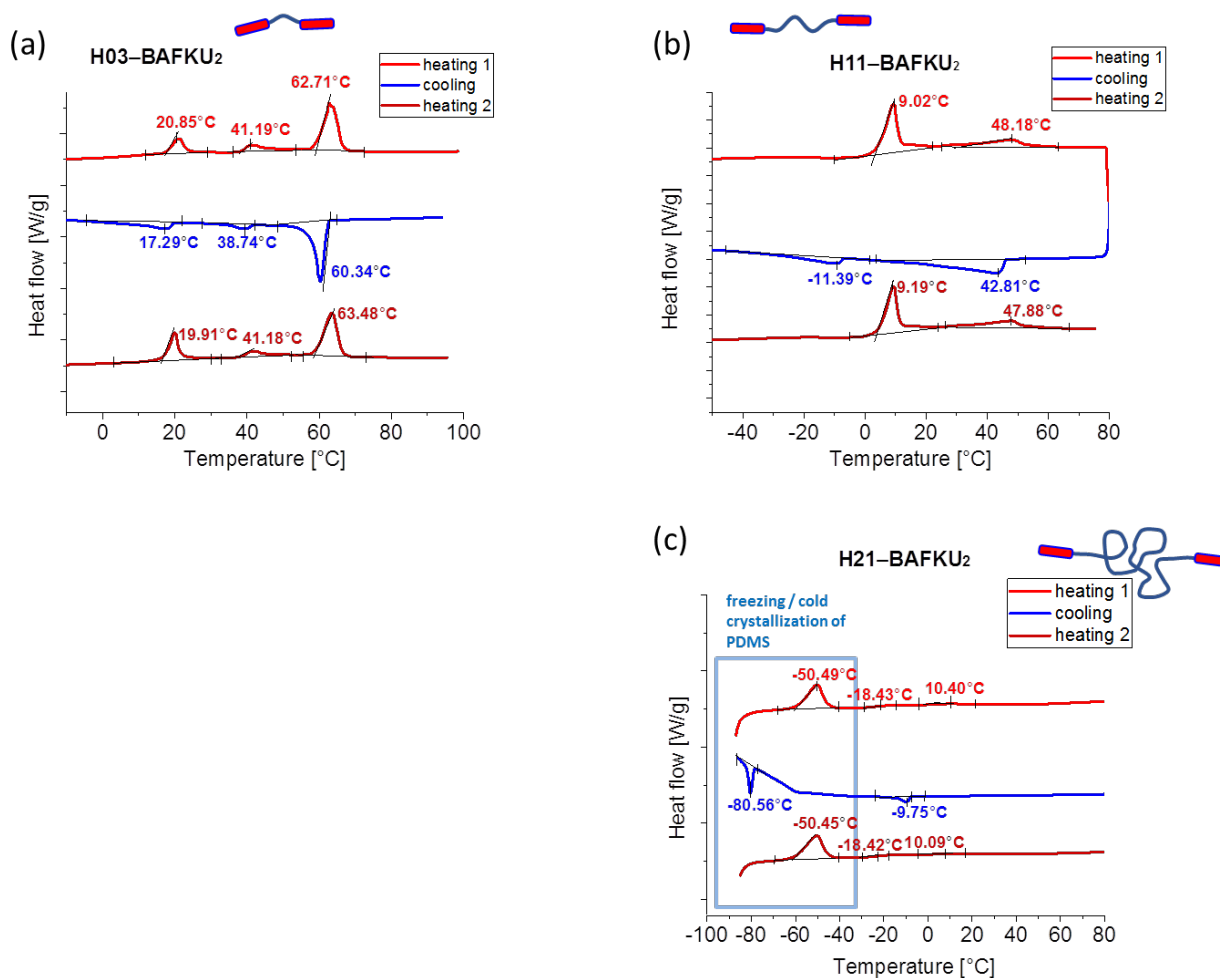


Figure 22: DSC traces of the LC-end-capped copolymers: (a) H03-BAFKU₂; (b) H11-BAFKU₂; and (c) H21-BAFKU₂.

The **linear infinite LC-PDMS copolymers with azo-type mesogens** A1 and A12 were found to display stronger crosslinking than the LC-end-capped ones, but weaker than the LC-grafted ones (with very similar mesogens), as was discussed further above (thermo-mechanical properties). Also in case of their thermal transition behaviour, this family of copolymers behaved in a somewhat intermediate way between the two above-discussed copolymer families: From the

exemplary DSC results in **Figure 23** it can be seen, that the linear infinite azoLC-PDMS copolymers display multiple (namely two) discrete thermal transitions, if the dilution by the PDMS spacer is not too high. However, these transitions are flatter and broader than in case of the LC-end-capped copolymers, but similarly like in case of the grafted copolymers. The whole collection of DSC results for the copolymers with the A1 and A2 mesogens is shown in **Appendix 4**.

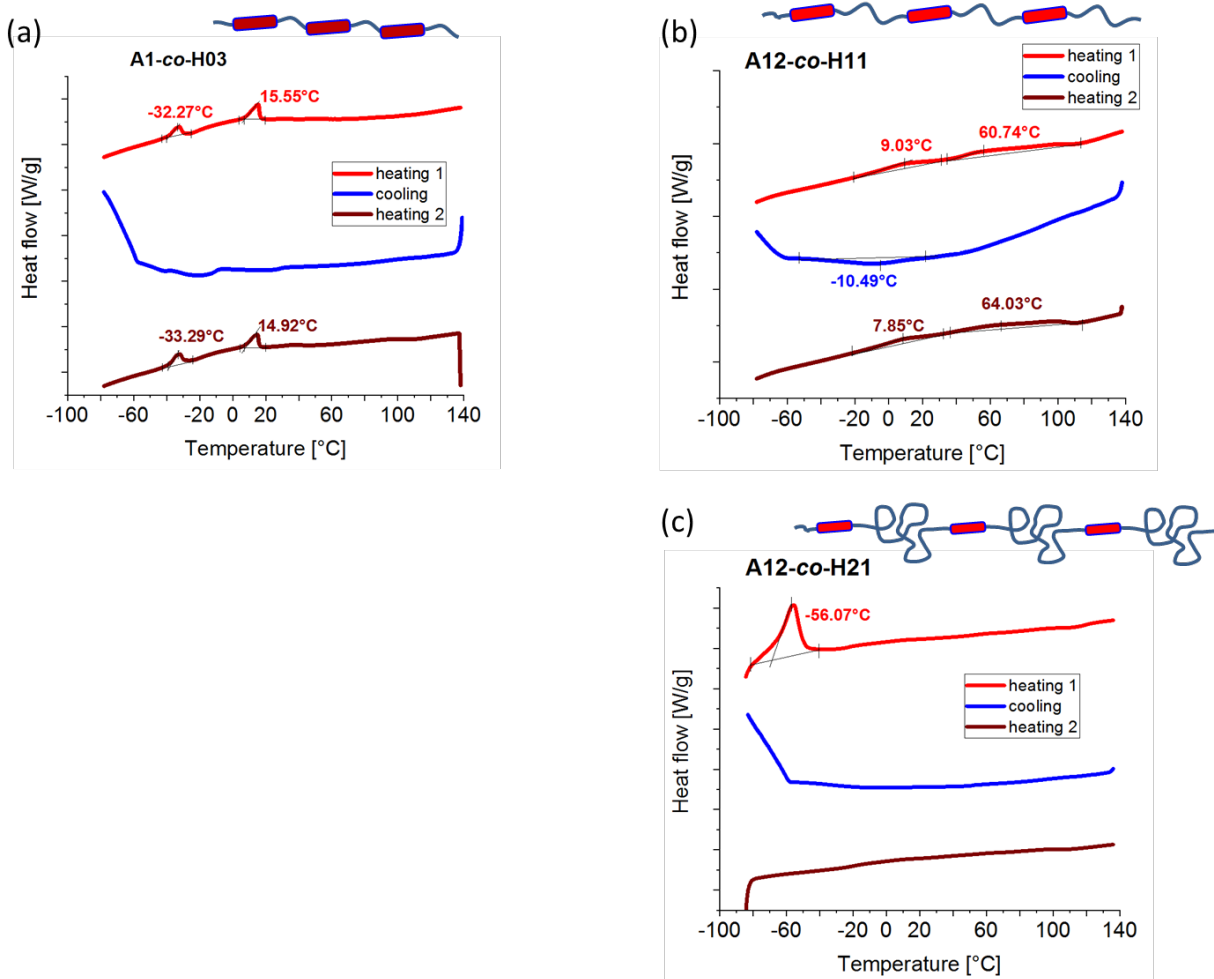


Figure 23: DSC traces of exemplary linear infinite LC-PDMS copolymers with azo-type mesogens: (a) A1-co-H03; (b) A12-co-H11; and (c) A12-co-H21.

The copolymers A1-co-H03, A12-co-H03 (**Appendix 4**), and A12-co-H11 display visible pairs of DSC transitions, while the remaining copolymers (A1-co-H11, A1-co-H21, and A12-co-H21), display only the freezing / cold crystallization effects of PDMS. In A1-co-H11 (see DSC in **Appendix 4**), the crystallization and melting of PDMS is surprisingly distinct and regular, and

might be nucleated by nano-crystallization of the LC-units. The DSC traces of the copolymers A12-co-H03 and A12-co-H11 are very similar, but the transitions are more intense with the shorter spacer. The longer spacer (H11 instead of H03) also shifts the thermal transitions to somewhat lower temperatures, but only by 10°C (see DSC in *Appendix 4*). Hence, the structure-property trend can be considered intermediate between the ones observed for grafted and LC-end-capped copolymers: **The PDMS chains moderately interfere with the thermal transitions of the LC nano-domains. The small specific heat values and the flat DSC peaks indicate rather an imperfect order in the LC nano-aggregates.** A correlation of the DSC transitions with the thermo-mechanical properties (see complete DMTA and DSC data in *Appendix 4*, or compare *Figure 17b* and *23b*) indicates, that in case of the copolymers with A12, the **thermotropic transitions correlate with the onset of the melting** (first transition: possibly via the formation of a nematic phase in the LC aggregates) **and with its final stage** (second transition: viscoelasticity change in the melt, possibly due to isotropization of the liquid-like LC-aggregates). In case of A1-co-H03, the DSC transitions occur at less specific temperatures in the course of gradual softening and melting.

The azo-free polyaromatic linear infinite LC-PDMS copolymers based on the mesogens M12, M22, and M32 displayed mutually similar trends concerning their thermal transition behaviour (see *Figure 24* and *25*; all data: see *Appendix 6*). Especially similar is the behaviour of the copolymers with the larger mesogens M22 and M32. In general, the latter two groups of copolymers display one somewhat broadened transition, which is found in the temperature region of the melting of the rubbery phase of the copolymer, and which can be correlated to the crystalline → smectic transition of the respective mesogen, shifted down by ca. 30°C. This single broadened transition in the copolymers (into which the higher-temperature transitions of the mesogen likely are merged) seems to be practically independent of the PDMS spacer length. Hence it seems, that the **phase behaviour of the LC units in the nano-aggregates is strongly affected by the bonding situation in the copolymer** (the mentioned down-shift of the transition), but otherwise **not affected by the PDMS phase** (no temperature shift of the transitions with changing PDMS spacer length).

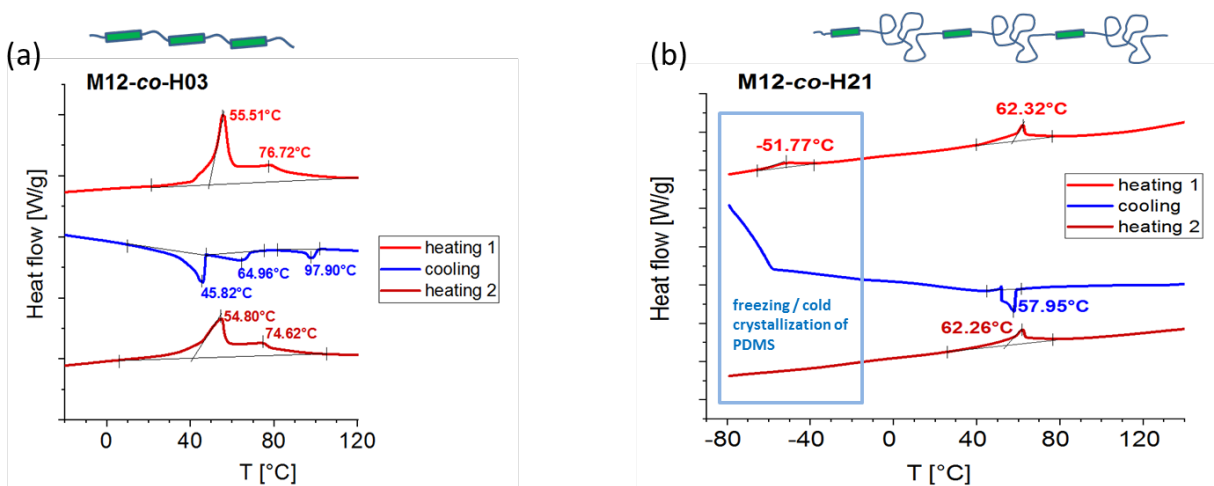


Figure 24: DSC traces of exemplary azo-free polyaromatic linear infinite LC-PDMS copolymers containing the LC unit M12: (a) M12-co-H03; and (b) M12-co-H21.

The **M12-based copolymers** display a somewhat different behaviour, than the ones with the larger mesogens: The transition region in M12-based systems is somewhat broader and structured (see **Figure 24a**). In case of the M12 copolymer with the shortest spacer H03, three separate transitions even can be observed during the cooling run, which indicates the formation of considerably ordered mesophases (the transitions are less separated in the heating scan). The thermal transitions in M12-co-H03 begin at its melting temperature and continue in the melt, so that the material could be of interest as a ‘smart oil’ with T -switchable viscoelasticity. The copolymer M12-co-H21 already shows similar trends in DSC, like the ones with larger mesogens and mid-sized spacers.

The **copolymers based on the mesogen M32** display one additional interesting DSC feature, namely the Cr1 \rightarrow Cr2 transition in the LC nano-aggregates, which occurs at approximately the same temperature like in the neat mesogen. This indicates at least a **partly similar packing of LC units in the M32 nano-aggregates and in neat M32**. In case of the copolymer M32-co-H21, none of the DSC transitions of the LC units is intense enough to generate a visible DSC peak (albeit mechanical effects of the main transition can be detected, similarly like in other H21-based copolymers). Interestingly, the main transition is faintly visible in the homologue with the smaller mesogen M22 (in M22-co-H21, see DSC in **Appendix 6**), and even better in case of M12-co-H21 (see **Figure 24b**). The reason might be, that the smaller

mesogens easier arrange to more regular nano-aggregates, which then generate sharper and hence more visible DSC peaks.

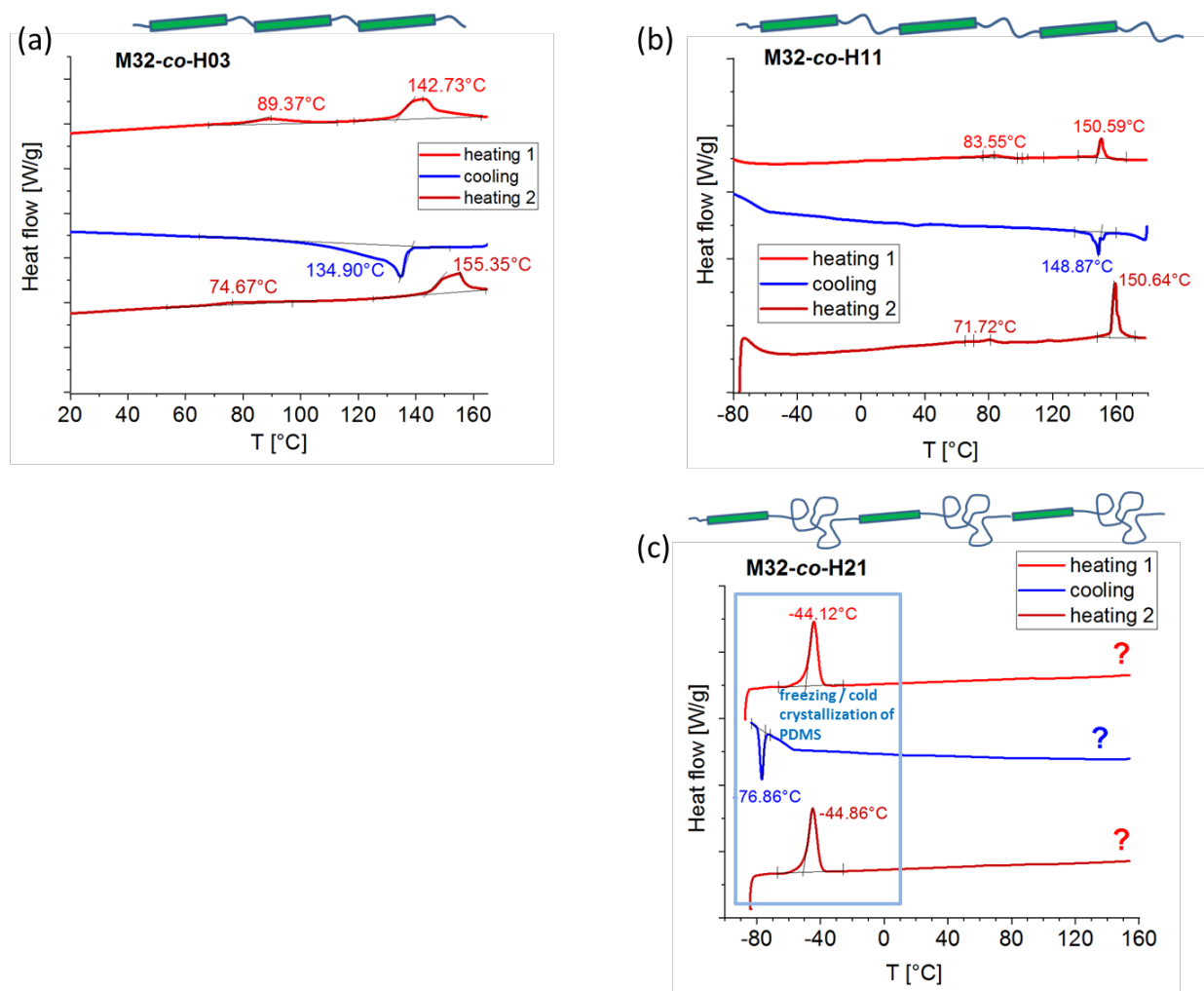


Figure 25: DSC traces of exemplary azo-free polyaromatic linear infinite LC-PDMS copolymers containing the LC unit M12: (a) M12-co-H03; and (b) M12-co-H21.

5.4.2 X-ray scattering analysis of the phase behaviour

The phase transition behaviour of the studied copolymers was deeper investigated by means of temperature-dependent X-ray scattering (SAXS and WAXS) investigations. The scattering patterns of the neat mesogens were compared with the patterns of the copolymers of different architecture.

LC-grafted copolymers: In *Figure 26*, the temperature-dependent X-ray scattering patterns of the **neat mesogen BAFKU**, and of the BAFKU-grafted copolymer BAFKU₄₁–HMS 064 are compared (detailed discussion: *Appendix 1*). The neat mesogen displays numerous crystalline reflections (in the logarithmic intensity scale), among which the peak at the scattering vector value of $q = 0.242 \text{ \AA}^{-1}$ (scattering angle $2\theta = 3.40^\circ$) is the most prominent (a second order reflection of this peak also is observed at $0.484 \text{ \AA}^{-1}/6.80^\circ$). Its Bragg distance, 2.60 nm, corresponds to the length of a BAFKU unit. The pattern shown by BAFKU is characteristic for a well ordered organic molecular crystal. It can be seen, that at 85°C , all the reflections of BAFKU disappear, and are replaced by two very broad amorphous halo features. Upon cooling, the peaks rapidly re-appear. Only small temperature-induced peak shifts were observed in neat BAFKU (see detailed discussion in *Appendix 1*), so that its thermotropic transitions are not ‘highlighted’ by marked changes in XRD pattern.

In case of the **rubbery copolymer BAFKU₄₁–HMS 064** which contains ca. 22.7 Vol.% of BAFKU, the XRD pattern is much simpler, and practically no peaks of neat BAFKU are found in the pattern of the copolymer (compare *Figure 26a* vs. *b*). The pattern of the copolymer is dominated by the amorphous halo of PDMS (centered at $0.84 \text{ \AA}^{-1}/11.9^\circ$), but some reflections stemming from BAFKU also can be found: The peak associated with the mesogen length is found at $0.183 \text{ \AA}^{-1}/2.57^\circ$, which corresponds to a crystallographic distance of 3.43 nm. The second-order reflection of this most prominent LC peak also is observed in the copolymer ($0.366 \text{ \AA}^{-1}/5.14^\circ$), as well as weak reflections close to the second-order-peak, and also small peaks at $1.44 \text{ \AA}^{-1}/20.3^\circ$ (these latter also occurred in neat BAFKU at a similar position; they correspond to Van der Waals distances between organic molecules). The XRD pattern of the copolymer generally indicates a **different and somewhat less ordered packing of BAFKU in the LC nano-aggregates of the copolymer**. A very important finding is, however, that **the moderate order in the aggregates is not destroyed in the molten state of the copolymer**, at a temperature well above the clearing (isotropization) point of neat BAFKU (see curve for 85°C in *Figure 26b*). The preserved order in the liquid state of the LC aggregates in the copolymer likely is caused by the fact, that the LC units are attached in quartets (see structure in *Scheme 26* further above), which tend to stay aligned along the multiple LC axes also in the state of high segmental mobility. (Temperatures much higher than 85° could not be investigated with XRD, due to equipment limitations).

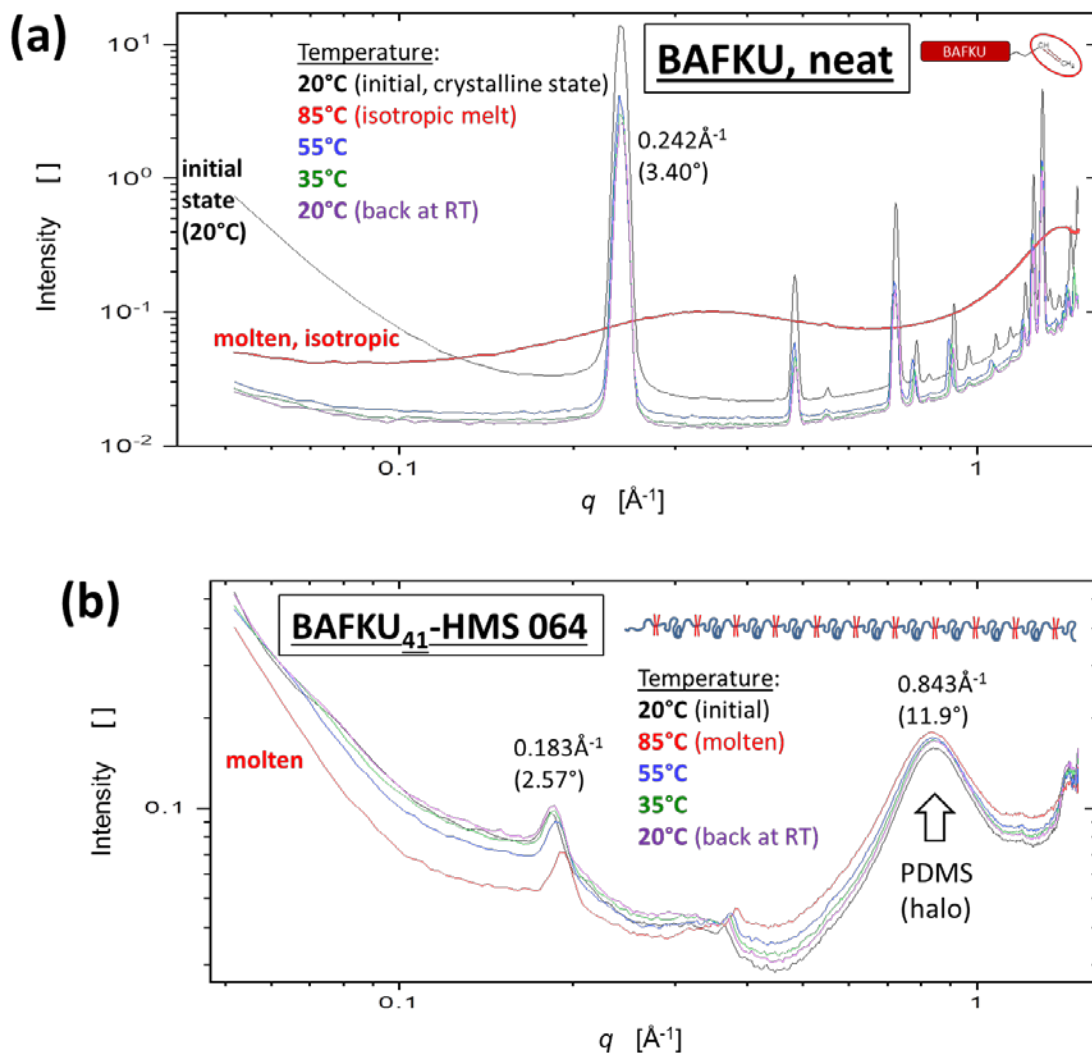


Figure 26: X-ray scattering patterns in the combined SAXS and WAXS range, in the format Scattering intensity = $f(q)$, with both axes in logarithmic format: (a) neat BAFKU; (b) the grafted BAFKU₄₁-HMS064 copolymer; the patterns were recorded at room temperature (20°C), then at 85°C (molten), and after subsequent cooling to 55°C, to 35°C and to 20°C (back at room temperature).

Another interesting feature in the T -dependent XRD patterns of the copolymer BAFKU₄₁-HMS064 is the temperature-dependence of the position of the main LC peak at $0.183\text{ \AA}^{-1}/2.57^\circ$. With increasing temperature, this peak (as well as its second order reflection) shifts to higher q values (scattering angles), which indicates shortening distances in the BAFKU nano-aggregates (more compact packing at higher T ; the effect occurs practically reversibly). Together with the higher ‘nominal LC length’ in the copolymer, this effect also points at a looser packing of BAFKU units in nano-aggregates in the copolymer.

LC-end-capped copolymers: *Figure 27* shows selected results concerning the temperature-dependent X-ray diffraction patterns of the BAFKU-end-capped PDMS copolymers (the complete set of results and a more detailed discussion can be found in *Appendix 1*).

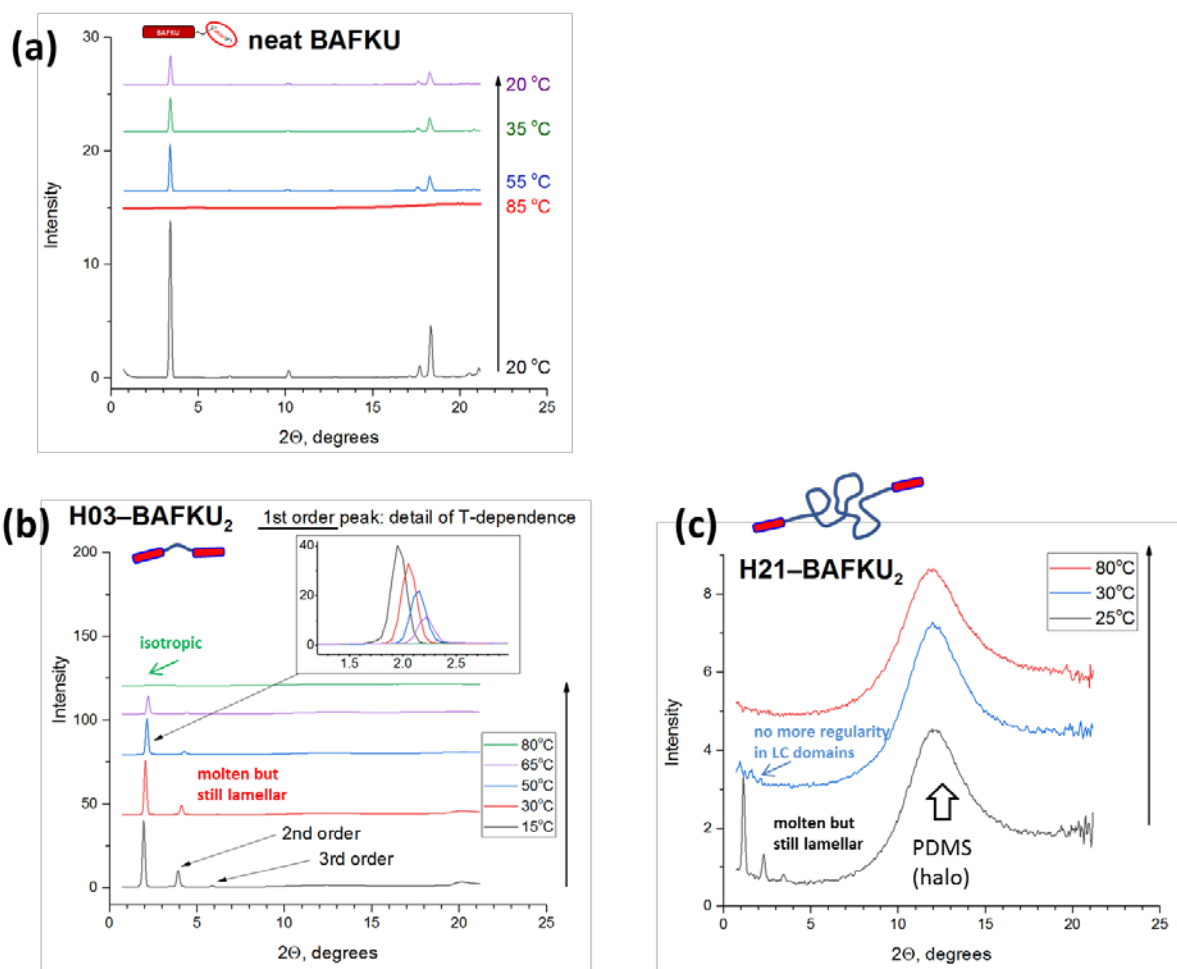


Figure 27: Temperature-dependent XRD patterns of: (a) neat BAFKU, (b) the LC-end-capped H03-BAFKU₂, and (c) H21-BAFKU₂; the sequence of applied temperatures is indicated by arrows besides the legend of each sub-image.

The BAFKU-end-capped copolymers display completely different scattering patterns and also wholly different temperature-induced changes in XRD, if compared with the further above-discussed BAFKU-grafted PDMS copolymer. In all copolymers, even with the H21 central chain (64 PDMS repeat units, 13.5 Vol.% of BAFKU), diffraction peaks caused by the LC units are distinct and sharp. Evaluation of the sharp ‘LC peaks’ indicated, that they represent

the 1st, 2nd, and 3rd order reflections on a single crystallographic distance, while no other ‘LC peaks’ are observed. The characteristic distance causing this set of reflections was found to be highly different in each of the copolymers, and also highly different from the approximate length of the BAFKU mesogen. Additionally, the observed reflection pattern (namely: well visible 1st to 3rd order) is characteristic of lamellar structures. If the characteristic distance of the observed lamellar reflections is compared with the size of the mesogen BAFKU and with the approximate size of the differently coiled PDMS chains H03, H11 and H21, as shown in **Figure 28**, it can be seen that the observed 3-order reflections correspond to distances between **lamellae of BAFKU units, separated by the different PDMS chains**. No reflections caused by the internal structure of the lamellae were observed by XRD (in the experiment range).

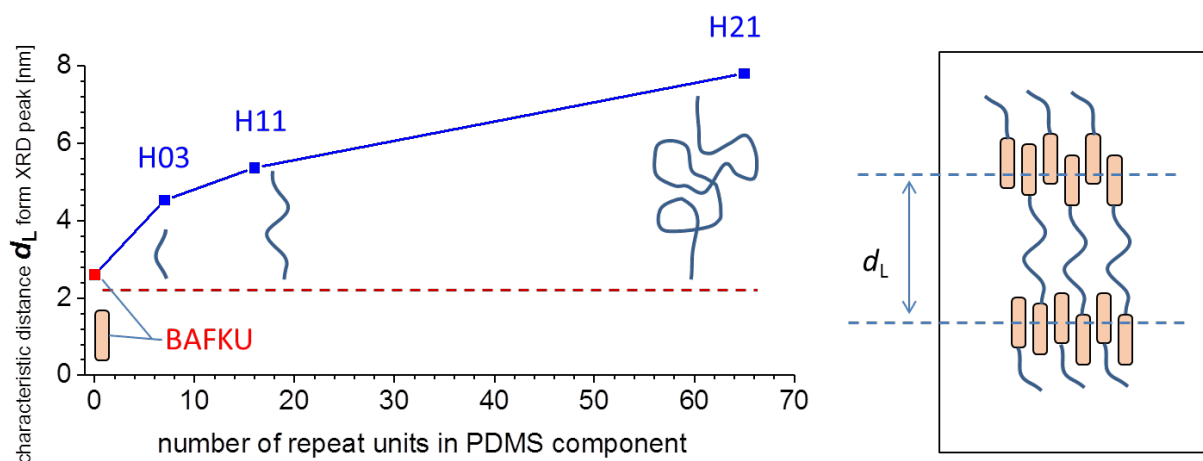


Figure 28: Lamellar structure of the LC-end-capped copolymers and the effect of the chain length of the PDMS component on the characteristic distance observed by X-ray diffraction. **(Left):** plot of the observed (XRD) characteristic distance with in-laid approximate relative sizes of the segments of the studied copolymers; the coiling of PDMS chains plays an important role; **(Right):** idealized representation of the lamellar nanoaggregates of the BAFKU end-groups present in the copolymers below the isotropization temperature.

Another notable difference between the BAFKU-end-capped and BAFKU-grafted copolymers was, that the ‘LC reflections’ in the end-capped ones disappeared at critical temperatures well below the isotropization temperature of neat BAFKU. On the other hand, the XRD experiments also indicated, **that the lamellar structures persisted in the low-temperature-melt state of the BAFKU-end-capped copolymers** (e.g. at room temperature), **but disappeared above their last thermotropic transition**. In case of H21–BAFKU₂, the last phase transition was not visible by DSC, but the XRD data indicate that it occurs at $T \leq 30^\circ\text{C}$, while further-below discussed polarized light microscopy (PLM) and rheology investigations indicate that this temperature is close to 30°C . The persistence of lamellar aggregates in low-temperature melt, and their thermally induced replacement by isotropic nano-droplet-like aggregates explains the interesting temperature-switched viscoelastic behaviour of the liquid BAFKU-end-capped copolymers (‘smart oils’).

Linear infinite alternating LC-PDMS copolymers: The XRD characterization of the linear infinite copolymers based on the azo mesogens A1 and A12 is still not finished in the moment of submission of this Thesis (other results concerning these copolymers can be found in *Appendix 4* and *5*). The azo-free linear infinite copolymers based on the mesogens M12, M22 and M32, some of which displayed promising material properties, were characterized nearly completely, however, and representative results are shown in *Figure 29* and *30* (the complete sets of results are shown in *Appendix 6*).

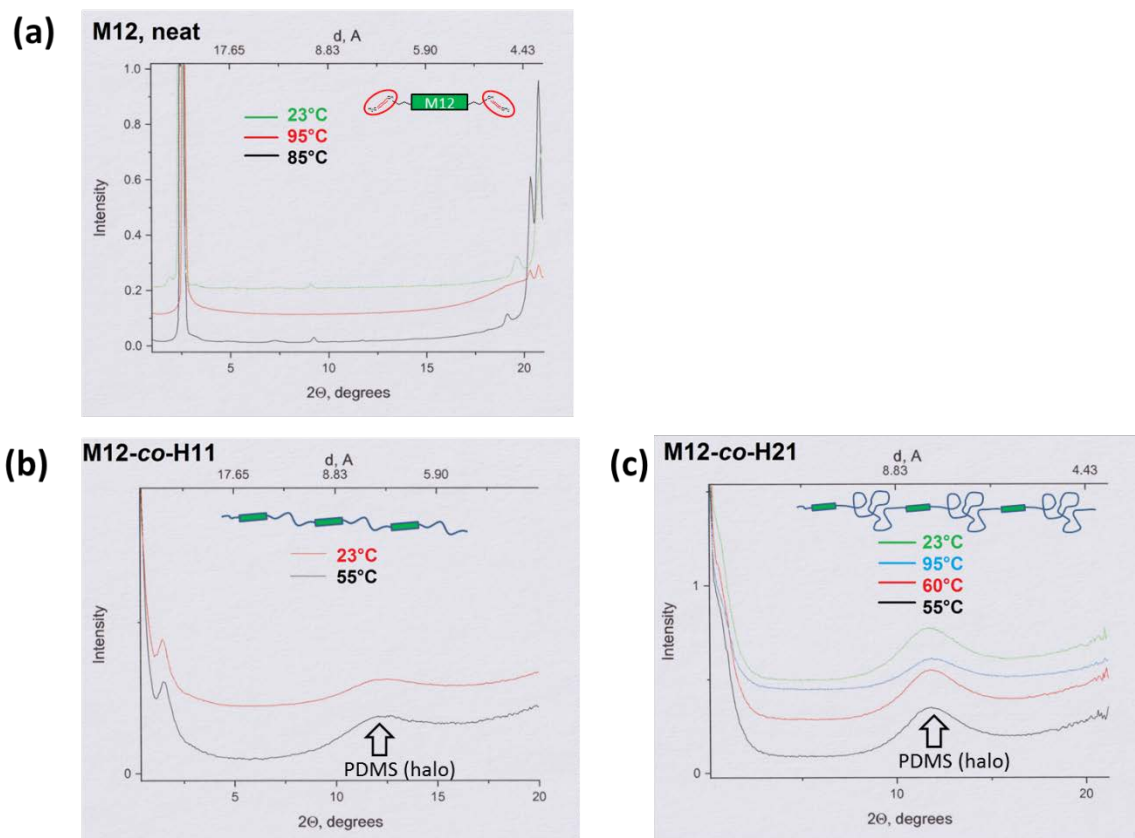


Figure 29: Temperature-dependent XRD patterns of: (a) neat M12, (b) of the linear infinite M12-co-H11, and (c) M12-co-H21; the sequence of applied temperatures is given in the legend of each sub-image, starting from top.

The **Figure 29** shows the results of temperature-dependent XRD experiments with the **neat mesogen M12**, as well as with the copolymers M12-co-H11 and M12-co-H21. The mesogen M12 has nearly an identical shape, and was found to be only a somewhat weaker crosslinker than A12, which can be considered to be the divinyl-analogue of BAFKU. The neat mesogen displays a very intense characteristic reflection at $2.6^\circ/0.184 \text{ \AA}^{-1}$ (distance: 3.4 nm), which can be assigned to its length (it is somewhat longer than BAFKU). Several additional sharp reflections of M12 are found near $20^\circ/1.44 \text{ \AA}^{-1}$, and correspond to inter-molecular Van der Waals distances. At 95°C , the molten mesogen M12 approaches the isotropic state (DSC in **Figure 20a**: N \rightarrow I: peak maximum at 94.2°C): the peaks near 20° practically completely transformed to amorphous halo, while the one at 2.6° still persists (see **Figure 29a**; temperatures higher than 95°C could not be investigated, due to equipment limitations). In contrast to BAFKU,

for M12, some differences clearly can be seen in the positions of the smaller peaks, if comparing the smectic (85°C) and the crystalline state (23°C; see both curves in *Figure 29a*).

In the **copolymer M12-co-H11** (*Figure 29b*), one LC reflection near $1.8^\circ/0.128 \text{ \AA}^{-1}$ (distance: 4.9 nm) and a steep increase of scattering at lower angles is observed. The latter scattering feature is likely due to nano-domains, similarly like in the BAFKU₄₁-HMS 064 copolymer – visible in *Figure 26a*, or also in **Fig.6/Appendix 1**, where the same axes formats are used like in *Figure 29*. No other LC-related features are observed in *Figure 29b*. The described pattern persists at 55°C, where the physical crosslinks (M12 nano-aggregates) are in a liquid crystalline state (see DSC of M12-co-H11 in **Appendix 6**). Unfortunately, the experiment at 95°C still has to be done yet, which would show, if the nano-aggregates become more irregular above the last LC transition, as would be expected in view of the XRD patterns of the ‘more PDMS-diluted’ analogue M12-co-H21 (*Figure 29c*). Generally, the LC-related features in *Figure 29b* suggest, that M12-co-H11 could have a similar structure of aggregates like the copolymer BAFKU₄₁-HMS 064: stronger small primary ones, assembled to larger looser secondary ones, the latter not exceeding several tens of nanometres (see detailed discussion of XRD data in *Appendix 1* and its Supporting Information file). The LC reflection near $1.8^\circ/0.128 \text{ \AA}^{-1}$, which might be related to the ‘mesogen length reflection’ of neat M12 at $2.6^\circ/0.184 \text{ \AA}^{-1}$, would suggest a loose packing in the M12 nano-aggregates (similarly like in the branched copolymer BAFKU₄₁-HMS 064).

In case of the **copolymer M12-co-H21** (*Figure 29c*), which is close to melting at room temperature, the XRD patterns are very similar like in its homologue with the shorter H11 spacer. The only difference is, that the LC units do not generate a distinct reflection peak near 2° , but this reflection (a shoulder still is visible) is merged with the increase of scattering at small angles. Thus, expectedly, the M12 aggregates are less ordered in M12-co-H21 than in M12-co-H11.

Representative results of XRD investigations with **linear infinite LC-PDMS copolymers with larger M-type mesogens** are given in *Figure 30*, where the system **M32-co-PDMS** is evaluated (all collected data are in *Appendix 6*).

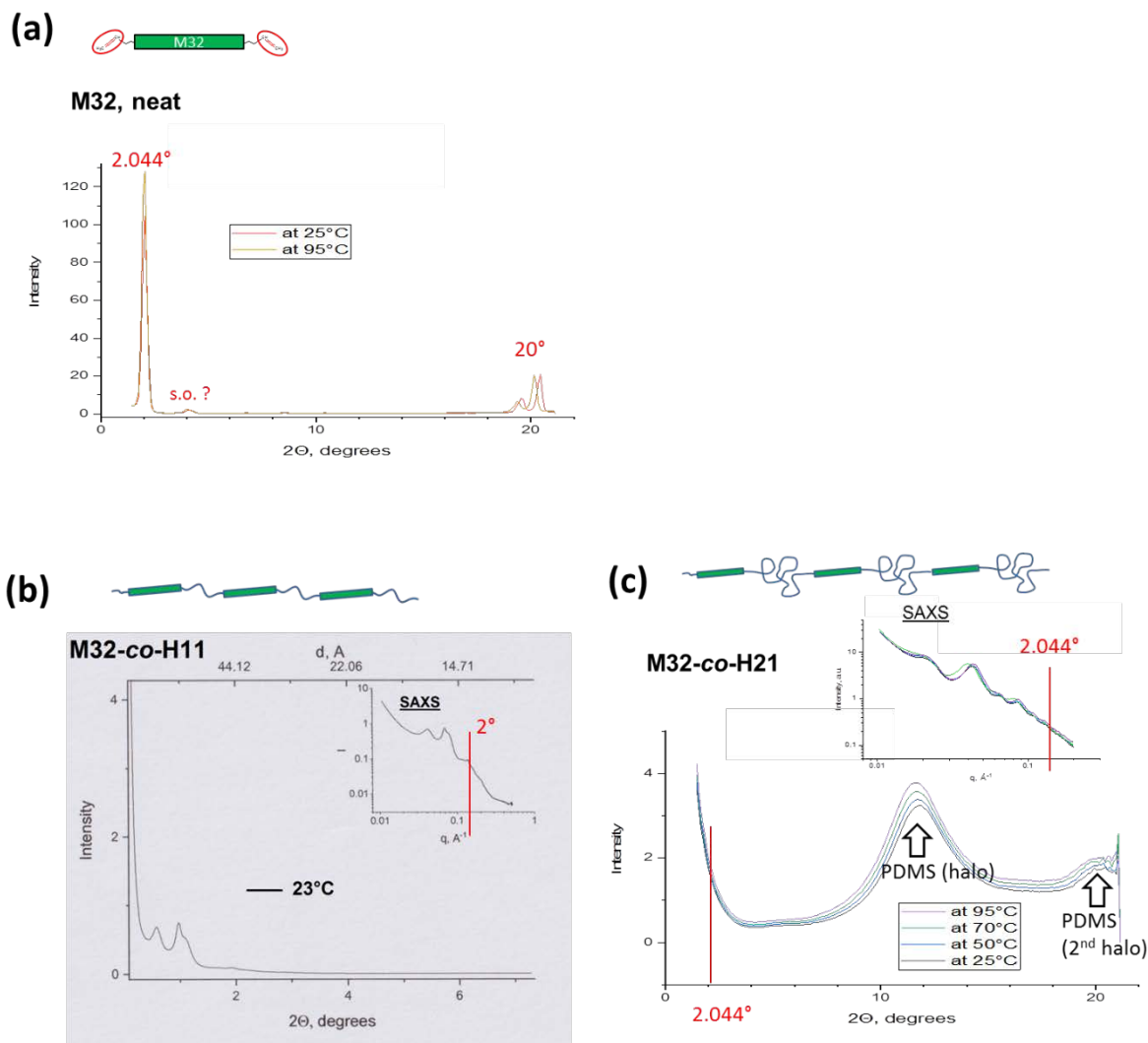


Figure 30: Temperature-dependent XRD patterns of: (a) neat M32, (b) linear infinite M32-co-H11 (room temperature only), and (c) M32-co-H21; each sample was first measured at room temperature, and subsequently at the higher ones.

It can be seen in **Figure 30**, that the system M32-co-PDMS displayed the same trends in the XRD experiments, like M12-co-PDMS (e.g. structured reflections of LC aggregates with shorter PDMS spacer). The temperature-dependent scattering patterns of M22-co-PDMS (shown in **Appendix 6**) also are very similar to the ones of M12-co-H21 and M32-co-H21 (shown in **Figure 29** and **30**).

To sum up, the X-ray diffraction analysis suggested a distinct lamellar structure for the BAFKU-end-capped PDMS copolymers, with a fairly regular internal structure in the lamellae,

which made possible multiple thermotropic transitions in them, and thus in the whole copolymer. The lamellae were also shown to exist in the molten LC-end-capped polymers. On the other hand, the LC-nano-aggregates were shown to be rather loose and less well ordered in the LC-grafted, and in the linear infinite LC-PDMS copolymers. A specific feature of the LC-grafted copolymers was the persistent alignment of the LC units also in the molten copolymer, above of the clearing point of the neat mesogen, which seems to originate from the occurrence of the grafted LC units in quartets.

5.4.3 PLM observation of anisotropy and of mesophase textures

The phase transition behaviour, as well as ordering effects in the domains of the mesogenic units of the prepared copolymers were additionally evaluated by means of polarized light microscopy (PLM), in order to eventually combine the DSC, XRD and PLM results, and elucidate the complex phase behaviour.

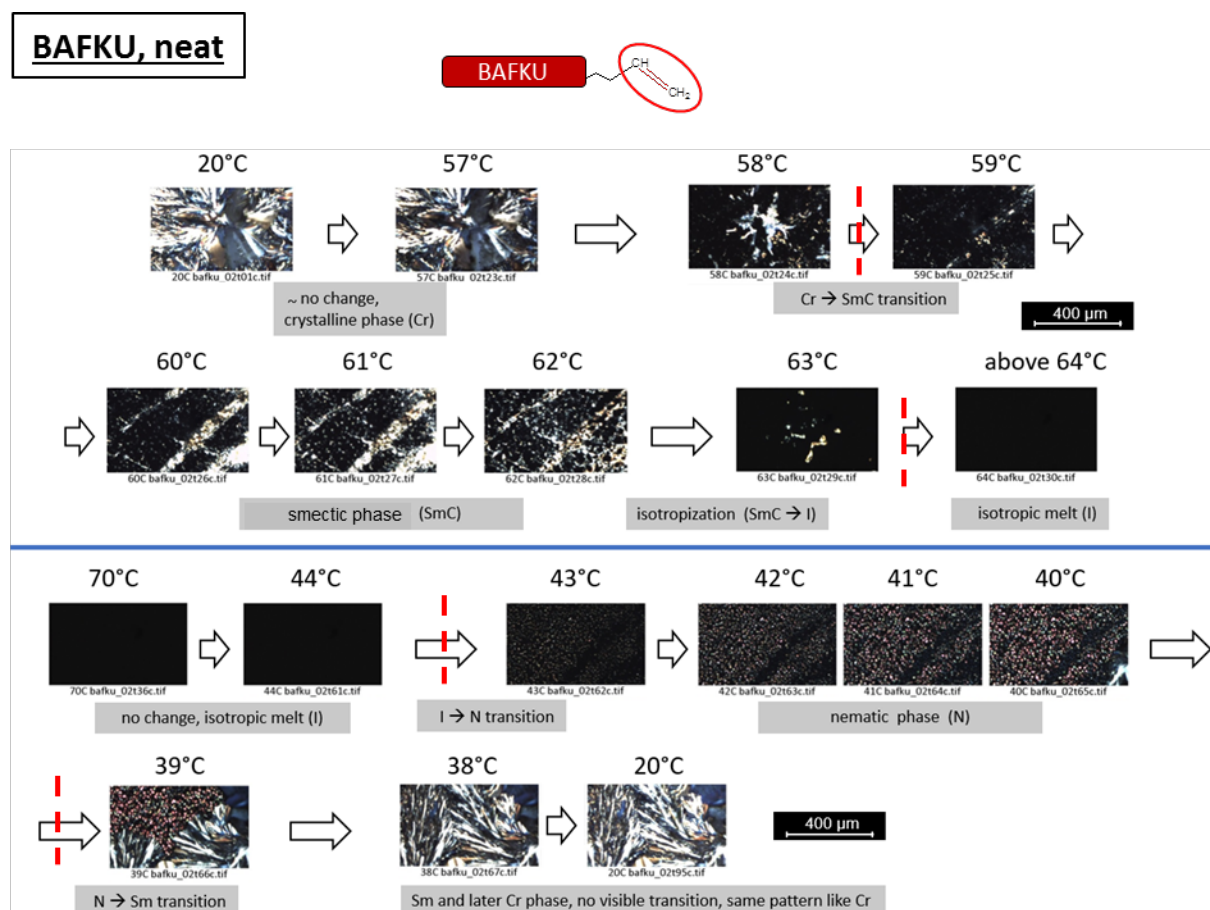


Figure 31: Textures observed in neat BAFKU mesogen, top: heating run; bottom: cooling run; positions of thermotropic transitions are marked with red dotted lines; large representative images of each characteristic texture are shown in the Supplementary Information File of Appendix 2, SI-Fig. 20, 21.

Neat mesogen BAFKU: The mono-vinyl-functional mesogen BAFKU was incorporated as LC unit into the LC-grafted- and into the LC-end-capped copolymers. Its textures observed by polarized light microscopy at different temperatures are shown in **Figure 31**. The mesogen

displays several monotropic transitions in the heating and cooling scan, as was shown in **Figure 19a** (DSC, further above). The changes in textures in the heating scan well-correspond with DSC, while in the cooling scan, they seem to appear somewhat belatedly (undercooling). The white colour dominates in most of the textures of the mesogen, but other ones also are prominent, like purple/brown, or blue. (The neat mesogen appears orange in daylight). Detail PLM images of BAFKU are shown in the Supplementary Information part of **Appendix 2**.

LC-grafted copolymers: From the group of LC-grafted copolymers, only the rubber-like BAFKU₄₁-HMS 064 was investigated in PLM, which had the most promising material properties. The results are illustrated in **Figure 32**.

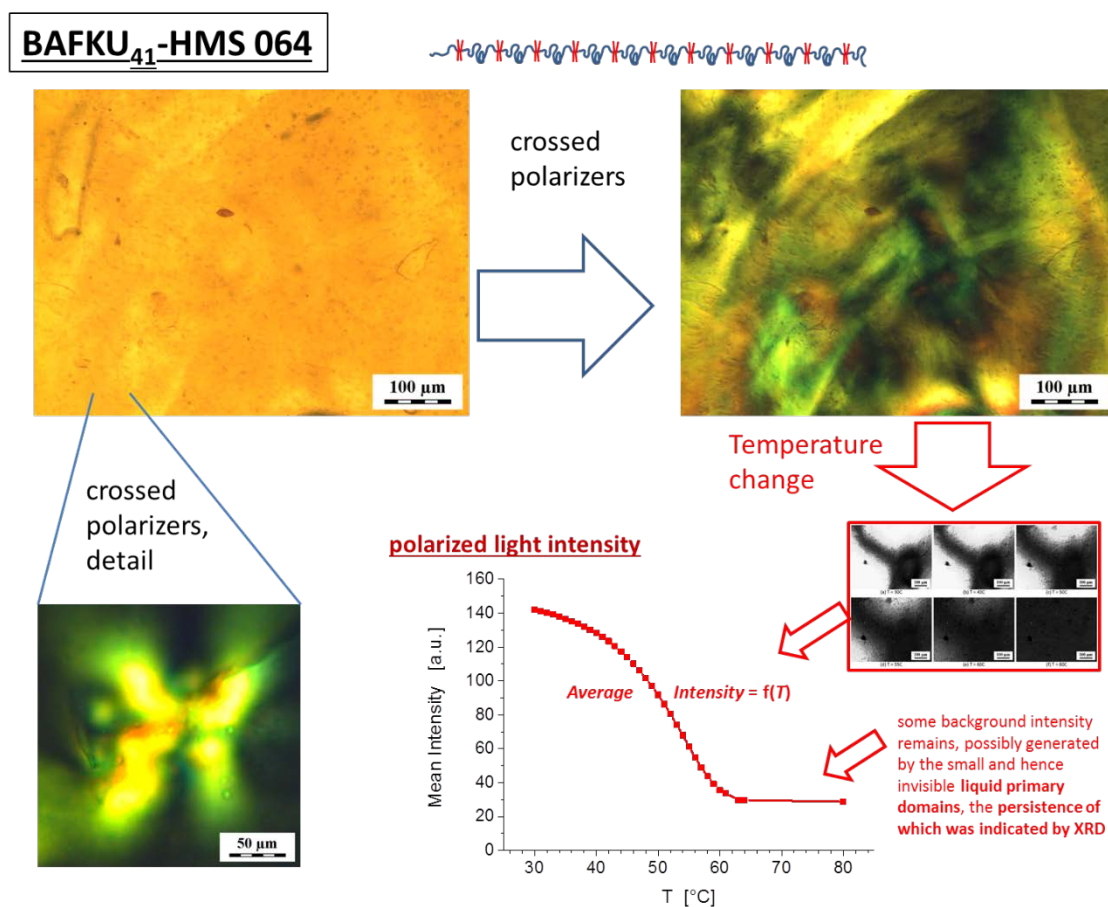


Figure 32: Images of a sample of the LC-grafted copolymer BAFKU₄₁-HMS 064 in transmitted polarized light, without second polarizer, and with crossed polarizers; the non-specific colourful texture did not change with temperature, but its intensity gradually decreased, while approaching the melting point of the copolymer.

No anisotropy was observed if the copolymer was melted (upon installation between microscopy glasses) and subsequently cooled-down to room temperature. However, widespread **anisotropy** (see textures in *Figure 32*) **could be induced by gently shearing** the molten sample between the glasses, prior to its solidification. The colourful texture was highly different from the ones observed in neat BAFKU, also in matter of colours. **The texture in BAFKU₄₁–HMS 064 also was non-characteristic, which is in good agreement with the postulated rather irregular arrangement in the LC nano-aggregates.** The texture in the grafted copolymer did not change with temperature, but upon approaching the mechanically observable melting point of the copolymer, it gradually lost intensity. The mean polarized light intensity from a selected image area was quantitatively followed, and its temperature dependence is shown in *Figure 32*, as a measure for gradual melting and isotropization of LC-aggregates in the copolymer. The texture did not reappear upon sample cooling, unless shear was applied. (A more detailed discussion of the PLM analysis of this copolymer is in *Appendix 1*).

LC-end capped copolymers: Similarly like with other properties, the LC-end-capped copolymers displayed also highly different PLM textures (and their *T*-induced changes), if compared to the LC-grafted copolymer BAFKU₄₁–HMS 064. The PLM analyses of the PDMS–BAFKU₂ copolymers are presented in *Figure 33–35* (detailed: *Appendix 2*).

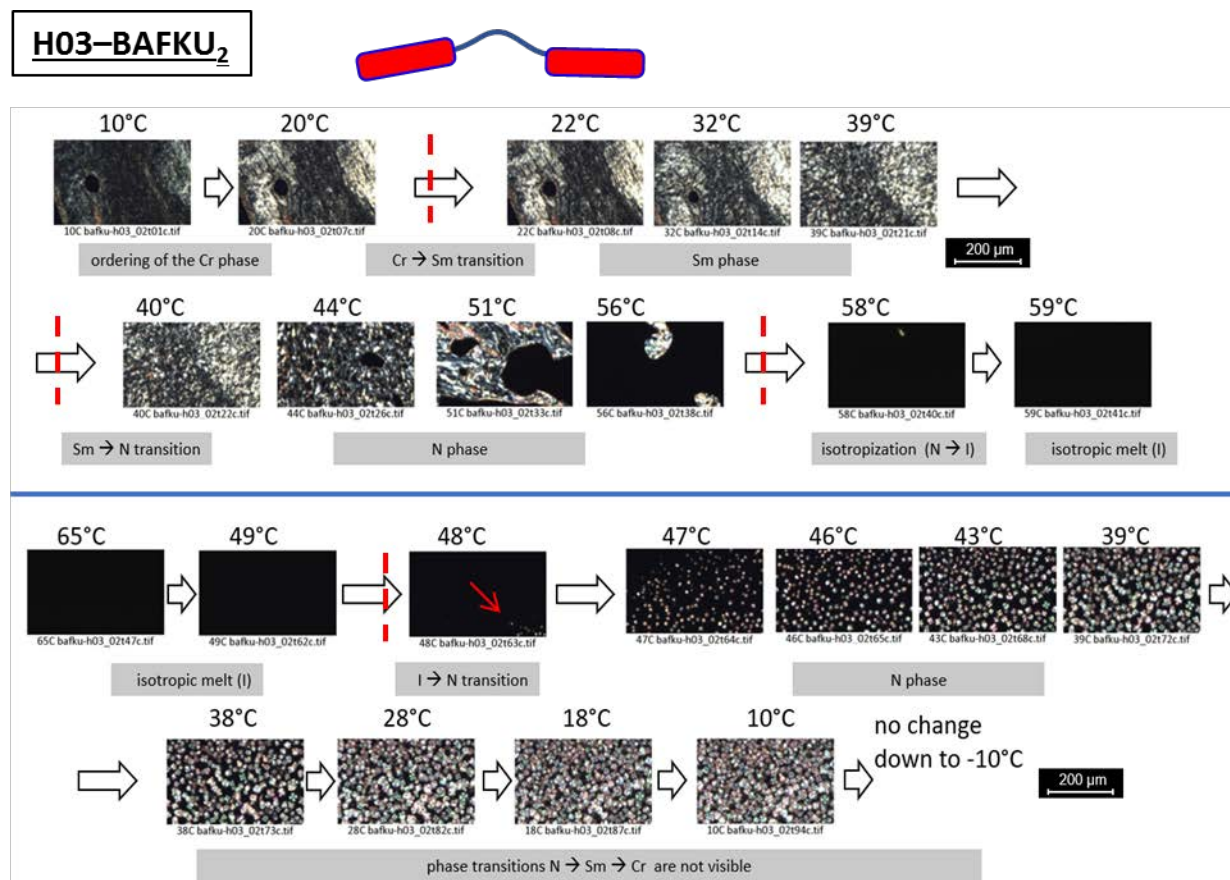


Figure 33: Textures observed in the LC-end-capped H03-BAFKU₂, top: heating run; bottom: cooling run; positions of thermotropic transitions observed by DSC are marked with red dotted lines; large representative images of each characteristic texture are shown in the Supplementary Information File of Appendix 2, SI-Fig. 22–24.

H03-BAFKU₂ displays similar mesophases like neat BAFKU, which are even stable at similar temperatures, but in H03-BAFKU₂, the phase transitions are all enantiotropic (there is even nearly no difference in characteristic temperatures in heating and cooling scans, see DSC in Figure 22a). Three different textures can be recognized in the PLM heating scan (see Figure 33; detail PLM images of H03-BAFKU₂ are shown in the Supplementary Information part of Appendix 2), which are different from the ones observed in neat BAFKU, but the colours of the textures are very similar. Another difference is that the interconversions of textures in the copolymer are gradual and not as abrupt like in BAFKU. In case of the cooling scan, in contrast to DSC, the copolymer H03-BAFKU₂ displays only one texture (instead of three) which additionally appears ‘belatedly’, as an apparent undercooling. The contrast between the fast DSC scan (10°C/min) and the slow, but still undercooling PLM analysis (1°C/min) is interesting: A

certain undercooling was observed even with the neat BAFKU (albeit eventually most of the involved phases appeared). In case of the LC-end-capped copolymers, the apparent undercooling effect concerning the reappearance of PLM textures was found to be standard. As the LC-end-capped copolymers contain considerable amounts of PDMS spacer units, and also lamellae from BAFKU (which were observed by XRD), the **observed PLM textures are likely resulting from the anisotropy generated by both the alignment of BAFKU in lamellae, and by the lamellae themselves**. The relatively slow growth of lamellae to their final equilibrium sizes might be the reason for the apparent undercooling in PLM, which coincides with no undercooling in DSC.

H11-BAFKU₂ is characterized by simpler phase transition behaviour, and also by less sophisticated textures (see *Figure 34* and *Appendix 2* including its Supplementary Information), than H03-BAFKU₂. This copolymer displays only two thermotropic transitions (see DSC in *Figure 22b*). Moreover, the texture with the lamellae in the crystalline state does not significantly differ from the one with nematic lamellae. Similarly like its shorter homologue, also the copolymer H11-BAFKU₂ displays an apparent undercooling effect (with respect to DSC), concerning the reappearance of the PLM textures in the cooling scan, which can be attributed to analogous causes, namely the slow growth of the large lamellar structure in the sample.

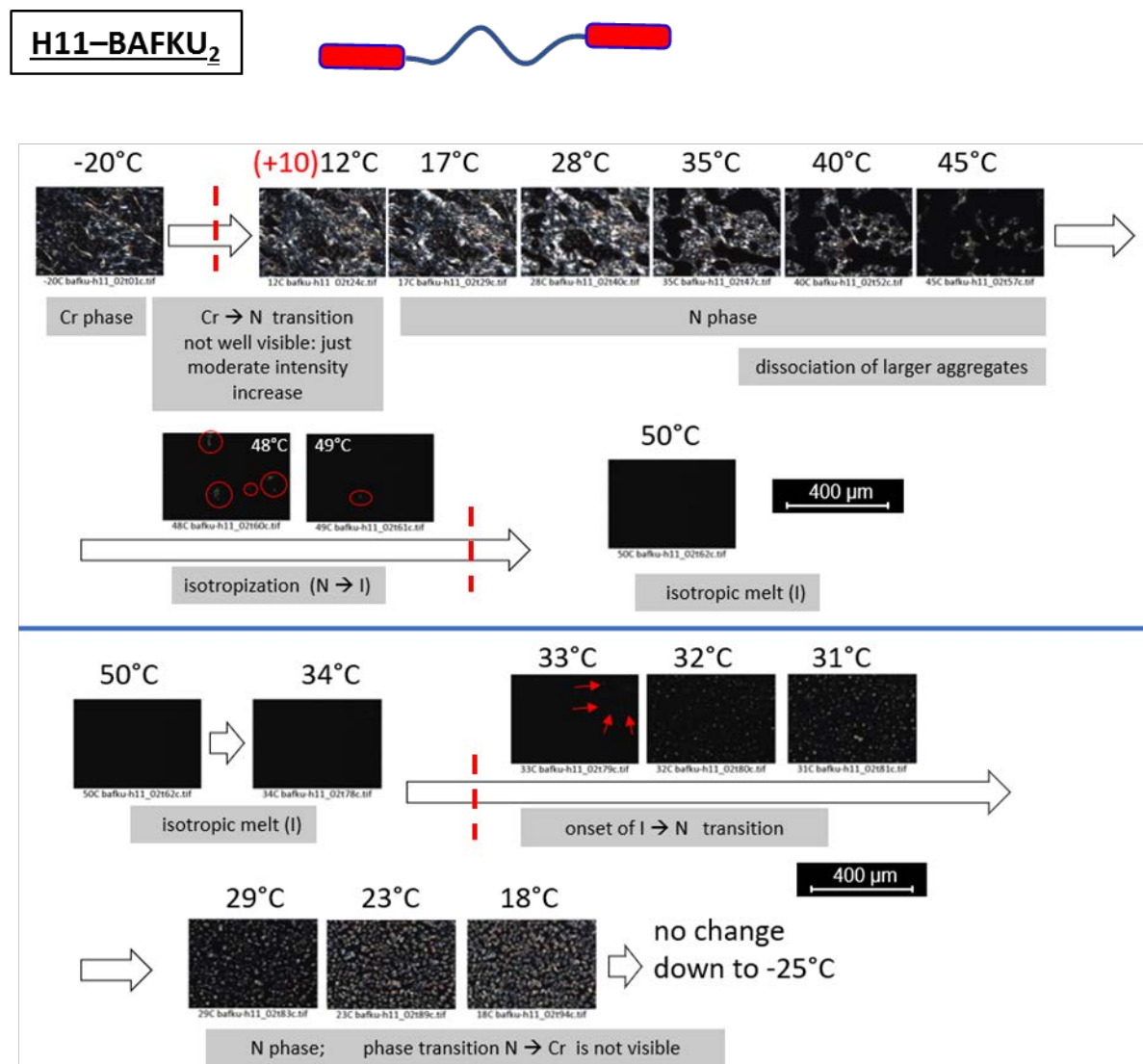


Figure 34: Textures observed in the LC-end-capped H11-BAFKU₂, top: heating run; bottom: cooling run; positions of thermotropic transitions observed by DSC are marked with red dotted lines; large representative images of each characteristic texture are shown in the Supplementary Information File of *Appendix 2, SI-Fig. 25–27*.

The copolymer H21-BAFKU₂ displays the most modest textures among the LC-end-capped copolymers, as shown in *Figure 35* (see also *Appendix 2* and its Supplementary Information). These consist in barely visible dot-like domains scattered over a darker field. Between +26 and +28°C, the dots brighten, and subsequently disappear between +28 and +32°C. In the cooling scan, the dots do not reappear, but the homogeneously dark image field becomes brighter, obviously due to the formation of sub-micrometre-sized anisotropic domains. The phase

transitions during both scans were evaluated using the mean polarized light intensity from a selected image area, which indicated nearly reversible changes on the time scale of the PLM experiment (see *Appendix 2, Supplementary Information File, SI-Fig. 19*). The reversible transition near 30°C is not visible in DSC (compare *Figure 22c*), but was observed (besides by PLM) also by XRD (see further above), and by rheological tests (see further below). The N→Cr transition, which leads to the solidification of H21–BAFKU₂ to a rubbery phase, and which correlates with the DSC peak at -9.75°C (in cooling scan only, see *Figure 22c*), does not cause any texture change in the PLM cooling scan in *Figure 35*.

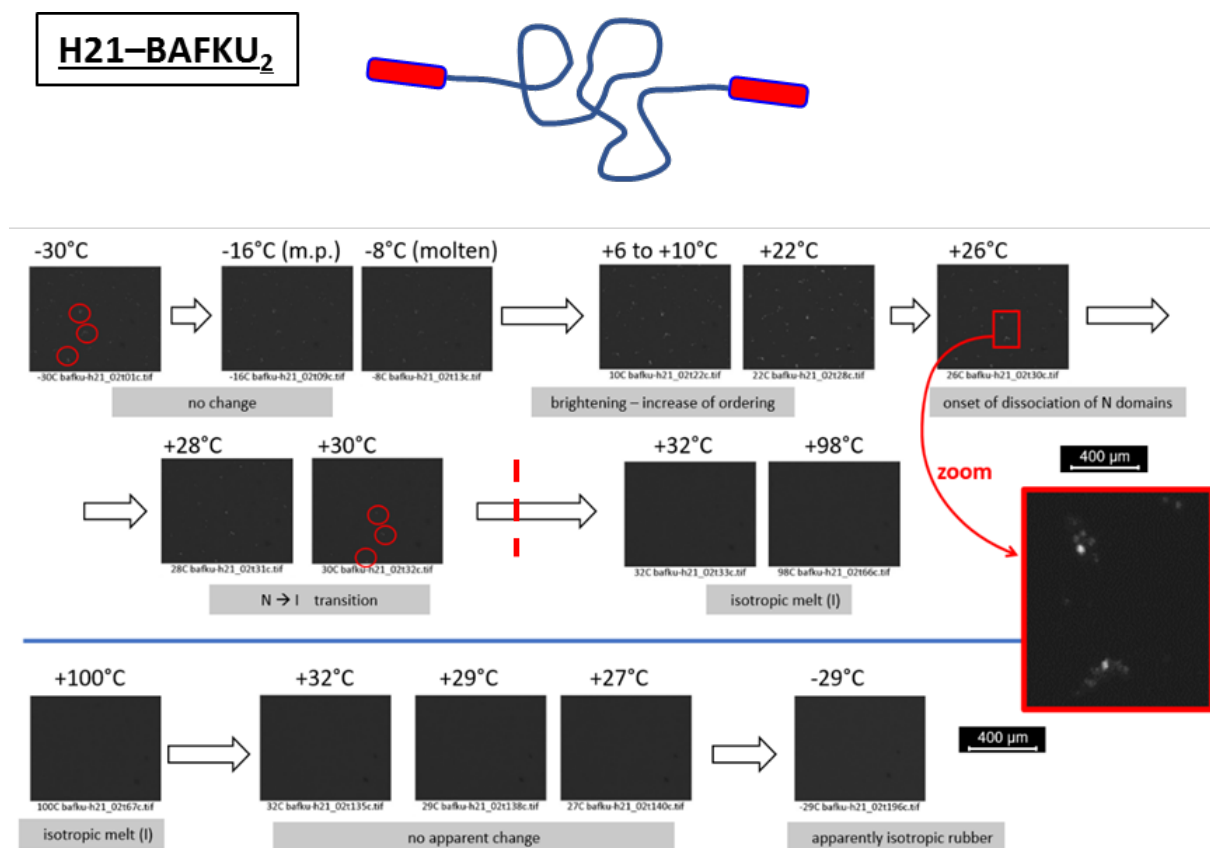


Figure 35: Textures observed in the LC-end-capped H21–BAFKU₂, top: heating run; bottom: cooling run; positions of thermotropic transitions observed by DSC are marked with red dotted lines; large representative images of each characteristic texture are shown in the Supplementary Information File of *Appendix 2, SI-Fig. 28–30*.

Linear infinite alternating LC-PDMS copolymers: Extensive PLM characterization was done for the linear infinite copolymers based on the azo-free mesogens M12, M22 and M32.

Results were also obtained for the copolymers based on the mesogen A1, which however did not display visible anisotropy in PLM analyses. Copolymers based on A12 still have to be characterized (other results concerning the azo-type linear copolymers can be found in *Appendix 4* and *5*).

Neat mesogens M12, M22 and M32: The mesogens M12, M22 and M32 display numerous thermotropic transitions (see DSC in *Figure 20*). The PLM textures of these mesogens are fairly similar, an example is shown in *Figure 36* (*T*-dependent textures of M22; the PLM analyses of all three mesogens are shown in *Appendix 6*). The temperatures of interconversions in PLM textures approximately correspond with the characteristic transition temperatures observed by DSC (M22: compare *Figure 20b* further above with *Figure 36*). It can be further noted, that the textures of the colorless mesogens have exclusively black and white colours. Additionally, the textures which reappear in cooling scans are fairly similar to their analogues observed in the heating scans.

In case of the mesogen **M12** (PLM: see *Appendix 6*), all the occurring mesophases can be observed reversibly without thermal damage to the compound during the heating scan, similarly like in case of M22. On the other hand, the mesogen **M32** undergoes thermally-induced reactions above 200°C, as was shown by detailed DSC investigations, so that its PLM analysis (see *Appendix 6*) above this temperature does not describe the pure compound, as well as the whole subsequent cooling scan.

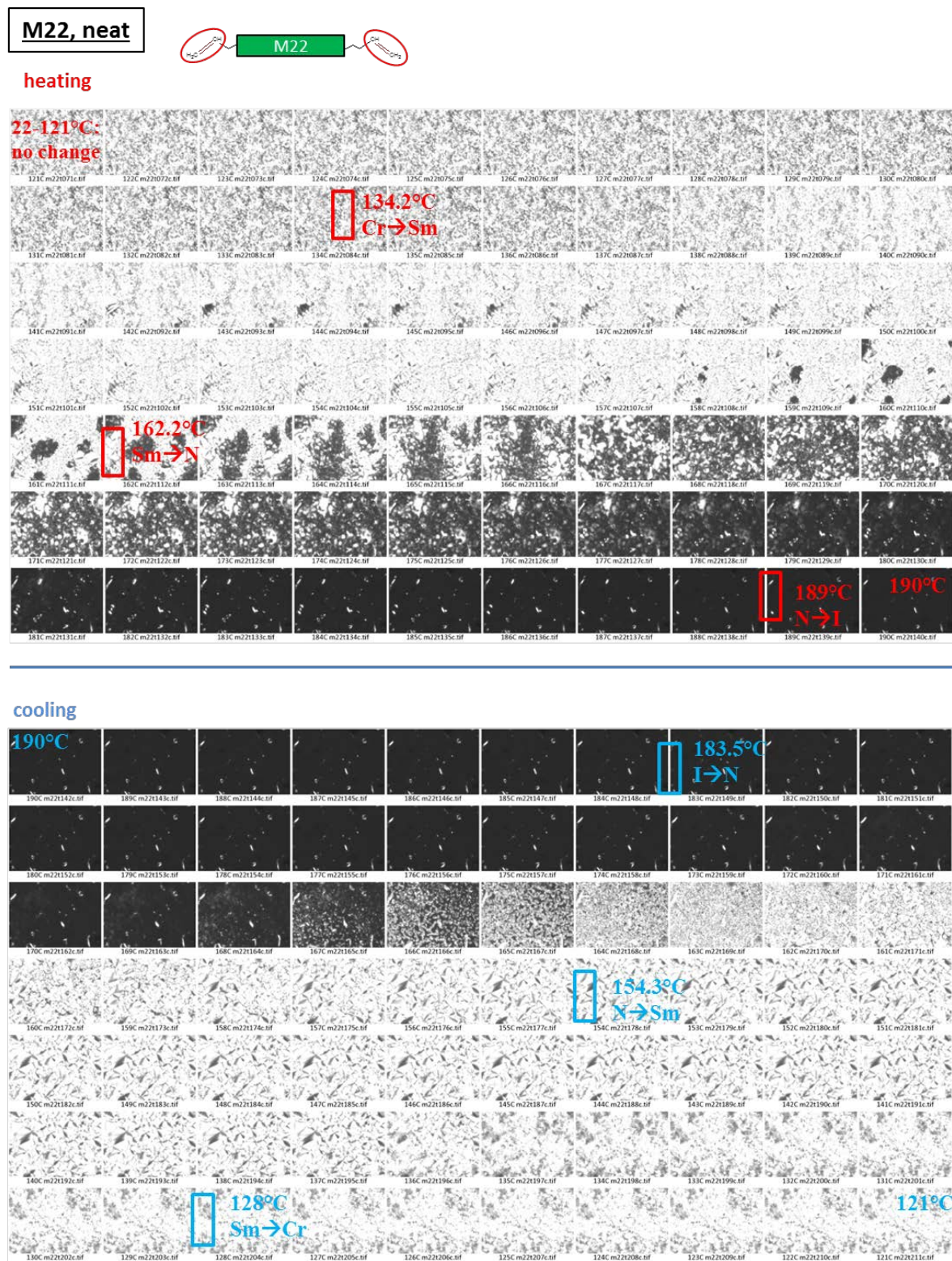


Figure 36: Textures observed in the neat mesogen M22, top: heating run; bottom: cooling run; the positions of thermotropic transitions as observed by DSC are marked.

Linear infinite copolymers with M12 mesogen: The smallest azo-free divinyl-functional mesogen provided only weak crosslinking in the linear infinite copolymers. This led to rather fine and bleak textures in the PLM analysis (see selected examples in *Figure 37*; all images are shown in *Appendix 6*). Similarly like in case of the neat mesogen, the textures in the **M12-co-PDMS copolymers** are black black and white. The texture was the richest in **M12-co-H03** with the shortest PDMS spacer (see *Figure 37a*). Upon heating, this texture was gradually fading, but the fading process did not follow the mechanically observable melting, but rather the final DSC transition (N→I) of the copolymer, which was fairly extended (maximum: 77°C; end of transition: ca. 100°C; disappearance of texture: ca. 84°C. Similarly like in case of the LC-end-capped copolymers, the anisotropy appeared in the PLM cooling run of M12-co-PDMS with a considerable delay relatively to DSC, but the pattern of the re-appearing texture was the same like the initial one observed at room temperature.

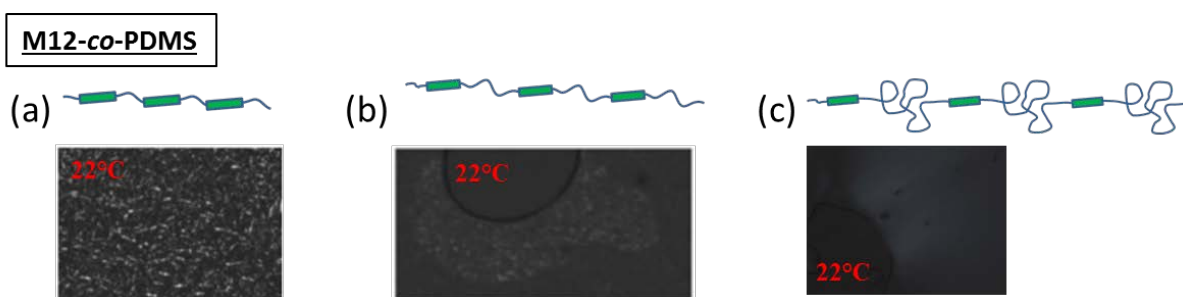


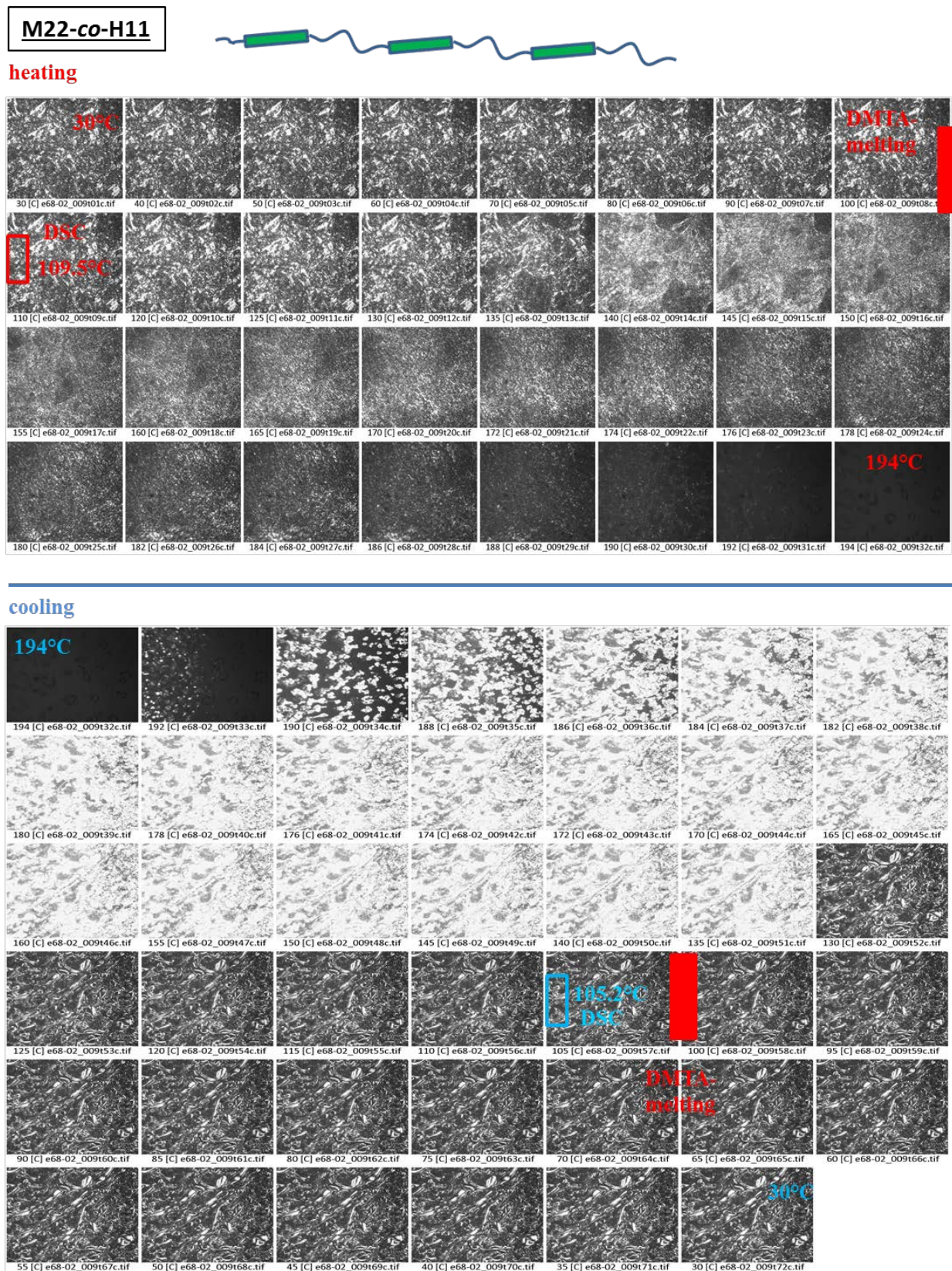
Figure 37: PLM textures in the M12-co-PDMS copolymers: (a) M12-co-H03; (b) M12-co-H11; (c) M12-co-H21; all the depicted textures were observed at room temperature.

In case of **M12-co-H11** with the mid-sized spacer segment, the PLM texture is much fainter (barely visible at room temperature, see *Figure 37b*) and it gradually fades upon the onset of the broad thermotropic transition (DSC maximum at 55°C; texture practically invisible at this point). Upon cooling, no re-generation of the texture is visible by naked eye in the PLM cooling scan. The copolymer with the longest mesogen **M12-co-H21** displays analogous trends like M12-co-H11, but no discrete texture pattern is observed in its anisotropic state, only a faint light grey colour (see *Figure 37c*), which suggests sub-micrometer size of the oriented domains. Except for the copolymer with the shortest spacer H03, the remaining ones display **isotropization (PLM) as well as a single broad DSC transition at temperatures ca. 20°C below the clearing point of the neat mesogen.** M12-co-H03, which was the richest in the M12

mesogen, displays a similar DSC transition region, and also a similar clearing point temperature, like the neat mesogen M12.

The linear infinite copolymers with the larger mesogens M22 and M32 displayed very similar trends in PLM analyses. Representative results characterizing some of the most attractive products (reversible rubbers) are shown in *Figure 38* (M22-co-H11) and *39* (M32-co-H11). The complete PLM results are presented in *Appendix 6*. In contrast to the copolymers with the M12 mesogens, the PLM textures are distinct in the M22- and M32- based products, especially with the shorter H03 and H11 PDMS spacers. In case of the longest spacer H21, similar textures are observed with M22-co-H21 (*Appendix 6*) and M32-co-H21 (*Figure 39*), like with M12-co-H03.

In case of the **shorter spacer segments H03 and H11**, the textures of the **M-co-PDMS copolymers** are fairly similar to the ones of the neat mesogens, or are even more structured (see M32-co-H03 and M32-co-H11 in *Appendix 6*, as well as M22-co-H11 in *Figure 38*; M22-co-H03 has to be characterized, but is expected to be highly similar to M32-co-H03). With a smaller mesogen and a lower melting temperature, the copolymer M22-co-H11 (see *Figure 38*) can be molten and heated up to the apparent clearing point without decomposition, while M32-co-H03 and M32-co-H11 (see *Appendix 6*) decompose prior to clearing point. The Cr1→Cr2 transition observed by DSC in the M32-based copolymers near 80-90°C does not lead to any visible change in PLM texture (see *Appendix 6*). On the other hand, the broadened ‘main transition’ (the only one in M22-based products), assigned as “Cr→N” in view of the PLM images, and connected with mechanically observable melting, leads to a distinctly visible texture change in the copolymers, which consists in a dramatic change of brightness (M32-co-H11 in *Appendix 6*), or in a moderate change in brightness combined with a change in the ‘micro-pattern’ of the texture (M22-co-H11, in *Figure 38*). In case of M32-co-H03, the main transition already cannot be discerned from the thermal decomposition (see *Appendix 6*). In general, in case of the products based on M32, the texture interconversions observable by PLM are sharper, and follow more closely the transitions visible in DSC.



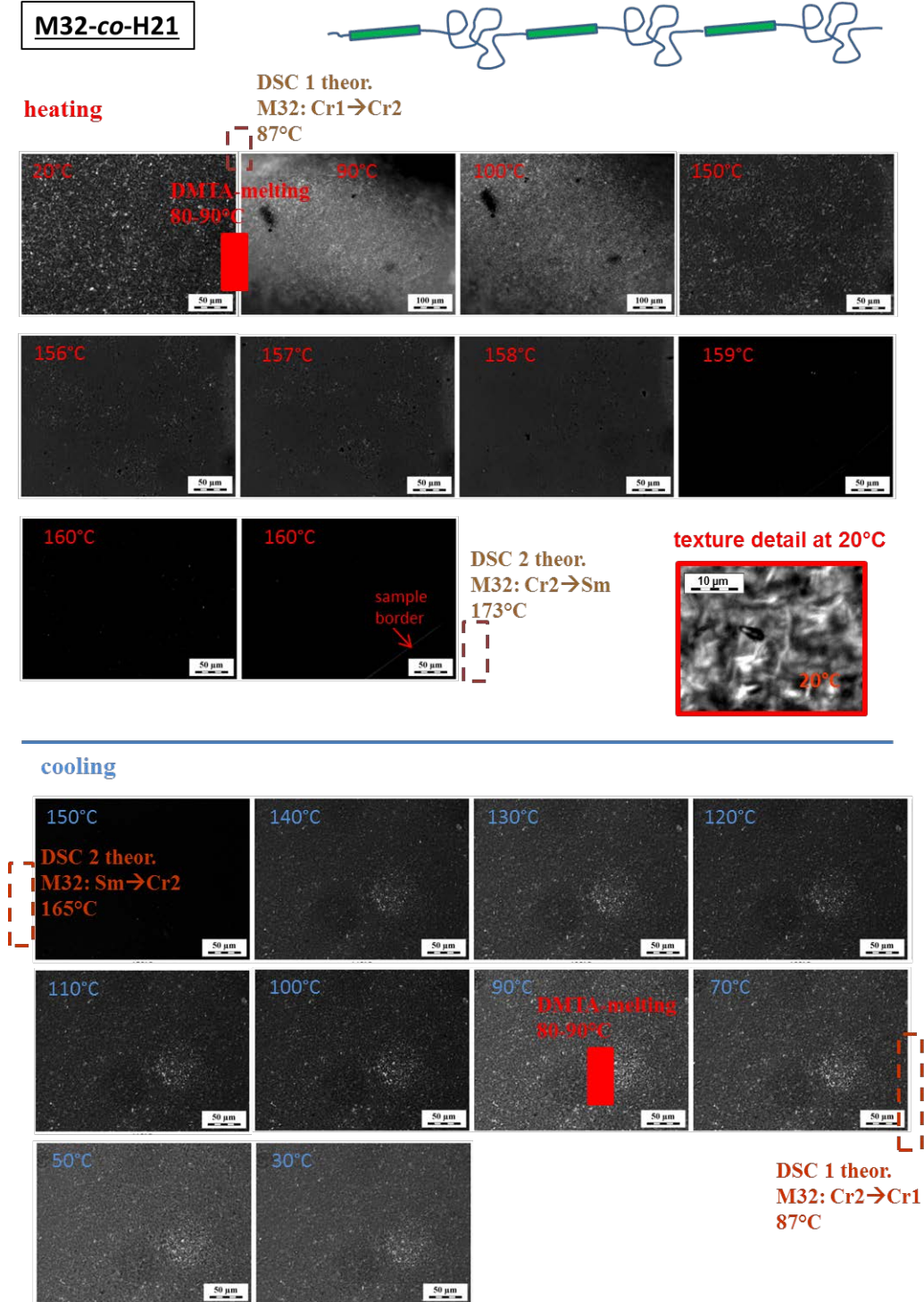


Figure 39: Textures observed in the copolymer M32-co-H21, top: heating run; bottom: cooling run; the positions of thermotropic transitions as observed by DSC, as well as of the mechanically observed melting/freezing are marked.

In case of the longer spacer segment H21, the **M-co-PDMS copolymers** display a faint and fine pattern (see M32-co-H21 in *Figure 39*), similar to the one observed for M12-co-H11 (see further above, *Figure 37a*). In case of M22-co-H21 (*Appendix 6*), the anisotropy is more uniform, rather than fine particulate. Even with the longest spacers, however, the anisotropy in the M-co-PDMS copolymers reappears in the cooling run without a marked delay (small apparent undercooling). This effect might be enhanced by the high nano-phase-separation tendency of the large mesogens.

To sum up, the PLM investigations greatly contributed to the elucidation of the phase- and nano-aggregation behaviour of the different LC units in the studied LC-PDMS copolymers of several architecture types.

-PLM confirmed the relatively low degree of ordering in the BAFKU-grafted elastomeric copolymer: non-characteristic textures only appeared if anisotropy was induced by shear.

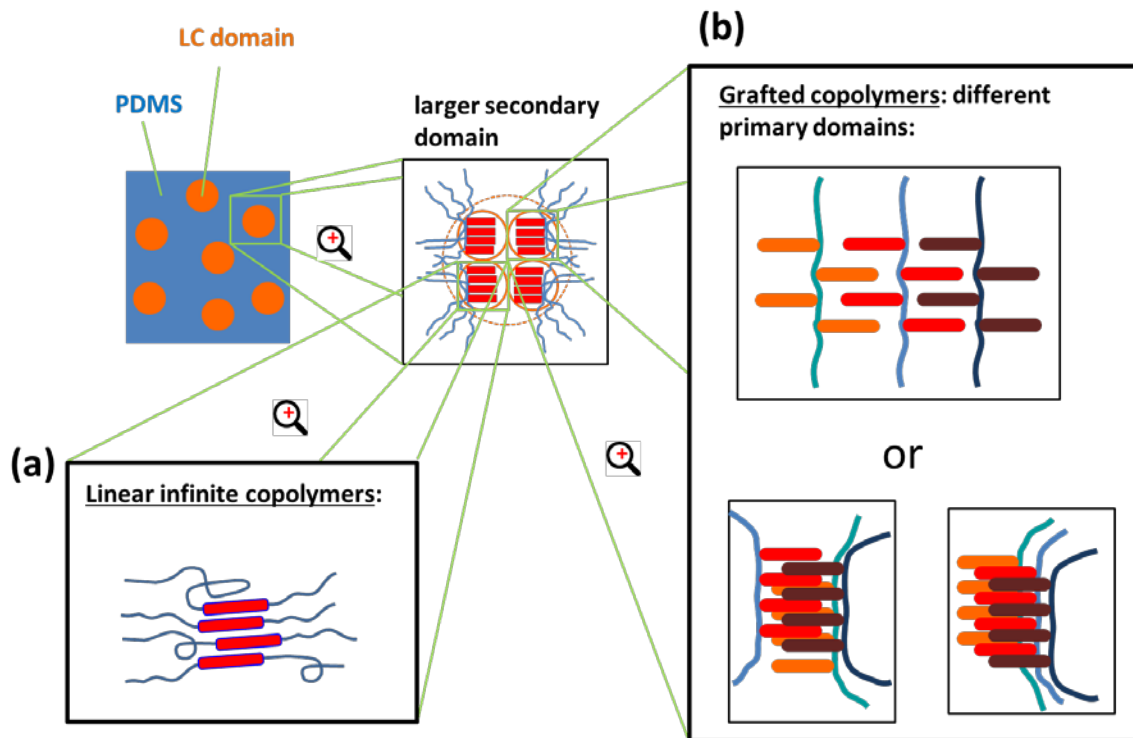
-The much higher degree of ordering in the BAFKU-end-capped copolymers also was confirmed by PLM, with especially sophisticated textures appearing and interconverting if the shortest PDMS spacer was employed. The spacer effect on the textures was dramatic, and they became very simple with the long H21 as spacer. But a thermotropic phase transition in liquid H21-BAFKU₂, invisible by DSC, and suggested by X-ray diffraction, could be clearly and most conveniently visualized by PLM. In the LC-end-capped copolymers, the anisotropy formed spontaneously after melt cooling. Because the relatively slowly growing lamellar structure had a decisive influence on the textures, the textures of frozen LC-end-capped copolymer melts displayed a longer development before reaching their final appearance.

-A moderately disordered nano-aggregate structure was confirmed by PLM for the linear infinite M-co-PDMS copolymers. A higher regularity associated with more distinct textures, and their more abrupt interconversions expectedly were observed with larger mesogens (like M32) and shorter spacers (like H11 and H03). In these copolymers, the textures formed spontaneously after cooling. Because no large superstructures were formed, the textures of cooled linear infinite copolymer melts (with M22 and M3) quickly reached the final appearance.

5.4.4 Aggregation behaviour of the copolymers

In view of the combined data from DMTA, DSC, X-ray and PLM analysis, models of aggregation behaviour in the studied copolymers can be suggested.

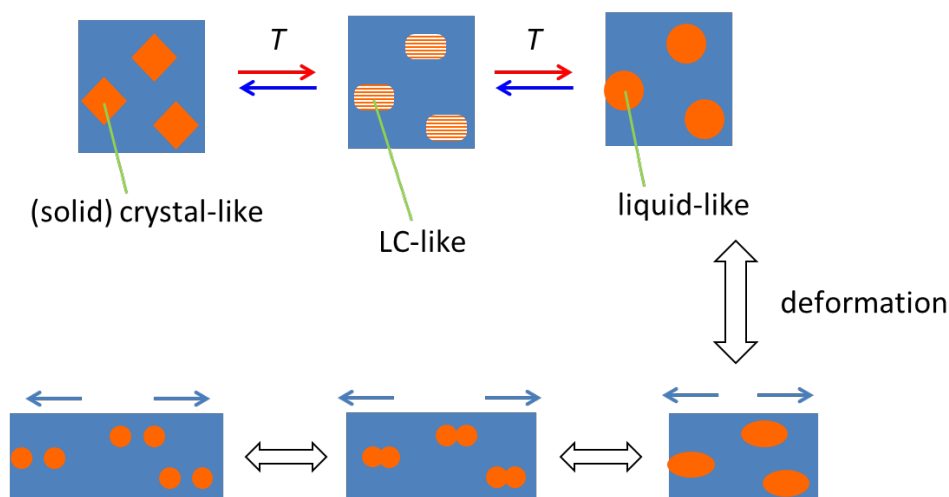
In case of the **LC-grafted**, as well as of the **linear infinite PDMS-LC copolymers**, the following structure can be postulated (see *Scheme 30*): Small nanometre-sized primary aggregates of LC units, which typically were found to possess a somewhat different and looser packing than the neat mesogens, are arranged to larger and less strong secondary aggregates, sized up to tens of nanometres (which caused the scattering features at the low angles in XRD analyses).



Scheme 30: Symbolic representation of the nano-structured morphology, and especially of the LC nano-aggregates in the (a) linear-infinite-LC-PDMS-, and (b) LC-grafted copolymers.

The regularity of the primary aggregates is not very high in the grafted copolymers, and moderate in the linear infinite ones, as documented by XRD and PLM. This is likely due to local mechanical strains, or to steric effects. Nevertheless, at different temperatures, structures are

formed, which are more or less related to crystalline, smectic, or nematic phases of neat mesogens (see *Scheme 31* top). Above the clearing point, the aggregates are isotropic-liquid like.

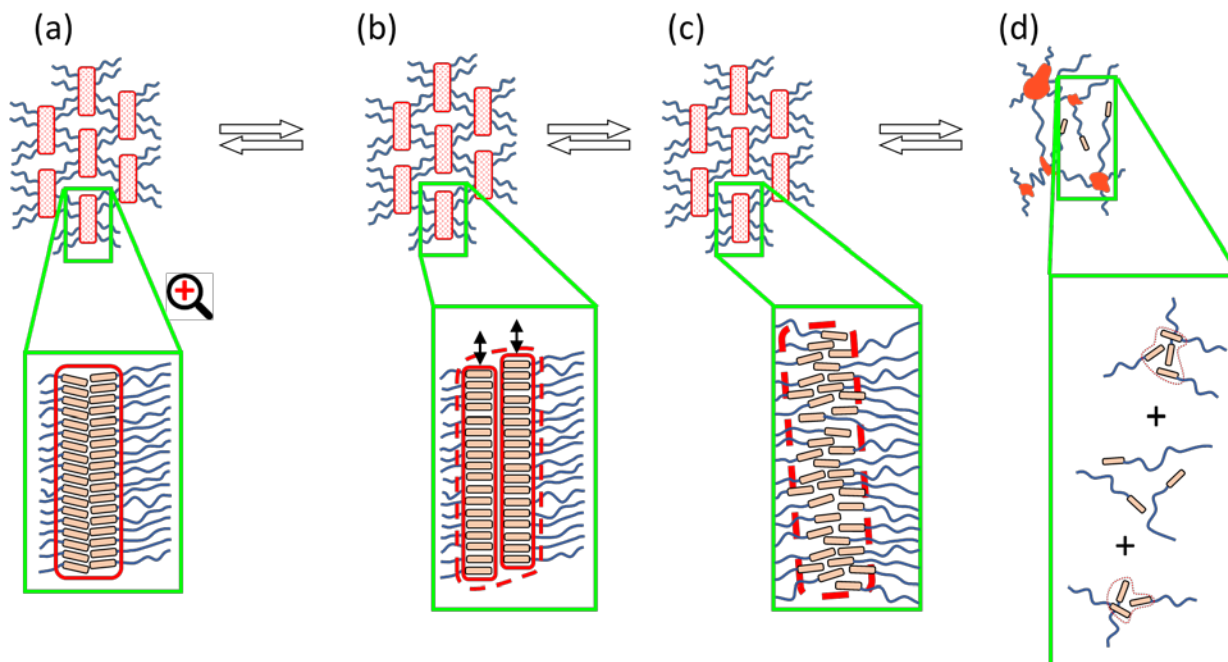


Scheme 31: LC nano-domains in linear-infinite-LC-PDMS-, and in LC-grafted copolymers, their transition from crystalline to liquid-crystalline (LC) and liquid state, under domain preservation; mechanical disconnection to smaller domains and recombination (coalescence) to bigger ones upon large shear deformation in the liquid or LC state.

The liquid-like LC nano-domains in the copolymer can split or coalesce (see *Scheme 31* bottom), but the primary and secondary aggregates are expected to persist (as supported by WAXS and SAXS data, see *Appendix 1*), because of the incompatibility, and hence phase-separation-tendency of PDMS and the mesogen.

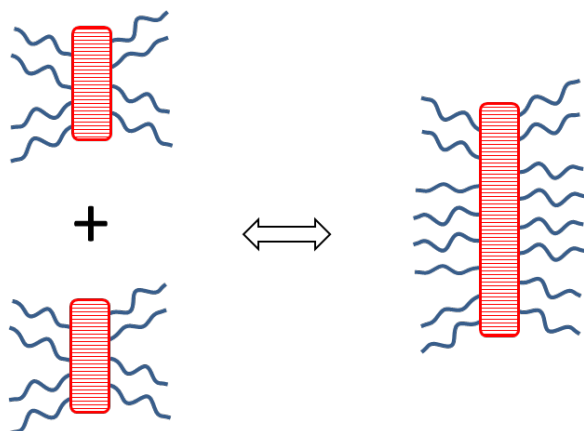
LC-end-capped copolymers: The lamellar structure, which was found in the LC-end-capped copolymers, is illustrated in *Scheme 32*. This Scheme also depicts postulated changes in the lamellae in the course of their internal thermotropic transitions, which control the mechanical properties of the whole copolymeric material: Depending on the temperature, the LC aggregates change their internal arrangement, as indicated by DSC and PLM, but below the isotropization temperature, they always keep their lamellar shape, and the lamellae stay at regular distances (like in the example in *Scheme 32*), in order to generate the above-discussed relatively sharp XRD reflection combined with its higher order peaks. The smectic state (*Scheme 32b*) is only observed in the copolymer H03–BAFKU₂. Larger areas with regularly and hence anisotropically

arranged LC aggregates (lamellae) generate well-visible PLM textures, in contrast to small regions of regularity. The latter nevertheless can produce significant background intensity in PLM, which was evaluated as the mean intensity of polarized light from the whole image area, as mentioned further above.



Scheme 32: *LC-end-capped copolymers: lamellar nano-aggregates of BAFKU, and the thermotropic transitions in their interior: (a) crystalline lamellae in the rubbery state, (b) smectic lamellae in the LC melt, (c) nematic lamellae in the LC melt, (d) isotropic small droplet like aggregates in the isotropic melt.*

The splitting and recombination of LC lamellae is depicted in **Scheme 33**. This process is expected to occur during the flow of the liquid crystalline melt of the LC-end-capped copolymers, or after cooling them down from the isotropic molten state (in which small droplet-like isotropic aggregates are expected to occur, as shown in **Scheme 32d**).



Scheme 33: Splitting and growth of LC lamellae in the LC-end-capped copolymers.

The process most probably plays a key role in the viscoelasticity and thixotropy of the liquid crystalline melt of the LC-end-capped copolymers, as well as in the ‘aging’ / undercooling of their PLM textures (which was discussed above).

5.5 Advanced tests of mechanical properties: disconnection of crosslinks in the reversible elastomers

Advanced mechanical tests were conducted in order to evaluate the strength, as well as the eventual failure and subsequent regeneration of the physical crosslinks in the studied copolymers. To this end, strain sweep tests (eventual network disconnection at high deformations), creep and stress relaxation tests (longer-time stability of the crosslinks under load) were conducted. The prepared copolymers also were subjected to frequency sweep tests, in order to compare them with the behavior of classical covalently crosslinked elastomers. As was eventually observed, this latter characterization method (or more precisely its chosen experimental setup) also made possible to visualize strain damage and its eventual rapid self-healing.

The advanced mechanical tests were most systematically conducted in case of the LC-end-capped copolymers (in a dedicated publication, see *Appendix 3*), but were also performed with the rubbery LC-grafted copolymer BAFKU₄₁–HMS 064 (*Appendix 1*), or with the linear infinite copolymers with azo-type mesogens (unpublished work, *Appendix 5*).

5.5.1 Strain sweep tests

The strain sweep tests with the studied copolymers (see example in *Figure 40*) were carried out in the oscillatory regime, with re-melted samples installed between very small (typically 6.1 mm) parallel plates. Fortunately, the re-melted copolymers showed good adhesion to the steel plates. The standard range of applied deformations (oscillatory strains, at 1 Hz) was from 0.1 to 1000%. The strain-dependent change of the (shear-) storage and loss modulus was observed. *Figure 40* shows representative results (graphs characteristic for different material states), as obtained for the LC-end-capped copolymer H11–BAFKU₂. In case of the other copolymer types, generally similar sets of results are obtained.

In *Figure 40*, several characteristic situations can be seen at different temperatures on the example of H11–BAFKU₂: at very low temperatures far from the melting region (e.g. -50°C in *Figure 40*) the physical network in the rubbery phase is rather robust: The sample undergoes macroscopic destruction (separation from the plates) at sufficiently high strains, which manifests itself as irregularities and sudden downward steps in the graphs. The mechanical destruction can also be observed visually. The limiting strain is between 1 and 2% for stiff rubbery H11–BAFKU₂, while for stiff rubbery H21–BAFKU₂ (at -70°C) with longer PDMS chains it is between 10 and 20%, and in stiff rubbery BAFKU₄₁–HMS 064 (at 0°C), this limit is 30–60% (see *Appendix 1*, Supplementary information).

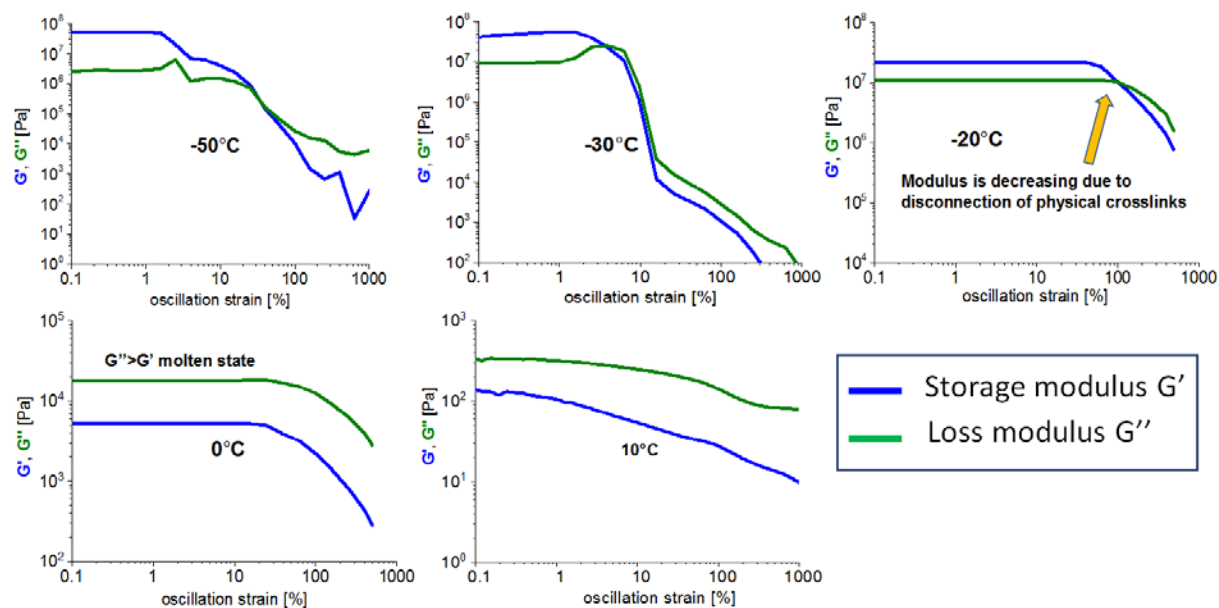


Figure 40: Disconnection of the physical crosslinks in H11-BAFKU₂ by mechanical strain: strain-dependence of storage (G') and loss (G'') modulus of H11-BAFKU₂ at temperatures from -50 to +10°C – selected results; the full results collection is shown in SI-Fig. 6/Appendix 3.

The linear infinite copolymers based on the mesogens A1 and A12 display similar or somewhat higher (100%, see *Appendix 5*) destruction limits in the stiff rubbery state than BAFKU₄₁-HMS 064. This destructive damage to the stiff rubbery samples occurs practically without dynamic disconnection of the physical crosslinks. At somewhat higher temperatures (-30°C in *Figure 40*), a smoother destruction occurs, which besides macroscopic damage likely also includes some shear thinning in the material (crosslink disconnection). At even higher temperatures (-20°C in *Figure 40*) no mechanical destruction is observed any more visually, the measured curves are smooth, and the samples are able to endure even high deformations. The moduli smoothly decrease at sufficiently high deformations (100% and more at -20°C in *Figure 40*), due to the disconnection of the physical crosslinks. At such a high deformation, the sample becomes liquid-like as G'' exceeds G' ($G'' > G'$ crossover). At even higher temperatures, e.g. 0 and 10°C in *Figure 40*, the strain dependence of the moduli shows similar trends like before, but G'' always is higher than G' , as the material already is a melt, and also the ‘shear degradation’ of the moduli starts at lower strains. The curves also become flatter and the moduli smaller.

To sum up, it can be concluded, that the physical crosslinks in the studied copolymers can be reversibly disconnected by large mechanical strain in the rubbery state and also in the melt. The investigations also suggested (and further below-discussed thixotropy tests confirmed that the ‘warmer’ rubbery phase of the longer copolymers, especially of the LC end-capped ones, can be relatively easily transformed into liquid by strong shear. Copolymers with the longest PDMS spacer segments between the LC units expectedly displayed the highest resistance at all temperatures against strain-induced degradation of their physical crosslinks.

5.5.2 **Creep test**

In case of the elastomeric LC-end-capped copolymers (H11–BAFKU₂ and H21–BAFKU₂), the mechanical strength of the physical crosslinks also was studied in multi-step creep experiments (details see *Appendix 3*), in which a constant stress was applied in each step, and the resulting time-dependent strain was observed. After each loading step, a recovery step with stress automatically adjusted to zero was carried out. The LC-end-capped copolymers with different PDMS spacers displayed similar trends in their respective characteristic temperature regions. Their crosslinks were found to be robust (on the time scale of the tests) only in the low-temperature part of the rubbery region.

H11–BAFKU₂ at -50°C (deep in the rubbery region) did not exhibit any visible creep up to 10 000 Pa (*SI-Fig. 9/Appendix 3*). At a higher temperature in the rubbery region (-20°C), a distinct creep starts at 10 000 Pa but most of the deformation still is recovered. At -5°C, not far from the melting region (which is near +8°C according to DMTA), creep is observed already at the lowest loadings, although significant elastic recovery still occurs, especially at lower stress loadings. By applying the relatively high stress of 10 000 Pa at -5°C, the sample is ‘shear-liquefied’ and an extreme deformation results. At +5°C and at higher temperatures, only plastic deformation without any recovery occurs, and the strains resulting from the applied stresses become very large, as the sample becomes liquid, albeit a nematic viscoelastic one.

The copolymer H21–BAFKU₂ (*SI-Fig. 10/Appendix 3*) displayed similar trends like H11–BAFKU₂, but at the highest stresses, it is the longer copolymer which creeps more.

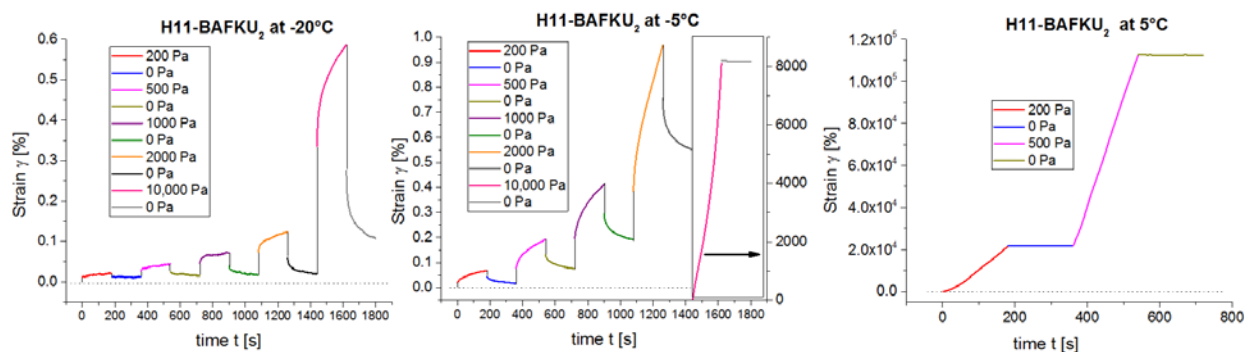


Figure 41: Multi-step creep tests of H11-BAFKU₂ at the temperatures of -20, -5 and +5°C; stresses ranging between 200 and 10 000 Pa were applied, followed by recovery steps (at 0 Pa); more results at different temperatures are shown in **SI-Fig. 9/Appendix 3**.

5.5.3 Stress relaxation

The mechanical stability of the physical crosslinks in the elastomeric LC-end-capped copolymers (H11-BAFKU₂ and H21-BAFKU₂) was further evaluated by means of stress relaxation test, which practically studied “internal creep phenomena”. Both copolymers exhibited the same trends in their characteristic temperature regions, like in case of creep tests. Exemplary results for H21-BAFKU₂ are shown in **Figure 42**.

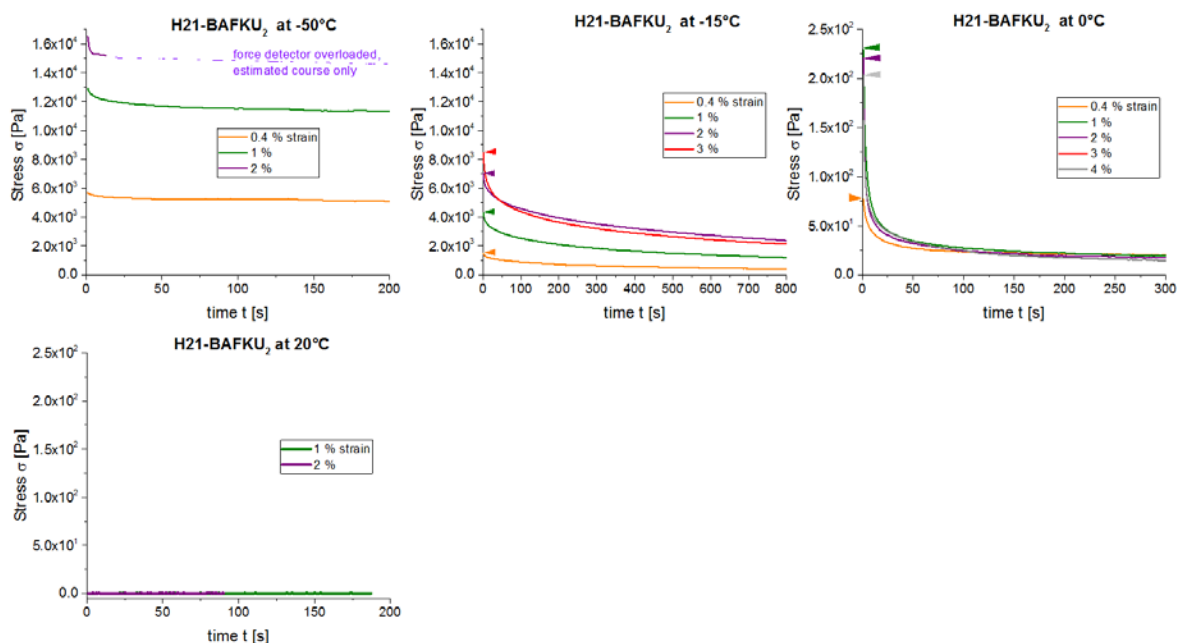


Figure 42: Stress relaxation tests of H21-BAFKU₂ at different temperatures; at each temperature, several constant strain values were applied.

Deep in the rubbery region (-50°C), the copolymer H21–BAFKU₂ exhibits a small and fast relaxation (see *Figure 42*), and subsequently no significant effects on the timescale of 3 min. At higher temperature (-15°C), (in analogy with the creep test), relaxation is much more prominent, especially if higher initial stress is applied, but the measured relaxing stress does not seem to approach a zero final value (in the mid-term). At 0°C (in the early nematic state), the stress relatively quickly relaxes ca. 85% of its value and stabilizes on a slowly decreasing course. This behaviour could be connected with presence of permanent entanglements due to the long H21 chains, and due to the stabilization of entanglements via residual of physical crosslinking (BAFKU lamellae in the nematic phase). At 20°C , in the warmer region of the nematic phase, the stress relaxation is nearly immediate. The value of the measured stress runs constantly at 0 Pa.

H11–BAFKU₂ exhibits very similar trends like H21–BAFKU₂ (see *Appendix 3/SI-Fig. 12*), with an interesting feature at 5°C (in the nematic phase). There, after applying the highest stress values, the relaxation is very rapid. The relaxing stress eventually crosses the zero value and reaches a small negative value ('relaxation overshoot'). This likely is caused by shear-induced ordering of the nematic lamellae and of the whole lamellar structure, which is dynamic at this temperature. A similar effect of higher strength was observed for H03–BAFKU₂, which contains more of the mesogen, while the effect is absent in H21–BAFKU₂.

In case of H03–BAFKU₂, investigated in its early melting region (see *Appendix 3/SI-Fig. 13*), the relaxation trends are similar to the warm H11–BAFKU₂, but relaxation in the smectic H03–BAFKU₂ is much faster and the relaxation overshoot effect is more intense (especially at 25°C).

5.5.4 Frequency stiffening tests and ability to self-healing

Eventual sample stiffening at high oscillatory deformation frequencies and eventual frequency-induced transitions between liquid-like and rubber-like behaviour was studied by means of frequency sweep tests at several temperatures for all of the groups of copolymers (LC-grafted copolymers: *Appendix 1*, LC-end capped copolymers: *Appendix 3*, linear infinite copolymers of azo type: *Appendix 5*). Generally it can be concluded that frequency-stiffening

was observed in all the copolymers in the rubbery state, as well as in the melt. Such a behaviour is characteristic of classical elastomers and of molten linear polymers.

The studied copolymers generally exhibit analogous trends in the frequency sweep tests. As an example, several characteristic situations can be seen at different temperatures on the example of the copolymer **H11-BAFKU₂** (see **Figure 43**, selected graphs only, all results are in **Appendix 3/SI-Fig. 14**). The following trends can be observed: At low temperatures deep in the rubbery region (e.g. at -60°C in **Figure 43**), G' always prevails over G'' , even at the lowest frequency of 1 mHz, and the samples hence are truly rubber-like. The physical crosslinks are robust in this temperature region, so that the test at -60°C with high applied strains results in macroscopic mechanical damage: irregular curves, similarly like in the strain sweep test of the same copolymer at -50°C shown in **Figure 40**; the damage worsens during the delays between frequency decades (steps in the curves; the delays of the duration of several seconds were given by the operation mode of the employed rheometer/DMTA analyser).

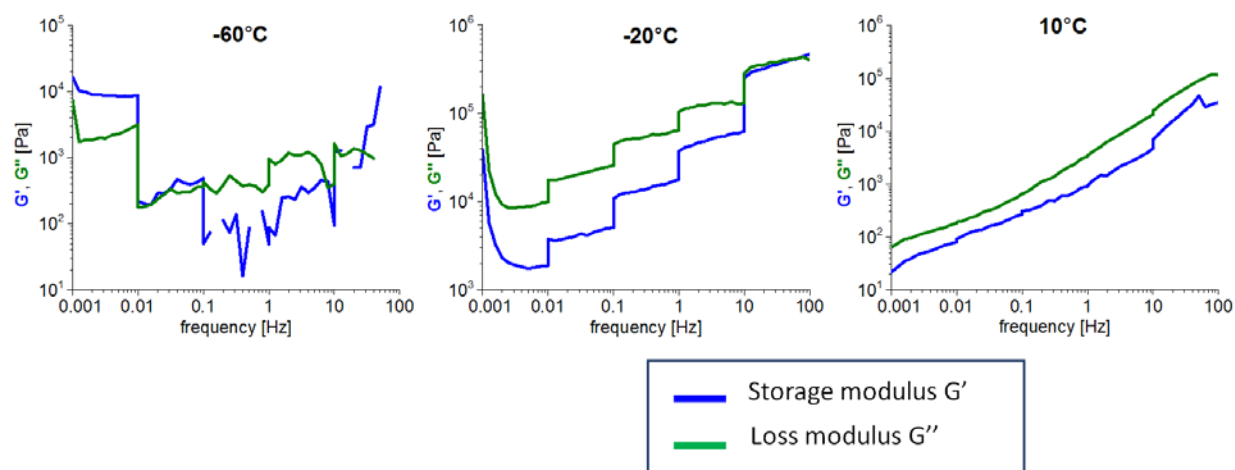


Figure 43: Frequency-stiffening of H11-BAFKU₂ observed in frequency sweep tests (1 mHz to 100 Hz) conducted at -60 to $+10^{\circ}\text{C}$ – selected results; the full results collection is shown in **Appendix 3/SI-Fig. 14**; the strain amplitude was different in each frequency decade, ranging from 50% at 1 mHz to 1% at 100 Hz; the effect of strain-induced damage to the network, as well as of its recovery between the frequency decades is clearly visible, especially in case of G' curves at lower temperatures.

At higher temperatures in the rubbery region (-20°C), no macroscopic destruction is observed, but only shear-thinning damage to the crosslink density. During the delays between frequency decades, the internal damage is at least partly repaired by crosslink re-combination. This **internal**

self-healing is very fast, as it generates marked effects during the brief (multi-second) delays. As the rubbery phase is fully molten (see example in *Figure 43*: 10°C), the crosslink destruction at low frequency (due to large deformation amplitude), as well as the self-healing effects completely disappear, and the measured curves become nearly linear in the nematic melt. Already before T reaches the melting region, G'' starts to dominate over G' , but G' increases more steeply with frequency. In the nematic melt, and at higher temperatures, G' and G'' have a parallel course.

To sum up, it should be underlined that in all copolymers, the stiffening effect was the highest in the molten state: 4–5 orders of magnitude, while it was the lowest in the stiff rubbery state (low temperature): 1–3 orders of magnitude. The strain damage and self-healing effects, which were also observed in the frequency sweep tests, were found to be prominent especially in the temperature range of the thermotropic transitions of the LC aggregates in the studied copolymers (see also results for BAFKU₄₁–HMS064 in *Appendix 1*).

5.6 Rheological properties

The dynamic aspects of the reversible physical crosslinking in the studied copolymers were investigated by rheological methods. These included the **multi-frequency study of temperature-controlled gelation vs. melting** of the copolymers (multi-frequency temperature scans). Another method was the rheological **study of the kinetics of the gelation of copolymer melt after its abrupt cooling** to a given temperature (single-frequency time sweep tests). Finally, the **thixotropic properties of the molten copolymers** were investigated (destruction and regeneration of crosslinks in melt). Most extensively studied were the LC-end-capped copolymers (in a dedicated publication, see *Appendix 3*), but rheology tests (except thixotropy) also were performed with the rubbery LC-grafted copolymer BAFKU₄₁-HMS 064 (*Appendix 1*), or with the linear infinite copolymers with azo-type mesogens (unpublished work, *Appendix 5*).

In general, the rheological behaviour of the copolymers was found to be controlled by an interplay of nano-phase separation of the LC moieties (growth and splitting of their aggregates), and of the thermotropic transitions in these aggregates (which change their stiffness). Entanglements of the elastic PDMS chains also were found to play a role.

5.6.1 Reversible gelation near the melting point

Rheological multi-frequency temperature scans were performed in order to determine gelation temperatures in the tested copolymers. Normally, a material displays only one gel point, as consequence of thermally or chemically induced crosslinking. The point of gelation is most accurately defined by the Chambon-Winter theory [217], as the point of the cross-over of $\tan \delta$ (loss factor) for several frequencies.

The **LC-grafted copolymer BAFKU₄₁-HMS064**, in which the LC aggregates were found to be less than perfectly ordered, nevertheless, was found to display an interesting temperature-controlled gelation behaviour (see *Figure 44*, heating scan). In the heating multi-frequency scan, two $\tan \delta$ crossovers can be seen, at 44.9 and 68.5°C, which hence correspond to two gel points. The gel point at 68.5°C can be regarded as the expected one, because the rubbery copolymer gradually melts near this temperature (it also is close to the clearing point of neat BAFKU). The second, ‘anomalous’ gel point at 44.9°C, occurs at the position of the nematic/smectic transition, which in the neat mesogen occurs only in the cooling scan. In the

copolymer, however, this transition apparently is included into the broader transition region observed both in heating and cooling scans. This transition might contribute to considerable stiffening of primary and of the larger secondary aggregates (see discussion of aggregation behaviour further above), and thus of the whole rubbery phase, which transforms from a plastic elastomer to a stiffer rubber. In the cooling regime a similar behaviour is observed, but the low-temperature gel point is less pronounced (see detailed discussion in *Appendix I*).

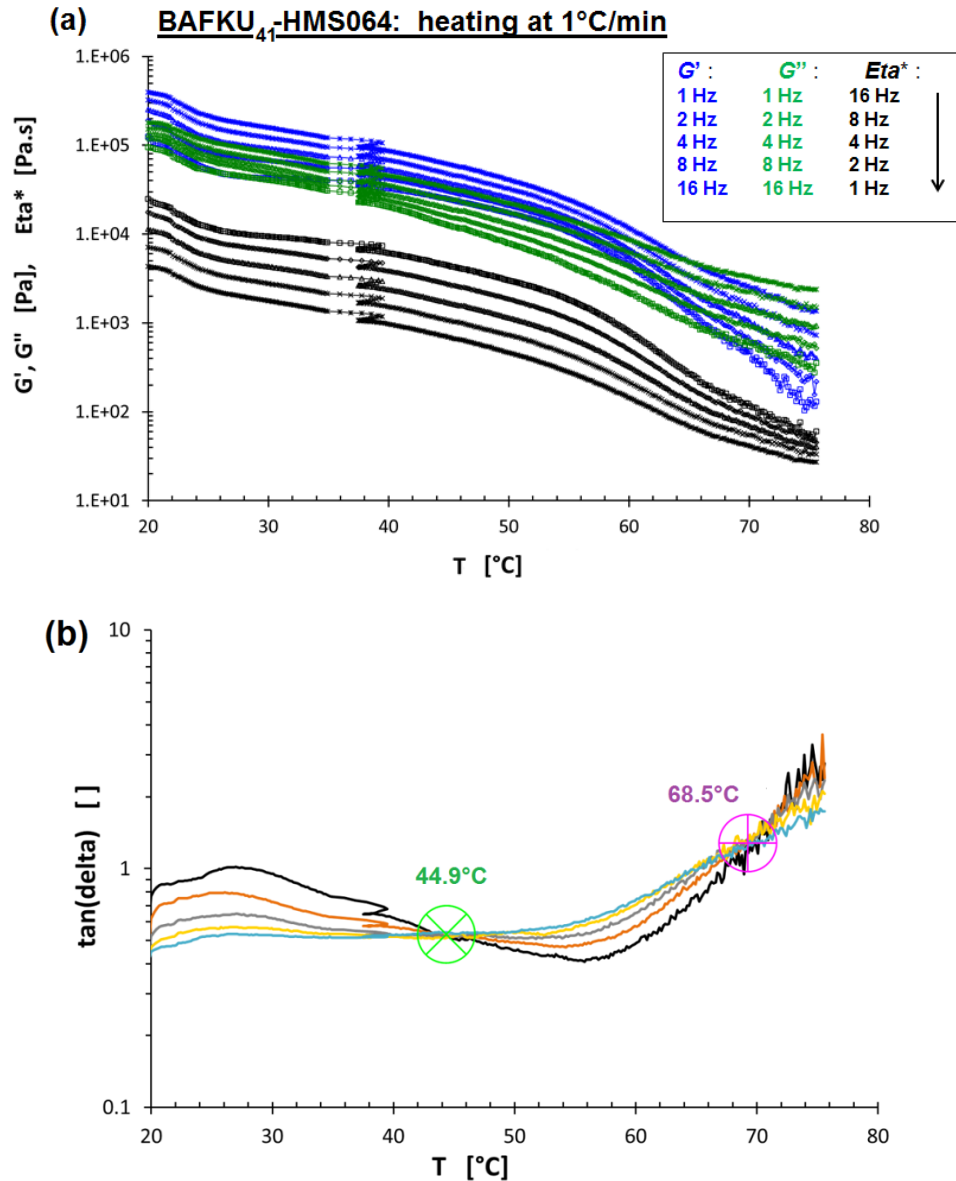


Figure 44: Multi-frequency temperature ramp test: Determination of temperature-induced gel in BAFKU₄₁-HMS064: (a) temperature dependence of the storage shear moduli G' , of the loss moduli G'' , and of the complex viscosity Eta^* recorded at the simultaneously applied frequencies

of 1, 2, 4, 8 and 16 Hz; (b): detail of the set of the $\tan \delta$ curves for the same experiment, with marked crossover points.

In case of the **LC-end-capped copolymers**, the gelation behaviour is even more complex than in case of LC-grafted BAFKU₄₁-HMS064. As an example, the **Figure 45** shows results of multi-frequency temperature scans for the copolymer **H03-BAFKU₂**, which was shown to display the richest phase behaviour (as discussed further above), and which also displays the most sophisticated gelation behaviour.

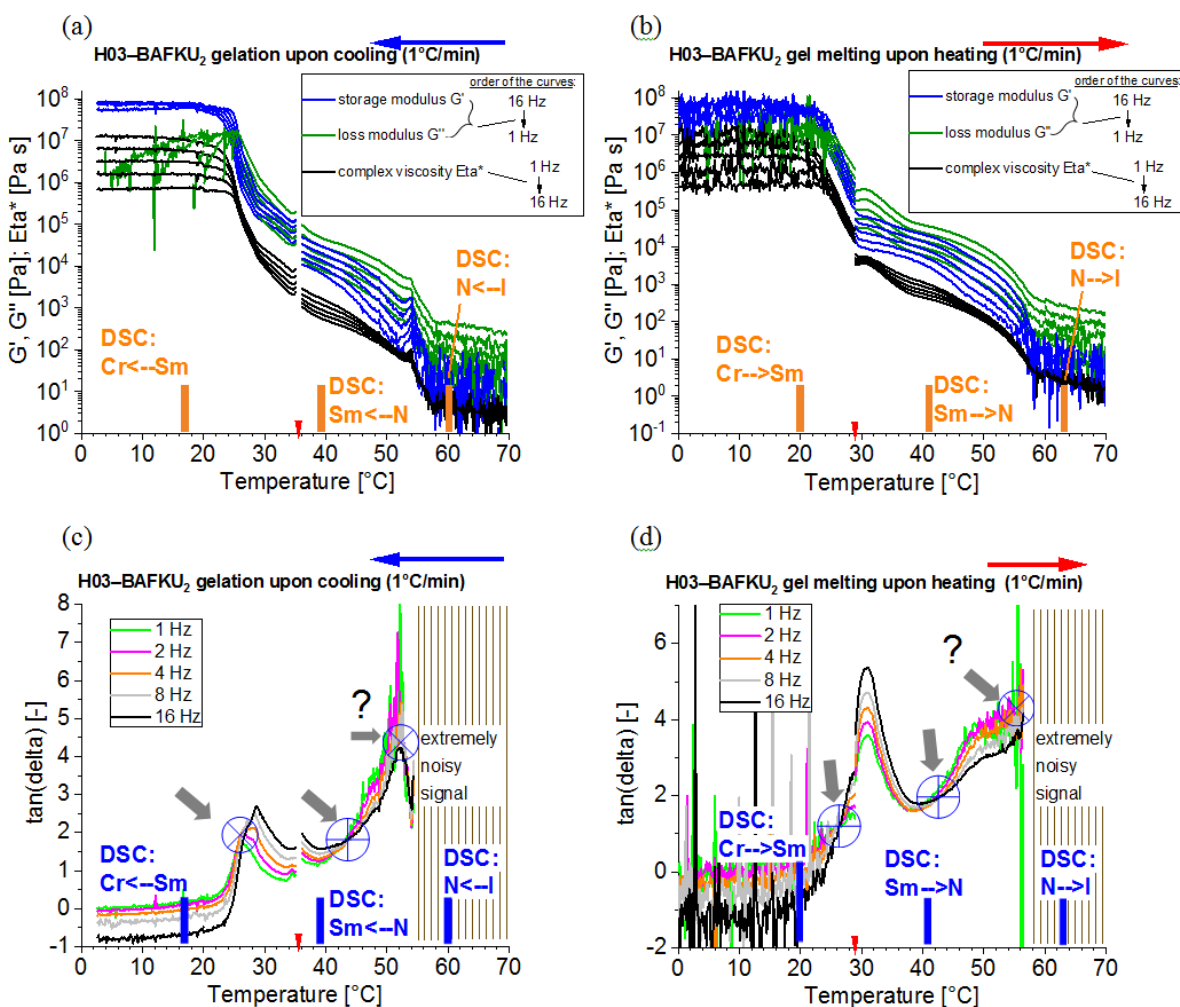


Figure 45. Multi-frequency temperature ramp tests carried out in the melt- and rubbery temperature regions of the LC-end-capped copolymer H03-BAFKU₂: (a), (b): temperature dependence of the storage shear moduli G' , of the loss moduli G'' , of the complex viscosities Eta^* recorded at the simultaneously applied frequencies of 1, 2, 4, 8 and 16 Hz; (a): cooling scan; (b): heating scan; (c), (d): detail of the sets of the $\tan \delta$ curves with marked crossover (or

near-crossover) points; (c): cooling scan , (d): heating scan; red markers indicate change in strain.

It can be seen in **Figure 45**, that three gel points can be recognized (or at least suspected in case of the one at the highest temperature). These gel points appear to closely correlate with the distinct transitions observable by DSC, and assigned as transitions between material with aggregates in crystalline, smectic, nematic and isotropic state. Additionally, the wider scale effects of nano-phase-separation (LC lamellae fragmentation vs. growth) appear to play an important role (a detailed discussion is given in **Appendix 3**).

The **H11–BAFKU₂** copolymer with longer central chains displays similar trends like its shorter homologue, but it possesses ‘only’ two gel points, as it also possesses only two thermotropic transitions (between material with aggregates in crystalline, nematic and isotropic state). The involved transitions are at lower temperatures than in case of H03–BAFKU₂. The copolymer **H21–BAFKU₂** closely resembles H11–BAFKU₂ in its gelation behaviour its transition temperatures are even lower (a detailed discussion concerning the gelation of both copolymers is given in **Appendix 3**)

Finally, it should be noted, that **in case of the LC-end-capped copolymers**, the **additional “anomalous’ gel points are all located in the liquid region**, while the ‘normal’ gel point occurs at the lowest temperature and corresponds to the melting/freezing of the rubbery phase. Hence, these copolymers could be of interest as ‘smart liquids’, with temperature-switchable viscoelastic properties.

Among the **linear infinite copolymers**, only the rheological properties of the ones containing the relatively weakly crosslinking mesogens A1 and A12 were investigated (the results were not yet published; they are summarized in **Appendix 5**). These copolymers were shown to display intermediate properties in many aspects between the LC-grafted and the LC-end-capped copolymers. An exemplary set of rheology results is shown in **Figure 46**, namely for the LC-rich product A1-co-H03. It can be seen, that this material clearly displays three well-visible $\tan \delta$ crossovers (another hidden in noise cannot be excluded). This finding correlates with the relatively transition-rich behaviour of this copolymer in DSC (discussed further above). While the rich transition behaviour of A1-co-H03 and its numerous gel points are reminiscent of the LC-end-capped copolymers, all the transitions in A1-co-H03 nevertheless are found in the

rubbery (or eventually plastic rubbery) state, and none (even suspected) of them is in the melt region. This is an analogy with the LC-grafted copolymers, which also do not display additional gel points in the melt phase, and which are postulated (as discussed further above) to exhibit a similar aggregation behaviour. Other linear infinite copolymers of azo type display similar trends like A1-co-H03, but the ones with longer PDMS chains tend to display fewer gel points.

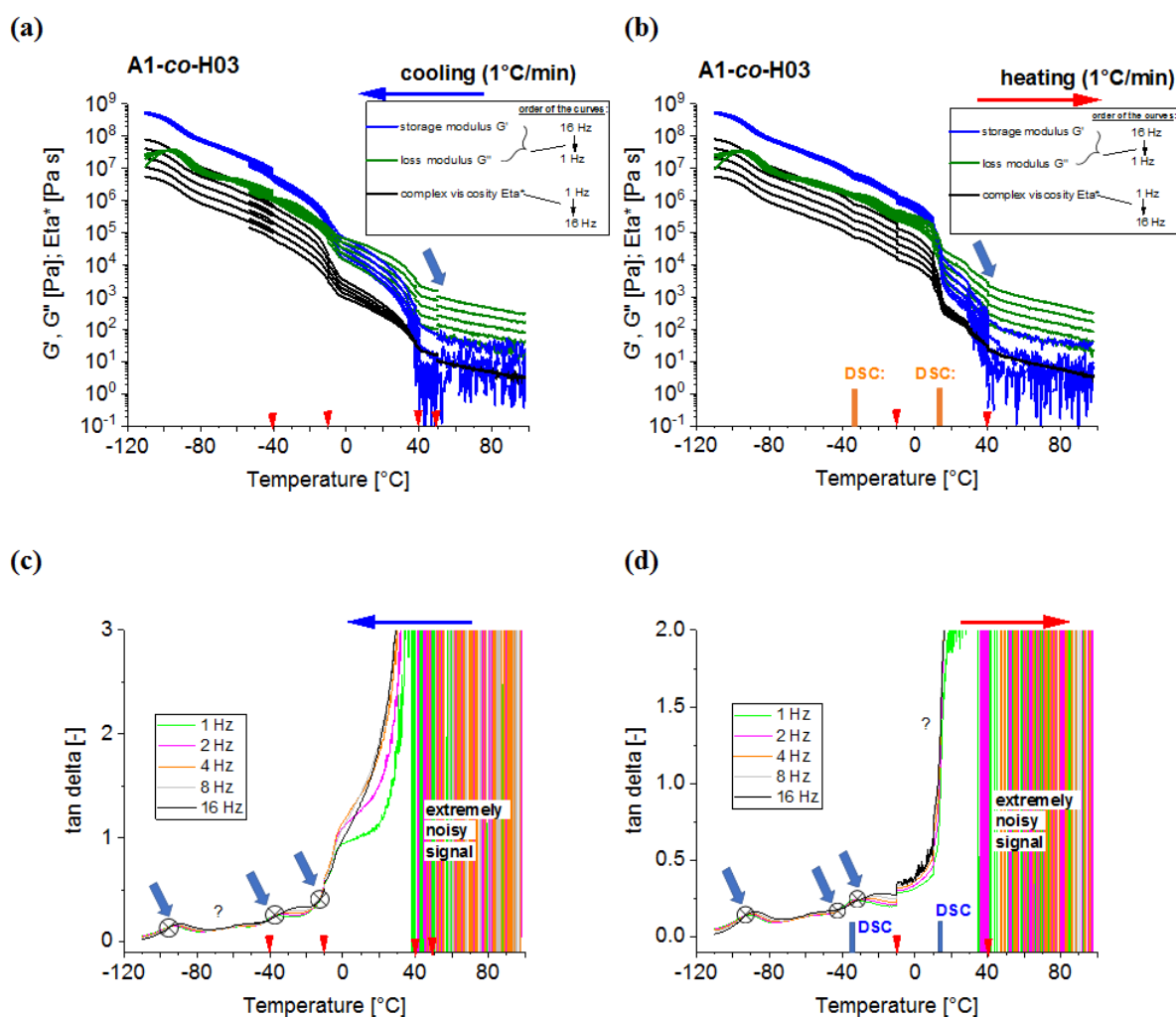


Figure 46. Multi-frequency temperature ramp tests carried out in the melt- and rubbery temperature regions of the LC-end-capped copolymer A1-co-H03: (a), (b): temperature dependence of the storage shear moduli G' , of the loss moduli G'' , and of the complex viscosities Eta^* recorded at the simultaneously applied frequencies of 1, 2, 4, 8 and 16 Hz; (c), (d): sets of the $\tan \delta$ curves with marked crossover (or near-crossover) points; red signs indicate change in strain.

Finally, it should be noted, that **in contrast to LC-rich liquid crystalline (co)polymers (LCPs) known from the literature, the novel copolymers studied in this work display a viscosity increase if going from isotropic to nematic** (or further to the smectic) state, because their viscoelasticity is controlled by the larger-scale morphology, which is responsible for the physical crosslinking. The latter in turn is controlled by nano-phase separation and by the strengthening or loosening of the aggregates of LC units via thermotropic transitions.

5.6.2 Rate of thermally induced physical gelation

An interesting aspect of the temperature-induced reversible crosslinking of via nano-aggregation of LC units in the studied copolymers is the kinetics of this process. The kinetics could not be directly observed in the above-discussed multi-frequency experiments which sought to find temperatures of gel points.

The gelation kinetics was studied via ‘quenching’ polymer melt samples from the ‘isotropic temperature’ of of the respective copolymer down to different test temperatures. During the quenching and in the subsequent time period where the temperature was constant, the moduli of the tested samples were measured via an applied oscillatory deformation of constant frequency (1 Hz) and of a constant small strain (1%). Observation of the build-up and of the subsequent equilibration of the moduli gave a picture of the kinetics. The kinetics of temperature-induced gelation was studied in detail in case of the LC-end-capped copolymers (in a dedicated publication, see *Appendix 3*), but with the rubbery LC-grafted copolymer BAFKU₄₁–HMS 064 (*Appendix 1*), or with the linear infinite copolymers with azo-type mesogens (unpublished work, *Appendix 5*).

The studied copolymers all displayed similar trends concerning the kinetics of crosslinking upon the quenching of their melt. Only in case of the LC-end-capped copolymers, some additional specific effects were observed. The rates of gelation also were generally similar. The LC-grafted copolymer BAFKU₄₁–HMS 064 (*Appendix 1*) needed ca. 2 to 3 min for completed gelation, depending on experiment temperature. The LC-end-capped copolymers needed between 0.5 and 3 min, but typically ca. 1 min. Linear infinite LC-PDMS copolymers with azo-type mesogens A1 and A12 typically needed 2 to 3 min for complete gelation, similarly like the LC-grafted ones.

In **Figure 47** and **48**, exemplary results are shown, which were obtained for the LC-end-capped copolymers H11-BAFKU₂ and H21-BAFKU₂, respectively. It can be seen, that if these copolymers are quenched to very low temperatures, deep in the rubbery region, the kinetics of gelation is the fastest and has a simple course. If the melt is quenched to higher temperatures, which is closer to a LC transition or to the clearing point, the kinetics slows down and the gelation often starts with some delay after temperature equilibration (and the achieved final moduli are lower). Finally, in case of H21-BAFKU₂, a slow two-step gelation kinetics is observed if quenching to temperatures close to the melting point of the rubbery phase. This can be assigned to a rapid formation of small ‘primary’ nano-aggregates of the BAFKU end-groups, which subsequently more slowly (second step in the curves) grow to larger, higher-functional-crosslinking ones.

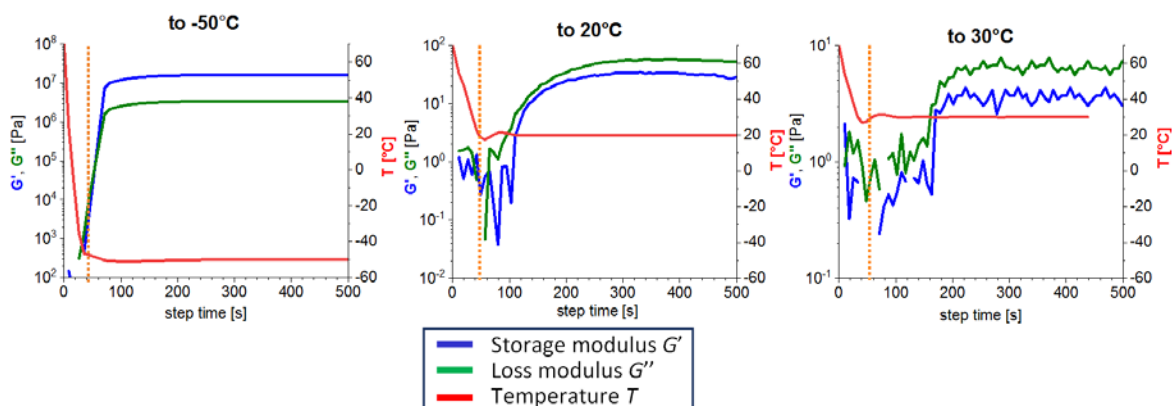


Figure 47: Exemplary kinetics of the change in storage (G') and loss (G'') modulus (kinetics of physical gelation) upon quenching molten H11-BAFKU₂ from 70°C down to -50°C (left), to +20°C (centre) and to +30°C (right); the entire set of results for the different final temperatures tested is shown in **SI-Fig. 3/Appendix 3**; at final temperatures above +45°C, practically no change in moduli is observed upon quenching.

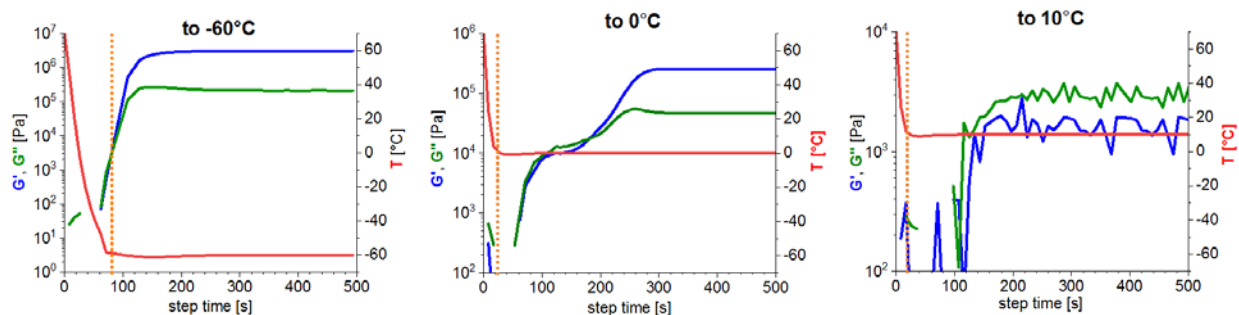


Figure 48: Exemplary kinetics of the change in storage (G') and loss (G'') modulus (kinetics of physical gelation) upon quenching molten H21–BAFKU₂ from 70°C down to temperatures between -60°C and +10°C; the complete set of results for all the different final temperatures tested is shown in **SI-Fig. 4/Appendix 3**; at final temperatures above +45°C, practically no change in moduli is observed upon quenching the melt.

A specific feature of the LC end-capped copolymers was the higher sensitivity of the gelation time to the quenching temperature (including very fast gelations), and also the mentioned two-step kinetics which was most pronounced with H21–BAFKU₂ at higher final temperatures of the melt quenching experiments. Both aspects are related to the complex phase behaviour and lamellae growth in the LC end-capped copolymers.

5.6.3 Thixotropic properties

The reversible nature of the crosslinking in the studied copolymers suggests that thixotropy (a time-dependent shear thinning property) effects could possibly occur in the molten state or at the edge of the rubbery state, if the temperature is not far away from the melting point. Especially in the case of LC-end-capped copolymers, several of the above-discussed experimental methods already indicated thixotropy. Hence, the thixotropic behaviour of this group of copolymers was investigated in detail in **Appendix 3**.

Direct simple tests of thixotropy and of the recovery of viscoelastic properties are shown in **Figure 49**, on the example of H11–BAFKU₂: The sample was subjected to an oscillatory shear deformation with the constant frequency of 1 Hz, while the deformation amplitude was multi-step-wise changed between the values of 0.1% and 5030%.

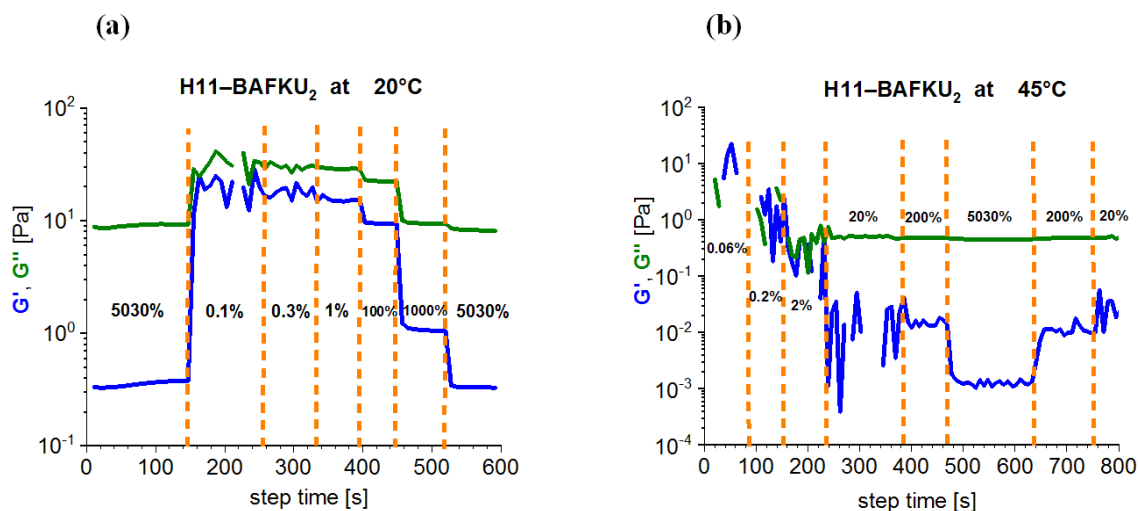


Figure 49: Simple thixotropy tests carried out on the copolymer H11-BAFKU₂ at 20°C (a) and 45°C (b); the tests (b, d) were carried out after a preparatory procedure, which consisted in heating up to the isotropic state, followed by cooling down to the experiment temperature, and after subsequent resting time of 5 min during which no deformation occurred, the thixotropy tests were carried out as rheological time sweeps conducted in several subsequent stages differing in the value of the applied constant deformation (strain).

The tests were conducted at two temperatures: at +20°C, not far above the melting point of the tested H11-BAFKU₂ copolymer, and at 45°C, close to the point of isotropization of its nematic melt. It can be seen that at both temperatures, the storage (elasticity) modulus increases by more than two orders if going from the very high deformation amplitude of ca. 5 000% to the small one of ca. 0.1%. The loss modulus displays a markedly lower sensitivity to deformation amplitude than the storage modulus.

Most importantly, it can be noted, that the thinning or the thickening of the copolymer melt occurs practically immediately upon the change of the deformation amplitude, also in case of smaller step-wise changes.

As a more comprehensive characterization, the **thixotropic loop tests** were carried out as follows: In the first stage of these tests, the shear rate was continuously raised from 0 to 100 s⁻¹ and subsequently continuously reduced again to 0 s⁻¹. In a second stage, a fast scan was done of the higher shear rates, where several points were measured, namely at 100, 200, 300, 400, 300, 200 and 100 s⁻¹, in this order. In case of sufficiently slow re-generation of the elastic structures in

the liquids, a distinct hysteresis would be expected between the ‘shear-rate-up-curve’ and the ‘shear-rate-down-curve’. It was found that the copolymers display mutually similar trends in their respective characteristic temperature regions. The results indicate very fast recovery of flow-induced damage to crosslinking.

The thixotropy loop tests indicated that the LC-end-capped copolymers display mutually similar trends in their respective characteristic temperature regions (see *Appendix 3*). The results generally indicate very fast recovery of flow-induced damage to physical crosslinks in the melt. In *Figure 50*, representative results are shown for the copolymer H11–BAFKU₂. A notable feature is, that although the same copolymer displayed tremendous changes in viscoelasticity in dependence on the applied deformation in the above simple tests (*Figure 49*), it displays only very small hysteresis in the thixotropy loop tests in *Figure 50*. The hysteresis is the widest near the melting point of the rubbery phase, but already very nearly absent in the middle of the temperature region of the nematic phase (20°C). It is completely absent in the isotropic state.

To sum up, the results of the thixotropy tests indicate a very fast regeneration of destroyed physical crosslinks, so that only very small hysteresis is observed in these tests, in spite of very strong shear-thinning tendency in all the copolymers in wide temperature ranges. Nevertheless, in contrast to oscillation experiments, the crosslink regeneration in continuous flow is not immediate, as witnessed by small but still not completely negligible hysteresis in the thixotropic loops.

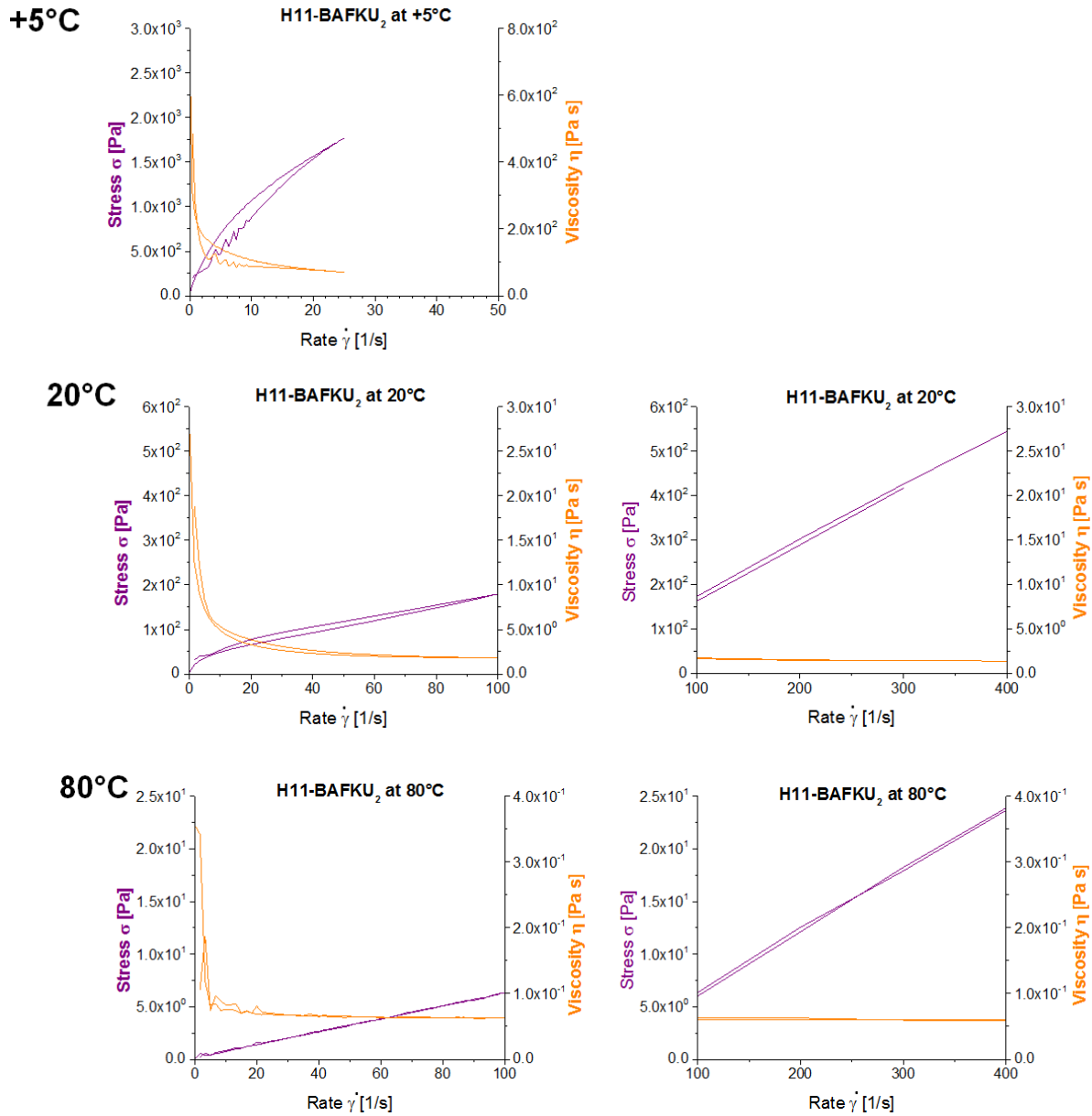


Figure 50: Thixotropic loop tests (dependence of shear stress and of viscosity on the shear rate) for the copolymer H11-BAFKU₂ at +5, 20 and 80°C: at the left are continuous tests with shear rates rising up to 100 s⁻¹, at the right are step-wise tests with shear rates between 100 and 400 s⁻¹.

6 Conclusions

- Several series of reversible physical networks based on polydimethylsiloxane (PDMS) chains and liquid crystalline (LC) structural units were synthesized, which belong to three different architecture types:

- (1) LC-grafted PDMS (with LC quartets at the grafting sites),

- (2) LC-end-capped linear PDMS,

- (3) and linear ‘infinite’ LC-PDMS copolymers (with alternating LC and PDMS segments).

- PDMS spacers of different lengths were tested, as well as 6 different polyaromatic mesogens of azo type and azo-free type.

- Hydrosilylation coupling of vinyl-functional mesogens, obtained as part of an international cooperation, with commercial Si-H-functional PDMS was employed to synthesize all the studied materials.

- In case of the linear ‘infinite’ LC-PDMS copolymers, molecular masses between 6 200 and 36 000 g/mol were achieved, corresponding to numbers of ‘macro-repeat-units’ [LC-PDMS] ranging between 2.6 and 13. The smallest numbers of macro-repeat units were obtained in the copolymers with the longest PDMS spacers, which at the same time had the highest molecular masses in their respective series.

- The main aim of this Thesis was fulfilled by obtaining numerous reversible rubbery copolymers with attractive thermotropic properties, which belonged to the LC-grafted and to the linear ‘infinite’ LC-PDMS type.

- Other copolymers, mainly from the LC-end-capped, and some from the linear ‘infinite’ LC-PDMS group, were of interest as ‘smart oils’ whose viscoelastic properties are switchable by temperature in a wide range.

- The copolymers were physically crosslinked by the nano-aggregation of their LC moieties. The thermotropic properties of the LC-nano-aggregates lent interesting physical properties to the whole material.

- The PDMS spacer segments were selected because of their extreme flexibility, which lent high elasticity to the physically crosslinked copolymers, and also because of their (desired) incompatibility with the mesogens, which supported nano-segregation and hence physical crosslinking.

- The efficiency of physical crosslinking in dependence of copolymer architecture decreased in the following order: LC-grafted PDMS > linear ‘infinite’ LC-PDMS copolymers >> LC-end-capped copolymers. In order to evaluate the ‘architecture effect’, copolymers with identical (or nearly) identical mesogens, and with PDMS spacers of the same length were compared.

- The crosslinking strength in the grafted copolymers is apparently greatly enhanced by the occurrence of LC units as quartets at the graft sites.

- The LC-grafted and the linear ‘infinite’ LC-PDMS copolymers were found to contain strongly or partly disordered LC-nano-aggregates, most likely composed of stronger primary and larger looser secondary ones. The LC-end-capped copolymers, on the other hand, contained a highly regular superstructure of LC-lamellae, which persisted also in low-temperature melt (irregular liquid isotropic LC domains form at higher T), and which caused interesting mechanical and rheological properties, in addition to sophisticated anisotropic textures in PLM.

- The melting points of the most efficiently crosslinked LC-grafted copolymers appear to occur near the temperature of the melting transition of the neat mesogen, and do not depend on the PDMS spacer. In case of the linear ‘infinite’ LC-PDMS copolymers with strongly crosslinking larger mesogens, the melting point also does not vary with the PDMS spacer length, but it is markedly lower than in case of neat mesogen. Finally, in case of the LC-end-capped copolymers, the melting point markedly decreases with increasing length of the PDMS segment, and it is also markedly lower than in the neat mesogen.

- Textures observed by polarized light microscopy (PLM) were not characteristic in the linear ‘infinite’, and especially in the LC-grafted copolymers, but were very sophisticated in the LC-end-capped ones. In the latter case, the textures seem to result from both the alignment of the LC units in their nano-aggregates, as well as from the ordering of the lamellar aggregates themselves.

- In the series of the linear ‘infinite’ LC-PDMS copolymers, it was possible to vary the strength of the physical crosslinking by changing the size of the incorporated mesogen

(tremendous change if going from diaromatic to triaromatic LC, and large change if going from triaromatic to tetraaromatic one). The melting point of the elastomers could be increased up to temperatures exceeding 160°C in the extreme case.

- Copolymers based on the very short polydimethylsiloxane spacers were brittle waxy (vitrimeric) materials, which transform directly from glass to melt. This was the result of a dominant volume fraction of mesogen in them.

- Self-healing of strain damage to network structure was found to occur in all the investigated copolymers, deep in the rubbery region, close to the melting point, and even in the viscoelastic (low-temperature-) melt region.

- The expected self-healing of disrupted samples also was proven on the example of a rubbery LC-grafted copolymer.

- The thermotropic properties of the LC nano-aggregates which physically crosslink the studied copolymers lead to interesting viscoelastic properties and rheological: the LC-grafted rubbery copolymer displays an additional gel point in its rubbery phase; the linear infinite LC-PDMS copolymers (at least the selected ones which were investigated) display additional gel points in the rubbery, as well as in the molten phase; the LC-end-capped copolymers display one or two additional gel points in the melt phase (they become thin liquids at temperatures above the last gel point).

- The rheological behaviour of the copolymers generally was found to be controlled by the interplay of growth and splitting of their aggregates, and of the thermotropic transitions in these aggregates (which change their stiffness). Entanglements of the elastic PDMS chains also were found to play a role.

- In contrast to LC-rich liquid crystalline (co)polymers (LCPs) known from the literature, the copolymers studied in this work display viscosity increase if going from isotropic to nematic (or further to the smectic) state, because their viscoelasticity is controlled by the larger-scale morphology, and not by the LC domains themselves.

- The kinetics of temperature-induced gelation of copolymer melt to network was found to be fairly fast: between 0.5 and 3 min (typically ca. 1 min). It slows down at higher final

temperatures. This kinetics is controlled by temperature-dependent nano-phase-separation dynamics.

- The physical crosslinks (LC nano-aggregates) can be reversibly disconnected by large mechanical strain in the rubbery state and in the melt (thixotropy in the latter case). The kinetics of subsequent re-generation was found to be extremely fast: ca. 1 s in oscillatory tests.

- Thixotropic tests, in which the samples were subjected to continuous flow or to larger oscillatory deformations, also indicate a very fast regeneration of destroyed physical crosslinks, combined with a very strong shear-thinning tendency in all the copolymers in wide temperature ranges.

- Very attractive, application-related material properties of the prepared copolymers include their re-processibility (useful e.g. for 3D printing, recycling, or simple processing), multiple temperature-induced viscoelastic transitions in the rubbery or molten state (interesting for smart applications), as well as self-healing in the rubbery state (connected with the physical nature of the crosslinking).

7 List of publications

7.1 List of the articles constituting the Thesis:

1. „Melttable copolymeric elastomers based on polydimethylsiloxane with multiplets of pendant liquid-crystalline groups as physical crosslinker: a self-healing structural material with a potential for smart applications“

S. Horodecka, A. Strachota*, B. Mossety-Leszczak, M. Šlouf, A. Zhigunov, M. Vyroubalová, D. Kaňková, M. Netopilík.

European Polymer Journal 2020, 137, 109962_1–109962_23.

DOI: <https://doi.org/10.1016/j.eurpolymj.2020.109962>

2. „Low-temperature melttable elastomers based on linear polydimethylsiloxane chains alpha, omega-terminated with mesogenic groups as physical crosslinker: a passive smart material with potential as viscoelastic coupling. Part I: synthesis and phase behavior“

S. Horodecka, A. Strachota*, B. Mossety-Leszczak, B. Strachota, M. Šlouf, A. Zhigunov, M. Vyroubalová, D. Kaňková, M. Netopilík, Z. Walterová. Polymers 2020, 12, 2476_1–2476_27.

DOI: <https://doi.org/10.3390/polym12112476>

3. „Low temperature-melttable elastomers based on linear polydimethylsiloxane chains alpha, omega-terminated with mesogenic groups as physical crosslinekr: a passive smart material with potential as viscoelastic coupling. Part II: viscoelastic and rheological properties“

S. Horodecka, A. Strachota*, B. Mossety-Leszczak, M. Kisiel, B. Strachota, M. Šlouf. Polymers 2020, 12, 2840_1–2840_31.

DOI: <https://doi.org/10.3390/polym12122840>

7.2 List of articles not included in the Thesis:

„Polyurethane nanocomposites containing the chemically active inorganic Sn-POSS cages“

B. Strachota, A. Strachota*, S. Horodecka, M. Steinhart, J. Kovářová, E. Pavlova, F. Ribot. Reactive & Functional Polymers 2019, 143, 104338_1–104338_16.

DOI: <https://doi.org/10.1016/j.reactfunctpolym.2019.104338>

8 APPENDICES

Appendix 1: “Melttable copolymeric elastomers based on polydimethylsiloxane with multiplsets of pendant liquid-crystalline groups as physical crosslinker: a self-healing structural material with a potential for smart applications”.

S. Horodecka, A. Strachota*, B. Mossety-Leszczak, M. Šlouf, A. Zhigunov, M. Vyroubalová, D. Kaňková, M. Netopilík.

European Polymer Journal 2020, 137, 109962_1–109962_23.

DOI: <https://doi.org/10.1016/j.eurpolymj.2020.109962>.

Appendix 2: “Low-temperature melttable elastomers based on linear polydimethylsiloxane chains alpha, omega-terminated with mesogenic groups as physical crosslinker: a passive smart material with potential as viscoelastic coupling. Part I: synthesis and phase behavior”.

S. Horodecka, A. Strachota*, B. Mossety-Leszczak, B. Strachota, M. Šlouf, A. Zhigunov, M. Vyroubalová, D. Kaňková, M. Netopilík, Z. Walterová. Polymers 2020, 12, 2476_1–2476_27.

DOI: <https://doi.org/10.3390/polym12112476>.

Appendix 3: “Low temperature-melttable elastomers based on linear polydimethylsiloxane chains alpha, omega-terminated with mesogenic groups as physical crosslinker: a passive smart material with potential as viscoelastic coupling. Part II: viscoelastic and rheological properties”.

S. Horodecka, A. Strachota*, B. Mossety-Leszczak, M. Kisiel, B. Strachota, M. Šlouf. Polymers 2020, 12, 2840_1–2840_31.

DOI: <https://doi.org/10.3390/polym12122840>.

Appendix 4: unpublished work: “Thermo-reversible elastomers and smart oils based on linear infinite copolymers of azo-type mesogens and elastic polydimethylsiloxane blocks”.

S. Horodecka, A. Strachota*, B. Mossety-Leszczak, M. Šlouf, A. Zhigunov, M. Vyroubalová, D. Kaňková, M. Netopilík, Z. Walterová.

Appendix 5: unpublished work: “Rheological and viscoelastic properties of low-temperature-meltable elastomers and smart oils based on linear infinite copolymers of azo-type mesogens and elastic polydimethylsiloxane blocks”.

S. Horodecka, A. Strachota*, B. Mossety-Leszczak.

Appendix 6: unpublished work: “Thermo-reversible and soluble elastomers based on linear infinite copolymers of polyaromatic mesogens and elastic polydimethylsiloxane blocks”.

S. Horodecka, A. Strachota*, B. Mossety-Leszczak, B. Strachota, M. Šlouf, A. Zhigunov, M. Vyroubalová, D. Kaňková, M. Netopilík, Z. Walterová.

9 References

- ¹ M. Warner, E. Terentjev, Liquid crystal elastomers, published by Oxford University Press, Oxford (UK) (2003). ISBN: 9780198527671.
- ² J. C. Dubois, P. LeBarny, M. Mauzac, C. Noel, D. Demus, J. W. Goodby, G. W. Gray, H. W. Spiess, V. Vill, Handbook of Liquid Crystals, published by Verlag Chemie (Now Wiley-VCH); Weinheim (Germany) (1998), Part I: Fundamentals. DOI: 10.1002/9783527619276
- ³ G. W. Gray, Liquid Crystals and Plastic Crystals, Volume 1 and 2. published by Ellis Horwood Ltd., Chichester (UK) (1974), ISBN-10: 0470323396. ISBN-13: 978-0470323397.
- ⁴ J. Kupfer, H. Finkelmann, Liquid-crystal elastomers - Influence of the orientational distribution of the cross-links on the phase-behavior and reorientation processes, *Macromolecular Chemistry and Physics* 195 (1994) 1353–1367.
DOI: <https://doi.org/10.1002/macp.1994.021950419>.
- ⁵ F. C. Bawden, N. W. Pirie, The isolation and some properties of liquid crystalline substances from solanaceous plants infected with three strains of tobacco mosaic virus, *Proceedings of the Royal Society of London, Part B* 123 (1937) 274-320. DOI: 10.1098/rspb.1937.0054.
- ⁶ F. Rodriguez, Principles of polymer systems, published by Taylor & Francis, Washington (1996), ISBN: 1-56032-325-6. DOI: <https://doi.org/10.1021/ja9657162>.
- ⁷ I. M. Ward, D. W. Hadley, An introduction to the mechanical properties of solid polymers, published by J. Wiley & Sons, Chichester (1993). ISBN: 0-471-93874-2.
DOI: <https://doi.org/10.1002/actp.1996.010470110>.
- ⁸ V. Shibaev, Liquid crystalline polymers, *Elsevier* (2016) 1–46. DOI: 10.1016/B978-0-12-803581-8.01301-1.
- ⁹ P. J. Flory, Statistical thermodynamics of semi-flexible chain molecules, *Proceedings of the Royal Society of London, Part A* 234 (1956) 60–73.
DOI: <https://doi.org/10.1098/rspa.1956.0015>.
- ¹⁰ P. J. Flory, Phase equilibria in solutions of rod-like particles, *Proceedings of the Royal Society of London, Part A* 234 (1956) 73–89. DOI: <https://doi.org/10.1098/rspa.1956.0016>.
- ¹¹ V. Luzzati, H. Mustacchi, A. Skoulios, Structure of the Liquid-Crystal Phases of the Soap–water System: Middle Soap and Neat Soap, *Nature* 180 (1957) 600–601.
DOI: 10.1038/180600a0

-
- ¹² W. R. Burghardt, Molecular orientation and rheology in sheared lyotropic liquid crystalline polymers, *Macromolecular Chemistry and Physics* 199 (1998) 471–488.
DOI: 10.1002/(SICI)1521-3935(19980401)199:4<471::AID-MACP471>3.0.CO;2-9
- ¹³ G. Kiss, R. S. Porter, Rheology of concentrated solutions of helical polypeptides, *Journal of Polymer Science: Polymer Physics Edition* 18 (1980) 361–388.
DOI: <https://doi.org/10.1002/pol.1980.180180217>
- ¹⁴ J. M. Lehn, *Supramolecular chemistry: concepts and perspectives*, published by Wiley-VCH, New York (1995), ISBN: 9783527607433. DOI: 10.1002/3527607439.
- ¹⁵ S. V. Fridrikh, E. M. Terentjev, Order-disorder transition in an external field in random ferromagnets and nematic elastomers, *Physical Review Letters* 79 (1997) 4661–4664.
DOI: <https://doi.org/10.1103/PhysRevLett.82.3380>.
- ¹⁶ C. J. Booth, *Handbook of liquid crystals Vol- 2A*, (eds.: D. Demus, J. W. Goodbye, G. W. Gray, H. -W. Spiess, V. Vill, published by Wiley-VCH, Verlag GmbH, Weinheim (1998). ISBN: 978-3-527-62056-2.
- ¹⁷ H. S. Kitzerow, C. Bahr, *Chirality in liquid crystals*, published by Springer-Verlag, New York (2001). ISBN: 978-0-387-21642-3.
- ¹⁸ G. W. Gray, J. W. Goodbye, *Smectic liquid crystals: textures and structures*, published by Leonard Hill, Glasgow (1984). ISBN: 0863440258 9780863440250 0249441683 9780249441680.
- ¹⁹ P. S. Pershan, *Structure of liquid crystal phases; World Scientific Lecture Notes in Physics 23*, published by World Scientific Pub. Co Inc, Singapore (1988). ISBN: 9971507056.
- ²⁰ D. Vorländer, A. Apel, Die Richtung der Kohlenstoff-Valenzen in Benzol-Abkömmlingen, *Berichte der Deutschen Chemischen Gesellschaft* 62 (1929) 2831–2835.
DOI: <https://doi.org/10.1002/cber.19290621026>
- ²¹ T. Akutagawa, Y. Matsunaga, K. Yashuhara, Mesomorphic behaviour of 1,3-phenylene bis[4-(4-alkoxyphenyliminomethyl)benzoates] and related compounds, *Liquid Crystals* 17 (1994) 659–666. DOI: 10.1080/02678299408037337
- ²² S. Chandrasekhar, Liquid crystals of disk-like molecules, *Advances in Liquid Crystals* 5 (1982) 47–78. DOI: 10.1016/B978-0-12-025005-9.50008-4
- ²³ L. Wang, D. Huang, L. Lam, Z. Cheng, Bowlics: history, advances and applications, *Liquid Crystals Today* 26 (2017) 85–111. DOI: 10.1080/1358314X.2017.1398307
- ²⁴ G. Pelzl, S. Diele, W. Weissflog, Banana-Shaped Compounds—A New Field of Liquid Crystals, *Advanced Materials* 11 (1999) 707–724. DOI: 10.1002/(SICI)1521-4095(199906)11:9<707::AID-ADMA707>3.0.CO;2-D

-
- ²⁵ M. F. Achard, J. Ph. Bedel, J. P. Marceroua, H. T. Nguyen, J. C. Roui, Switching of banana liquid crystal mesophases under field, *The European Physical Journal E* 10 (2003) 129–134. DOI: 10.1140/epje/e2003-00016-y
- ²⁶ J. A. Castellano, *Liquid Gold: The Story of Liquid Crystal Displays and the Creation of an Industry*, published by World Scientific Publishing, Singapore (Singapore) (2005). ISBN-10: 9789812389565; ISBN-13: 978-9812389565
- ²⁷ A. K. Jain, R. R. Deshmukh, *An Overview of Polymer-Dispersed Liquid Crystals Composite Films and Their Applications*, published by IntechOpen Ltd., London (UK) (2020). DOI: 10.5772/intechopen.91889
- ²⁸ Patent: US 4738549, Plimpton RG, "Pool thermometer"
- ²⁹ J. Beeckman, K. Neyts, P. Vanbrabant, Liquid-Crystal Photonic Applications, *Optical Engineering* 50 (2011) article# 081202 1–17. DOI: 10.1117/1.3565046
- ³⁰ S. Sato, Liquid-Crystal Lens-Cells with Variable Focal Length, *Japanese Journal of Applied Physics* 18 (1979) 1679–1684. DOI: 10.1143/JJAP.18.1679
- ³¹ Y. H. Lin, Y. J. Wang, V. Reshetnyak, Liquid crystal lenses with tunable focal length, *Liquid Crystals Reviews* 5 (2017) 111-143. DOI: 10.1080/21680396.2018.1440256
- ³² S. D. Jacobs, K. A. Cerqua, K. L. Marshall, A. Schmid, M. J. Guardalben, K. J. Skerrett, Liquid-crystal laser optics: design, fabrication, and performance, *Journal of the Optical Society of America B* 5 (1988) 1962-1979. DOI: 10.1364/JOSAB.5.001962
- ³³ T. Ube, K. Kawasaki, T. Ikeda, Photomobile Liquid-Crystalline Elastomers with Rearrangeable Networks, *Advanced Materials* 28 (2016) 8212–8217. DOI: 10.1002/adma.201602745.
- ³⁴ M. O. Saed, R. H. Volpe, N. A. Traugutt, R. Visvanathan, N. A. Clark, C. M. Yakacki, High strain actuation liquid crystal elastomers via modulation of mesophase structure, *Soft Matter* 13 (2017) 7537–7547. DOI: 10.1039/c7sm01380a.
- ³⁵ W. Lehmann, H. Skupin, C. Tolksdorf, E. Gebhard, R. Zentel, P. Kruger, M. Losche, F. Kremer, Giant lateral electrostriction in ferroelectric liquid-crystalline elastomers, *Nature* 410 (2001) 447–450. DOI: 10.1038/35068522.
- ³⁶ M. C. Coutinho Varela da Silva, J. L. Maia Figueirinhas, J. C. da Silva Barbosa Sotomayor, Improvement of permanent memory effect in PDLC films using TX-100 as an additive, *Liquid Crystals* 43 (2016) 124–130. DOI: 10.1080/02678292.2015.1061713
- ³⁷ C. K. Ober, J. I. Jin, Q. Zhou, R. W. Lenz, Liquid crystals polymers I, *Advances in Polymer Science* 59 (1984) 103–146. DOI: https://doi.org/10.1007/3-540-12818-2_8.

-
- ³⁸ M. G. Dobb, J. E. McIntyre, Properties and applications of liquid-crystalline main-chain polymers in Liquid Crystal Polymers II/III, *Advances in Polymer Science* 60/61 (1984) 61–98. DOI: https://doi.org/10.1007/3-540-12994-4_2.
- ³⁹ H. Finkelmann, G. Rehage, Liquid crystal side chain polymers in Liquid Crystal Polymers II/III, *Advances in Polymer Science* 60/61 (1984) 99–172. DOI: https://doi.org/10.1007/3-540-12994-4_3.
- ⁴⁰ V. Shibaev, N. A. Platé, Thermotropic liquid-crystalline polymers with mesogenic side groups in Liquid Crystal Polymers II/III, *Advances in Polymer Science* 60/61 (1984) 173–252. DOI: https://doi.org/10.1007/3-540-12994-4_4.
- ⁴¹ C. B. McArdle, Side chain liquid crystal polymers, published by Blackie and Son, Ltd., Glasgow (1989). ISBN: 0-216-92503-7.
- ⁴² A. Ciferri, Liquid crystallinity in polymers-principles and fundamental properties, published by VCH Publisher, New York (1991). DOI: <https://doi.org/10.1002/pola.1992.080300530>.
- ⁴³ A. M. Donald, A. H. Windle, Liquid crystalline polymers, published by Cambridge University Press, Cambridge (1992). ISBN: 0-521-30666-3.
- ⁴⁴ V. Shibaev, L. Lam, Liquid crystalline and mesomorphic polymers, published by Springer-Verlag, New York (1994). ISBN: 978-1-4613-8333-8.
- ⁴⁵ T. S. Chung, Thermotropic liquid crystal polymers: thin-film polymerization, characterization, blends, and applications, published by Technomic Publishing Company, Lancaster (2001). ISBN: 9781566769433.
- ⁴⁶ D. Demus, J. W. Goodby, G. W. Gray, H. W. Spiess, V. Vill, Handbook of liquid crystals Vol. 3: high molecular weight liquid crystals, published by Wiley-VCH, Weinheim (1998). ISBN: 978-3527292707.
- ⁴⁷ R. A. Guadiana, R. A. Minns, R. Sinta, N. Weeks, H. G. Rogers, Amorphous rigid-rod polymers, *Progress in Polymer Science* 14 (1989) 47–89. DOI: [https://doi.org/10.1016/0079-6700\(89\)90017-8](https://doi.org/10.1016/0079-6700(89)90017-8).
- ⁴⁸ C. De Ruijter, E. Mendes, H. Boerstoel, S. J. Picken, Orientational order and mechanical properties of poly (amide-block-aramid) alternating block copolymer films and fibers, *Polymer* 47 (2006) 8517–8526. DOI: [10.1016/j.polymer.2006.10.006](https://doi.org/10.1016/j.polymer.2006.10.006).
- ⁴⁹ J. I. Jin, C. S. Kang, Thermotropic main chain polyesters, *Progress in Polymer Science* 22 (1997) 937–973. DOI: [https://doi.org/10.1016/S0079-6700\(97\)00013-0](https://doi.org/10.1016/S0079-6700(97)00013-0).
- ⁵⁰ C. Noël, Synthesis, characterization and recent developments of liquid crystalline polymers, *Macromolecular chemistry, Macromolecular Symposia* 22 (1988) 95–139. DOI: <https://doi.org/10.1002/masy.19880220108>.

-
- ⁵¹ J. I. Jin, C. S. Kang, I. H. Lee, Y. K. Yun, Synthesis and characterization of regioregularly ring – substituted, liquid crystalline aromatic polyesters, *Macromolecules* 27 (1994) 2664–2670. DOI: <https://doi.org/10.1021/ma00088a003>.
- ⁵² B. K. Chen, S. Y. Yuan, J. Y. Chen, Synthesis and properties of liquid crystalline polymers with low T_m and broad mesophase temperature ranges, *Polymer* 46 (2005) 8624–8633. DOI: <https://doi.org/10.1016/j.polymer.2005.06.084>.
- ⁵³ K. U. Jeong, B. S. Knapp, J. J. Ge, M. J. Graham, Y. Tu, S. Leng, H. Xiong, F. W. Harris, S. Z. D. Cheng, Structures and phase transformations of odd-numbered asymmetric main-chain liquid crystalline polyesters, *Polymer* 47 (2006) 3351–3362. DOI: [10.1016/j.polymer.2006.03.025](https://doi.org/10.1016/j.polymer.2006.03.025).
- ⁵⁴ M. Bagheri, R. Z. Rad, Synthesis and characterization of thermotropic liquid crystalline polyesters with biphenyl unit in the main chain, *Reactive and Functional Polymers* 68 (2008) 613–622. DOI: <https://doi.org/10.1016/j.reactfunctpolym.2007.10.029>.
- ⁵⁵ P. Penczek, K. Frisch, B. Szczepaniak, E. Rudnik, Synthesis and properties of liquid crystalline polyurethanes, *Journal of Polymer Science Part A Polymer Chemistry* 31 (1993) 1211–1220. DOI: [10.1002/pola.1993.080310517](https://doi.org/10.1002/pola.1993.080310517).
- ⁵⁶ J. B. Lee, T. Kato, S. Ujiie, K. Iimura, T. Uryu, Thermotropic polyurethanes prepared from 2,5 - tolylene diisocyanates and 1,4 - bis(omega-hydroxyalkoxy) benzenes containing no mesogenic unit, *Macromolecules* 28 (1995) 2165–2171. DOI: <https://doi.org/10.1021/ma00111a010>.
- ⁵⁷ T. Padmavathy, K. S. V. Srinivasan, Synthesis and properties of segmented main-chain liquid-crystalline polyurethanes with a high aspect ratio mesogenic diol as a chain extender, *Journal of Polymer Science Part A Polymer Chemistry* 40 (2002) 1527–1538. DOI: <https://doi.org/10.1002/pola.10237>
- ⁵⁸ J. Y. W. Lam, X. X. Kong, Y. P. Dong, K. K. L. Cheuk, K. Xu, B. Z. Tang, Synthesis and properties of liquid crystalline polyacetylenes with different spacer lengths and bridge orientations, *Macromolecules* 33 (2000) 5027–5040. DOI: <https://doi.org/10.1021/ma992097j>.
- ⁵⁹ J. Y. W. Lam, B. Z. Tang, Functional polyacetylenes, *Accounts of Chemical Research* 38 (2005) 745–754. DOI: <https://doi.org/10.1021/ar040012f>.
- ⁶⁰ A. Roviello, A. Sirigu, Mesophasic behaviour of some polycarbonates of 4,4' dihydroxy- α,α' -dimethylbenzalazine, *European Polymer Journal* 15 (1979) 423–430. DOI: [https://doi.org/10.1016/0014-3057\(79\)90054-5](https://doi.org/10.1016/0014-3057(79)90054-5).
- ⁶¹ C. D. Baker, M. V. Beylen, R. Ottenburgs, C. Samyn, Synthesis and liquid-crystalline properties of thermotropic homopolycarbonates, *Macromolecular Chemistry and Physics* 196 (1995) 1495–1514. DOI: <https://doi.org/10.1002/macp.1995.021960512>.

-
- ⁶² V. Percec, R. Yourd, Liquid crystalline polyethers and copolyethers based on conformational isomerism. 3. The influence of thermal history on the phase transitions of the thermotropic polyethers and copolyethers based on 1-(4-hydroxyphenyl)-2-(2-methyl-4-hydroxyphenyl)ethane and flexible spacers containing an odd number of methylene units, *Macromolecules* 22 (1989) 3229–3242. DOI: <https://doi.org/10.1021/ma00198a007>.
- ⁶³ V. Srinivasa Rao, A. B. Samui, Structure–property relationship of photoactive liquid crystalline polyethers containing benzylidene moiety, *Journal of Polymer Science Part A Polymer Chemistry* 47 (2009) 2143–2155. DOI: <https://doi.org/10.1002/pola.23303>.
- ⁶⁴ H. R. Kricheldorf, V. Linzer, Liquid crystalline polyimides: 18. Thermotropic polyimides based on biphenyl-3,3',4,4'-tetracarboxylic anhydride, *Polymer* 36 (1995) 1893–1902. DOI: [https://doi.org/10.1016/0032-3861\(95\)90937-W](https://doi.org/10.1016/0032-3861(95)90937-W).
- ⁶⁵ W. J. Jackson, Liquid Crystal Polymers. IV. Liquid Crystalline Aromatic Polyesters, *Polymer International* 12 (1980) 154–162. DOI: <https://doi.org/10.1002/pi.4980120405>.
- ⁶⁶ C. Aguilera, J. Bartulin, B. Hisgen, H. Ringsdorf, Liquid crystalline main chain polymers with highly flexible siloxane spacers, *Die Makromolekulare Chemie / Macromolecular Chemistry (since 1994: Macromolecular Chemistry and Physics)* 184 (1983) 253–262. DOI: <https://doi.org/10.1002/macp.1983.021840202>.
- ⁶⁷ K. A. Burke, I. A. Rousseau, P. T. Mather, Reversible actuation in main-chain liquid crystalline elastomers with varying crosslink densities, *Polymer* 55 (2014) 5897–5907. DOI: <http://dx.doi.org/10.1016/j.polymer.2014.06.088>
- ⁶⁸ M. Giamberini, E. Amendola, C. Carfagna, Curing of a rigid rod epoxy resin with an aliphatic diacid: an example of a lightly crosslinked liquid crystalline thermoset, *Macromolecular rapid communications* 16 (1995) 97–105. DOI: <https://doi.org/10.1002/marc.1995.030160201>.
- ⁶⁹ M. Giamberini, V. Ambrogi, P. Cerruti, C. Carfagna, Viscoelasticity of main chain liquid crystalline elastomers, *Polymer* 47 (2006) 4490–4496. DOI: <https://doi.org/10.1016/j.polymer.2006.04.021>.
- ⁷⁰ M. A. Espinosa, V. Cádiz, M. Galiá, New cholesteric liquid-crystal epoxy resins derived from 6-hydroxy-2-naphthoic acid, *Journal of Polymer Science, Part A, Polymer Chemistry* 39 (2001) 2847–2858. DOI: <https://doi.org/10.1002/pola.1264>.
- ⁷¹ D. Ribera, M. Giamberini, A. Serra, A. Mantecón, Lightly crosslinked, mesomorphic networks obtained through the reaction of dimeric, liquid-crystalline epoxy–imine monomers and heptanedioic acid, *Journal of Polymer Science, Part A, Polymer Chemistry* 44 (2006) 6270–6286. DOI: <https://doi.org/10.1002/pola.21681>.
- ⁷² N. A. Platé, V. Shibaev, Comb-shaped polymers and liquid crystals, published by Plenum Press, New York (1987). ISBN: 978-1-4613-1951-1.

-
- ⁷³ C. Noël, P. Navard, Liquid crystal polymers, *Progress in Polymer Science* 16 (1991) 55-110. DOI: [https://doi.org/10.1016/0079-6700\(91\)90007-8](https://doi.org/10.1016/0079-6700(91)90007-8).
- ⁷⁴ T. Ganicz, W. A. Stańczyk, E. Bialecka-Florjańczyk, I. Śledzińska, Liquid crystal dimers with organosilicon spacers as models for side chain LC polymers, *Polymer* 40 (1999) 4733-4739. DOI: [https://doi.org/10.1016/S0032-3861\(98\)00673-9](https://doi.org/10.1016/S0032-3861(98)00673-9).
- ⁷⁵ A. Blumstein, *Polymeric liquid crystals*, published by Plenum Press, New York (1985). ISBN: 978-1-4899-2299-1.
- ⁷⁶ A. A. Collyer, *Liquid crystal polymers: from structure to applications*, Elsevier Science Publishers, London (1992). ISBN: 978-94-011-1870-5.
- ⁷⁷ V. V. Tsukruk, V. N. Bliznyuk, Side chain liquid crystalline polymers at interfaces, *Progress in Polymer Science* 22 (1997) 1089-1132. DOI: [https://doi.org/10.1016/S0079-6700\(97\)00017-8](https://doi.org/10.1016/S0079-6700(97)00017-8).
- ⁷⁸ X. Han, R. A. Shanks, D. Pavel, The synthesis and thermal properties of polyepichlorohydrin side-chain liquid crystal polymers, *European Polymer Journal* 41 (2005) 984-991. DOI: <https://doi.org/10.1016/j.eurpolymj.2004.11.038>.
- ⁷⁹ M. Bagheri, Z. Pourmoazzen, Synthesis and properties of new liquid crystalline polyurethanes containing mesogenic side chain, *Reactive and Functional Polymers* 68 (2008) 507-518. DOI: <https://doi.org/10.1016/j.reactfunctpolym.2007.10.032>.
- ⁸⁰ T. Itahara, J. Inadome, Liquid crystalline polymers having dimetric moieties as side chains, *Reactive and Functional Polymers* 69 (2009) 851-856. DOI: <https://doi.org/10.1016/j.reactfunctpolym.2009.08.007>.
- ⁸¹ K. F. Wissbrun, Rheology of rod-like polymers in the liquid crystalline state, *Journal of Rheology* 25 (1981) 619-662. DOI: <https://doi.org/10.1122/1.549634>
- ⁸² G. Marrucci, Rheology of liquid crystalline polymers, *Pure and Applied Chemistry* 57 (1985) 1545-1552. DOI: <https://doi.org/10.1351/pac198557111545>
- ⁸³ S. M. Guskey, H. H. Winter, Transient shear behavior of a thermotropic liquid crystalline polymer in the nematic state, *Journal of Rheology* 35 (1991) 1191-1207. DOI: <https://doi.org/10.1122/1.550171>
- ⁸⁴ G. Marrucci, F. Greco, Flow behavior of liquid crystalline polymers, published by John Wiley & Sons, Inc., New York, USA (1993) (online: 2007); Volume 86, 331-404. Print ISBN: 9780471598459; Online ISBN: 9780470141458. DOI: <https://doi.org/10.1002/9780470141458.ch3>
- ⁸⁵ A. M. Jamieson, D. Gu, F. L. Chen, S. Smith, Viscoelastic behavior of nematic monodomains containing liquid crystal polymers, *Progress in Polymer Science* 21 (1996) 981-1033. DOI: [https://doi.org/10.1016/S0079-6700\(96\)00009-3](https://doi.org/10.1016/S0079-6700(96)00009-3)

-
- ⁸⁶ G. Kiss, R. S. Porter, Rheology of concentrated solutions of poly(γ -benzyl-glutamate), *Journal of Polymer Science: Polymer Symposia* 65 (1978) 193–211. DOI: <https://doi.org/10.1002/polc.5070650117>
- ⁸⁷ P. Moldenaers, J. Mewis, On the nature of viscoelasticity in polymeric liquid crystals, *Journal of Rheology* 37 (1993) 367–380. DOI: <https://doi.org/10.1122/1.550448>
- ⁸⁸ T. Asada, H. Muramatsu, R. Watanabe, S. Onogi, Rheoptical studies of racemic poly(γ -benzyl glutamate) liquid crystals, *Macromolecules* 13 (1980) 867–871. DOI: <https://doi.org/10.1021/ma60076a019>
- ⁸⁹ S. Onogi, T. Asada, Rheology and rheo-optics of polymer liquid crystals, published by Springer, Boston, MA, USA (1980); Volume 1, 127–147. Print ISBN: 978-1-4684-3742-3; Online ISBN: 978-1-4684-3740-9; DOI: https://doi.org/10.1007/978-1-4684-3740-9_9
- ⁹⁰ M. Doi, Molecular dynamics and rheological properties of concentrated solutions of rodlike polymers in isotropic and liquid crystalline phases, *Journal of Polymer Science: Polymer Physics Edition* 19 (1981) 229–243. DOI: <https://doi.org/10.1002/pol.1981.180190205>
- ⁹¹ M. Doi, S. F. Edwards, The theory of polymer dynamics, published by Oxford University Press, Oxford (1986). ISBN 10: 0198519761, ISBN 13: 9780198519768
- ⁹² R. G. Larson, M. Doi, Mesoscopic domain theory for textured liquid crystalline polymers, *Journal of Rheology* 35 (1991) 539–563. DOI: <https://doi.org/10.1122/1.550180>
- ⁹³ R. G. Larson, The Structure and Rheology of Complex Fluids, published by Oxford University Press, New York, USA, (1999). ISBN-10: 019512197X, ISBN-13: 978-0195121971
- ⁹⁴ S. G. Baek, J. J. Magda, R. G. Larson, Rheological differences among liquid-crystalline polymers. I. The first and second normal stress differences of PBG solutions, *Journal of Rheology* 37 (1993) 1201–1224. DOI: <https://doi.org/10.1122/1.550377>
- ⁹⁵ S. G. Baek, J. J. Magda, R. G. Larson, S. D. Hudson, Rheological differences among liquid-crystalline polymers. II. Disappearance of negative N1 in densely packed lyotropes and thermotropes, *Journal of Rheology* 38 (1994) 1473–1503. DOI: <https://doi.org/10.1122/1.550555>
- ⁹⁶ V. M. Ugaz, W. R. Burghardt, W. Zhou, J. A. Kornfield, Transient molecular orientation and rheology in flow aligning thermotropic liquid crystalline polymers, *Journal of Rheology* 45 (2001) 1029–1063. DOI: <https://doi.org/10.1122/1.1389317>
- ⁹⁷ A. Azoug, V. Vasconcellos, J. Dooling, M. Saed, C. M. Yakacki, T. D. Nguyen, Viscoelasticity of the polydomain-monodomain transition in main-chain liquid crystal elastomers, *Polymer* 98 (2016) 165–171. DOI: <http://dx.doi.org/10.1016/j.polymer.2016.06.022>
- ⁹⁸ K. M. Lee, C. D. Han, Rheology of nematic side-chain liquid-crystalline polymer: comparison with main-chain liquid-crystalline polymer, *Macromolecules* 35 (2002) 6263–6273. DOI: <https://doi.org/10.1021/ma012240k>

-
- ⁹⁹ S. S. Kim, C. D. Han, Effect of thermal history on the rheological behavior of a thermotropic liquid-crystalline polymer, *Macromolecules* 26 (1993) 3176–3186.
DOI: <https://doi.org/10.1021/ma00064a030>
- ¹⁰⁰ R. H. Colby, J. R. Gillmor, G. Galli, M. Laus, C. K. Ober, E. Hall, Linear viscoelasticity of side chain liquid crystal polymer, *Liquid Crystals* 13 (1993) 233–245.
DOI: <https://doi.org/10.1080/02678299308026297>
- ¹⁰¹ J. Berghausen, J. Fuchs, W. Richtering, Rheology and shear orientation of a nematic liquid crystalline side-group polymer with laterally attached mesogenic units, *Macromolecules* 30 (1997) 7574–7581. DOI: <https://doi.org/10.1021/ma970430i>
- ¹⁰² S. Chang, C. D. Han, Effect of flexible spacers on the rheological behavior of main-chain thermotropic liquid-crystalline polymers having bulky pendent side groups, *Macromolecules* 30 (1997) 2021–2034. DOI: <https://doi.org/10.1021/ma961729o>
- ¹⁰³ K. M. Lee, C. D. Han, Effect of flexible spacer length on the rheology of side-chain liquid-crystalline polymers, *Macromolecules* 36 (2003) 8796–8810.
DOI: <https://doi.org/10.1021/ma030303o>
- ¹⁰⁴ A. Wewerka, K. Viertler, D. Vlassopoulos, F. Stelzer, Structure and rheology of model side-chain liquid crystalline polymers with varying mesogen length, *Rheologica Acta* 40 (2001) 416–425. DOI: <https://doi.org/10.1007/s003970100177>
- ¹⁰⁵ I. K. Yang, S. H. Chang, The smectic rheology of a polysiloxane side chain liquid crystalline polymer, *Journal of Polymer Research* 9 (2002) 163–168.
DOI: <https://doi.org/10.1023/A:1021335507404>
- ¹⁰⁶ M. Gamberini, E. Amendola, C. Carfagna, A novel approach to the tailoring of polymers for advanced composites and optical applications, involving the synthesis of liquid crystalline epoxy resins, *Polymer Engineering and Science* 39 (1999) 534–542.
DOI: <https://doi.org/10.1002/pen.11443>.
- ¹⁰⁷ G. G. Barclay, C. K. Ober, K. I. Papatomas, D. W. Wang, Rigid-rod thermosets based on 1, 3, 5-triazine-linked aromatic ester segments, *Macromolecules* 25 (1992) 2947–2954.
DOI: <https://doi.org/10.1021/ma00037a025>.
- ¹⁰⁸ Y. Bouligand, P. E. Cladis, L. Liebert, L. Strzelecki, Study of sections of polymerized liquid crystals, *Molecular Crystals and Liquid Crystals* 25 (1974) 233–252.
DOI: <https://doi.org/10.1080/15421407408082803>.
- ¹⁰⁹ S. B. Clough, A. Blumstein, E. C. Hsu, Structure and thermal expansion of some polymers with mesomorphic ordering, *Macromolecules* 9 (1976) 123–127.
DOI: <https://doi.org/10.1021/ma60049a024>.
- ¹¹⁰ A. Shiota, C. K. Ober, Rigid rod and liquid crystalline thermosets, *Progress in Polymer Science* 22 (1997) 975–1000. DOI: [https://doi.org/10.1016/S0079-6700\(97\)00014-2](https://doi.org/10.1016/S0079-6700(97)00014-2).

-
- ¹¹¹ J. S. Hu, B. Y. Zhang, D. S. Yao, W. Q. Xiao, Y. L. Dong, Synthesis, structure, and characterization of nematic liquid-crystalline thermosets based on bisacrylates, *Journal of Polymer Science Part A: Polymer Chemistry* 43 (2005) 4478-4485.
DOI: <https://doi.org/10.1002/pola.20924>.
- ¹¹² E. P. Douglas, Structure-property relationships in liquid crystalline thermosets, *Journal of Macromolecular Science, Part C: Polymer Reviews* 46 (2006) 127-141.
DOI: <https://doi.org/10.1080/15321790600646745>.
- ¹¹³ B. Mossety-Leszczak, B. Strachota, A. Strachota, M. Steinhart, M. Šlouf, The orientation-enhancing effect of diphenyl aluminium phosphate nanorods in a liquid-crystalline epoxy matrix ordered by magnetic field, *European Polymer Journal* 72 (2015) 238–255.
DOI: <https://doi.org/10.1016/j.eurpolymj.2015.09.018>.
- ¹¹⁴ W. Mormann, M. Bröcher, Liquid crystalline thermosets from triaromatic ester group containing diepoxides and aromatic diamines, *Macromolecular Chemistry and Physics* 199 (1998) 853-859. DOI: [https://doi.org/10.1002/\(SICI\)1521-3935\(19980501\)199:5<853::AID-MACP853>3.0.CO;2-S](https://doi.org/10.1002/(SICI)1521-3935(19980501)199:5<853::AID-MACP853>3.0.CO;2-S).
- ¹¹⁵ W. Mormann, M. Bröcher, Liquid crystalline thermosets from triaromatic azomethine group containing diepoxides and 4,4'-methylenedianiline, *Macromolecular Chemistry and Physics* 199 (1998) 1935-1938. DOI: [https://doi.org/10.1002/\(SICI\)1521-3935\(19980901\)199:9<1935::AID-MACP1935>3.0.CO;2-2](https://doi.org/10.1002/(SICI)1521-3935(19980901)199:9<1935::AID-MACP1935>3.0.CO;2-2).
- ¹¹⁶ G. G. Barclay, C. K. Ober, K. I. Papathomas, D. W. Wang, Liquid crystalline epoxy thermosets based on dihydroxymethylstilbene: Synthesis and characterization, *Journal of Polymer Science Part A: Polymer Chemistry* 30 (1992) 1831-1843.
DOI: <https://doi.org/10.1002/pola.1992.080300906>.
- ¹¹⁷ B. A. Rozenberg, L. L. Gur'eva, Oriented Liquid Crystalline Network Polymers, published by Plenum Press, New York (1992) 147-164. ISBN: 978-1-4613-6314-9.
- ¹¹⁸ D. J. Broer, J. Lub, G. N. Mol, Synthesis and photopolymerization of a liquid-crystalline diepoxide, *Macromolecules* 26 (1993) 1244-1247. DOI: <https://doi.org/10.1021/ma00058a007>.
- ¹¹⁹ J. Y. Lee, J. Jang, S. M. Hong, S. S. Hwang, K. U. Kim, Relationship between the structure of the bridging group and curing of liquid crystalline epoxy resins, *Polymer* 40 (1999) 3197-3202.
DOI: [https://doi.org/10.1016/S0032-3861\(98\)00531-X](https://doi.org/10.1016/S0032-3861(98)00531-X).
- ¹²⁰ B. Ellis, Chemistry and technology of epoxy resins, published by Springer Netherlands (1993). ISBN: 978-94-011-2932-9.
- ¹²¹ B. Mossety-Leszczak, H. Galina, M. Włodarska, U. Szeluga, H. Maciejewski, Anisotropic epoxy networks, *Macromolecular Symposia* 291/292 (2010) 127-136.
DOI: <https://doi.org/10.1002/masy.201050516>.

-
- ¹²² M. Harada, K. Sumitomo, Y. Nishimoto, M. Ochi, Relationship between fracture toughness and domain size of liquid-crystalline epoxy resins having polydomain structure, *Journal of Polymer Science Part B: Polymer Physics* 47 (2009) 156-165. DOI: <https://doi.org/10.1002/polb.21626>.
- ¹²³ S. Jahromi, Liquid crystalline epoxide thermosets: A deuterium nuclear magnetic resonance study, *Macromolecules* 27 (1994) 2804-2813. DOI: <https://doi.org/10.1021/ma00088a022>.
- ¹²⁴ S. Jahromi, W. A. G. Kuipers, B. Norder, W. J. Mijs, Liquid crystalline epoxide thermosets. Dynamic mechanical and thermal properties, *Macromolecules* 28 (1995) 2201-2211. DOI: <https://doi.org/10.1021/ma00111a014>.
- ¹²⁵ Ch. Tan, H. Sun, B. Fung, B. P. Grady, Properties of liquid crystal epoxy thermosets cured in a magnetic field, *Macromolecules* 33 (2000) 6249-6254. DOI: <https://doi.org/10.1021/ma9916411>.
- ¹²⁶ M. Harada, M. Ochi, M. Tobita, T. Kimura, T. Ishigaki, N. Shimoyama, H. Aoki, Thermomechanical properties of liquid-crystalline epoxy networks arranged by a magnetic field, *Journal of Polymer Science Part B: Polymer Physics* 42 (2004) 758-765. DOI: <https://doi.org/10.1002/polb.10740>.
- ¹²⁷ P. Castell, A. Serra, M. Galiá, M. Giamberini, C. Carfagna, Anisotropic thermosets from liquid-crystalline azomethynic epoxy resins and primary aromatic diamines, *Journal of Polymer Science Part A: Polymer Chemistry* 41 (2003) 1-12. DOI: <https://doi.org/10.1002/pola.10544>.
- ¹²⁸ B. Mossety-Leszczak, M. Włodarska, H. Galina, G. W. Bąk, T. Pakuła, Development of liquid crystalline order during cure of mesogenic epoxy resins, *Macromolecular Symposia* 227 (2005) 149-160. DOI: <https://doi.org/10.1002/masy.200550915>.
- ¹²⁹ B. C. Benicewicz, M. E. Smith, J. D. Earls, R. D. Priester, S. M. Setz, R. S. Duran, E. P. Douglas, Magnetic field orientation of liquid crystalline epoxy thermosets, *Macromolecules* 31 (1998) 4730-4738. DOI: <https://doi.org/10.1021/ma980058m>.
- ¹³⁰ G. G. Barclay, S. G. McNamee, C. K. Ober, K. I. Papathomas, D. W. Wang, The mechanical and magnetic alignment of liquid crystalline epoxy thermosets, *Journal of Polymer Science Part A: Polymer Chemistry* 30 (1992) 1845-1853. DOI: <https://doi.org/10.1002/pola.1992.080300907>.
- ¹³¹ P. G. De Gennes, Possibilities offered by polymer crosslinking in the presence of a liquid crystal, *Physics Letters A* 28 (1969) 725-726. DOI: [https://doi.org/10.1016/0375-9601\(69\)90584-2](https://doi.org/10.1016/0375-9601(69)90584-2).
- ¹³² C. Ohm, M. Brehmer, R. Zentel, Liquid crystalline elastomers as actuators and sensors, *Advanced Materials* 22 (2010) 3366-3387. DOI: <https://doi.org/10.1002/adma.200904059>.

-
- ¹³³ L. B. Braun, T. G. Linder, T. Hessberger, R. Zentel, Influence of a crosslinker containing an azo group on the actuation properties of a photoactuating LCE system, *Polymers* 8 (2016) 1–14. DOI: <https://doi.org/10.3390/polym8120435>.
- ¹³⁴ E. M. Terentjev, Liquid-crystalline elastomers, *Journal of Physics: Condensed Matter* 11 (1999) R239–R257. DOI: <https://doi.org/10.1088/0953-8984/11/24/201>.
- ¹³⁵ S. Mayer, R. Zentel, Liquid crystalline polymers and elastomers, *Current Opinion in Solid State and Materials Science* 6 (2002) 545–551. DOI: [https://doi.org/10.1016/S1359-0286\(03\)00011-1](https://doi.org/10.1016/S1359-0286(03)00011-1).
- ¹³⁶ P. Xie, R. B. Zhang, Liquid crystal elastomers, networks and gels: advanced smart materials, *Journal of Materials Chemistry* 15 (2005) 2529–2550. DOI: <https://doi.org/10.1039/B413835J>.
- ¹³⁷ H. R. Brand, H. Pleiner, P. Martinoty, Selected macroscopic properties of liquid crystalline elastomers, *Soft Matter* 2 (2006) 182–189. DOI: <https://doi.org/10.1039/B512693M>.
- ¹³⁸ K. Urayama, Selected issues in liquid crystal elastomers and gels, *Macromolecules* 40 (2007) 2277–2288. DOI: <https://doi.org/10.1021/ma0623688>.
- ¹³⁹ M. Bispo, D. Guillon, B. Donnio, H. Finkelmann, Main-chain liquid crystalline elastomers: monomer and cross-linker molecular control of the thermotropic and elastic properties, *Macromolecules* 41 (2008) 3098–3108. DOI: <https://doi.org/10.1021/ma7026929>.
- ¹⁴⁰ H. Wermter, H. Finkelmann, Liquid crystalline elastomers as artificial muscles, *e-Polymers* 1 (2001) 1–13. DOI: <https://doi.org/10.1515/epoly.2001.1.1.111>.
- ¹⁴¹ T. H. Ware, Z. P. Perry, C. M. Middleton, S. T. Iacono, T. J. White, Programmable liquid crystal elastomers prepared by thiol–ene photopolymerization, *ACS Macro Letters* 4 (2015) 942–946. DOI: <https://doi.org/10.1021/acsmacrolett.5b00511>.
- ¹⁴² J. C. Dubois, P. LeBarny, M. Mauzac, C. Noel, D. Demus, J. W. Goodby, G. W. Gray, H. W. Spiess, V. Vill, Handbook of liquid crystals, published by Verlag Chemie (now Wiley-VCH), Weinheim (DE) (1998), Print ISBN: 9783527295029, Online ISBN: 9783527619276, DOI: <https://doi.org/10.1002/9783527619276>.
- ¹⁴³ C. S. Hsu, The application of side-chain liquid-crystalline polymers, *Progress in Polymer Science* 22 (1997) 829–871. DOI: [https://doi.org/10.1016/S0079-6700\(97\)00008-7](https://doi.org/10.1016/S0079-6700(97)00008-7).
- ¹⁴⁴ H. Finkelmann, G. Rehage, Investigations on liquid crystalline polysiloxanes, 1. Synthesis and characterization of linear polymers, *Macromolecular Rapid Communications* 1 (1980) 31–34. DOI: <https://doi.org/10.1002/marc.1980.030010107>.
- ¹⁴⁵ H. Finkelmann, G. Rehage, Investigations on liquid crystalline polysiloxanes, 2. Optical properties of cholesteric phases and influence of the flexible spacer on the mobility of the mesogenic groups, *Macromolecular Rapid Communications* 1 (1980) 733–740. DOI: <https://doi.org/10.1002/marc.1980.030011206>.

-
- ¹⁴⁶ H. Finkelmann, H. J. Kock, G. Rehage, Investigations on liquid crystalline polysiloxanes 3. Liquid crystalline elastomers — a new type of liquid crystalline material, *Macromolecular Rapid Communications* 2 (1981) 317–322. DOI: <https://doi.org/10.1002/marc.1981.030020413>.
- ¹⁴⁷ H. Finkelmann, G. Rehage, Investigations on liquid crystalline polysiloxanes, 4. Cholesteric homopolymers—synthesis and optical characterization, *Macromolecular Rapid Communications* 3 (1982) 859–864. DOI: <https://doi.org/10.1002/marc.1982.030031203>.
- ¹⁴⁸ H. Finkelmann, H. J. Kock, W. Gleim, G. Rehage, Investigations on liquid crystalline polysiloxanes 5. Orientation of LC-elastomers by mechanical forces, *Macromolecular Rapid Communications* 5 (1984) 287–293. DOI: <https://doi.org/10.1002/marc.1984.030050508>.
- ¹⁴⁹ B. Donnio, H. Wermter, H. Finkelmann, A Simple and Versatile Synthetic Route for the Preparation of Main-Chain, Liquid-Crystalline Elastomers, *Macromolecules* 33 (2000) 7724–7729. DOI: <https://doi.org/10.1021/ma0002850>.
- ¹⁵⁰ H. P. Patil, J. Liao, R. C. Hedden, Smectic Ordering in Main-Chain Siloxane Polymers and Elastomers Containing p-Phenylene Terephthalate Mesogens, *Macromolecules* 2007, 40, 6206–6216. DOI: <https://doi.org/10.1021/ma0706374>.
- ¹⁵¹ J. Küpfer, H. Finkelmann, Nematic liquid single crystal elastomers, *Macromolecular Rapid Communications* 12 (1991) 717–726. DOI: <https://doi.org/10.1002/marc.1991.030121211>.
- ¹⁵² M. Wang, L. X. Guo, B. P. Lin, X. Q. Zhang, Y. Sun, H. Yang, Photo-responsive polysiloxane-based azobenzene liquid crystalline polymers prepared by thiol-ene click chemistry, *Liquid Crystals* 43 (2016) 1626–1635. DOI: <https://doi.org/10.1080/02678292.2016.1191686>.
- ¹⁵³ G. F. Wang, Y. Xiong, H. D. Tang, Synthesis and characterization of a graft side-chain liquid crystalline polysiloxane, *Journal of Organometallic Chemistry* 775 (2015) 50–54. DOI: <https://doi.org/10.1016/j.jorganchem.2014.10.026>.
- ¹⁵⁴ W. Zhao, B. P. Lin, X. Q. Zhang, Y. Sun, H. Yang, Polysiloxane Side-chain Liquid Crystalline Polymers Prepared by Alkyne Hydrosilylation, *Chinese Journal of Polymer Science* 33 (2015) 1431–1441. DOI: <https://doi.org/10.1007/s10118-015-1697-9>.
- ¹⁵⁵ S. Pandey, S. P. Mishra, B. Kolli, T. Kanai, A. B. Samui, Hyperbranched Photo Responsive and Liquid Crystalline Azo-Siloxane Polymers Synthesized by Click Chemistry, *Journal of Polymer Science, Part A: Polymer Chemistry* 50 (2012) 2659–2668. DOI: <https://doi.org/10.1002/pola.26042>.
- ¹⁵⁶ I. G. Shenouda, L. C. Chien, New ferroelectric liquid-crystalline polysiloxanes containing cyanohydrin chiral mesogens: L-norleucine series, *Macromolecules* 26 (1993) 5020–5023. DOI: <https://doi.org/10.1021/ma00071a006>.
- ¹⁵⁷ Q. L. Zhou, J. T. Zhang, Z. J. Ren, S. K. Yan, P. Xie, R. B. Zhang, A stable and high-efficiency blue-light emitting terphenyl-bridged ladder polysiloxane, *Macromolecular Rapid Communications* 29 (2008) 1259–1263. DOI: <https://doi.org/10.1002/marc.200800188>.

-
- ¹⁵⁸ H. Kawakami, Y. Mori, H. Abe, S. Nagaoka, Gas transport properties of liquid crystalline polysiloxane with laterally attached side chain, *Journal of Membrane Science* 133 (1997) 245–253. DOI: [https://doi.org/10.1016/S0376-7388\(97\)00086-0](https://doi.org/10.1016/S0376-7388(97)00086-0).
- ¹⁵⁹ H. X. Rao, Z. Y. Zhang, Preparation, Characterization and permeation property of a liquid crystal/PDMS membrane material, *Journal of Applied Polymer Science* 123 (2012) 191–199. DOI: <https://doi.org/10.1002/app.34450>
- ¹⁶⁰ T. Ganicz, W. A. Stanczyk, J. Chmielecka, J. Kowalski, Liquid crystalline polycarbosilanes and poly(di-n-butylsiloxane) as stationary phases in gas chromatography, *Polymer International* 58 (2009) 248–254. DOI: <https://doi.org/10.1002/pi.2527>.
- ¹⁶¹ M. Warner, E. Terentjev, Liquid crystal elastomers, published by Oxford University Press, Oxford (UK) (2003). ISBN: 9780198527671.
- ¹⁶² T. Ikeda, J. Mamiya, Y. Yu, Photomechanics of liquid-crystalline elastomers and other polymers, *Angewandte Chemie International Edition* 46 (2007) 506–528. DOI: <https://doi.org/10.1002/anie.200602372>.
- ¹⁶³ C. Ohm, M. Brehmer, R. Zentel, Liquid crystalline elastomers as actuators and sensors, *Advanced Materials* 22 (2010) 3366–3387. DOI: <https://doi.org/10.1002/adma.200904059>.
- ¹⁶⁴ X. L. Pang, B. Xu, X. Qing, J. Wei, Y. L. Yu, Photo-induced bending behavior of post-crosslinked liquid crystalline polymer/polyurethane blend films, *Macromolecular Rapid Communications* 39 (2018) 1-7. DOI: <https://doi.org/10.1002/marc.201700237>.
- ¹⁶⁵ A. B. Samui, S. Pandey, S. P. Mishra, Main chain photoresponsive liquid crystalline polymer synthesized through hydrosilylation, *RSC Advances* 5 (2015) 68351–68355. DOI: <https://doi.org/10.1039/c5ra14818a>.
- ¹⁶⁶ S. Pandey, B. Kolli, S. P. Mishra, A. B. Samui, Siloxane polymers containing azo moieties synthesized by click chemistry for photo responsive and liquid crystalline applications, *Journal of Polymer Science, Part A: Polymer Chemistry* 50 (2012) 1205–1215. DOI: <https://doi.org/10.1002/pola.25885>.
- ¹⁶⁷ J. J. Xu, S. Chen, W.L. Yang, B. Qin, X. X. Wang, Y. C. Wang, M. S. Cao, Y. C. Gao, C. S. Li, Y. M. Dong, Photo actuation of liquid crystalline elastomer nanocomposites incorporated with gold nanoparticles based on surface plasmon resonance, *Soft Matter* 15 (2019) 6116–6126. DOI: <https://doi.org/10.1039/c9sm00984a>.
- ¹⁶⁸ M. Wang, S. M. Sayed, L. X. Guo, B. P. Lin, X. Q. Zhang, Y. Sun, H. Yang, Multi-stimuli responsive carbon nanotube incorporated polysiloxane azobenzene liquid crystalline elastomer composites, *Macromolecules* 49 (2016) 663–671. DOI: <https://doi.org/10.1021/acs.macromol.5b02388>.
- ¹⁶⁹ "Linear Polydimethylsiloxanes", Joint Assessment of Commodity Chemicals, September 1994 (Report No. 26). ISSN: 0773-6339-26.

-
- ¹⁷⁰ M. P. Wolf, G.B. Salieb-Beugelaar, P. Hunziker, PDMS with designer functionalities-properties, modifications strategies, and applications, *Progress in Polymer Science* 83 (2018) 97–134. DOI: <https://doi.org/10.1016/j.progpolymsci.2018.06.001>
- ¹⁷¹ W. Noll, *Chemistry and Technology of Silicones*, 1st Edition published by Academic Press, New York (1968). ISBN: 9780323141406.
- ¹⁷² R. J. Hofmann, M. Vlatković, F. Wiesbrock, Fifty years of hydrosilylation in polymer science: A review of current trends of low-cost transition-metal and metal-free catalysts, Non-thermally triggered hydrosilylation reactions and industrial applications, *Polymers* 9 (2017) 1–37. DOI: <https://doi.org/10.3390/polym9100534>.
- ¹⁷³ J. F. Carpentier, V. Bette, Chemo- and enantioselective hydrosilylation of carbonyl and imino groups. An emphasis on non-traditional catalyst systems, *Current Organic Chemistry* 6 (2002) 913–936. DOI: <https://doi.org/10.2174/1385272023373851>.
- ¹⁷⁴ J. L. Speier, Homogeneous catalysis of hydrosilylation by transition metals, *Advances in Organometallic Chemistry* 17 (1979) 407–447. DOI: [https://doi.org/10.1016/S0065-3055\(08\)60328-7](https://doi.org/10.1016/S0065-3055(08)60328-7).
- ¹⁷⁵ A. J. Chalk, J. F. Harrod, Homogeneous catalysis. II. The mechanism of the hydrosilylation of olefins catalyzed by group VIII metal complexes, *Journal of the American Chemical Society* 87 (1965) 16–21. DOI: <https://doi.org/10.1021/ja01079a004>.
- ¹⁷⁶ B. Marciniec, *Comprehensive handbook on hydrosilylation*, published by Pergamon Press, Oxford (1992). ISBN: 9780080402727.
- ¹⁷⁷ S. H. Bergens, P. Noheda, J. Whelan, B. Bosnich, Asymmetric catalysis. Production of chiral diols by enantioselective catalytic intramolecular hydrosilylation of olefins, *Journal of the American Chemical Society* 114 (1992) 2121–2128. DOI: <https://doi.org/10.1021/ja00032a028>.
- ¹⁷⁸ M. Brookhart, B. E. Grant, Mechanism of a cobalt (III)-catalyzed olefin hydrosilylation reaction: direct evidence for a silyl migration pathway, *Journal of the American Chemical Society* 115 (1993) 2151–2156. DOI: <https://doi.org/10.1021/ja00059a008>.
- ¹⁷⁹ M. Spirkova, J. Pavlicevic, A. Strachota, R. Poreba, O. Bera, L. Kapralkova, J. Baldrian, M. Slouf, N. Lazic, J. Budinski-Simendic, Novel polycarbonate-based polyurethane elastomers: composition–property relationship, *European Polymer Journal* 47 (2011) 959–972. DOI: <https://doi.org/10.1016/j.eurpolymj.2011.01.001>.
- ¹⁸⁰ P. Cordier, F. Tournilhac, C. Soulié-Ziakovic, L. Leibler, Self-healing and thermoreversible rubber from supramolecular assembly, *Nature* 451 (2008) 977–980. DOI: <https://doi.org/10.1038/nmat711>.

-
- ¹⁸¹ A. S. Fawcett, M. A. Brook, Thermoplastic silicone elastomers through self-association of pendant coumarin groups, *Macromolecules* 47 (2014) 1656–1663.
DOI: <https://doi.org/10.1021/ma402361z>
- ¹⁸² M. Knight, W. J. & R. D. Lundberg, Thermoplastic elastomers 3rd edition, 261–283, published by Hanser Publications, Munich (2004). ISBN: 9781569903643.
- ¹⁸³ Y. Miwa, J. Kurachi, Y. Kohbara, S. Kutsumizu, Dynamic ionic crosslinks enable high strength and ultrastretchability in a single elastomer, *Communications Chemistry* 1 (2018) 1–8.
DOI: <https://doi.org/10.1038/s42004-017-0004-9>.
- ¹⁸⁴ T. Dollase, H. W. Spiess, M. Gottlieb, R. Yerushalmi-Rozen, Crystallization of PDMS: The effect of physical and chemical crosslinks, *Europhysics Letters* 60 (2002) 390–396.
DOI: <https://doi.org/10.1209/epl/i2002-00276-4>
- ¹⁸⁵ C. J. Kloxin, C. N. Bowman, Covalent adaptable networks: smart, reconfigurable and responsive network systems, *Chemical Society Reviews* 42 (2013) 7161–7173.
DOI: <https://doi.org/10.1039/c3cs60046g>.
- ¹⁸⁶ J. M. Lehn, Dynamic combinatorial chemistry and virtual combinatorial libraries, Chemistry-A, *European Journal* 5 (1999) 2455–2463. DOI: [https://doi.org/10.1002/\(SICI\)1521-3765\(19990903\)5:9<2455::AID-CHEM2455>3.0.CO;2-H](https://doi.org/10.1002/(SICI)1521-3765(19990903)5:9<2455::AID-CHEM2455>3.0.CO;2-H)
- ¹⁸⁷ A. V. Tobolsky, I. B. Prettyman, J. H. Dillon, Stress relaxation of natural and synthetic rubber stocks, *Journal of Applied Physics* 15 (1944) 380–395.
DOI: <https://doi.org/10.1063/1.1707442>.
- ¹⁸⁸ S. Y. An, S. M. Noh, J. H. Nam, J. K. Oh, Dual sulfide–disulfide crosslinked networks with rapid and room temperature self-healability, *Macromolecular Rapid Communications* 36 (2015) 1255–1260. DOI: <https://doi.org/10.1002/marc.201500123>.
- ¹⁸⁹ B. D. Fairbanks, S. P. Singh, C. N. Bowman, K. S. Anseth, Photodegradable, photoadaptable hydrogels via radical-mediated disulfide fragmentation reaction, *Macromolecules* 44 (2011) 2444–2450. DOI: <https://doi.org/10.1021/ma200202w>.
- ¹⁹⁰ K. N. Plunkett, M. L. Kraft, Q. Yu, J. S. Moore, Swelling kinetics of disulfide cross-linked microgels, *Macromolecules* 36 (2003) 3960–3966. DOI: <https://doi.org/10.1021/ma025874f>.
- ¹⁹¹ X. Chen, A. D. Matheus, O. Kanji, M. Ajit, S. Hongbin, S. R. Nutt, K. Sheran, F. Wudl, A thermally re-mendable cross-linked polymeric material, *Science* 295 (2002) 1698–1702.
DOI: <https://doi.org/10.1126/science.1065879>.
- ¹⁹² E. B. Murphy, E. Bolanos, C. Schaffner-Hamann, F. Wudl, S. R. Nutt, M. L. Auad, Synthesis and characterization of a single-component thermally remendable polymer network: Staudinger and Stille Revisited, *Macromolecules* 41 (2008) 5203–5209.
DOI: <https://doi.org/10.1021/ma800432g>.

-
- ¹⁹³ K. Sharavanan, K. J. Eichhorn, B. Voit, F. Bohme, Formation and stability of hydrogen bonds and ionic complexes in polyacetamidine and its mixtures with proton donors- a vibrational spectroscopy study, *Polymer* 44 (2003) 2601–2605. DOI: [https://doi.org/10.1016/S0032-3861\(03\)00169-1](https://doi.org/10.1016/S0032-3861(03)00169-1).
- ¹⁹⁴ A. Gandini, The furan/maleimide Diels-Alder reaction: A versatile click-unclick tool in macromolecular synthesis, *Progress in Polymer Science* 38 (2013) 1–29. DOI: <https://doi.org/10.1016/j.progpolymsci.2012.04.002>.
- ¹⁹⁵ M. Capelot, D. Montarnal, F. Tournilhac, L. Leibler, Metal-catalyzed transesterification for healing and assembling of thermosets, *Journal of the American Chemical Society* 134 (2012) 7664–7667. DOI: <https://doi.org/10.1021/ja302894k>.
- ¹⁹⁶ D. Montarnal, M. Capelot, F. Tournilhac, L. Leibler, Silica-like malleable materials from permanent organic networks, *Science* 334 (2011) 965–968. DOI: <https://doi.org/10.1126/science.1212648>.
- ¹⁹⁷ R. W. Layer, The chemistry of imines, *Chemical reviews* 63 (1963) 489–510. DOI: <https://doi.org/10.1021/cr60225a003>.
- ¹⁹⁸ P. Zheng, T. J. McCarthy, A surprise from 1954: Siloxane equilibration is a simple, robust, and obvious polymer self-healing mechanism, *Journal of the American Chemical Society* 134 (2012) 2024–2027. DOI: <https://doi.org/10.1021/ja2113257>.
- ¹⁹⁹ H. Y. Park, C. J. Kloxin, A. S. Abuelyaman, J. D. Oxman, C. N. Bowman, Stress relaxation via addition–fragmentation chain transfer in high T_g , High conversion methacrylate-based systems, *Macromolecules* 45 (2012) 5640–5646. DOI: <https://doi.org/10.1021/ma300228z>.
- ²⁰⁰ C. H. Li, C. Wang, C. Keplinger, J. L. Zuo, L. Jin, Y. Sun, P. Zheng, Y. Cao, F. Lissel, C. Linder, X. Z. You, Z. Bao, A highly stretchable autonomous self-healing elastomer, *Nature Chemistry* 8 (2016) 618–624. DOI: <https://doi.org/10.1038/nchem.2492>
- ²⁰¹ O. Colombani, C. Barioz, L. Bouteiller, C. Chaneac, L. Fomperie, F. Lortie, H. Montes, Attempt toward 1D cross-linked thermoplastic elastomers: structure and mechanical properties of a new system, *Macromolecules* 38 (2005) 1752–1759. DOI: <https://doi.org/10.1021/ma048006m>
- ²⁰² N. E. Botterhuis, D. J. M. van Beek, G. M. L. van Gemert, A. W. Bosman, R. P. Sijbesma, Self-assembly and morphology of polydimethylsiloxane supramolecular thermoplastic elastomers, *Journal of Polymer Science: Part A: Polymer Chemistry* 46 (2008) 3877–3885. DOI: <https://doi.org/10.1002/pola.22680>
- ²⁰³ M. L. Ślęczkowski, E. W. Meijer, A. R. A. Palmans, Cooperative folding of linear poly(dimethyl siloxane)s via supramolecular interactions, *Macromolecular Rapid Communications* 38 (2017) 1–5. DOI: <https://doi.org/10.1002/marc.201700566>

-
- ²⁰⁴ T. Rambarran, A. Bertrand, F. Gonzaga, F. Boisson, J. Bernard, E. Fleury, F. Ganachaud, M. A. Brook, Sweet supramolecular elastomers from α , α '-(β -cyclodextrin terminated) PDMS, *Chemical Communications* 52 (2016) 6681–6684. DOI: <https://doi.org/10.1039/c6cc02632j>
- ²⁰⁵ B. A. G. Lamers, R. Graf, B. F. M. de Waal, G. Vantomme, A. R. A. Palmans, E. W. Meijer, Polymorphism in the assembly of phase-segregated block molecules: pathway control to 1D and 2D nanostructures, *Journal of the American Chemical Society* 141 (2019) 15456–15463. DOI: <https://doi.org/10.1021/jacs.9b08733>
- ²⁰⁶ B. A. G. Lamers, M. L. Ślęczkowski, F. Wouters, T. A. P. Engels, E. W. Meijer, A. R. A. Palmans, Tuning polymer properties of non-covalent crosslinked PDMS by varying supramolecular interaction strength, *Polymer Chemistry* 11 (2020) 2847–2854. DOI: <https://doi.org/10.1039/d0py00139b>
- ²⁰⁷ V. G. Vasilev, T. A. Pryakhina, D. I. Shragin, Y. N. Kononevich, V. S. Papkov, A. M. Muzafarov, Formation of a physical crosslinked structure in polydimethylsiloxanes modified with long-chain hydrocarbon substituents with polar fragments, *Polymer Science, Series B* 59 (2017) 320–327. DOI: <https://doi.org/10.1134/S1560090417030150>
- ²⁰⁸ M. Petr, B. Katzman, W. DiNatale, P. T. Hammond, Synthesis of a new, low-T_g siloxane thermoplastic elastomer with a functionalizable backbone and its use as a rapid, room temperature photoactuator, *Macromolecules* 46 (2013) 2823–2832. DOI: <https://doi.org/10.1021/ma400031z>
- ²⁰⁹ L. Dodge, Y. Chen, M. A. Brook, Silicone boronates reversibly crosslink using Lewis acid–Lewis base amine complexes, *Chemistry - A European Journal* 20 (2014) 9349–9356. DOI: <https://doi.org/10.1002/chem.201402877>
- ²¹⁰ X. Li, D. Zhang, K. Xiang, G. Huang, Synthesis of polyborosiloxane and its reversible physical crosslinks, *RSC Advances* 4 (2014) 1–8. DOI: <https://doi.org/10.1039/c4ra01877j>
- ²¹¹ N. Seetapan, A. Fuongfuchat, D. Sirikittikul, N. Limpanyoon, Unimodal and bimodal networks of physically crosslinked polyborodimethylsiloxane: viscoelastic and equibiaxial extension behaviors, *Journal of Polymer Research* 20 (2013) 1–9. DOI: <https://doi.org/10.1007/s10965-013-0183-8>
- ²¹² T. Stukenbroeker, W. Wang, J. M. Winne, F. E. Du Prez, R. Nicolaÿ, L. Leibler, Polydimethylsiloxane quenchable vitrimers, *Polymer Chemistry* 8 (2017) 6590–6593. DOI: <https://doi.org/10.1039/c7py01488k>
- ²¹³ M. Kathan, C. Jurissek, P. Kovaříček, S. Hecht, Imine-based dynamic polymer networks as photoprogrammable amine sensing devices, *Journal of Polymer Science, Part A: Polymer Chemistry* 57 (2019) 2378–2382. DOI: <https://doi.org/10.1002/pola.29518>
- ²¹⁴ A. Miniewicz, J. Girones, P. Karpinski, B. Mossety-Leszczak, H. Galina, M. Dutkiewicz, Photochromic and nonlinear optical properties of azo-functionalized POSS nanoparticles dispersed in nematic liquid crystals, *Journal of Materials Chemistry C* 2 (2014) 407–584. DOI: <https://doi.org/10.1039/c3tc31791a>

-
- ²¹⁵ B. Mossety-Leszczak, M. Włodarska, H. Galina, G. W. Bąk, Comparing liquid crystalline properties of two epoxy compounds based on the same azoxy group, *Molecular Crystals and Liquid Crystals* 490 (2008) 52–66. DOI: <https://doi.org/10.1080/15421400802305830>.
- ²¹⁶ B. Mossety-Leszczak, P. Wojciechowski, H. Galina, J. Ulański, Synteza monomerów epoksydowych zawierających grupy mezogeniczne, *Polimery-W* 46 (2001) 374-376. DOI: <https://doi.org/10.14314/polimery.2001.374>.
- ²¹⁷ H. H. Winter, F. Chambon, Analysis of linear viscoelasticity of a crosslinking polymer at the gel point, *Journal of Rheology* 30 (1986), 367–382. DOI: <https://doi.org/10.1122/1.549853>